

The Photochemical and Photophysical Characterization of
Chromium(III) Polypyridyl Complexes in Fluid Media

Mary Alain Jamieson

A Thesis
in
The Department
of
Chemistry

Presented in Partial Fulfillment of the Requirements
for the Degree of Doctor of Philosophy at
Concordia University
Montréal, Québec, Canada

November, 1982

© Mary Alain Jamieson, 1982

ABSTRACT

THE PHOTOCHEMICAL AND PHOTOPHYSICAL CHARACTERIZATION OF
CHROMIUM(III) POLYPYRIDYL COMPLEXES IN FLUID MEDIA

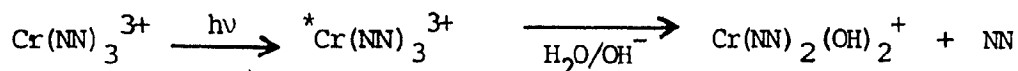
Mary Alain Jamieson, Ph.D. Chemistry
Concordia University, 1982

The photophysical and photochemical behavior of $\text{Cr}(\text{NN})_3^{3+}$ complexes in aqueous solution has been investigated using techniques of continuous and flash photolyses and luminescence intensity and emission measurements. These investigations have allowed for an intensive characterization of the lowest excited state(s) of these complexes, including the identity, the lifetime and the factors affecting the lifetime, and the chemical reactivity in aqueous and mixed solvent solutions.

The transient absorption produced on flash excitation of $\text{Cr}(\text{NN})_3^{3+}$ has been identified as the lowest excited doublet state, ${}^2\text{E}$, through comparison with the 727-nm phosphorescence emission lifetime and quenching studies. The $({}^2\text{E})\text{Cr}(\text{NN})_3^{3+}$ lifetimes were found to be sensitive to the nature and pH of the solvent, the nature of (NN), the presence of added anions and temperature. Furthermore, $({}^2\text{E})\text{Cr}(\text{NN})_3^{3+}$ has been shown to be a strong oxidizing agent, capable of undergoing excited-state bimolecular reductive electron transfer reactions. The product of such a reaction, $\text{Cr}(\text{NN})_3^{2+}$, has been characterized with respect to absorption spectra. Also, $({}^2\text{E})\text{Cr}(\text{NN})_3^{3+}$ undergoes excited-state bimolecular energy transfer reactions with molecular oxygen.

Continuous photolysis (313 - 450 nm) of $\text{Cr}(\text{NN})_3^{3+}$ in aqueous alkaline solution reveals that $({}^2\text{T}_1/{}^2\text{E})\text{Cr}(\text{NN})_3^{3+}$ is produced with near-unitary efficiency from the initially-produced Franck-Condon quartet

excited states. The photolysis results in the release of one polypyridine ligand:



Photolysis experiments have shown that the quenchable reaction component exhibits a pH dependence identical to that of the thermal reaction.¹ From the pH dependences, and the activation parameters obtained from temperature dependence studies, an associative interchange mechanism is proposed involving nucleophilic attack by H₂O on the Cr(III) center to yield a seven-coordinate intermediate species. The excited state responsible for this reaction component is the lowest excited doublet manifold, (²T₁/²E). The unquenchable photoaquation reaction component has been ascribed to direct reaction from the ⁴T₂ excited manifold, via a similar associative interchange mechanism; this assignment was based on pH- and temperature-dependence studies of the quantum yields of reaction under conditions where > 99.9% of the (²T₁/²E) reaction is quenched.

Wavelength dependence studies of the quenchable and unquenchable reaction components, as well as the phosphorescence intensity, of the Cr(bpy)₃³⁺ complex was investigated to determine if a chemical reaction and/or an intersystem crossing process is capable of competing with vibrational relaxation down the quartet manifold. The coincidental decrease of all parameters at 470 - 510 nm is interpreted in terms of the presence of prompt intersystem crossing to (²T₁/²E) and prompt chemical reaction from the ⁴T₂ manifold.

Photosolvolytic of Cr(bpy)₃³⁺ in CH₃CN/H₂O mixtures reveals that Cr(bpy)₃³⁺ is preferentially solvated by CH₃CN, and the reactivity

is attributed to dynamic effects, rather than static effects. Also, the reaction appears to proceed through the ($^2T_1/{}^2E$) manifold via an associative interchange mechanism.

TO GORDON

ACKNOWLEDGEMENTS

I would like to convey my sincere appreciation and gratitude to Dr. Nick Serpone for his continued guidance and active participation throughout this project. A more dedicated mentor cannot be found. He also receives my appreciation for financial support (NSERC, FCAC and NATO) during the last three years.

I would also like to extend my thanks to Drs. Robin T. Rye and Peter H. Bird for serving on my research committee, and for their constructive criticism of this thesis.

I wish to acknowledge and thank Dr. Silvano Emmi for performing the pulse radiolysis experiments, and Dr. Nick Serpone for the flash photolysis experiments. I also wish to thank and extend my appreciation to Professors Morton Z. Hoffman and Mauro Maestri for their collaboration in this project and for their friendship.

I am always indebted to my mother, and to Jim and Gordon for their continued encouragement in all of my endeavors.

TABLE OF CONTENTS

	page
1.0. INTRODUCTION	1
2.0. EXPERIMENTAL SECTION	3
2.1. Preparation of Chromium(III) polypyridyl Complexes ..	3
2.1.0. Reagents and Solvents	3
2.1.1. Elemental Analyses	3
2.1.2. Techniques	3
2.1.3. Synthesis Procedure	4
2.1.4. Elemental Analysis Results	5
2.2. Chemicals and Solutions	6
2.2.0. Solvents	6
2.2.1. Solvent Systems	6
a. Britton-Robinson buffer solutions	6
b. Acetonitrile/water solutions	7
2.3. Photochemical Techniques and Apparati	7
2.3.0. Continuous Photolyses	7
2.3.1. Emission Lifetimes	8
2.3.2. Flash Photolyses	8
2.3.3. Luminescence Intensity Measurements	10
a. Intensity measurements for $\text{Cr}(\text{bpy})_3^{3+}$ in $\text{CH}_3\text{CN}/\text{H}_2\text{O}$ mixtures	10
b. Intensity measurements for $\text{Cr}(\text{bpy})_3^{3+}$ at various excitation wavelengths	10
c. Intensity measurements at 77K	11
2.4. Actinometry	11
2.4.0. Chemical Actinometric Systems	11
2.4.1. Reinecke Actinometry	12

a.	Actinometric procedure	12
b.	Calculations	13
2.4.2.	Ferrioxalate Actinometry	14
a.	Preparation of actinometric solutions ...	15
b.	Ferrous ion calibration curve	15
c.	Actinometric procedure	17
d.	Determination of the light intensity	20
2.5.	Quantum Yield Determinations	21
2.5.0.	Quantum Yield of Reaction by Extraction Procedure	21
a.	Extraction procedure	22
2.5.1.	Spectrophotometric Determination of Quantum Yields of Reaction	23
a.	Experimental procedure	24
2.6.	Emission Lifetime Determinations	26
3.0.	RESULTS AND DISCUSSION	29
3.1.	The Ground State of Cr(III) Complexes	29
3.2.	Ground State Absorption Spectra of Cr(NN) ₃ ³⁺ Complexes	32
3.3.	Ground-state Reactivity of Cr(bpy) ₃ ³⁺ and Cr(phen) ₃ ³⁺ in Solution	37
3.4.	Excited-state Characterization of Cr(NN) ₃ ³⁺ Complexes	42
3.4.0.	Previous Work of Related Cr(III) Complexes ..	42
3.4.1.	Excited-state Absorption of Cr(NN) ₃ ³⁺ Complexes	48
3.4.2.	Luminescence from Cr(NN) ₃ ³⁺ Complexes	56
3.5.	Excited-state Lifetimes of Cr(NN) ₃ ³⁺ Complexes	61
3.5.0.	Quartet State Lifetimes	62
3.5.1.	Doublet State Lifetimes and Substituent Effects	62

3.5.2. Pressure Effects on Doublet-state Lifetimes of $\text{Cr}(\text{bpy})_3^{3+}$	70
3.6. Solution Medium Effects on Doublet-state Lifetimes of $\text{Cr}(\text{NN})_3^{3+}$	71
3.6.0. Solvent Effects	71
3.6.1. Effect of Added Anions	74
3.6.2. Anion-induced Ground-state Quenching	75
3.7. Excited-state Bimolecular Quenching Reactions of $\text{Cr}(\text{NN})_3^{3+}$	101
3.7.0. Bimolecular Electron Transfer	103
a. The $\text{Cr}(\text{bpy})_3^{3+}/\text{Ru}(\text{bpy})_3^{2+}$ system	113
b. $\text{Cr}(\text{bpy})_3^{3+}$ /organic molecules systems	114
c. The $\text{Cr}(\text{NN})_3^{3+}$ /iodide ion systems	120
d. The $\text{Cr}(\text{bpy})_3^{3+}/\text{M}(\text{CN})_x^{n-}$ systems	121
e. The $\text{Cr}(\text{NN})_3^{3+}/\text{Fe}^{2+}(\text{aq})$ systems	122
f. Other $\text{Cr}(\text{NN})_3^{3+}$ /quencher systems	169
3.7.1. Bimolecular Energy Transfer	171
a. The $\text{Cr}(\text{NN})_3^{3+}/\text{Cr}(\text{CN})_6^{3-}$ system	174
b. The $\text{Cr}(\text{NN})_3^{3+}/\text{O}_2$ systems	175
3.8. Chemical Reactivity of $(^2T_1/^2E)\text{Cr}(\text{NN})_3^{3+}$ in Aqueous Solution	189
3.8.0. Continuous Photolysis of $\text{Cr}(\text{NN})_3^{3+}$	190
3.8.1. Temperature Dependence of $^{4+2}\phi_{\text{rx}}$	210
3.8.2. Photosolvolysis in Dimethylformamide	227
3.9. The Unquenchable Photoreaction	229
3.9.0. $\text{Cr}(\text{bpy})_3^{3+}$	229
a. pH dependence of $^4\phi_{\text{rx}}$	232
b. Temperature dependence of $^4\phi_{\text{rx}}$	237

3.9.1.	Cr(phen) ₃ ³⁺	258
	a. Temperature dependence of $^4\phi_{rx}$	258
3.10.	Evaluation of $^4T_2 \rightarrow ^2T_1/{}^2E$ Intersystem Crossing Yield	265
	3.10.0. Evaluating $^4\eta_{isc}$ by Doublet-state Irradiation	269
	3.10.1. Photochemical Evaluation of $^4\eta_{isc}$	243
3.11.	Wavelength Dependence of $^{4+2}\phi_{rx}$, $^4\phi_{rx}$ and I' for Cr(bpy) ₃ ³⁺	286
3.12.	Excited-state Behavior of Cr(bpy) ₃ ³⁺ in CH ₃ CN/H ₂ O Mixtures	313
4.0.	CONCLUSIONS	340
	ADDENDA	346
5.0.	REFERENCES	352

LIST OF FIGURES

FIGURE	page
2-1 : Schematic Representation of N ₂ Laser System for Emission Lifetime Measurements	9
2-2 : Ferrous Ion Calibration Curve for Ferrioxalate Actinometry	18
2-3 : Plots of Cr(NN) ₃ ³⁺ vs Total Irradiation Time for Cr(bpy) ₃ ³⁺ , Cr(5-Brphen) ₃ ³⁺ and Cr(5-Phphen) ₃ ³⁺	27
3-1 : Simplified Energy Level Diagram for CrL ₆ ³⁺ Complexes	30
3-2 : a. Absorption Spectra (log ε vs λ) of Cr(bpy) ₃ ³⁺ , Cr(terpy) ₂ ³⁺ , Cr(4,4'-Me ₂ bpy) ₃ ³⁺ , Cr(4,4'-Ph ₂ bpy) ₃ ³⁺ , Cr(phen) ₃ ³⁺ , Cr(5-Clphen) ₃ ³⁺ , and Cr(5-Brphen) ₃ ³⁺ in Aqueous Solution....	32
b. Absorption Spectra (log ε vs λ) of Cr(4,7-Me ₂ phen) ₃ ³⁺ , Cr(3,4,7,8-Me ₄ phen) ₃ ³⁺ , Cr(5-Mephen) ₃ ³⁺ , Cr(5-Phphen) ₃ ³⁺ , and Cr(5,6-Me ₂ phen) ₃ ³⁺ in Aqueous Solution	32
3-3 : Dependence of the Observed Rate Constant of the Thermal Aquation Reactions on pH for (a) Cr(bpy) ₃ ³⁺ at 11°C, and (b) Cr(phen) ₃ ³⁺ at 31.1°C.....	39
3-4 : Absorption Spectrum of the Primary Transient Measured 150 μsec After the Flash Photolysis of Cr(bpy) ₃ ³⁺ in 0.93 M HClO ₄ and 1.0 M NaCl. [Cr(bpy) ₃ ³⁺] : A = 1.3 x 10 ⁻⁴ M; B = 1.7 x 10 ⁻⁵ M; C = 6.7 x 10 ⁻⁶ M.....	49
3-5 : Absorption Spectrum of the Primary Transient from the Flash Photolysis of Cr(phen) ₃ ³⁺ (1 x 10 ⁻⁵ M) at pH 2.4 and 22°C.	51
3-6 : Absorption Spectra of the Ground-state Cr(NN) ₃ ³⁺ Complexes (dashed lines), and of the Primary Transient Species (² E)-Cr(NN) ₃ ³⁺ (solid lines and points) Obtained by Flash Photolysis Absorption, in N ₂ -purged 1 M HCl.	54

3-7 : Luminescence Spectrum of $\text{Cr}(\text{bpy})_3^{3+}$ in Aqueous Solution at 22°C	57
3-8 : Schematic Energy-level Diagram of Chemical and Physical Processes Important to Chromium(III) Complexes	63
3-9 : Values of $^4\eta_{\text{isc}}$ (relative to $\chi_D = 0.0$) vs χ_D for $\text{Cr}(\text{bpy})_3^{3+}$ (O) and $\text{Cr}(\text{phen})_3^{3+}$ (●) at 22°C	73
3-10: Lifetime of $(^2\text{E})\text{Cr}(\text{phen})_3^{3+}$ as a Function of [Substrate] in Argon-purged Aqueous Solutions at 22°C : —, 1.0 M HCl; each point represents the average of 3-10 individual experiments; - - -, neat H_2O ; the line represents the average of 10 individual experiments performed at different [substrate].....	77
3-11: Quenching Plot of the Data for $(^2\text{E})\text{Cr}(\text{phen})_3^{3+}$ in Argon-purged 1 M HCl Solutions at 22°C ; points at [Substrate] < 2×10^{-4} M cannot be shown owing to scale used. Correlation Coefficient of Least-Squares Plot of all the Points = 0.995.	80
3-12: Lifetime of $(^2\text{E})\text{Cr}(\text{bpy})_3^{3+}$ as a Function of [Substrate] in Argon-purged Solutions at 22°C : —, 5 M HCl; each point represents the average of 3-10 individual experiments; - - -, neat H_2O ; the line represents the average of 10 individual experiments performed at different [substrate] ...	83
3-13: Quenching Plot of the Data for $(^2\text{E})\text{Cr}(\text{bpy})_3^{3+}$ in Argon-purged 5 M HCl Solutions at 22°C ; points at [substrate] < 2×10^{-4} M cannot be shown owing to the scale used. Correlation Coefficient of Least-Squares Plot of all the Points = 0.962	85

3-14: Plot of $1/\tau^2$ for $\text{Cr}(\text{NN})_3^{3+}$ as a Function of [Substrate] in Argon-purged 1 M HCl Solution at 22°C: (O), 5-Phphen in 4% v/v CH_3CN ; (■), 5-Clphen; (●), phen.....	92
3-15: Dependence of $\log k_q$ on ΔG_e^0 Calculated From Equation (3-19) (see text) where ΔG_e^0 is Given by the Marcus and Rehm-Weller Relationships.....	107
3-16: Plot of $\log k_q$ vs ΔE^f (see text) for Reductive Electron Transfer Quenching of $(^2T_1/^2E)\text{Cr}(\text{NN})_3^{3+}$ by $\text{Fe}^{2+}(\text{aq})$	125
3-17: $\log k_q$ vs $\log K_{12}$ Plot (●) for the Quenching of $(^2T_1/^2E)\text{Cr}(\text{NN})_3^{3+}$ by $\text{Fe}^{2+}(\text{aq})$ in Air-equilibrated 1 M HCl Aqueous Solutions; (O) $\log k_{12}$ vs $\log K_{12}$ Plot for the Reduction of $\text{Fe}^{3+}(\text{aq})$ by $\text{Cr}(\text{NN})_3^{2+}$ Transients	128
3-18: Absorption Spectra of $\text{Cr}(\text{NN})_3^{2+}$ Species:	
a. $\text{Cr}(\text{bpy})_3^{2+}$ and $\text{Cr}(4,4'\text{-Me}_2\text{bpy})_3^{2+}$	140
b. $\text{Cr}(4,4'\text{-Ph}_2\text{bpy})_3^{2+}$	142
c. $\text{Cr}(\text{phen})_3^{2+}$	144
d. $\text{Cr}(5\text{-Clphen})_3^{2+}$	146
e. $\text{Cr}(5\text{-Brphen})_3^{2+}$	148
f. $\text{Cr}(5\text{-Mephen})_3^{2+}$	150
g. $\text{Cr}(5\text{-Phphen})_3^{2+}$	152
h. $\text{Cr}(5,6\text{-Me}_2\text{phen})_3^{2+}$	154
i. $\text{Cr}(4,7\text{-Me}_2\text{phen})_3^{2+}$	156
j. $\text{Cr}(4,7\text{-Ph}_2\text{phen})_3^{2+}$	158
3-19: Plots of $\log k_q$ vs the Energy of the 2E States for the Reaction Between $(^2E)\text{Cr}(\text{NN})_3^{3+}$ and O_2 ; $\mu = 1.0$ M (HCl), Aqueous Solutions, 25°C	180

3-20: Theoretical Plot of $\log k_q$ vs the Free Energy Change ΔG^\ddagger (●) represent experimental quenching constants of the phenanthroline complexes; (○) indicate the k_q values for the bipyridyl complexes	184
3-21: Dependence of $\log k_q$ on ΔE^\ddagger (see text) for Oxygen Quenching of $(^2E)Cr(NN)_3^{3+}$ Species	187
3-22: A Potential Energy Surface Diagram (in two dimensions) for Octahedral Cr(III) Complexes	191
3-23: Spectral Variations upon 365-nm Irradiation of $2.2 \times 10^{-5} M$ $Cr(phen)_3^{3+}$ at pH 10.4 and $15^\circ C$ in 0.008 M Britton-Robinson Buffer and 1.0 M NaCl; Irradiation Times are: A, 0 min; B, 8 min; C, 20 min; D, 40 min; E, 180 min.....	193
3-24: Energy-level Diagram for $Cr(NN)_3^{3+}$ Complexes Depicting Important Chemical and Physical Processes.....	195
3-25: Dependence of the Quantum Yield of Photoaquation on pH for $Cr(bpy)_3^{3+}$ at $22^\circ C$ in Argon-purged Solutions Containing 0.008 M Britton-Robinson Buffer and 1.0 M NaCl.....	202
3-26: Dependence of the Quantum Yield of Photoaquation on pH for $Cr(phen)_3^{3+}$ at $15^\circ C$ in Air-equilibrated Solutions Containing 0.008 M Britton-Robinson Buffer and 1.0 M NaCl	204
3-27: Plot of $\ln {}^2k_o$ as a Function of Temperature for $Cr(bpy)_3^{3+}$ at pH 9.8 in Argon-purged Solutions	215
3-28: Plots of $\ln {}^2k_{rx}$ and $\ln {}^2k_{nr}$ vs $1/T$ for $Cr(bpy)_3^{3+}$ at pH 9.8 in Argon-purged Solutions	217
3-29: Arrhenius-type Plot for Temperature Dependences of ${}^{4+2}\phi_{rx}$, ${}^4\phi_{rx}$ and ${}^2\phi_{rx}$ for $Cr(phen)_3^{3+}$ at pH 10.0 and $\mu = 1.0$	221

- 3-30: Dependence of the Quantum Yield for Photoaquation of $\text{Cr}(\text{bpy})_3^{3+}$ (●) and $\text{Cr}(\text{phen})_3^{3+}$ (○) Complexes on I^- Concentration; 22°C , $\mu = 1.0 \text{ M}$, 0.008 M Britton-Robinson Buffer, pH 9-10, argon-purged solutions..... 233
- 3-31: $^4\phi_{\text{rx}}$ as a Function of pH for $\text{Cr}(\text{bpy})_3^{3+}$ at 22°C ; 313-nm Photolysis of Argon-purged Solutions of $1.6 \times 10^{-4} \text{ M}$ $\text{Cr}(\text{bpy})_3^{3+}$ Containing 0.008 M Britton-Robinson Buffer, 0.15 M NaI and 0.85 M NaCl, pH 9.6..... 235
- 3-32: Plot of $\ln ^4\phi_{\text{rx}}$ vs $1/T$ for $\text{Cr}(\text{bpy})_3^{3+}$ at 22°C ; 313-nm Photolysis of Argon-purged Solutions of $1.6 \times 10^{-4} \text{ M}$ $\text{Cr}(\text{bpy})_3^{3+}$ Containing 0.008 M Britton-Robinson Buffer, 0.15 M NaI and 0.85 M NaCl, pH 9.6..... 239
- 3-33: Schematic Representation of the t_{1u} Buckle Vibrational Mode Which Accompanies Excitation of $\text{Cr}(\text{NN})_3^{3+}$ in the Quartet Manifold 247
- 3-34: Plot of $\ln \lambda$ vs $1/T$ (see text) for $\text{Cr}(\text{bpy})_3^{3+}$ at 22°C
- 3-35: Stern-Volmer Plot for Quenching of ϕ_{rx} by I^- for $\text{Cr}(\text{phen})_3^{3+}$ at pH 10.5 and 15°C ; from reference 35. Superscript 0 refers to solutions without iodide ion..... 259
- 3-36: Arrhenius-type Plot of $\ln ^4\phi_{\text{rx}}$ vs $1/T$ for $\text{Cr}(\text{phen})_3^{3+}$ at pH 10.0 in Argon-purged Solutions 262
- 3-37: Simplified Energy Level Diagram of the Biacetyl/ $\text{Cr}(\text{bpy})_3^{3+}$ Couple Used in the Determination of the Intersystem Crossing Efficiency of $\text{Cr}(\text{bpy})_3^{3+}$; SA and SF denote spin-allowed and spin-forbidden states, respectively; k_1, k_2, k_3, k_4, k_i and k_{et} refer to the rate constants for non-radiative, radiative, non-radiative, quenching, intersystem and energy transfer processes 267

3-38: Plot of k_0 vs $[\text{OH}^-]$ in the Range 0.10 - 1.00 M OH^- for $\text{Cr}(\text{bpy})_3^{3+}$ at 5°C	277
3-39: Plots of F_{gsq} vs $[\text{OH}^-]$, (\blacktriangle), and $[\text{OH}^-]$ vs $[\text{OH}^-]$ (\blacksquare), in the Range 0.10 - 1.00 M OH^- for $\text{Cr}(\text{bpy})_3^{3+}$ at 5°C.....	281
3-40: Plots of $[\text{OH}^-]$ vs $[\text{OH}^-]$, (\blacksquare), and $F_{\text{OH}^-}^{-2}$ vs $[\text{OH}^-]$, (\bullet), for $\text{Cr}(\text{bpy})_3^{3+}$ at 5°C in the Range 0.10 - 1.00 M OH^-	282
3-41: Plot of $1/^{4+2}\phi_{\text{rx}}$ vs $1/[\text{OH}^-]^2$ in the Range 0.30 - 1.00 M OH^- for $\text{Cr}(\text{bpy})_3^{3+}$ at 5°C	284
3-42: Plots of $^4\phi_{\text{rx}}$ and I' vs Excitation Wavelength for $\text{Cr}(\text{bpy})_3^{3+}$ at pH 9.6 and 22°C in Air-equilibrated Solutions.....	287
3-43: Plot of $\phi_{\text{rx}}^{\text{tot}}$ vs Excitation Wavelength for $\text{Cr}(\text{bpy})_3^{3+}$ at pH 9.6 and 22°C in Air-equilibrated Solutions.....	289
3-44: Normalized Plots of $^4\phi_{\text{rx}}$, $\phi_{\text{rx}}^{\text{tot}}$ and $^2\phi_{\text{p}}^{\text{rel}}$ vs Excitation Wavelength for $\text{Cr}(\text{bpy})_3^{3+}$ at pH 9.6 and 22°C in Air-equilibrated Solutions.....	293
3-45: Simplified Energy-level Diagram for the Wavelength Dependence of the Photoaquation of $\text{Cr}(\text{bpy})_3^{3+}$ at pH 9.6 and 22°C in Air-equilibrated Solutions.....	295
3-46: Schematic Representation of the Quartet-doublet Excited-state Mixing in <u>trans</u> - $\text{Cr}(\text{en})_2(\text{NCS})_2^+$; from Figure 5 in Reference 120.....	299
3-47: Energy-level Diagram Depicting Wavelength of $\phi_{\text{rx}}^{\text{tot}}$, $^4\phi_{\text{rx}}$ and I' for $\text{Cr}(\text{bpy})_3^{3+}$ in Air-equilibrated Solutions at pH 9.6 and 22°C	304
3-48: Energy-level Diagram Depicting the Wavelength Dependence and Reaction Pathways from the Various Ground- and Excited-state Manifolds of $\text{Cr}(\text{bpy})_3^{3+}$	308

- 3-49: η/η_0 vs $\chi_{\text{CH}_3\text{CN}}$ for a Complex Undergoing Preferential Solvation; dashed lines represent the case of no preferential solvation. From reference 129..... 316
- 3-50: Preferential Solvation Data for $\text{Cr}(\text{bpy})_3^{3+}$ at 25°C Plotted as η/η_0 vs Mole Fraction of CH_3CN for $\text{CH}_3\text{CN}/\text{H}_2\text{O}$ Mixtures. Solid circles show value of η/η_0 derived from NMR linewidths of H_2O protons; open circles refer to data derived from the NMR linewidths of the methyl protons of CH_3CN ; from reference 129..... 318
- 3-51: Dependence of Emission Lifetime of $(^2T_1/^2E)\text{Cr}(\text{bpy})_3^{3+}$ Species on Solvent Composition Expressed as Mole Fraction CH_3CN . Closed circles denote data obtained in air-equilibrated solutions; open circles refer to data for argon-purged solutions..... 322
- 3-52: Effect of Added CH_3CN on the Luminescence Intensity and Emission Lifetime of $(^2T_1/^2E)\text{Cr}(\text{bpy})_3^{3+}$ Species Expressed as A Function of Mole Fraction of CH_3CN . Temperature, 22°C; air-equilibrated solutions; $[\text{Cr}(\text{bpy})_3^{3+}] = 1.5 \times 10^{-4} \text{ M}$ 324
- 3-53: Stern-Volmer Plot for the Water Quenching of the Phosphorescence Intensity and Emission Lifetimes of $\text{Cr}(\text{bpy})_3^{3+}$ in $\text{CH}_3\text{CN}/\text{H}_2\text{O}$ Mixtures (0.80 - 1.00 mole fraction CH_3CN). Solid circles denote intensity data; open circles denote lifetime data. Temperature, 22°C; argon-purged solutions; $[\text{Cr}(\text{bpy})_3^{3+}] = 1.5 \times 10^{-4} \text{ M}$ 328
- 3-54: Dependence of the Photosolvolytic Quantum Yield on the Solvent Composition for $\text{Cr}(\text{bpy})_3^{3+}$ in $\text{CH}_3\text{CN}/\text{H}_2\text{O}$ Mixtures. Temperature, 22°C; air-equilibrated solutions; $[\text{Cr}(\text{bpy})_3^{3+}] = 1.5 \times 10^{-4} \text{ M}$ 331

- 3-55: Preferential Solvation Data of trans-Cr(NH₃)₂(NCS)₄⁻ at 25°C. Circles denote data from the NMR linewidths of CH₃CN protons; squares show values derived from the NMR linewidths of H₂O protons; reproduced from reference 135..... 334
- 3-56: Effect of Water on the Emission Lifetimes of trans-Cr(NH₃)₂(NCS)₄⁻ in CH₃/H₂O Mixtures. Open circles denote τ_0/τ vs Mole Fraction of Water; Solid Circles denote τ_0/τ against η/η_0 of Water; reproduced (in part) from reference 132)... 335
- 3-57: Geometry of the cis-Cr(bpy)₂(H₂O)Cl²⁺ Cation; made available by N. Serpone..... 348

LIST OF TABLES

TABLE	page
2-1 : Solution Composition, Absorbance and Fe^{2+} Concentration for Fe^{2+} Calibration Curve	16
3-1 : Ground-state Absorption Spectra of $\text{Cr}(\text{NN})_3^{3+}$ Complexes	36
3-2 : Thermal Activation Parameters for $\text{Cr}(\text{bpy})_3^{3+}$ and $\text{Cr}(\text{phen})_3^{3+}$	43
3-3 : Luminescence Spectra for Several $\text{Cr}(\text{NN})_3^{3+}$ Complexes in Aqueous Solution at Room Temperature	60
3-4 : Lifetimes of $(^2\text{E})\text{Cr}(\text{NN})_3^{3+}$ and $(^3\text{CT})\text{Ru}(\text{NN})_3^{2+}$	66
3-5 : Phosphorescence Lifetimes of Some Chromium(III) Complexes in Fluid Media	68
3-6 : Lifetime of $(^2\text{E})\text{Cr}(\text{phen})_3^{3+}$ in Deaerated Aqueous 1 M HCl Solutions at 22°C	76
3-7 : Lifetime of $(^2\text{E})\text{Cr}(\text{bpy})_3^{3+}$ in Deaerated Aqueous 5 M HCl Solutions at 22°C	82
3-8 : Rate Constants in the Ground-state Quenching of $(^2\text{T}_1/^2\text{E})\text{-Cr}(\text{NN})_3^{3+}$	88
3-9 : Ground-state Quenching Parameters for $\text{Cr}(\text{NN})_3^{3+}$ at 22°C ...	94
3-10: Medium Dependence of Lifetimes of $(^2\text{T}_1/^2\text{E})\text{Cr}(\text{bpy})_3^{3+}$ and $(^2\text{T}_1/^2\text{E})\text{Cr}(\text{phen})_3^{3+}$ in Argon-purged Solutions at 22°C	96
3-11: Redox Potentials (vs NHE) of $^*\text{Cr}(\text{NN})_3^{3+/2+}$ and X/X^- Couples in Fluid Media	99
3-12: Absorption Spectral Properties of $\text{Cr}(\text{phen})_3^{3+}$, $\text{Cr}(\text{bpy})_3^{3+}$ and X/X^- Couples	100
3-13: Excited-state Identification, Lifetimes, Energies and Redox Potentials for Various $\text{M}(\text{NN})_3^{n+}$ Complexes in Fluid Media ..	110
3-14: Formal Reduction Potentials of $\text{Cr}(\text{NN})_3^{n+}$ Complexes at 25°C.	112
3-15: Electron Transfer Rate Constants (2k_q) for Quenching of $^*\text{Cr}(\text{NN})_3^{3+}$ Complexes	115
3-16: Electron Transfer Rate Constants (2k_q) and Thermal-back Electron Transfer Rate Constants (k_{bet}) for the $\text{Cr}(\text{NN})_3^{3+}/\text{Fe}^{2+}(\text{aq})$ Systems at 22 - 24°C	135

3-17: Rate Constants (k) and Monitoring Wavelength for the Formation of $\text{Cr}(\text{NN})_3^{2+}$	139
3-18: Absorption Spectra of $\text{Cr}(\text{NN})_3^{2+}$ Transients	160
3-19: Calculated Values of f_{ligand} and $\Delta(\text{Cr}(\text{III}))$ and $\Delta(\text{Cr}(\text{II}))$..	167
3-20: Energy Transfer Rate Constants (2k_q) for Quenching by Oxygen and Excited-state Energies ($E^{\text{O-O}}$) of (${}^2T_1/{}^2E$)- $\text{Cr}(\text{NN})_3^{3+}$ Complexes in Fluid Media	177
3-21: Photoaquation Quantum Yields for $\text{Cr}(\text{NN})_3^{3+}$ Complexes at 22°C in Deaerated Solutions	199
3-22: Quantum Yields of Photoaquation and Doublet-state Rate Constants for (${}^2T_1/{}^2E$)- $\text{Cr}(\text{bpy})_3^{3+}$ as a Function of Temperature in Deaerated Solutions	211
3-23: Temperature Profile of the Total Photoaquation, Unquenchable Photoaquation and Quenchable Photoaquation Quantum Yields for $\text{Cr}(\text{phen})_3^{3+}$ in Deaerated Solutions	212
3-24: Temperature Profile of the Ground-state Quenching Phenomenon for (${}^2T_1/{}^2E$)- $\text{Cr}(\text{phen})_3^{3+}$ at pH 10.0 in Deaerated Solutions .	223
3-25: Quantum Yields of Photoaquation and Doublet-state Rate Constants for (${}^2T_1/{}^2E$)- $\text{Cr}(\text{phen})_3^{3+}$ as a Function of Temperature in Deaerated Solutions	225
3-26: Activation Parameters for the (${}^2T_1/{}^2E$) Reaction of $\text{Cr}(\text{bpy})_3^{3+}$ and $\text{Cr}(\text{phen})_3^{3+}$ in Deaerated Solutions at pH 9.5-10.0 ...	226
3-27: a. Photoaquation Quantum Yields for $\text{Cr}(\text{bpy})_3^{3+}$ as a Function of Iodide Ion Concentration at pH ~9.6 in Deaerated Solutions at 22°C	231
b. Photoaquation Quantum Yields for $\text{Cr}(\text{phen})_3^{3+}$ as a Function of Iodide Ion Concentration at pH ~9.6 in Deaerated Solutions at 22°C	232
3-28: Quantum Yields of Photoaquation at 313 nm of $\text{Cr}(\text{bpy})_3^{3+}$ as a Function of Temperature	238

3-29: Temperature Profile of the Photoaquation Quantum Yield and Reactive Decay Rate Constant for the Unquenchable Reaction Component of $\text{Cr}(\text{phen})_3^{3+}$ in Deaerated Solutions	261
3-30: Rate Constants for the Intrinsic Decay, Ground-state Quenching, and Observed Decay of $(^2T_1/^2E)\text{Cr}(\text{bpy})_3^{3+}$ at 5°C as a Function of $[\text{OH}^-]$	275
3-31: Values of $^2k_{\text{rx}}$, $^2k_{\text{rx}}^{\text{OH}^-} [\text{OH}^-]$, and $^2k_{\text{rx}}^{\text{H}_2\text{O}}$ for $\text{Cr}(\text{bpy})_3^{3+}$ at 5°C	276
3-32: Calculated Values of $^2k_{\text{gsq}}$, F_{gsq} , $F_{\text{OH}^-}^{-2}$ and $^2k_{\text{nr}}$ for $\text{Cr}(\text{bpy})_3^{3+}$ at 5°C	279
3-33: Photoaquation Quantum Yields in the Absence and Presence of Iodide Ion and Phosphorescence Intensities of $\text{Cr}(\text{bpy})_3^{3+}$ as a Function of Excitation Wavelength in Air-equilibrated Solutions at pH ~ 9.5 and 22°C	291
3-34: Known Values of the "bite", b , and the Pitch Angle, ψ , for Some Tris(bidentate) Transition Metal Complexes	311
3-35: Relative Values of $(\eta/\eta_0)_{\text{CH}_3\text{CN}}$, Phosphorescence Intensities I , and Lifetimes for $\text{Cr}(\text{bpy})_3^{3+}$ at 22°C as a Function of CH_3CN Composition	326

LIST OF ABBREVIATIONS

bpy	2,2'-bipyridine
4,4'-Me ₂ bpy	4,4'-dimethyl-2,2'-bipyridine
4,4'-Ph ₂ bpy	4,4'-diphenyl-2,2'-bipyridine
phen	1,10-phenanthroline
5-Clphen	5-chloro-1,10-phenanthroline
5-Brphen	5-bromo-1,10-phenanthroline
5-Mephen	5-methyl-1,10-phenanthroline
4,7-Me ₂ phen	4,7-dimethyl-1,10-phenanthroline
5,6-Me ₂ phen	5,6-dimethyl-1,10-phenanthroline
3,4,7,8-Me ₄ phen	3,4,7,8-tetramethyl-1,10-phenanthroline
5-Phphen	5-phenyl-1,10-phenanthroline
4,7-Ph ₂ phen	4,7-diphenyl-1,10-phenanthroline
trpy	2,2',2''-terpyridine
en	ethylenediamine
DMF	dimethylformamide
CH ₃ CN	acetonitrile
η_i	efficiency of the i^{th} process
k_i	rate constant for the i^{th} process
ϕ_i	quantum yield for the i^{th} process
isc	intersystem crossing process
pisc	prompt intersystem crossing process
bisc	back intersystem crossing process
rad	radiative process
nr	non-radiative process
rx	reactive process

q quenching process
bet back-electron transfer process
gsq ground-state quenching process

1.0. INTRODUCTION

Formidable progress has been made over the last twenty years in the study of the photochemical and photophysical behavior of chromium(III) coordination complexes. These complexes remain the object of continued controversy with regard to the identification of the excited state(s) responsible for the photochemical reaction. Photochemistry provides a new dimension in chemistry inasmuch as an electronically-excited species may possess properties different from those of the corresponding ground-state species. While the dominant reaction mode of chromium(III) complexes is photo-substitution by solvent upon irradiation in the ligand-field (LF) bands, photo-racemization, -isomerization, -anation and redox reactions have been investigated for some complexes. Interest in the study of the photoreactivity of chromium(III) complexes revolves around the following considerations: i) the origin of excited-state reactivity with respect to ground-state symmetry; ii) the relationship between the nature of the electronic excited state and the mode of chemical reaction; iii) the mechanistic evaluation of the process(es) which deactivates excited state(s); iv) the adequacy (or inadequacy) of various theories to predict photochemical and photophysical behavior; and v) the comparison of the observed behavior of chromium(III) complexes with that of other transition metal complexes.

Chromium(III) polypyridyl complexes merit particular attention in this respect since their metal-centered (MC) excited states exhibit relatively long lifetimes which can be further prolonged by ligand modification, and by changes in solution medium or ground-state substrate concentration. These excited-state species can thus engage in homogeneous bimolecular energy and electron transfer reactions as a result of

favorable energetics and redox properties. To some extent, the electronic absorption spectra of these complexes overlap the solar emission spectrum, thereby prompting investigations of such complexes as potential photosensitizers in solar energy conversion and storage processes. Investigation of several $\text{Cr}(\text{NN})_3^{3+}$ complexes (NN = 2,2'-bipyridine, 1,10-phenanthroline, or some substituted analogue) in aqueous solution reveals that photosubstitution by solvent is the dominant reaction mode, occurring principally from the doublet excited state with a small unquenchable fraction originating directly from the quartet excited state. The nature of the doublet excited state has been studied intensively in an effort to determine the efficiency with which it is formed, and the various parameters which affect its deactivation. Reactivity of the lowest energy, short-lived quartet excited state has also been probed.

2.0. EXPERIMENTAL SECTION.

2.1. PREPARATION OF CHROMIUM(III) POLYPYRIDYL COMPLEXES.

2.1.0. Reagents and Solvents.

The following chemicals were used as supplied, without further purification: anhydrous chromium(II) chloride (98%) (Alfa or Fluka); 5-chloro-1,10-phenanthroline (G.F. Smith Chemical); 4,4'-diphenyl-2,2'-bipyridine (Chemical Procurement Laboratory); 4,7-dimethyl-1,10-phenanthroline (Chemical Procurement Laboratory or Anachemia); 4,7-diphenyl-1,10-phenanthroline (G.F. Smith Chemical); 2,2'-bipyridine (Anachemia); 1,10-phenanthroline monohydrate (Anachemia Reagent ACS or Aldrich); and 4,4'-dimethyl-2,2'-bipyridine, 2,2',2''-terpyridine, 5-methyl-1,10-phenanthroline monohydrate, 5-nitro-1,10-phenanthroline, 5,6-dimethyl-1,10-phenanthroline, 5-bromo-1,10-phenanthroline, 5-phenyl-1,10-phenanthroline (G.F. Smith Chemical); chlorine gas (Matheson).

Solvents were of reagent or spectrophotometric and used without further purification, including the following: tetrahydrofuran (Fisher Scientific; Certified), absolute methanol (Anachemia, Reagent), 95% ethanol (Anachemia, Reagent). Saturated sodium perchlorate solutions were prepared from purified sodium perchlorate (Fisher Scientific).

2.1.1. Elemental Analysis.

All elemental analyses of the chromium(III) polypyridyl complexes were performed by Galbraith Laboratories, Inc., Knoxville, Tennessee.

2.1.2. Techniques.

In the syntheses of the chromium(III) polypyridyl complexes, the preparations were carried out in a nitrogen-purged glove bag using deoxygenated solvents to avoid premature oxidation of the chromous complex.

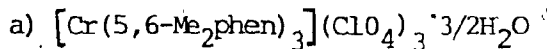
Thus, a stream of nitrogen gas was bubbled through the solvents for ca. 45 min. immediately prior to use. All filtrations were performed using sintered-glass funnels connected to a water-aspirator. Oxidation with chlorine gas was carried out in a well ventilated fumehood. Tygon tubing was connected between the lecture bottle and a sintered-glass dispersion tube, and the chlorine gas bubbled through the reaction mixture. Drying of the product was carried out in air, followed by drying in vacuo.

2.1.3. *Synthesis Procedure.*

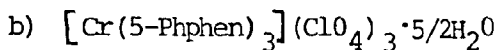
The preparation of $[\text{Cr}(\text{bpy})_3](\text{ClO}_4)_3 \cdot 1/2\text{H}_2\text{O}$, $[\text{Cr}(\text{phen})_3](\text{ClO}_4)_3 \cdot 2\text{H}_2\text{O}$, $[\text{Cr}(4,4'\text{-Ph}_2\text{bpy})_3](\text{ClO}_4)_3 \cdot 2\text{H}_2\text{O}$, $[\text{Cr}(4,7\text{-Ph}_2\text{phen})_3](\text{ClO}_4)_3 \cdot 4\text{H}_2\text{O}$, $[\text{Cr}(4,7\text{-Me}_2\text{phen})_3](\text{ClO}_4)_3 \cdot 2\text{H}_2\text{O}$, and $[\text{Cr}(5\text{-Clphen})_3](\text{ClO}_4)_3 \cdot 2\text{H}_2\text{O}$ have been described previously.¹ For the other complexes, a solution of 5 mmole of chromium(II) chloride, dissolved in 100 ml deoxygenated, distilled water (made slightly acidic with hydrochloric acid) was slowly added to a solution of .15 mmole of free polypyridine dissolved in a minimum of deoxygenated solvent. The choice of solvent was dictated by the ligand solubility. The resulting solution immediately turns a very dark purple or dark green color, indicative of the formation of the chromous²⁺ cation $\text{Cr}(\text{NN})_3^{2+}$. This solution was stirred in a nitrogen atmosphere for 30 min. to ensure complete reaction. Subsequently, 10 ml of saturated sodium perchlorate solution was added, and the solution exposed to oxidation by chlorine gas for ca. 10 min. at which time the solution turned yellow, indicating the formation of $\text{Cr}(\text{NN})_3^{3+}$. The crude product was filtered, collected and recrystallized from a minimum amount of warm water acidified with hydrochloric acid. In cases where the crude product was not soluble in this medium, dissolution was effected with a few mls of acetonitrile, followed by the normal recrystallization procedure. The

final product was obtained by addition of concentrated sodium perchlorate solution and cooling. The mixture was filtered, and the product collected and dried in air and then in vacuo.

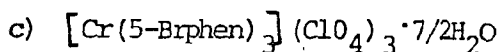
2.1.4. *Elemental Analysis Results.*



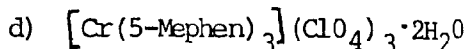
Calculated for $\text{CrC}_{42}\text{H}_{39}\text{N}_6\text{O}_{13.5}\text{Cl}_3$: C, 50.34; H, 3.92; N, 8.31; Cl, 10.52; Cr, 5.19; Found: C, 50.20; H, 3.56; N, 8.24; Cl, 10.80; Cr, 4.99.



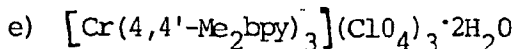
Calculated for $\text{CrC}_{54}\text{H}_{41}\text{N}_6\text{O}_{14.5}\text{Cl}_3$: C, 55.71; H, 3.55; N, 7.22; Cl, 9.13; Cr, 4.46; Found: C, 55.52; H, 3.55; N, 7.36; Cl, 9.31; Cr, 4.19.



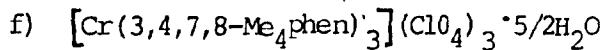
Calculated for $\text{CrC}_{36}\text{H}_{28}\text{N}_6\text{O}_{15.5}\text{Br}_3$: C, 36.31; H, 2.30; N, 7.06; Cl, 8.93; Br, 20.13; Cr, 4.37; Found: C, 36.34; H, 2.24; N, 7.03; Cl, 9.13; Br, 19.98; Cr, 4.55.



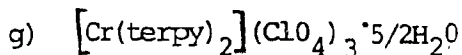
Calculated for $\text{CrC}_{39}\text{H}_{34}\text{N}_6\text{O}_{14}\text{Cl}_3$: C, 48.79; H, 3.46; N, 8.75; Cl, 11.08; Cr, 5.42; Found: C, 48.68; H, 3.52; N, 8.65; Cl, 10.89; Cr, 5.16



Calculated for $\text{CrC}_{36}\text{H}_{40}\text{N}_6\text{Cl}_3\text{O}_{14}$: C, 46.24; H, 4.31; N, 8.99; Cr, 5.56; Found: C, 46.33; H, 4.40; N, 8.90; Cr, 5.36.



Calculated for $\text{CrC}_{48}\text{H}_{53}\text{N}_6\text{O}_{14.5}\text{Cl}_3$: C, 52.23; H, 4.79; N, 7.61; Cr, 4.71; Found: C, 52.25; H, 4.88; N, 7.59; Cr, 4.91.



Calculated for $\text{CrC}_{30}\text{H}_{27}\text{N}_6\text{O}_{14.5}\text{Cl}_3$: C, 41.80; H, 3.16; N, 9.75;

Found: C, 41.88; H, 2.83; N, 9.97.

2.2. CHEMICALS AND SOLUTIONS.

2.2.0. Solvents.

Sodium hydroxide solutions were prepared by dilution of concentrates (Anachemia Acculute). Acid concentrations were prepared volumetrically from the appropriate concentrated acids: hydrochloric acid (Fisher Reagent ACS, 0.2 ppm Fe), perchloric acid, 70% (Fisher Reagent ACS, 0.001% Fe). Reagent grade sodium chloride (Fisher Scientific) was used to maintain constant ionic strength. Boric acid (Fisher Scientific), reagent grade acetic acid (Fisher Scientific), and ortho-phosphoric acid, 85% w/w (Fisher Scientific) were used to prepare the Britton-Robinson buffers. Spectroanalyzed hexanes and n-heptane (Fisher Scientific or Photorex J.T. Baker) were used as supplied. Spectroanalyzed acetonitrile (MCB Chemicals) was used as supplied.

Quenching experiments were performed using sodium iodide (Fisher Scientific), $\text{Fe}(\text{NH}_4)_2(\text{SO}_4)_2 \cdot 6\text{H}_2\text{O}$ (0.005% Fe^{3+}), sodium bromide (Mallinckrodt), potassium nitrate (Macco, reagent), sodium thiocyanate (Fisher Scientific, Certified Reagent), sulphuric acid (Fisher Scientific), and sodium sulphate (Fisher Scientific, reagent).

Deionized, mono-distilled water was used in all solution preparations, as well as in all experiments.

2.2.1. Solvent Systems.

a. Britton-Robinson Buffer Solutions.

The Britton-Robinson stock solution was prepared according

7

to the procedure of Mongay and Cerda.² Dilution of a mixture of 11.5 ml of acetic acid, 7.5 ml of ortho-phosphoric acid, and 12.4 g of boric acid to 1.00 liter with water gave a 0.20 M solution. A typical solvent contained 0.008 M Britton-Robinson buffer, 1.00 M NaCl to maintain constant ionic strength, and varying amounts of 0.1000 or 1.000 M sodium hydroxide depending on the pH desired. In those experiments involving the iodide ion, the ionic strength was maintained constant at 1.00 using sodium chloride and sodium iodide.

b. Acetonitrile/Water Solutions.

The mixed solvent studies on $\text{Cr}(\text{bpy})_3^{3+}$ were performed using a solvent system composed of spectroscopic grade acetonitrile (BDH) and mono-distilled water.³

2.3. *PHOTOCHEMICAL TECHNIQUES AND APPARATI.*

2.3.0. *Continuous Photolyses.*

Continuous photolyses were carried out with a 1-KW Oriol Hg-Xe lamp equipped with a Bausch and Lomb monochromator (22 nm bandwidth). The beam was passed through an 8-cm path of cooled, distilled water to improve the spectral purity of the incident light. Constant temperature ($\pm 0.5^\circ\text{C}$) during irradiation was maintained with a jacketed cell holder and a constant-temperature circulating water bath (Lauda, model K4R).

Continuous photolyses experiments were performed by pipeting 3.0 ml of photolyte into a 1-cm quartz cell fitted with a stopcock. When necessary, deaeration of the photolyte was carried out by bubbling pre-purified nitrogen or argon through the solution for at least 20 min. at the desired temperature prior to irradiation. Subsequently, irradiation was

carried out for the desired length of time at the appropriate wavelength, followed by spectrophotometric or extraction analysis to determine the quantum yield of reaction. During irradiation of the photolyte, the solution was stirred by bubbling nitrogen or argon through it. For air-equilibrated experiments, compressed air was bubbled through the photolyte during irradiation. The incident light intensity was measured by chemical actinometry, employing either the ferrioxalate or Reinecke actinometer, depending on the irradiation wavelength.

Absorption measurements were recorded on an Aminco-Bowman DW-2 or a Perkin-Elmer 552 UV/VIS spectrophotometer.

2.3.1. *Emission Lifetimes.*

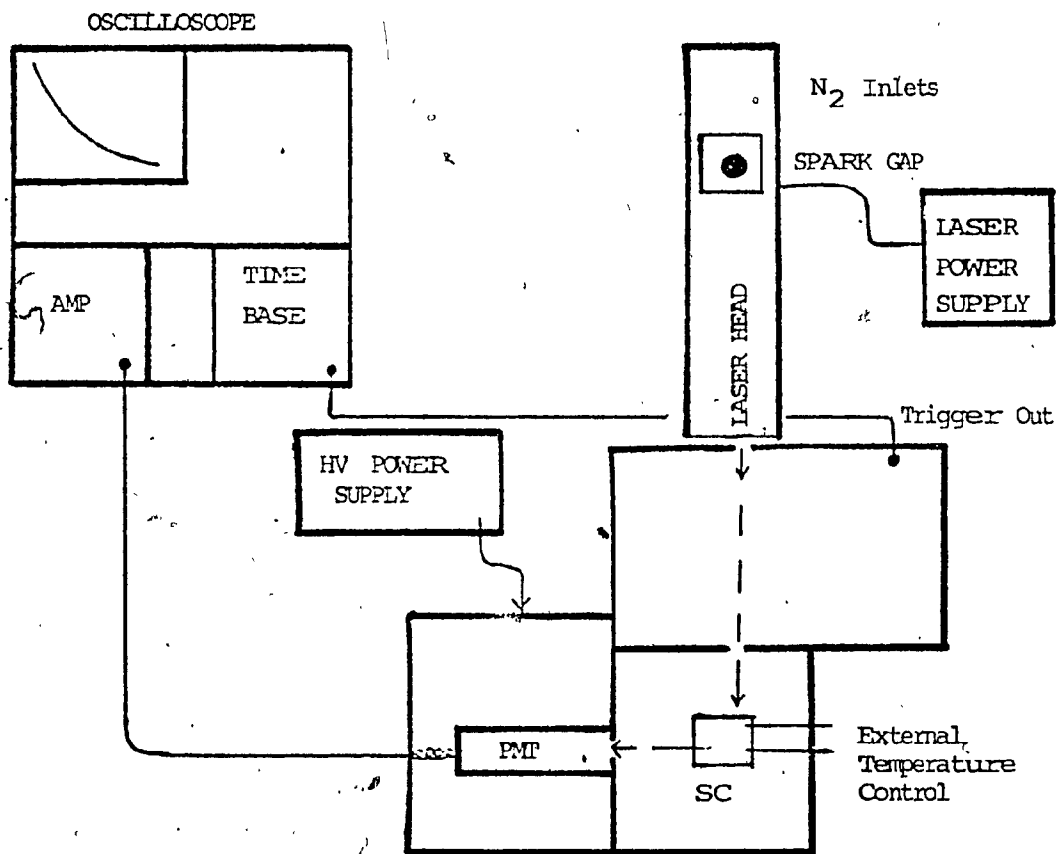
Emission lifetimes for $\text{Cr}(\text{NN})_3^{3+}$ complexes were determined using a Phase-R N21-000 1-KW nitrogen laser (4 nsec pulses at 337 nm) as described by Demas and Flynn.⁴ Luminescence decay curves were photographed from a Tektronix 7633 oscilloscope equipped with a 7A15A amplifier unit and a 7B80 time base unit. Experiments were carried out using 1400V input voltage and were performed with a 1-K Ω load resistance. The apparatus is schematically shown in Figure 2-1. Constant temperature of the analyte was maintained with a constant temperature circulating water bath.

Solutions of the appropriate $\text{Cr}(\text{NN})_3^{3+}$ concentration were dissolved in the desired medium. Where deaerated solutions were required, pre-purified nitrogen or argon was bubbled through the solution for at least 20 min. prior to analysis.

2.3.2. *Flash Photolysis.*

Flash photolysis experiments were performed at Boston University, Boston, MA. The apparatus consisted of a Xenon Corp. Model 720

FIGURE 2-1 : Schematic Representation of N_2 Laser System for Emission Lifetime Measurements.



SC :: sample cell

PMT : RCA C7164R Photomultiplier Tube

unit with xenon-filled flash lamps (500J; $1/e = 30\mu\text{sec}$) and an optical cell 22 cm in length. The 150-W xenon analyzing lamp was operated off a controlled voltage power supply. The output of the photomultiplier tube was displayed on a Tektronix 564 storage oscilloscope.

2.3.3. Luminescence Intensity Measurements.

Luminescence spectra and intensities of $^*\text{Cr}(\text{NN})_3^{3+}$ were recorded on either an Aminco-Bowman or a Perkin-Elmer MPF-44B spectrofluorimeter; the latter was equipped with a R406 (R446) photomultiplier tube, a 150-W xenon lamp source and a DSCU-2 corrected spectra unit.

a. Intensity measurements for $\text{Cr}(\text{bpy})_3^{3+}$ in $\text{CH}_3\text{CN}/\text{H}_2\text{O}$.

Luminescence intensities of $\text{Cr}(\text{bpy})_3^{3+}$ in various $\text{CH}_3\text{CN}/\text{H}_2\text{O}$ mixtures were measured at 22°C ; concentration of $\text{Cr}(\text{bpy})_3^{3+}$ was $1.54 \times 10^{-4} \text{ M}$. Excitation wavelength was 400 nm, and the emission intensity at 727 nm was obtained by recording the emission spectrum in the range 680-750 nm. Emission and excitation slits were 10 nm, and an emission cutoff filter ($< 430\text{nm}$) was employed to remove ultraviolet light and the harmonics of the exciting wavelength.

b. Intensity measurements for $\text{Cr}(\text{bpy})_3^{3+}$ at various excitation wavelengths.

Luminescence intensities at 727 nm of $\text{Cr}(\text{bpy})_3^{3+}$ in acidic and basic media at 22°C as a function of excitation wavelength were determined as follows. The emission spectrum of the xenon lamp source (400-600 nm) was recorded in the ENERGY DC mode against Rhodamine B as a quantum counter. Emission intensities were recorded for $\text{Cr}(\text{bpy})_3^{3+}$ in Britton-Robinson buffered solutions (0.008 M, 1.0 M NaCl, pH 9.53) having an absorbance of 0.043 at each excitation wavelength. Similarly, the emission intensities of solutions of $\text{Cr}(\text{bpy})_3^{3+}$ in 1.0 M HCl having an

absorbance of 0.011 at the various excitation wavelengths were recorded at 727 nm. Luminescence intensity at 727 nm, corrected for the variation in the lamp intensity, is given by $I' = I_{727\text{nm}} / I_x$, where $I_{727\text{nm}}$ is the emission intensity of the $\text{Cr}(\text{bpy})_3^{3+}$ at 727 nm and I_x is the emission intensity of the xenon lamp source at a particular excitation wavelength λ_{exc} . Emission intensities were determined at $\lambda_{\text{exc}} = 400, 420, 440, 460, 480, 505, 520, 540$ and 565 nm. All instrumental parameters were maintained constant for $I_{727\text{nm}}$ and I_x measurements.

c. Intensity measurements at 77K.

The sample compartment of the spectrofluorimeter was replaced with the Phosphorescence Accessory, which consists basically of a Dewar flask and a quartz appendage as the cell holder. $\text{Cr}(\text{bpy})_3^{3+}$ was dissolved, qualitatively, in 4:1 methanol:water and brought to 77 K by immersing in liquid nitrogen. Luminescence spectra of $\text{Cr}(\text{bpy})_3^{3+}$ at 77 K were recorded in the 600 - 1100 nm range. Detection sensitivity in the 800 - 1100 nm range was increased using a red-sensitive R406 photomultiplier tube.

2.4. ACTINOMETRY.

2.4.0. Chemical Actinometric Systems.

Chemical actinometric systems have proven very useful in determining the intensity of incident light, though they may be restricted to some extent by their light absorbing properties. The ferrioxalate actinometer was therefore used for excitation wavelengths in the 313 - 450 nm range, while the Reinecke actinometer was used in the 300 - ca. 700 nm range to measure incident light intensity from the continuous photolysis apparatus.

2.4.1. *Reinecke Actinometry.*

Reinecke's salt is commercially available (Fisher Certified ACS) as the ammonium salt, $\text{NH}_4[\text{Cr}(\text{NH}_3)_2(\text{NCS})_4]$. The ammonium salt was converted to the potassium salt, $\text{K}[\text{Cr}(\text{NH}_3)_2(\text{NCS})_4]$, by dissolution of ca. 20 g in 300 ml warm, distilled water (40-50°C). The warm solution was filtered through a medium-porosity sintered-glass frit (air-aspirator) to give a clear, dark red solution. Approximately 100 ml of a saturated solution of potassium chloride (at 35°C) was slowly added, whereupon the crude pink crystalline product, $\text{K}[\text{Cr}(\text{NH}_3)_2(\text{NCS})_4]$, immediately precipitated out. The solution was allowed to cool, filtered, and the crude product collected. Recrystallization of the crude product from ca. 200 ml of warm, distilled water containing 10 ml of the saturated potassium chloride solution afforded the product, $\text{K}[\text{Cr}(\text{NH}_3)_2(\text{NCS})_4]$, R^- , which was collected, air-dried for 4 hrs. and then in vacuo for 16 hrs. All procedures were carried out in dim, red light and the product was kept in vacuo over P_2O_5 .

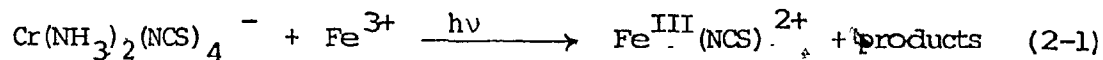
a. Actinometric procedure.

The procedure followed was that reported by Wegner and Adamson.⁵ A solution of R^- in water (pH 5.3-5.5) was prepared such that its absorbance at the excitation wavelength, λ_{rad} , is greater than 2, that is, for 100 % absorption of the incident light. A volume V_{rad} of the R^- solution was irradiated for the desired length of time, with stirring during irradiation. Then, 1.00 ml of the irradiated solution was pipeted into a vial containing 4.00 ml of Fe^{3+} (0.1M $\text{Fe}(\text{NO}_3)_3 \cdot 9\text{H}_2\text{O}$ in 0.5 M HClO_4). At the same time, 1.00 ml of non-irradiated R^- solution was pipeted into a vial containing 4.00 ml of Fe^{3+} solution, to account for the thermal

component of the reaction. The two solutions were shaken, and absorbance at 450 nm recorded for each solution. The entire procedure was performed in dim, red light.

b. Calculations.

In a photochemical experiment, the number of photons given by a lamp must be known. Using the Reinecke system, the following reaction occurs



where the optical density at 450 nm is that of the $\text{Fe}^{\text{III}}(\text{NCS})_2^{2+}$ species formed during the reaction. The difference in optical density between the irradiated and thermal component is given by (2-2), and the concentration

$$\Delta\text{OD}_{450} = \text{OD}_{450}(\text{irrad}) - \text{OD}_{450}(\text{thermal}) \quad (2-2)$$

of NCS^- released from $\text{Cr}(\text{NH}_3)_2(\text{NCS})_4^-$ is

$$[\text{NCS}^-] = \frac{\frac{1.00 \text{ ml} + 4.00 \text{ ml}}{1.00 \text{ ml}} (\Delta\text{OD}_{450})}{\epsilon_{450}(\text{Fe}^{3+})} \quad (2-3)$$

where $\epsilon_{450}(\text{Fe}^{3+}) = 4.3 \times 10^3$. To ensure less than 10% decomposition of the substrate, the percentage photolysis was calculated as in (2-4),

$$\% \text{ photolysis} = \frac{[\text{NCS}^-]}{R_0^-} * 100 \quad (2-4)$$

where R_0^- is the initial R^- concentration. Then the number of einsteins, $I_a t$, is given by (2-5), where I_a is the number of photons per second and

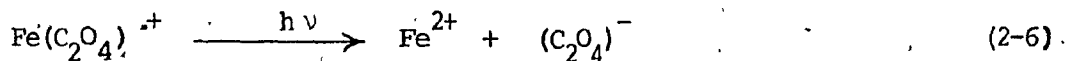
$$I_a t = \frac{[\text{NCS}^-] * v_{\text{rad}}(\lambda)}{\phi_{\text{NCS}^-}} \quad (2-5)$$

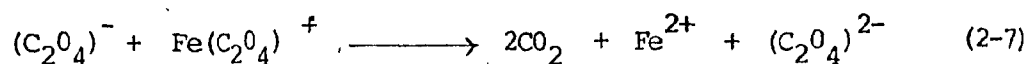
t is the irradiation time (in seconds). ϕ_{NCS^-} is the quantum yield for NCS^- release and is taken as equal to 0.285 (± 0.015) in the wavelength range 504 - 680 nm. The incident light intensity, I_a , can then be calculated as $I_a = I_a t / t$, in einsteins/second.

2.4.2. Ferrioxalate Actinometry.

The ferrioxalate system is normally used as a chemical actinometer to measure incident light intensities in the 250 - 450 nm wavelength range. This system is advantageous since it possesses a constant quantum efficiency and high absorption factor over a wide range of wavelengths, intensities and total irradiation time; also, it possesses high sensitivity and precision while being relatively simple to use.

The procedures used herein are those given by Parker and Hatchard.^{6,7} In general, the photolyte consists of a solution of potassium ferrioxalate, $\text{K}_3\text{Fe}(\text{C}_2\text{O}_4)_3 \cdot 3\text{H}_2\text{O}$, in 0.1 N sulphuric acid. Upon irradiation, reduction of Fe^{3+} occurs and the oxalate ion is oxidized. The ferrous ion





formed in reactions (2-6, 2-7) subsequently complexes with 1,10-phenanthroline, and the concentration of this complex is determined absorptometrically.

a. Preparation of actinometric solution.

Pure $\text{K}_3\text{Fe}(\text{C}_2\text{O}_4)_3 \cdot 3\text{H}_2\text{O}$ was prepared by recrystallizing (3 times) in total darkness reagent grade potassium ferric oxalate (Pfaltz and Bauer, Inc.) from warm, distilled water. The pure crystals were dried using a stream of nitrogen gas. For irradiation wavelengths of 313 and 365 nm, a 0.006 M actinometric solution was prepared by dissolving 2.947 g of $\text{K}_3\text{Fe}(\text{C}_2\text{O}_4)_3 \cdot 3\text{H}_2\text{O}$ in ca. 800 ml of distilled water; 100 ml of standardized 1.0 N sulphuric acid was added, and the solution diluted to 1.0 liter with water. The solution was stored in a brown plastic bottle in the dark to avoid photodecomposition.

b. Ferrous ion calibration curve.

The following solutions were prepared: (A) 4.0×10^{-2} M Fe^{2+} in 0.1 N H_2SO_4 , (B) 0.1% (wt/vol) 1,10-phenanthroline monohydrate in distilled water, (C) a buffer solution consisting of 600 ml of 1.0 N sodium acetate and 360 ml of 1.0 N H_2SO_4 diluted to 1.0 liter with distilled water, and (D) 0.1 N H_2SO_4 . Solutions (B) and (C) were also used in the actinometric procedure.

To a series of 25-ml volumetric flasks were added varying volumes of solution (A), 2.0 ml of solution (B), 5.0 ml of solution (C), and varying volumes of solution (D); the flasks were then diluted to 25 ml with water. The volumes of each solution (A-D) are given in Table 2-1. After thorough mixing, the solutions were allowed to stand for at least 30 min.

TABLE 2-1 : Solution Composition, Absorbance and Fe²⁺ Concentration for Fe²⁺ Calibration Curve.

Sol'n	Vol. (A) (ml)	Vol. (B) (ml)	Vol. (C) (ml)	Vol. (D) (ml)	Abs. (510nm)	Fe ²⁺ (M)
0	0.0	2.0	5.0	10.0	0.00	0.0
1	1.0	2.0	5.0	9.0	0.198	1.604×10^{-5}
2	2.0	2.0	5.0	8.0	0.451	3.208×10^{-5}
3	3.0	2.0	5.0	7.0	0.546	4.812×10^{-5}
4	4.0	2.0	5.0	6.0	0.728	6.416×10^{-5}
5	5.0	2.0	5.0	5.0	0.909	8.02×10^{-5}

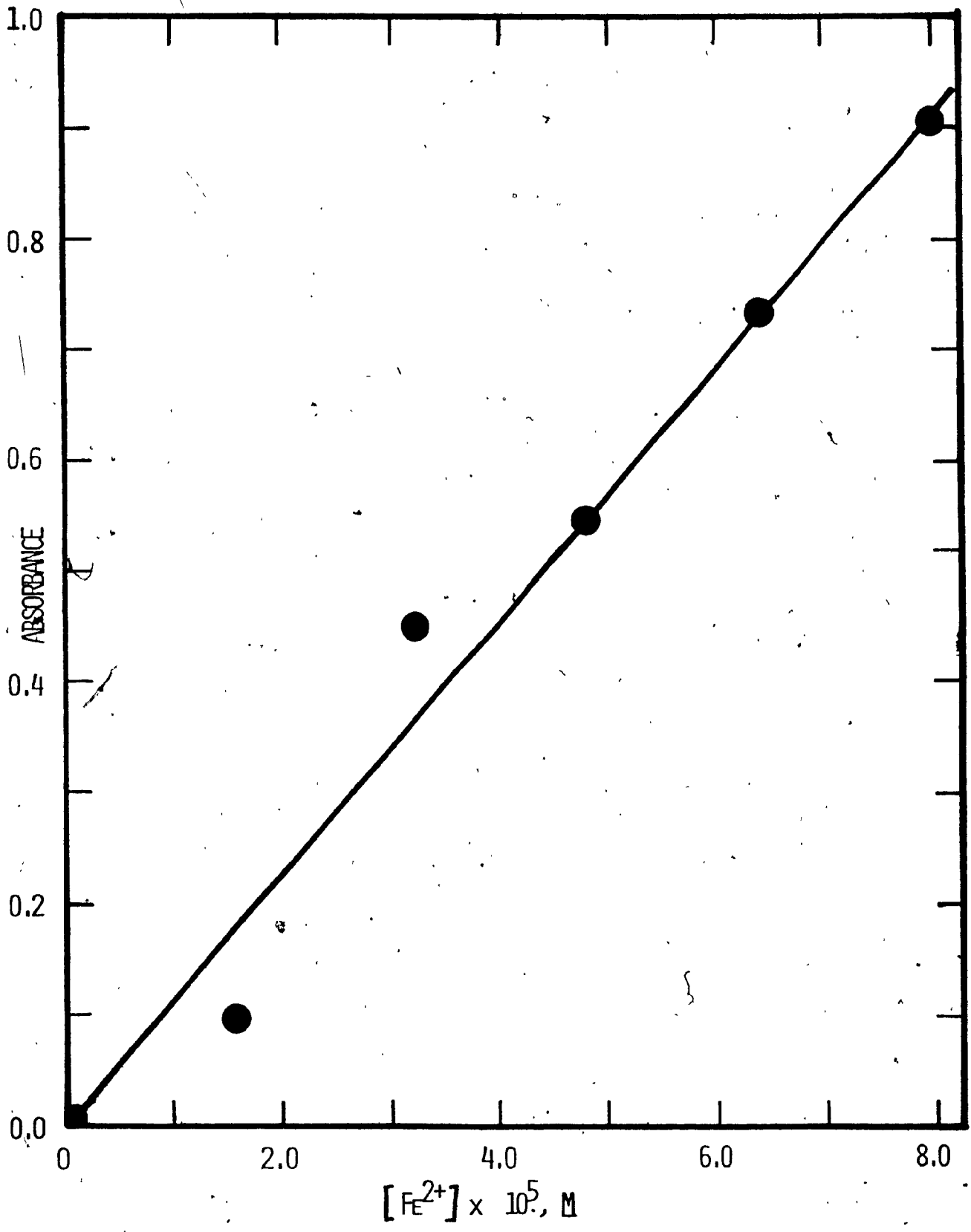
Subsequently, the absorbance at 510 nm was recorded of each solution on a spectrophotometer, using the solution without added Fe^{2+} as the blank. The absorbance values reflect the concentration of Fe^{2+} /1,10-phenanthroline complex formed; these values and the calculated $[\text{Fe}^{2+}]$ values are included in Table 2-1.

To construct the Fe^{2+} calibration curve, a plot of the absorbance at 510 nm vs $[\text{Fe}^{2+}]$ should be linear and yield a slope = $\text{Abs.}/[\text{Fe}^{2+}] = \epsilon$, and intercept = 0. A typical calibration curve is shown in Figure 2-2, using the data of Table 2-1. The slope of the plot in Figure 2-2 is $(1.11 \pm 0.05) \times 10^4 = \epsilon$ in excellent agreement with the literature value⁷ of $\epsilon = 1.11 \times 10^4$.

c. Actinometric procedure.

To determine the light intensity in a photoreaction cell upon irradiation at 313 or 365 nm, 3.0 ml of 0.006 M $\text{K}_3\text{Fe}(\text{C}_2\text{O}_4)_3 \cdot 3\text{H}_2\text{O}$ solution (V_1) was pipeted into a 1-cm quartz cell and irradiated for the desired length of time (t). 2.0 ml of the irradiated solution (V_2) was added to a 25-ml volumetric flask containing 1.0 ml of buffer solution (C) and 2.0 ml of 1,10-phenanthroline solution (B). The flask was diluted to 25 ml (V_3) with water and allowed to stand in the dark for at least 30 min. A blank solution was prepared simultaneously in a similar manner using 2.0 ml of non-irradiated ferrioxalate solution. The absorbance of the solutions containing irradiated ferrioxalate vs non-irradiated ferrioxalate was recorded at 510 nm. This procedure was repeated for various irradiation times. All procedures were carried out in a dimly-lit room. During irradiation, the photolyte was stirred by bubbling compressed air through the solution.

FIGURE 2-2 : ~~Fe~~rous Ion Calibration Curve for Ferrioxalate
Actinometry.



d. Calculations.

The number of Fe^{2+} ions formed during photolysis ($\eta_{\text{Fe}^{2+}}$) was calculated according to equation (2-8) from the data obtained in the previous procedure (see Table 2-1), where l is the pathlength of the

$$\eta_{\text{Fe}^{2+}} = \frac{6.023 \times 10^{23} * v_1 * v_3 * \log I_0/I}{v_2 * l * \epsilon} \quad (2-8)$$

reaction cell and ϵ ($= 1.11 \times 10^4$) is the experimental value of the molar extinction coefficient of the Fe^{2+} ion; all other quantities are defined above. The incident light intensity, I_a , can then be calculated from equation (2-9), knowing the quantum yield for Fe^{2+} ($\phi_{\text{Fe}^{2+}}$) at the

$$I_a = \frac{\eta_{\text{Fe}^{2+}}}{\phi_{\text{Fe}^{2+}} * t} \quad (2-9)$$

desired irradiation wavelength, and for t irradiation time. $\phi_{\text{Fe}^{2+}}$ at 22°C was taken to be 1.22 at 365 nm and 1.24 at 313 nm.⁷ Dividing I_a by Avogadro's Number yields the incident light intensity in einsteins/sec.

If the incident light intensity is maintained constant, then one can assume that any reflection, scattering and/or absorption of incident light by the cell window will be identical whether the cell contains the actinometric solution or some other analyte B. Under conditions of >99% of light absorbed, constant light intensity assures identical numbers of quanta absorbed by any two analytes. If analyte B were irradiated for t_B seconds and formed η_B molecules of product B, and the actinometric

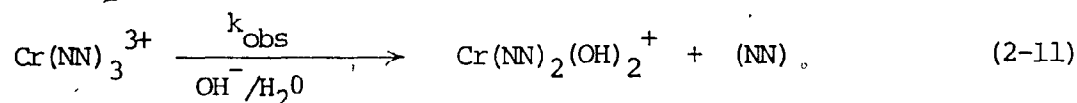
solution formed $\eta_{Fe^{2+}}$ molecules of its product when irradiated for $t_{Fe^{2+}}$ seconds, then the quantum yield of B is given by equation (2-10).

$$\phi_B = \frac{\eta_B * t_{Fe^{2+}} * \phi_{Fe^{2+}}}{\eta_{Fe^{2+}} * t_B} \quad (2-10)$$

2.5. QUANTUM YIELD DETERMINATION.

2.5.0. Quantum Yield of Reaction by Extraction Procedure.

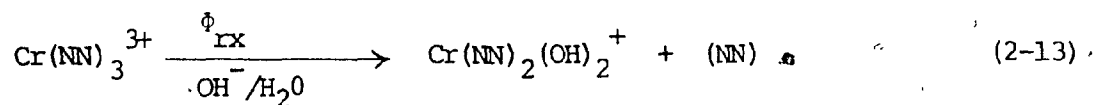
For the first-order reaction (2-11), the rate law for the appearance of reaction products is given in (2-12), where $[NN]$ is the



$$\frac{+d[NN]}{dt} = k_{obs} [Cr(NN)_3^{3+}]_t = k_{obs} \{C_0 - [NN]\} \quad (2-12)$$

concentration of free polypyridine released into solution and $[Cr(NN)_3^{3+}]_t$ is the complex concentration at time t during the reaction. $[Cr(NN)_3^{3+}]_t$ can be equated to the initial concentration of $Cr(NN)_3^{3+}$, C_0 , less the concentration of free polypyridine released, $[NN]$.

For the analogous photochemical reaction (2-13), the quantum yield of



reaction for formation of (NN) , ϕ_{rx} is defined as in (2-14). The

$$\phi_{rx} = \frac{\text{number of molecules of (NN) produced}}{\text{number of photons absorbed by Cr(NN)}_3^{3+}} \quad (2-14)$$

denominator of equation (2-14) was evaluated by measuring the incident light intensity by ferrioxalate actinometry; and the numerator determined by the extraction procedure outlined below. Using equation (2-9), one can write equation (2-15), where η_{Cr} is the number of (NN) molecules

$$\phi_{rx} = \frac{\eta_{Cr} \phi_{Fe^{2+}} t_{Fe^{2+}}}{t_{Cr} \eta_{Fe^{2+}}} \quad (2-15)$$

produced, and t_{Cr} is the irradiation time for the Cr(NN)_3^{3+} system. η_{Cr} is determined from equation (2-16), where V_0 (=3.00 ml) is the volume of photolyte.

$$\eta_{Cr} = \frac{[\text{NN}] * 6.023 * 10^{23} * V_0}{1000 \text{ ml/l}} \quad (2-16)$$

$$\eta_{Cr} = \frac{[\text{NN}] * 6.023 * 10^{23} * 3.00 \text{ ml}}{1000 \text{ ml/l}}$$

a. Extraction procedure.

Exactly 3.00 ml of the desired concentration of Cr(NN)_3^{3+} dissolved in the appropriate medium was pipeted in a 1-cm quartz cell fitted with a stopcock. The concentration must be such that > 99% of the incident light is absorbed by the sample. If necessary, deaeration was

carried out for a minimum of 20 min. at the desired temperature prior to irradiation. The photolyte was then irradiated at a specified temperature and irradiation wavelength for a period of time corresponding to less than 10 % substrate decomposition. Exactly 2.00 ml of the photolysed solution was vigorously shaken with 5.00 ml of n-heptane (for $\text{Cr}(\text{bpy})_3^{3+}$) or hexane (for $\text{Cr}(\text{phen})_3^{3+}$) for 1.0 min. and allowed to stand for 2.0 min. The absorbance spectrum of the upper layer (containing released polypyridine) was recorded in the ultraviolet region. Standard calibration plots of $[\text{NN}]$ vs absorbance maxima of free NN were subsequently employed to determine $[\text{NN}]$. A detailed procedure can be found in the MSc thesis of the author.¹ The thermal component of the reaction was accounted for by treating 2.00 ml of non-irradiated $\text{Cr}(\text{NN})_3^{3+}$ solution in exactly the same way.

2.5.1. Spectrophotometric Determination of Quantum Yields of Reaction.

The quantum yield for loss of complex, ϕ_{rx} , may be defined as the ratio of the rate of disappearance of the complex, Rate, to the rate of photons absorbed by the complex, I_a , as in (2-17). I_a is the

$$\phi_{\text{rx}} = \frac{(\text{Rate})_1}{I_a} \quad (2-17)$$

intensity of the light source at the excitation wavelength, λ_{rad} , in einsteins/sec, and is determined by ferrioxalate or Reinecke actinometry (see Section 2.4.). Then, equation (2-17) is the probability that absorption of a photon of light leads to chemical reaction. The rate is equal to the change in complex concentration as a function of irradiation time.

Equation (2-17) can be used to measure the relative quantum yield of any $\text{Cr}(\text{NN})_3^{3+}$ complex relative to $\text{Cr}(\text{bpy})_3^{3+}$. For the $\text{Cr}(\text{bpy})_3^{3+}$ cation, equations (2-17) becomes

$$\phi_{\text{rx}}(1) = \frac{(\text{Rate})_1}{I_a} = \frac{-d/dt [\text{Cr}(\text{bpy})_3^{3+}]}{I_a} \quad (2-18)$$

and for the $\text{Cr}(\text{NN})_3^{3+}$ cation, equation (2-19) may be written. If the

$$\phi_{\text{rx}}(2) = \frac{(\text{Rate})_2}{I_a} = \frac{d/dt [\text{Cr}(\text{NN})_3^{3+}]}{I_a} \quad (2-19)$$

intensity of the light source, I_a , remains constant for both $\text{Cr}(\text{bpy})_3^{3+}$ and $\text{Cr}(\text{NN})_3^{3+}$ and the concentration is such that the complexes absorb > 99% of the incident light, then equations (2-18) and (2-19) may be combined to yield (2-20). Rearrangement of (2-20) yields (2-21), which is

$$\frac{(\text{Rate})_1}{\phi_{\text{rx}}(1)} = I_a = \frac{(\text{Rate})_2}{\phi_{\text{rx}}(2)} \quad (2-20)$$

$$\phi_{\text{rx}}(2) = \phi_{\text{rx}}(1) \frac{(\text{Rate})_2}{(\text{Rate})_1} \quad (2-21)$$

the quantum yield for loss of $\text{Cr}(\text{NN})_3^{3+}$ relative to that for $\text{Cr}(\text{bpy})_3^{3+}$.

a. Experimental procedure.

Solutions of $\text{Cr}(\text{bpy})_3^{3+}$ and $\text{Cr}(\text{NN})_3^{3+}$ were prepared such

that there was >.99% absorption of light by the complex at the excitation wavelength. Exactly 3.00 ml of the solution was pipeted into a 1-cm quartz cuvet, and irradiated at the desired excitation wavelength λ_{rad} to produce a 1% change in absorbance in the quartet-quartet absorption region (360-460 nm). Successive irradiation and absorbance measurements were performed up to ca. 10% change in absorbance; beyond 10% loss of reactant complex, product absorption may interfere. During irradiation, the sample solution was stirred by bubbling gas (argon or compressed air) through a long needle inserted in the cuvet and immersed in the sample solution.

The absorbance was measured at the analysing wavelength λ_{anal} , and the $[\text{Cr}(\text{NN})_3^{3+}]$ determined from Beer's Law and equation (2-22), where

$$c = [\text{Cr}(\text{NN})_3^{3+}] = \frac{\text{Abs.}(\lambda_{\text{anal}})}{\epsilon(\lambda_{\text{anal}}) \cdot l} \quad (2-22)$$

$l = 1$ cm and $\epsilon(\lambda_{\text{anal}})$ is the molar extinction coefficient of $\text{Cr}(\text{NN})_3^{3+}$ at the analysing wavelength λ_{anal} .

A plot of $[\text{Cr}(\text{NN})_3^{3+}]$ vs total irradiation time ($t_{\text{rad}}^{\text{TOTAL}}$) yielded a slope equal to $(\text{Rate})_2$ and an intercept equal to the initial reactant concentration. This procedure was carried out for $\text{Cr}(\text{bpy})_3^{3+}$ at $\lambda_{\text{rad}} = 313$ nm and $\lambda_{\text{anal}} = 400$ nm, at 22°C, pH ca. 9.8, in air-equilibrated solutions, for which $\phi_{\text{rx}}(1) = 0.11 \pm 0.01$; and for the $\text{Cr}(\text{NN})_3^{3+}$ complex ion under the desired experimental conditions.

Thus, equation (2-21) was used to determine the quantum yield $\phi_{\text{rx}}(2)$ of any $\text{Cr}(\text{NN})_3^{3+}$ cation under any conditions, relative to that for

$\text{Cr}(\text{bpy})_3^{3+}$ under the above-specified conditions. Some typical plots of $[\text{Cr}(\text{NN})_3^{3+}]$ vs $t_{\text{rad}}^{\text{TOTAL}}$ are shown in Figure 2-3; the curvature at substrate decomposition of greater than 10% is observed for the 5-Brphen complex, and was attributed to product absorption.

2.6. EMISSION LIFETIME DETERMINATIONS.

In the absence of secondary processes, the decay of the $(^2T_1/{}^2E)$ state follows first-order kinetics, expressed mathematically as

$$\frac{d[{}^2T_1/{}^2E]}{dt} = -{}^2k_{\text{obs}} [{}^2T_1/{}^2E] \quad (2-23)$$

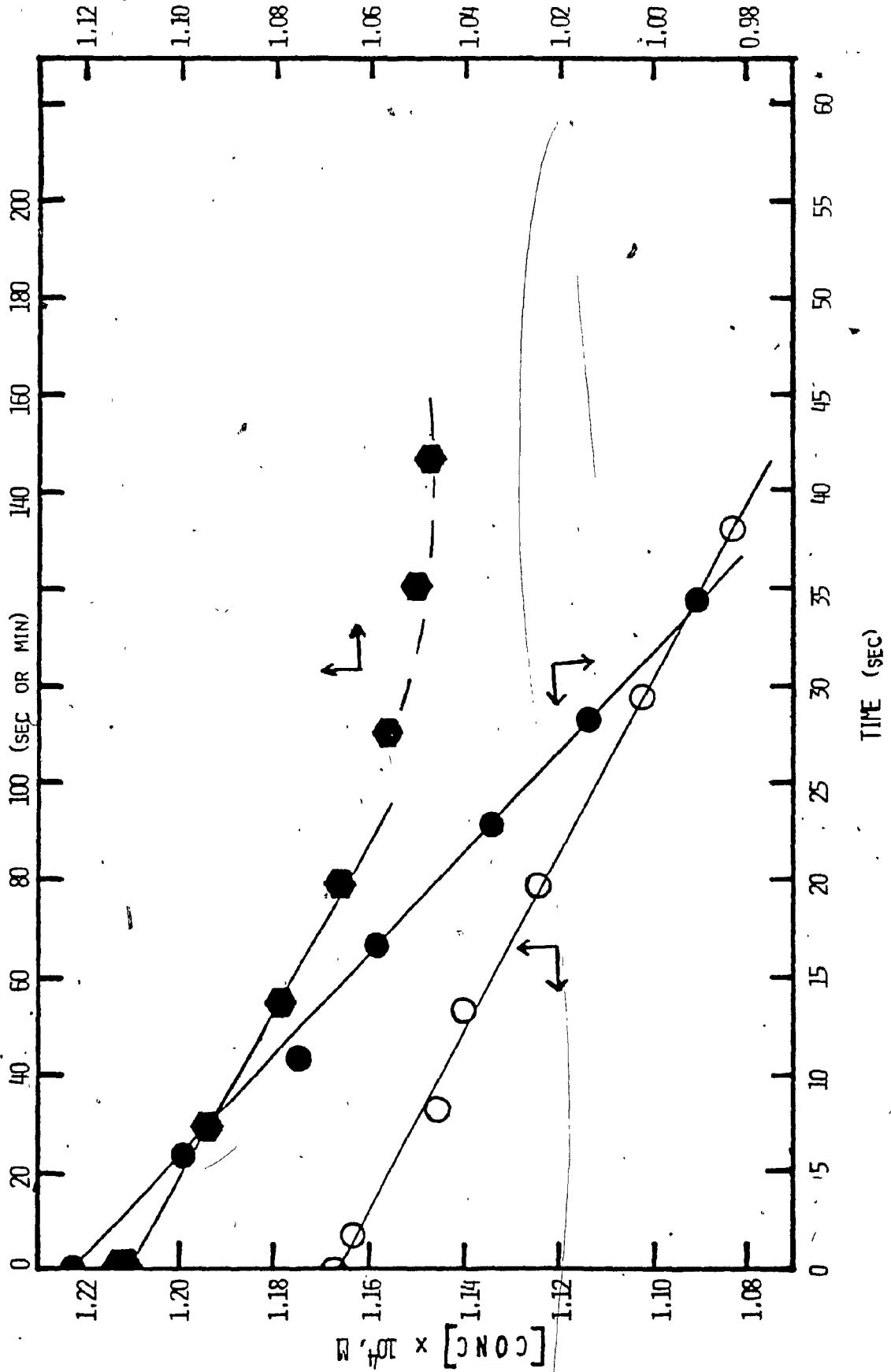
where ${}^2k_{\text{obs}}$ and $[{}^2T_1/{}^2E]$ are the decay constant and the concentration of the species in the $(^2T_1/{}^2E)$ state, respectively. Integration of (2-23) with respect to time, t , followed by rearrangement, yields (2-24).

$$[{}^2T_1/{}^2E]_t = [{}^2T_1/{}^2E]_0 e^{-{}^2k_{\text{obs}} t} \quad (2-24)$$

For an absorbing substrate $\text{Cr}(\text{NN})_3^{3+}$, the quantity $[{}^2T_1/{}^2E]$ is directly related to the relative intensity of the phosphorescence signal, I . Substitution of I for $[{}^2T_1/{}^2E]$ in equation (2-24) and taking natural logarithms of both sides yields (2-25). A plot of $\ln I_t$ vs time should yield a straight line with slope equal to $-{}^2k_{\text{obs}}$ and intercept $\ln I_0$. The reciprocal of the slope gives the experimental lifetime, ${}^2\tau_{\text{obs}}$.

$$\ln I_t = -{}^2k_{\text{obs}} t + \ln I_0 \quad (2-25)$$

FIGURE 2-3 : Plots of $[\text{Cr}(\text{NN})_3^{3+}]$ vs Total Irradiation Times for
 $\text{Cr}(\text{bpy})_3^{3+}$, (\bullet), $\text{Cr}(\text{5-Brphen})_3^{3+}$, (\blacklozenge), and
 $\text{Cr}(\text{5-Phphen})_3^{3+}$, (\circ).

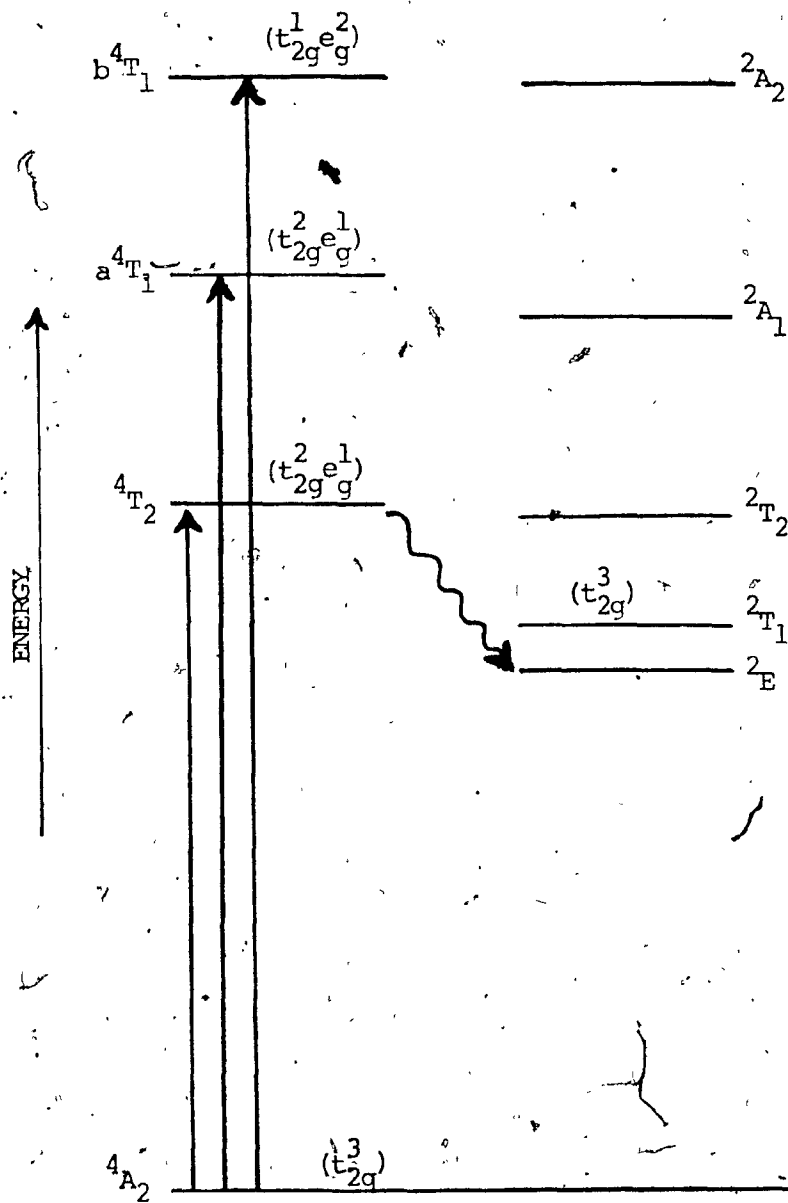


3.0. RESULTS AND DISCUSSION

3.1. THE GROUND STATE OF Cr(III) COMPLEXES.

Irrespective of the octahedral field strength, the ground state of a chromium(III) complex possesses a t_{2g}^3 electron configuration; the first two electronically excited states have $t_{2g}^2 e_g^1$ and $t_{2g}^1 e_g^2$ configurations, respectively. As the ligand field strength decreases, and interelectronic repulsion effects become important, the degeneracy of these states is removed to some extent and the energy level diagram shown in Figure 3-1 results for an octahedral d^3 complex of average ligand field. The splittings shown in Figure 3-1 are those for CrL_6^{3+} complexes, where L is a strong-field ligand. The ground state, 4A_2 , and the two lowest doublet excited states, 2E and 2T_1 , have the same formal electron configuration (t_{2g}^3); the difference among them is due only to spin. The excited quartet states, on the other hand, result from the promotion of an electron from a predominantly non-bonding orbital of π -symmetry (d_{xy} , d_{xz} , d_{yz}) to a σ -antibonding orbital (d_z^2 , $d_{x^2-y^2}$). The splitting of the t_{2g} and e_g orbitals, Δ , arises primarily from the antibonding character of the e_g orbitals, but may also be affected by π -bonding of the t_{2g} orbitals because the 4T_2 state has a $t_{2g}^2 e_g^1$ configuration. Thus, a large value of Δ implies that a complex in the 4T_2 state is expected to have considerably larger Cr-L separations than the 4A_2 complex, due to a decrease in the overall bond character when a t_{2g} electron is promoted to an antibonding e_g orbital. Furthermore, the energies of the quartet states are sensitive to the Cr-L bond strengths, whereas the energies of the doublet states are relatively insensitive.

FIGURE 3-1 : Simplified Energy Level Diagram for CrL_6^{3+} Complexes



3.2. GROUND STATE ABSORPTION SPECTRA OF $\text{Cr}(\text{NN})_3^{3+}$ COMPLEXES.

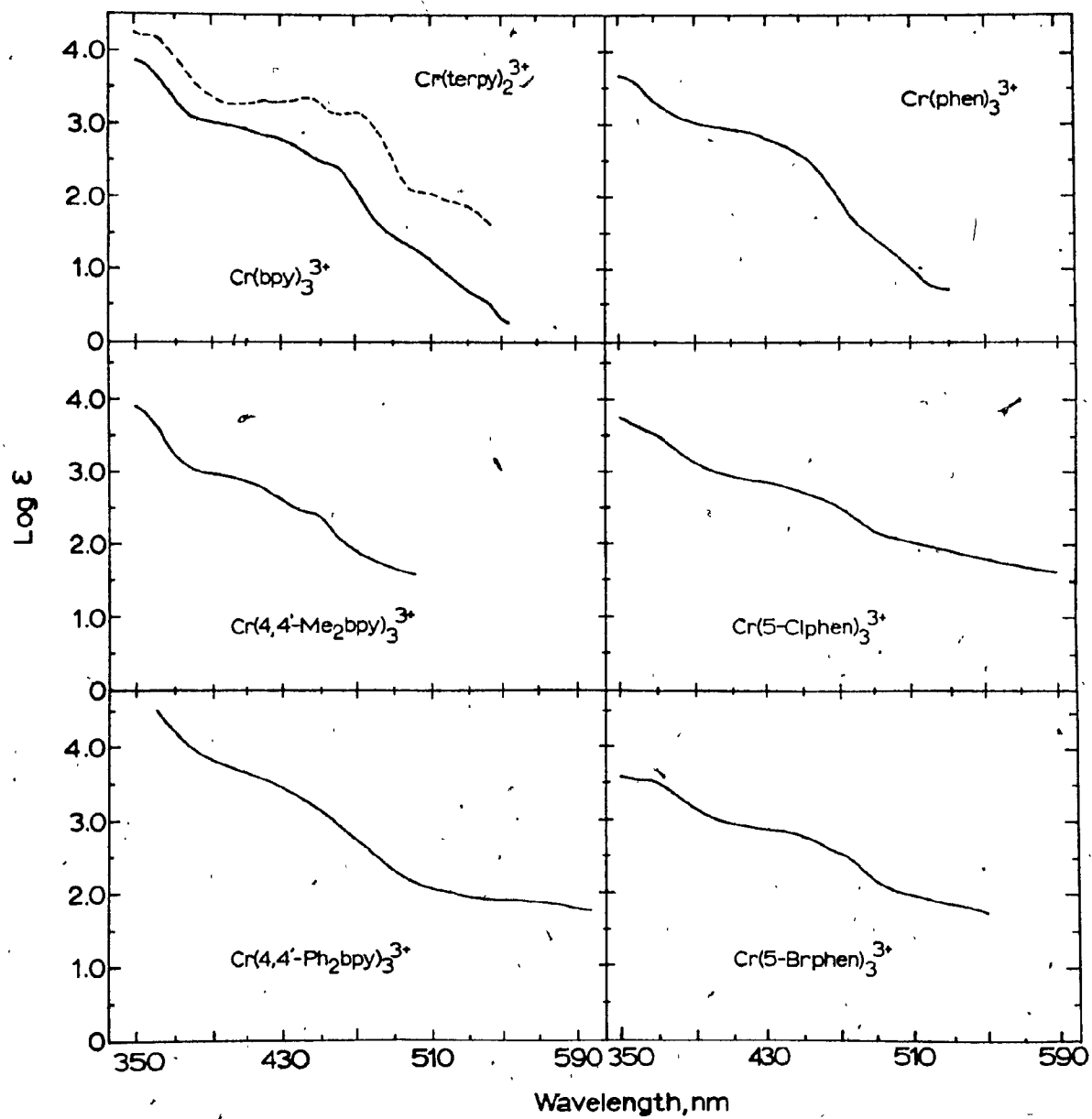
Typical absorption spectra of chromium(III) complexes reveal three weak absorption bands (quartet-quartet) in the ultraviolet and visible regions, and two very weak, spin-forbidden bands (quartet-doublet) in the red region. The quartet-quartet bands correspond to the spin-allowed transitions from the 4A_2 ground state to the excited quartet states 4T_2 , a^4T_1 and b^4T_1 . The quartet-doublet bands correspond to spin- and symmetry-forbidden transitions from the 4A_2 ground state to the excited doublet states 2E and 2T_1 .

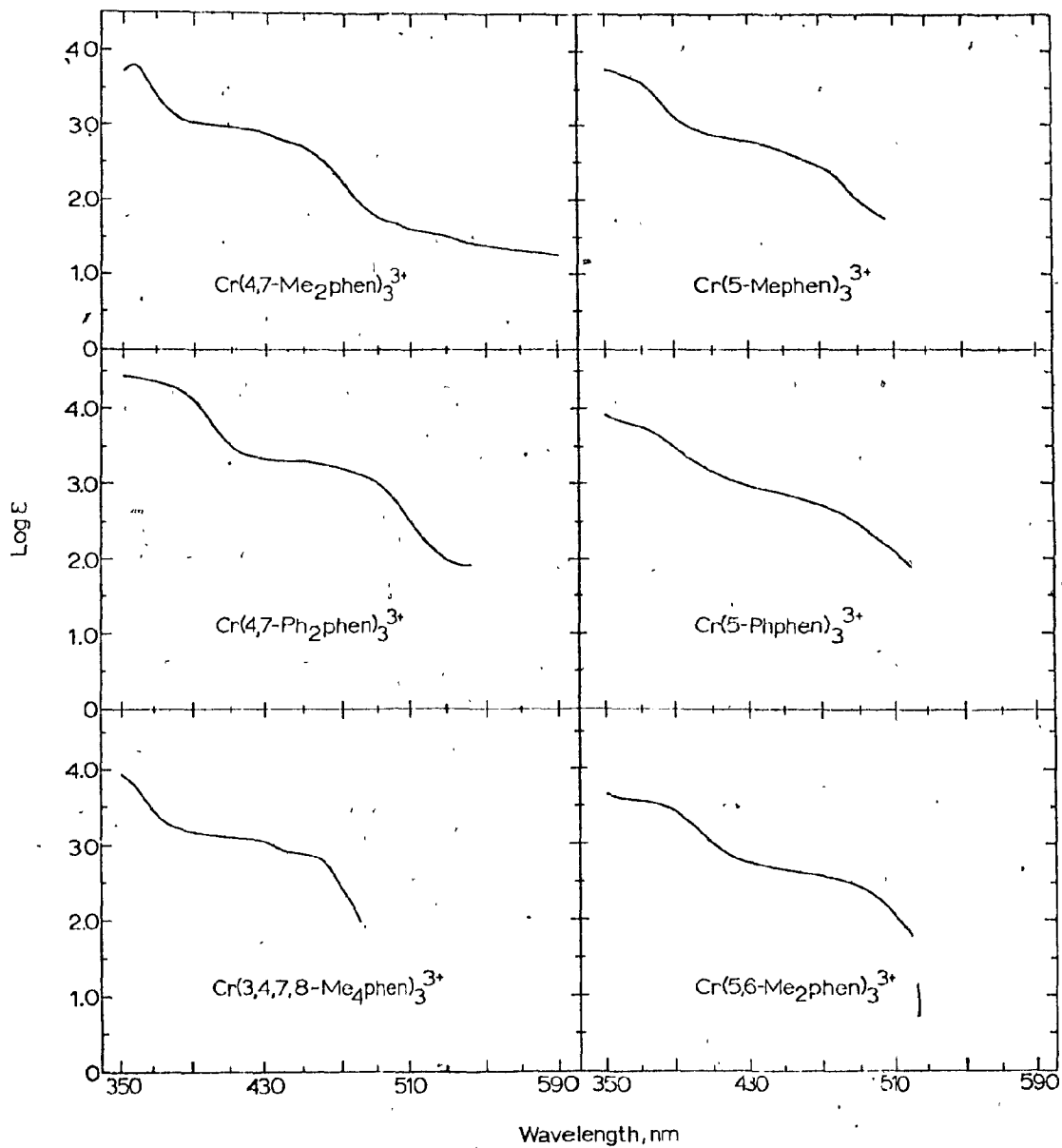
König and Herzog⁸ have thoroughly investigated the ground-state absorption spectrum of $\text{Cr}(\text{bpy})_3^{3+}$ and, assuming octahedral microsymmetry, have assigned the three spin-allowed quartet bands at 23.4 , 28.9 and $35.6 \times 10^3 \text{ cm}^{-1}$ (427nm, 346nm, and 281 nm, respectively) to the $^4A_2 \rightarrow ^4T_2$, $^4A_2 \rightarrow a^4T_1$, and $^4A_2 \rightarrow b^4T_1$ transitions, respectively. The three unresolved shoulders centered at $23.4 \times 10^3 \text{ cm}^{-1}$ (427 nm) were assigned⁸ to vibrational co-excitation involving the coupling of electronic d-d transitions and vibrational transitions within the bipyridyl ligand. This coupling then results in some electron delocalization within the excited states. The bands at $32.7 \times 10^3 \text{ cm}^{-1}$ (306 nm) and $42.1 \times 10^3 \text{ cm}^{-1}$ (238 nm) were interpreted⁸ as bipyridine ligand-centered transitions, $A_1 \rightarrow ^1B_1$ and $^1A_1 \rightarrow ^1A_1$, respectively.

The ground state absorption spectra of several chromium(III) polypyridyl complexes in aqueous solution have been investigated in this work and are illustrated in Figures 3-2a and b. The spectra include those of $\text{Cr}(\text{NN})_3^{3+}$ where $\text{NN} = \text{bpy}$, $4,4'\text{-Me}_2\text{bpy}$, $4,4'\text{-Ph}_2\text{bpy}$, phen, 5-Clphen, 5-Brphen, 5-Mephen, $5,6\text{-Me}_2\text{phen}$, $4,7\text{-Me}_2\text{phen}$, $3,4,7,8\text{-Me}_4\text{phen}$,

FIGURE 3-2 : a. Absorption Spectra ($\log \epsilon$ vs λ) of $\text{Cr}(\text{bpy})_3^{3+}$,
 $\text{Cr}(\text{terpy})_2^{3+}$, $\text{Cr}(4,4'\text{-Me}_2\text{bpy})_3^{3+}$, $\text{Cr}(4,4'\text{-Ph}_2\text{bpy})_3^{3+}$,
 $\text{Cr}(\text{phen})_3^{3+}$, $\text{Cr}(5\text{-Clphen})_3^{3+}$ and $\text{Cr}(5\text{-Brphen})_3^{3+}$
in Aqueous Solution.

b. Absorption Spectra ($\log \epsilon$ vs λ) of $\text{Cr}(4,7\text{-Me}_2\text{phen})_3^{3+}$,
 $\text{Cr}(3,4,7,8\text{-Me}_4\text{phen})_3^{3+}$, $\text{Cr}(5\text{-Mephen})_3^{3+}$, $\text{Cr}(5\text{-Phphen})_3^{3+}$
and $\text{Cr}(5,6\text{-Me}_2\text{phen})_3^{3+}$ in Aqueous Solution.





5-Phphen, and 4,7-Ph₂phen. Figures 3-2a and b show a marked decrease in absorption in the 350-400nm region. More importantly, the first ligand-field (LF) band often appears as two or three unresolved shoulders on the low-energy side of the very intense intraligand band. This makes it difficult to assess the positions and intensities of the ligand-field band. Observation of more than two components is probably the result of co-excitations of some appropriate vibrational modes of the very complex structure of the Cr(NN)₃³⁺ cations. Such interactions suggest some degree of electron delocalization. That there does exist some degree of back-π-bonding from the NN ligands to Cr(III) has also been suggested by Josephsen and Schaffer⁹ who separated the Δ parameter into its σ and π components ($\Delta = \Delta_{\sigma} - \Delta_{\pi}$). It was observed⁹ that $\Delta_{\text{bpy}}^{\sigma} - L_{\text{phen}}^{\sigma} = 300 \text{ cm}^{-1}$ in complexes of the type Cr(NH₃)_{6-2a}(NN)_a³⁺, where a = 0, 1, 2 or 3, and (NN) is bpy or phen. A comparison of the centers of gravity of the lowest-energy band of Cr(bpy)₃³⁺ and Cr(phen)₃³⁺ indicates that $\Delta_{\text{bpy}} \approx \Delta_{\text{phen}}$ (see Table 3-1).

The band maxima of the ground-state absorption spectra of Cr(NN)₃³⁺ are summarized in Table 3-1. For all of the spectra, the lowest-energy multicomponent band is assigned to the ${}^4A_2 \rightarrow {}^4T_2$ transition (denoted by an asterisk in Table 3-1); this band yields the value of the ligand field splitting parameter, Δ, which for the bipyridine complexes varies in the order 4,4'-Me₂bpy ≥ 4,4'-Ph₂bpy ≥ bpy, and for the phenanthroline complexes, Δ varies as 4,7-Ph₂phen ≥ 5-Mephen ≥ 5-Brphen ≈ 5-Clphen ≥ phen ≥ 3,4,7,8-Me₄phen ≥ 5,6-Me₂phen ≈ 4,7-Me₂phen ≥ 5-Phphen. It is evident from the spectral results that methyl or phenyl substitution at 4,4'-positions of the bpy ligand causes a slight blue shift in the bands corresponding to the ${}^4A_2 \rightarrow {}^4T_2$ transition. Methyl substitution on the

TABLE 3-1: Ground-state Absorption Spectra of Cr(NN)₃³⁺ Complexes. ^a

bpy	4,4'-Me ₂ bpy ^b	4,4'-Ph ₂ bpy ^b	phen	4,7-Me ₂ phen ^b
235 ^c (4.62)	240 (4.78)	268 (4.92)	225 (4.93)	230 (4.86)
265 (4.24)	278 (4.38)	320 (4.83)	269 (4.81)	237 (4.80)
276 (4.22)	307 (4.44)	332 (4.84)	285 (4.57)	269 (4.85)
305 (4.36)	342 (3.96)	404* (3.73)	323 (4.10)	308 (4.40)
313 (4.40)	354 (3.86)	422* (3.56)	342 (3.90)	340 (3.94)
346 (3.95)	394* (2.97)	445* (3.24)	358 (3.61)	357 (3.77)
360 (3.76)	418* (2.80)		405* (2.94)	402* (3.02)
402* (2.97)	446* (2.43)		435* (2.78)	424* (2.95)
428* (2.83)			454* (2.51)	450* (2.70)
458* (2.43)				
5-Clphen	4,7-Ph ₂ phen	3,4,7,8-Me ₄ phen		
238 (4.87)	220 (5.05)	234 (4.95)		
275 (4.79)	283 (4.90)	274 (4.90)		
368 (3.56)	308 (4.91)	295 (4.65)		
436* (2.85)	362 (4.43)	310 (4.42)		
466* (2.59)	380 (4.29)	327 (4.27)		
	445* (3.31)	400* (3.13)		
	484* (3.09)	428* (3.06)		
		456* (2.87)		

^a λ , nm ($\log \epsilon$, $M^{-1}cm^{-1}$); in aqueous HCl solutions, unless otherwise noted; positions marked with an asterisk are assigned to the lowest-energy spin-allowed quartet transition.

^b In methanol (spectroquality).

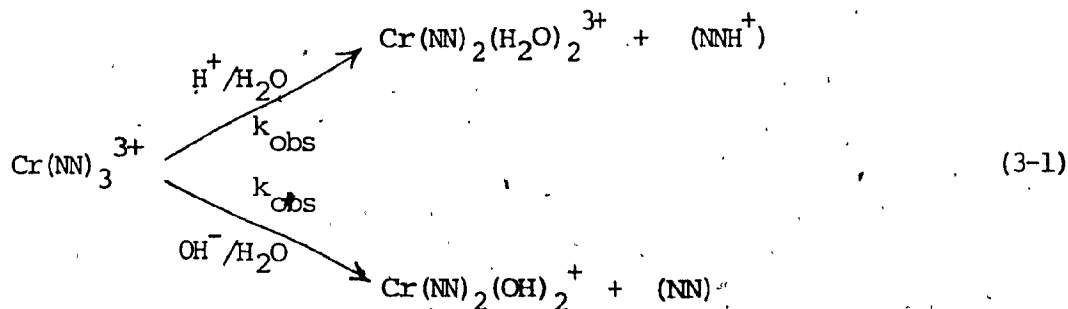
^c Shoulders.

phen ligand blue-shifts this low-energy transition, while phenyl- and halo-substitution cause a red shift. Additionally, the values of the molar extinction coefficient (ϵ) are significantly increased upon phenyl substitution on both bpy and phen frameworks (values in parentheses in Table 3-1).

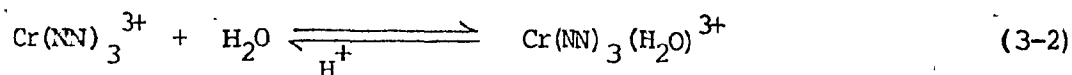
3.3. GROUND STATE REACTIVITY OF $\text{Cr}(\text{phen})_3^{3+}$ AND $\text{Cr}(\text{bpy})_3^{3+}$ IN SOLUTION.

Knowledge of the reactivity of ground-state (4A_2) $\text{Cr}(\text{NN})_3^{3+}$ complexes aids in elucidating the photochemical behavior of these complexes. To this extent, previous investigations by this author¹ and others¹⁰ have shown that the thermal aquation of $\text{Cr}(\text{bpy})_3^{3+}$ in the pH range 0 - 10.7 occurs via pH-dependent, first-order kinetics. Arguments were presented¹ against dissociative, ion-pair interchange, and Gillard-type¹¹ covalent-hydrate mechanisms for the aquation reaction (3-1). An associative interchange mechanism was proposed¹ in which the rate-determining step involved formation of a seven-coordinate intermediate via nucleophilic attack of a water molecule at the chromium(III) center. The thermal aquation was later extended to include the pH range 10.7 - 14.0 for $\text{Cr}(\text{bpy})_3^{3+}$ and $\text{Cr}(\text{phen})_3^{3+}$ in the pH range 0 - 14.¹

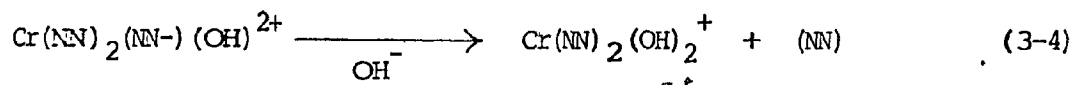
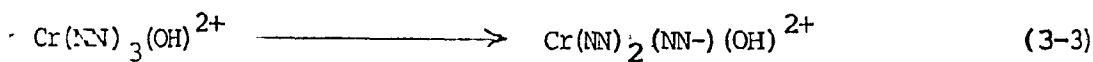
For both $\text{Cr}(\text{bpy})_3^{3+}$ and $\text{Cr}(\text{phen})_3^{3+}$, the stoichiometry of the solvolysis reaction in aqueous solution is described by reaction (3-1),



where NN refers to bpy or phen. At $\text{pH} \leq 6$, k_{obs} is very small and independent of solution pH. This was rationalized¹ in terms of relaxation of the initially-formed $\text{Cr}(\text{NN})_3(\text{H}_2\text{O})^{3+}$ intermediate back to $\text{Cr}(\text{NN})_3^{3+}$ via acid-dependent and acid-independent pathways for the bpy complex (reaction 3-2). The seven-coordinate intermediate, $\text{Cr}(\text{NN})_3(\text{H}_2\text{O})^{3+}$,



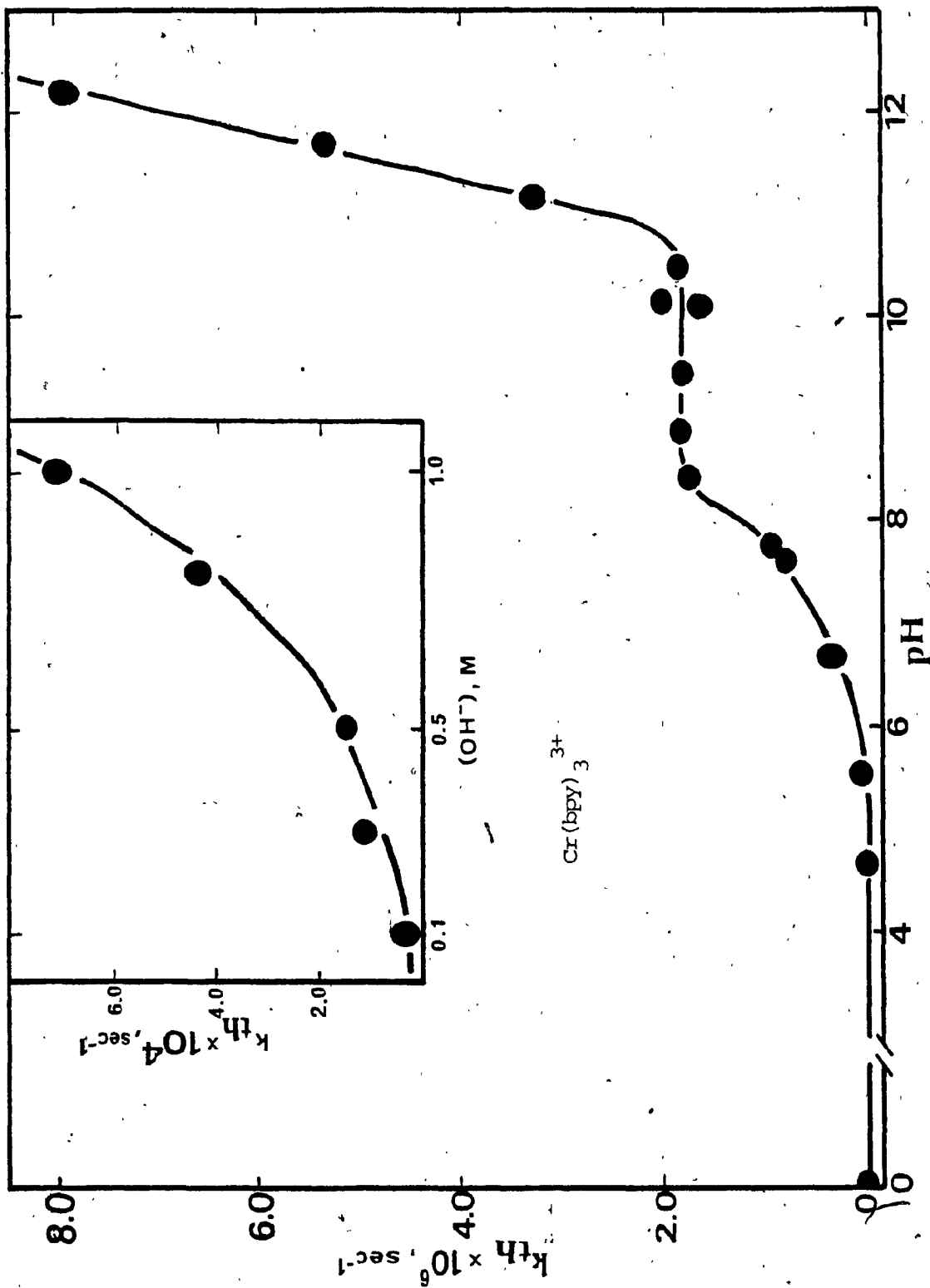
subsequently undergoes deprotonation to form the short-lived $\text{Cr}(\text{NN})_3(\text{OH})^{2+}$ species. This step is revealed by the inflection point at $\text{pH} 6 - 9$ in plots of k_{obs} vs pH (Figures 3-3a and b) for $\text{Cr}(\text{bpy})_3^{3+}$ and $\text{Cr}(\text{phen})_3^{3+}$, respectively. The hydroxy intermediate subsequently undergoes ring-opening and, ultimately and irreversibly, loss of monodentate NN.

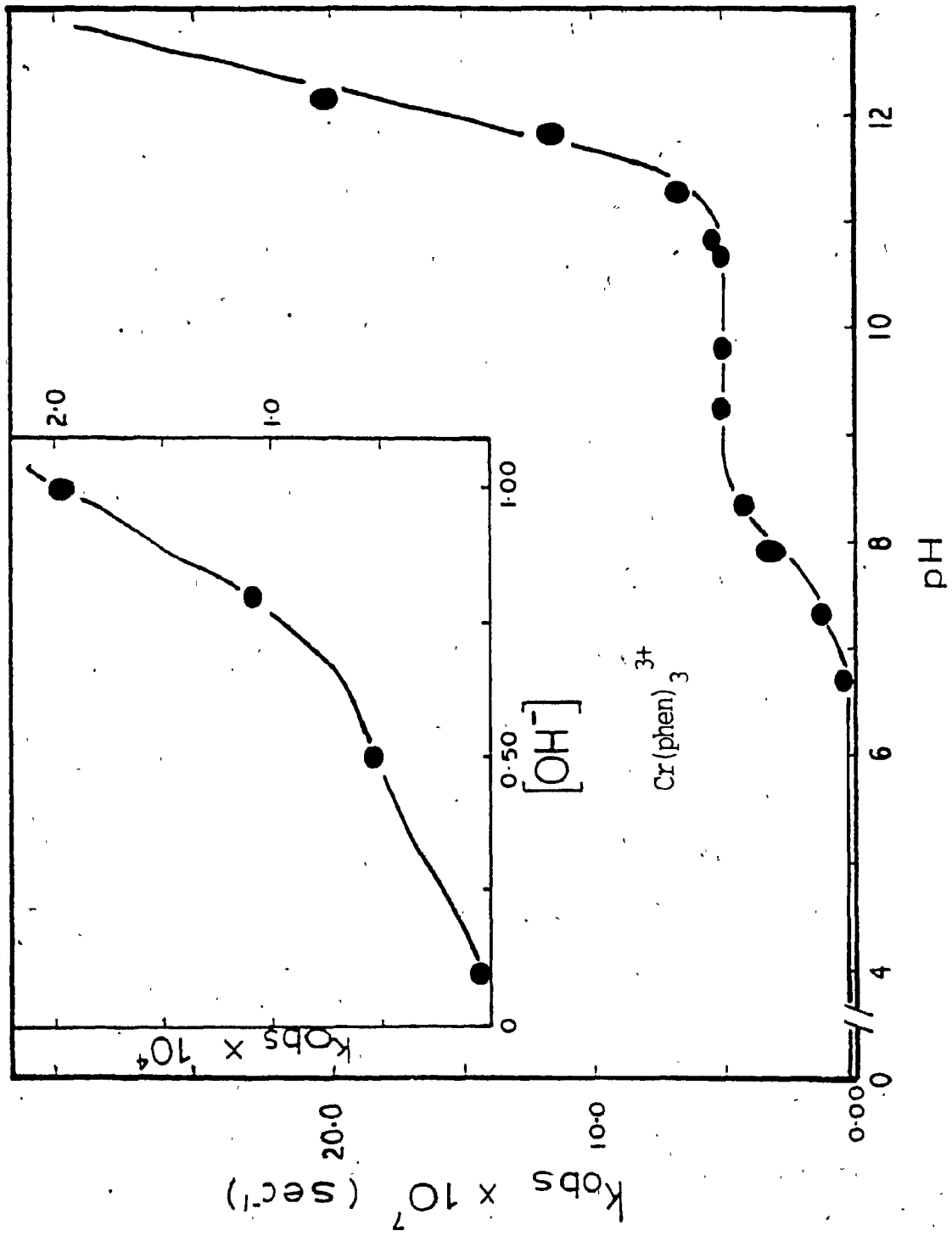


The existence of complexes containing monodentate bpy¹² and phen¹³ ligands has been suggested. The pH region 9 - 10.5 reflects the complete titration of $\text{Cr}(\text{NN})_3(\text{H}_2\text{O})^{3+}$, so that k_{obs} represents the rate constant for the rate-determining attack of H_2O on $\text{Cr}(\text{NN})_3^{3+}$.

Above $\text{pH} 10.7$, k_{obs} was observed¹ to be linearly dependent on $[\text{OH}^-]$ in the range $10.7 \leq \text{pH} \leq 12.2$; the slope of the line was identified with the rate constant for direct nucleophilic attack of OH^- on $\text{Cr}(\text{NN})_3^{3+}$, followed by reactions (3-3) and (3-4). Where $[\text{OH}^-] = 0.1 - 1.0 \text{ M}$, k_{obs} varies linearly with $[\text{OH}^-]^2$.¹ A plausible mechanism involves formation

FIGURE 3-3 : Dependence of the Observed Rate Constant of the Thermal Aquation Reactions on pH for (a) $\text{Cr}(\text{bpy})_3^{3+}$ at 41°C , and (b) $\text{Cr}(\text{phen})_3^{3+}$ at 31.1°C . From reference 1.





of ion-pairs between $\text{Cr}(\text{NN})_3^{3+}$ and OH^- , followed by attack on the ion-pair by another OH^- to form some seven-coordinate intermediate which, also, ultimately and irreversibly leads to polypyridine release. The rate constants, k_{obs} , in the various pH regimes (Figures 3-3a and b) and the activation parameters at $\text{pH} \sim 10$ are reproduced here (Table 3-2) from earlier work¹ for the thermal aquations of $\text{Cr}(\text{bpy})_3^{3+}$ and $\text{Cr}(\text{phen})_3^{3+}$ under the experimental conditions cited. The similarity in the activation parameters for the two chromium(III) complexes in the pH regimes > 6 supports a common mechanism for the two complexes.

3.4. EXCITED-STATE CHARACTERIZATION OF $\text{Cr}(\text{NN})_3^{3+}$ COMPLEXES.

3.4.O. Previous Work of Related Cr(III) Complexes.

Absorption of light into the first ligand-field (LF) band of a chromium(III) complex yields a vibrationally-excited Franck-Condon quartet state, ${}^4\text{FC}$, which subsequently relaxes (vibrational and orientational) to a thermally-equilibrated ("thexi")¹⁴ quartet state, ${}^4\text{T}_2^0$. The ${}^4\text{FC}$ state initially produced may be a mixed state of doublet and quartet character as Kirk suggests,¹⁵ although there is no definitive evidence to suggest that such is the case for $\text{Cr}(\text{NN})_3^{3+}$ complex ions. Clearly, the ${}^4\text{T}_2^0$ state is expected to be severely distorted with respect to the ${}^4\text{A}_2$ ground state as a result of electron promotion from a predominantly non-bonding orbital to an antibonding orbital. The distortion is revealed by increased Cr-L bond lengths in the ${}^4\text{T}_2^0$ state.

The energy of such distorted states should be sensitive to the nature of the coordinated ligand and the chromium-ligand bond strengths. In the solid state, fluorescence (${}^4\text{T}_2 \rightarrow {}^4\text{A}_2$) is expected to be broad and red-shifted with respect to the corresponding absorption band (${}^4\text{A}_2 \rightarrow {}^4\text{T}_2$).

TABLE 3-2 : Thermal Activation Parameters for $\text{Cr}(\text{bpy})_3^{3+}$ and $\text{Cr}(\text{phen})_3^{3+}$ a

ACTIVATION PARAMETER	pH ca. 10		pH ca. 12		0.50 M OH^-	
	bpy	phen	bpy	phen	bpy	phen
ΔH_{298}^+ , kcal/mole	22.3	23.3	20.7	21.6	18.9	20.8
ΔS_{298}^+ , eu	-8.8	-8.4	-12.6	-11	-11	-5

a. In 0.008 M Britton-Robinson buffer, $\mu = 1.0$ (NaCl), from reference 1.

Although fluorescence has been observed for some chromium(III) complexes at low temperature,¹⁶ only a few exhibit both room-temperature fluorescence and phosphorescence. Cr(urea)_6^{3+} exhibits both fluorescence and phosphorescence at room-temperature, with the fluorescence emission being strongly red-shifted to lower energy than that of the phosphorescence emission,¹⁷¹⁸ which implies that the ${}^4T_2^0$ state is at lower energy than the lowest doublet excited state. Also, trans- $\text{Cr(en)}_2F_2^+$ exhibits a weak but efficient ($\phi \approx 2 \times 10^{-4}$) emission with a large Stokes shift and broad spectral band width,¹⁹ and a 1.9 μsec lifetime¹⁵ which would be characteristic of delayed fluorescence.

Adams²⁰ originally proposed that the ${}^4T_2^0$ excited state was the direct precursor to the photochemical reactivity in chromium(III) complexes, on the basis of correlation of product yield with ligand field strength. Since then, the 4T_2 state has been implicated as the immediate precursor to photochemistry with the 2E state being chemically inert except via the 4T_2 state attained through back intersystem crossing.²⁰ Further, Adams²¹ suggested that stereochemically anti-thermal-type photosubstitution occurs from ${}^4T_2^0$, while thermal-type photosubstitution occurs from the doublet states and controls doublet-state lifetimes.

The lowest-energy doublet states, 2E and 2T_1 , are not expected to be distorted with respect to the 4A_2 ground state since the ${}^4A_2 \rightarrow {}^2T_1/{}^2E$ transitions do not involve electron promotion to an antibonding orbital; rather, electron spin-pairing or spin-flip occurs within the t_{2g} orbitals. The bond lengths are thus expected to be very similar for the 4A_2 and ${}^2T_1/{}^2E$ states. Indeed, the nuclear equilibrium geometries of the 4A_2 and ${}^2T_1/{}^2E$ species are essentially identical inasmuch as the absorption (${}^4A_2 \rightarrow {}^2T_1/{}^2E$) and emission (${}^2T_1/{}^2E \rightarrow {}^4A_2$) maxima are

coincident, there being no Stokes shift.¹⁶

Definitive identification of the excited state(s) responsible for chromium(III) photoreactivity remains somewhat elusive. Two principal pathways have been proposed to account for the photochemistry of Cr(III) complexes. Both the lowest spin-forbidden doublet state, 2E ,²²⁻²⁵ and the lowest spin-allowed quartet states, 4T_2 or $^4T_2^o$,²⁰ have been implicated. In support of photoreaction originating from the quartet excited state, Chen and Porter²⁶ have noted that only 50% of the photolysis reaction of $\text{trans-Cr}(\text{NH}_3)_2(\text{NCS})_4^-$ can be quenched by the doublet-quenching reagent $\text{Cr}(\text{CN})_6^{3-}$; this was taken as evidence that 50% of the thiocyanate loss occurs from the quartet excited state prior to intersystem crossing to the doublet excited manifold. Photolysis of $\text{Cr}(\text{NH}_3)_6^{3+}$, on the other hand, must arise from the 4T_2 state²⁷ inasmuch as the phosphorescence is completely quenched by the addition of doublet-quenching hydroxide ions, while the quantum yield of reaction is barely affected by this treatment. Furthermore, 40% of the photoreaction of $\text{Cr}(\text{en})_3^{3+}$ in aqueous solution originates from the quartet state prior to intersystem crossing to the doublet state; the remaining 60% is quenched and this is believed to result from molecules passing through the doublet state.²⁸ Ballardini²⁸ has suggested that the quenchable portion of the photoreaction also comes from the quartet state, subsequent to back intersystem crossing from the doublet state ($^2E \rightsquigarrow ^4T_2$). Cimolino and Linck²⁹ contend that the 4T_2 state is the sole precursor to reaction, based on the invariance to excitation wavelength of the isomeric distribution of photoproducts formed from $\text{Cr}(\text{en})_3^{3+}$. On the other hand, Fukuda et al.³⁰ have suggested that the thermally-equilibrated $^4T_2^o$ state is produced directly with ca. 70% efficiency from the initially-populated Franck-

Condon state, and then undergoes photoaquation; the thermally-equilibrated 2E state is produced with ca. 30% efficiency via prompt intersystem crossing and subsequent photoaquation from 2E . Quantum yields for photoaquation from the $(^4T_2)Cr(en)_3^{3+}$ and $(^2E)Cr(en)_3^{3+}$ species were reported³⁰ to be 0.17 and 0.8, respectively, using a pulsed laser technique. Kutal and coworkers³¹ have recently evaluated the quantum yield of reaction for $Cr(en)_3^{3+}$ by selective population of the 2E state. An increase in the quantum yield was observed³¹ upon direct 2E population relative to 4T_2 population; this was interpreted in terms of significant reactivity occurring from the 2E state.

The 4T_2 state is responsible for the photoaquation of $Cr(CN)_6^{3-}$ as the reaction is sensitized by the triplet states of pyrazine and xanthone, but not by the triplet states of Michler's ketone or $Ru(bpy)_3^{2+}$.³² The triplet energies of pyrazine and xanthone lie above the energy of $(^4T_2)Cr(CN)_6^{3-}$, while those of Michler's ketone and $Ru(bpy)_3^{2+}$ lie below the quartet energy level. Also, $Ru(bpy)_3^{2+}$ does sensitize the $Cr(CN)_6^{3-}$ phosphorescence, which implies that efficient sensitization of the doublet excited state is insufficient for chemical reaction to occur.³²

Photoracemization studies of $(+)-Cr(en)_3^{3+}$ ¹⁶ and $(+)-Cr(phen)_3^{3+}$ ³³,³⁴ have shown that both the quartet and doublet excited states are implicated in the photochemical reactivity of these complexes. Investigations^{33,34} of $(+)-Cr(phen)_3^{3+}$ have demonstrated that photoracemization is partially quenched by molecular oxygen and iodide ion, with an unquenched residual yield which was attributed³³ to a prompt reaction from the 4T_2 state prior to intersystem crossing to the quenchable 2E state. Fourteen (14) percent of the total photoracemization is not quenched by iodide ion, while 86% of the reaction occurs from excited-state species which have

passed through equilibrated doublet states. Intersystem crossing (${}^4T_2 \rightsquigarrow {}^2E$) appears to be a very rapid process in chromium(III) complexes, probably in the range of $10^{10} - 10^{11}$ sec.³⁵ Further, intersystem crossing has been shown^{34,36} to be wavelength-dependent, indicating that this process and vibrational relaxation probably occur within similar time frames. Sasseville and Langford observed³⁴ that the non-quenchable residual (14%) of the photoracemization reaction is wavelength dependent, and the quantum yields of racemization increase (to some extent) with increasing initial vibronic excitation across the low-energy side of the first quartet band. The parallel between the intersystem crossing and non-quenchable photoracemization in the 4T_2 state seems credible since the efficiency of both processes increases with increasing vibronic excitation to an upper limit. Also, there appears to be a significant contribution from the vibrationally-equilibrated ${}^4T_2^0$ state to the non-quenchable reaction.

Several early workers^{22-24,37} suggested that the 2E state was solely responsible for Cr(III) photosubstitution processes, because of the relatively long-lived 2E state in contrast to the absence of fluorescence, the 2E state possessing sufficient energy to promote such reaction, and based on the premise that the 2E electronic configuration (t_{2g}^3) promotes substitutional chemistry. At this point in chromium(III) photochemistry, it is generally believed that the 2E state serves as a source of subsequent quartet excited states via back intersystem crossing or merely as an electronic "sink" for energy dissipation, although there is growing evidence for direct 2E reaction in some complexes.

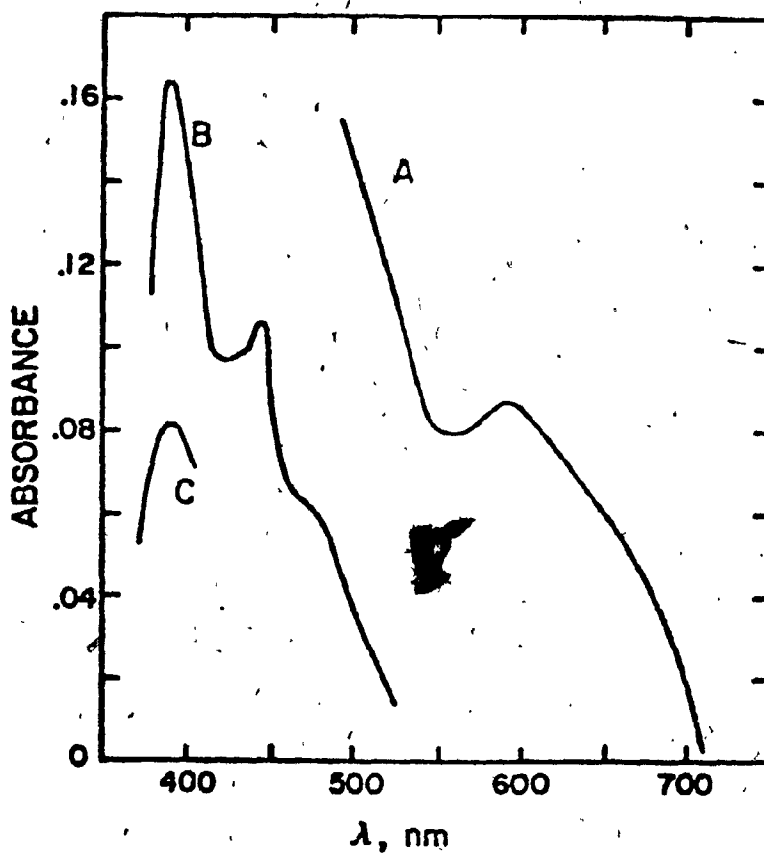
In light of these observations on the role(s) of the various excited states of Cr(III) complexes, and our investigation of the thermal behavior

of $\text{Cr}(\text{bpy})_3^{3+}$ and $\text{Cr}(\text{phen})_3^{3+}$, investigations into the photochemistry and photophysics of chromium(III) polypyridyl complexes have been undertaken in an effort to elucidate the nature and role(s) played by the excited states of these complexes.

3.4.1. Excited-state Absorption of $\text{Cr}(\text{NN})_3^{3+}$ Complexes.

Flash photolysis of acidic, neutral or alkaline solutions of $\text{Cr}(\text{bpy})_3^{3+}$ reveals a primary transient absorption spectrum reproduced from reference 38 and shown in Figure 3-4. The entire spectrum decays via first-order kinetics, with a rate constant $k = (1.6 \pm 0.3) \times 10^4 \text{ sec}^{-1}$ at 22°C .³⁸ Below pH 2, the entire spectrum returns to exactly the absorption level that existed before the flash; at $\text{pH} > 2$, the decay of the primary transient results in a solution of less absorbance in the 360 - 400 nm range than existed before the flash. This negative absorption effect (bleaching) represents the depletion of ground-state $\text{Cr}(\text{bpy})_3^{3+}$ and formation of a secondary transient. The extent of bleaching as well as the rate of ground-state recovery from the secondary transient are pH-dependent. In the range $2.35 \leq \text{pH} \leq 5.35$, recovery of the ground-state absorbance occurs via first-order kinetics, for which $k_{\text{obs}} = k_0 + k_a[\text{H}^+]$; $k_0 \leq 10 \text{ sec}^{-1}$ and $k_a = 4 \times 10^5 \text{ M}^{-1} \text{ sec}^{-1}$.³⁸ Whereas the primary transient is quenched by molecular oxygen ($k_q = 1.7 \times 10^7 \text{ M}^{-1} \text{ sec}^{-1}$),³⁸ iodide ion ($k_q = 1.2 \times 10^9 \text{ M}^{-1} \text{ sec}^{-1}$),³⁸ hydroxide ion ($k_q \approx 2 \times 10^4 \text{ M}^{-1} \text{ sec}^{-1}$),³⁸ and iron(II) ($k_q \approx 10^8 \text{ M}^{-1} \text{ sec}^{-1}$),³⁸ the rate of decay of the secondary transient is unaffected by the presence of I^- or O_2 , though the amount of this transient is reduced under such conditions.³⁸ In the range $4 \leq \text{pH} \leq 6$, the return of the signal to the original baseline is incomplete and a permanent change in solution absorption occurs. At $\text{pH} > 6$, no return of the signal was observed after the decay of the primary transient for

FIGURE 3-4 : Absorption Spectrum of the Primary Transient Measured
150 μ sec After the Flash Photolysis of $\text{Cr}(\text{bpy})_3^{3+}$ in
0.93 M HClO_4 and 1.0 M NaCl . $[\text{Cr}(\text{bpy})_3^{3+}] = 1.3 \times$
 10^{-4} M; B = 1.7×10^{-5} M; C = 6.7×10^{-6} M.



at least 20 msec, implying that the bleaching of the solution occurs in the decay of the primary transient. At pH 9.6, no further change at 360 nm was observed for up to 10 sec after the flash.³⁸

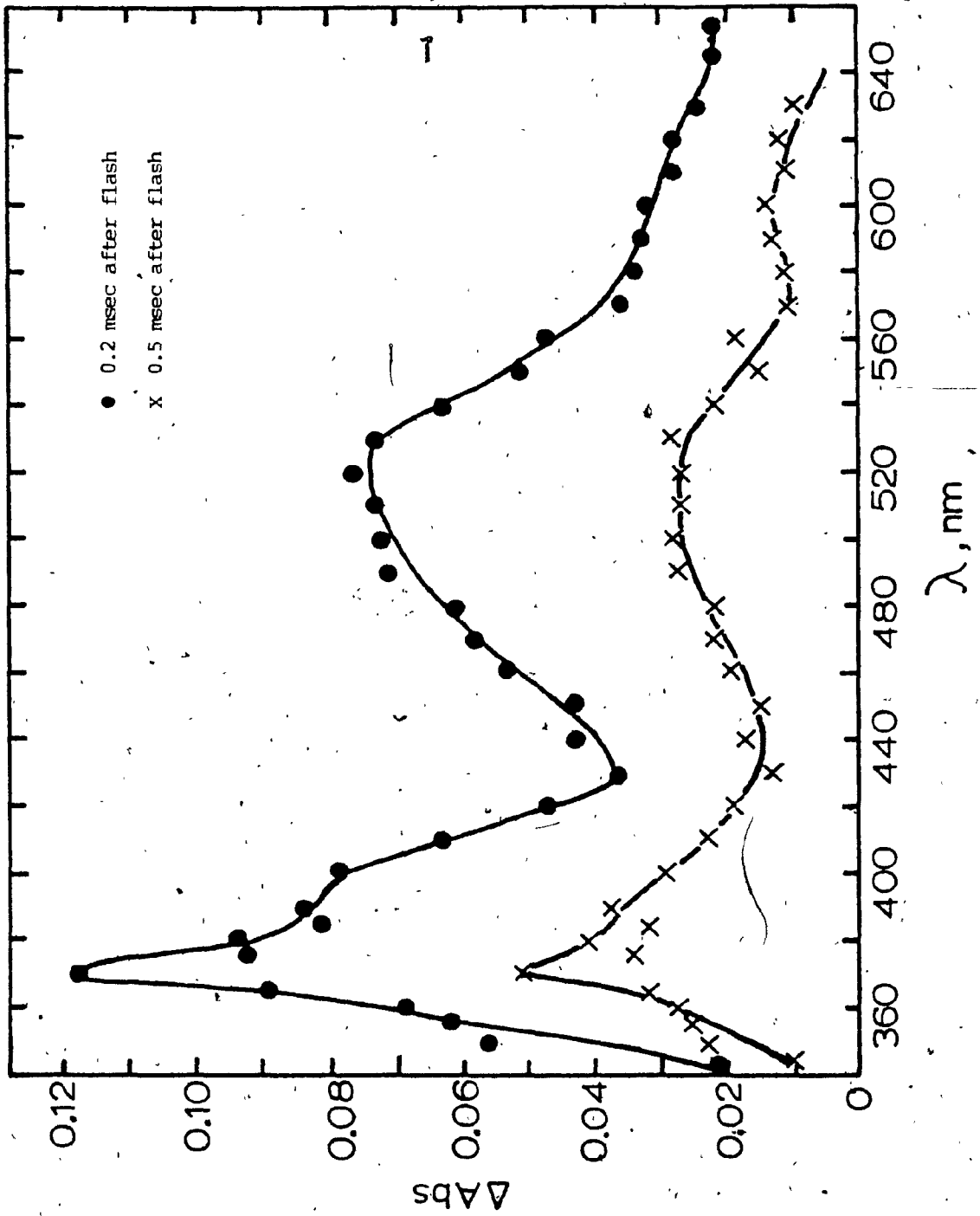
Inasmuch as the decay of the primary transient matches the decay of the phosphorescence emission, the primary transient was identified³⁸ as the 2E excited state. Such an assignment is supported by the temperature dependences of the transient decay and phosphorescence decay, as well as by the oxygen and iodide ion quenching data.³⁸

The absorption spectrum of $(^2E)Cr(bpy)_3^{3+}$ reveals bands at 390 nm, 445 nm, and 590 nm ($25.6 \times 10^3 \text{ cm}^{-1}$, $22.5 \times 10^3 \text{ cm}^{-1}$ and $16.9 \times 10^3 \text{ cm}^{-1}$, respectively), with shoulders at ca. 475 and 650 nm ($21.0 \times 10^3 \text{ cm}^{-1}$ and $15.4 \times 10^3 \text{ cm}^{-1}$, respectively).³⁸ Since the 2E state is $13.7 \times 10^3 \text{ cm}^{-1}$ above the 4A_2 ground state, the excited states attained by 2E absorption are $(30-40) \times 10^3 \text{ cm}^{-1}$ above the ground state.

Flash photolysis of an acidic solution (pH 2.4, HCl) of $Cr(phen)_3^{3+}$ also produces a primary transient absorption spectrum, shown in Figure 3-5, which decays via first-order kinetics with $k = (2.8 \pm 0.4) \times 10^3 \text{ sec}^{-1}$ at 22°C.³⁹ The excited-state decay process is accelerated at pH 11.14 ($k = 6.6 \times 10^3 \text{ sec}^{-1}$) and retarded in 11.7 M $HClO_4$ ($k = 1.5 \times 10^3 \text{ sec}^{-1}$).³⁹ In contrast to what is observed for $Cr(bpy)_3^{3+}$, no transient bleaching of the solution occurs for $Cr(phen)_3^{3+}$. The primary transient is, however, quenched by molecular oxygen ($k_q = 3.5 \times 10^7 \text{ M}^{-1} \text{ sec}^{-1}$ at pH 2.2 in $HClO_4$) and by SCN^- ($k_q = 1.0 \times 10^8 \text{ M}^{-1} \text{ sec}^{-1}$ at pH 2.7 in HCl).

³⁹ Inasmuch as the decay of the primary transient matches the inherent decay of the phosphorescence emission, the primary transient is identified as the 2E excited state. Further support for this assignment derives from the similar temperature dependences of the decays of the transient

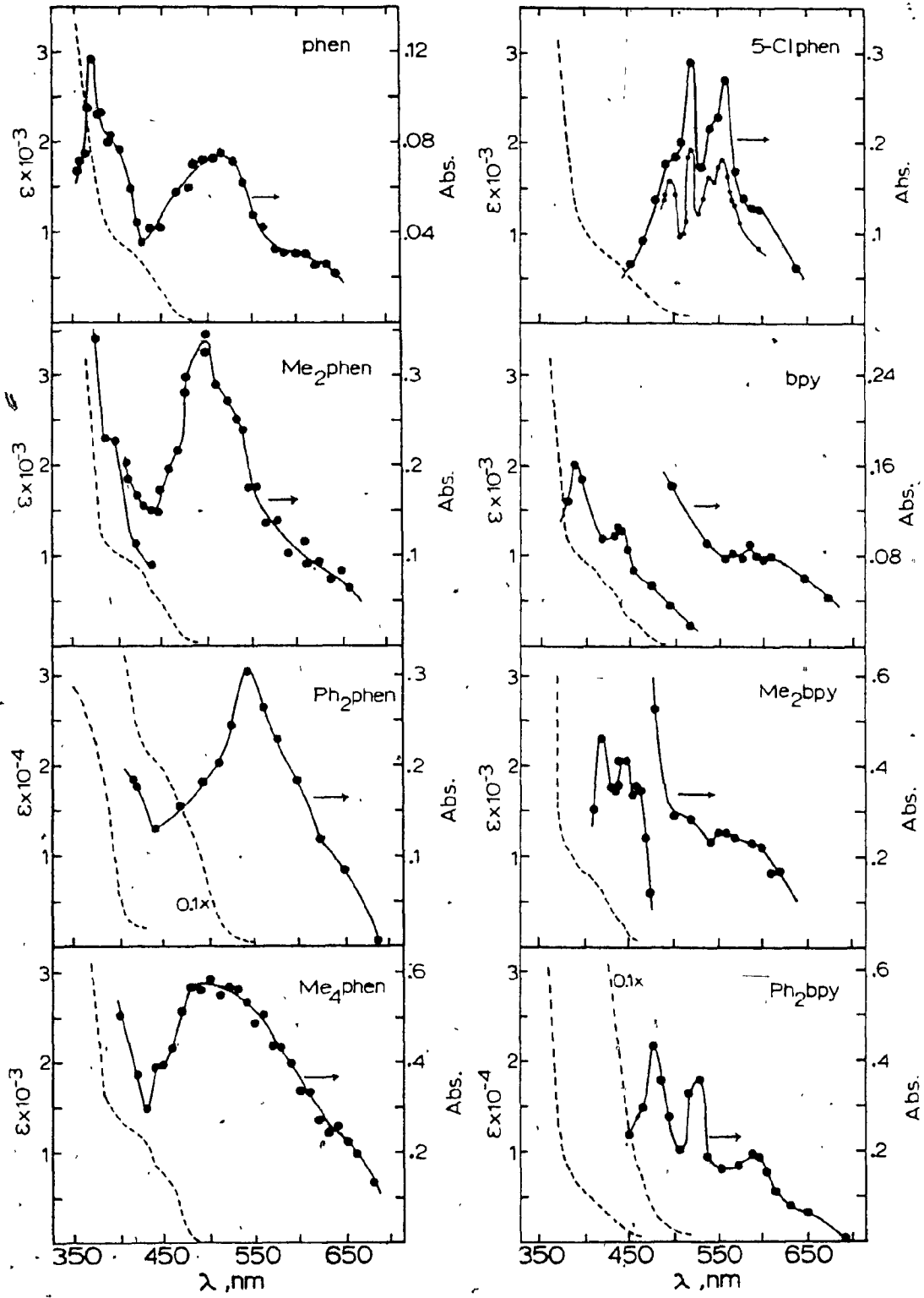
FIGURE 3-5 : Absorption Spectrum of the Primary Transient from the
Flash Photolysis of $\text{Cr}(\text{phen})_3^{3+}$ (1×10^{-5} M) at pH 2.4
and 22°C .



absorption ($E_a = 8.2$ kcal/mole at pH 3, HClO_4) and phosphorescence ($E_a = 9.1$ kcal/mole at pH 0, HCl), as well as from quenching results by the selective doublet quenchers O_2 and SCN^- .³⁹ The doublet absorption of $\text{Cr}(\text{phen})_3^{3+}$ shown in Figure 3-5 reveals bands at 368, 520 and 600 nm, with a shoulder at ca. 395 nm.

Flash photolysis of nitrogen-purged acidic solutions (1 M HCl) of several $\text{Cr}(\text{NN})_3^{3+}$ complexes produced transients which decayed via first-order kinetics at 23°C. The absorption spectra ($\lambda > 350$ nm) of the primary transient species (${}^2\text{E}$) $\text{Cr}(\text{NN})_3^{3+}$ are depicted by the solid lines and points in Figure 3-6 for $\text{NN} = \text{bpy}$, phen , 4,7- Me_2phen , 4,7- Ph_2phen , 3,4,7,8- Me_4phen , 5- Clphen , 4,4'- Me_2bpy and 4,4'- Ph_2bpy . The Figure reveals that the absorption spectra of the (${}^2\text{E}$) states of the bpy and substituted bpy complexes show overall similarity. Methyl substitution at the 4,4'-positions results in a red shift of the 390-nm band of (${}^2\text{E}$)- $\text{Cr}(\text{bpy})_3^{3+}$ to 420 nm; phenyl substitution at these positions red shifts both the 390- and 445-nm bands to 480 and 525 nm, respectively. The band at 590 nm in (${}^2\text{E}$) $\text{Cr}(\text{bpy})_3^{3+}$ does not appear to be very sensitive toward ligand substitution. Inasmuch as the ${}^2\text{E}$ excited states lie ca. $13.7 \times 10^3 \text{ cm}^{-1}$ above the ${}^4\text{A}_2$ ground states, the excited states reached by the ${}^2\text{E}$ absorption process are ca. $(30-40) \times 10^3 \text{ cm}^{-1}$ above the ground state, as expected from energy level diagrams.^{40,41} Such diagrams predict the existence of five metal-centered doublet transitions in the $(20-32) \times 10^3 \text{ cm}^{-1}$ (500 - 313 nm) region. Ohno and Kato⁴² noted that the energy levels of the doublet states of $\text{Cr}(\text{acac})_3$ are not far removed from the corresponding quartet states. On this basis, the upper doublet state corresponding to the ${}^4\text{T}_1$ state, which is $28.9 \times 10^3 \text{ cm}^{-1}$ above the ground state for $\text{Cr}(\text{bpy})_3^{3+}$,⁸ should occur at $15.2 \times 10^3 \text{ cm}^{-1}$ (ca. 660 nm) above the ${}^2\text{E}$.

FIGURE 3-6 : Absorption Spectra of the Ground-state $\text{Cr}(\text{NN})_3^{3+}$ Complexes (dashed lines), and of the Primary Transient Species $(^2\text{E})\text{Cr}(\text{NN})_3^{3+}$ (solid lines and points) Obtained by Flash Photolysis Absorption in N_2 -purged 1 M HCl. Spectra measured 40 μsec after the flash, except for the bpy and phen complexes, for which spectra were taken 150 μsec after the flash. Concentration of $\text{Cr}(\text{NN})_3^{3+}$ ca. 10^{-4} - 10^{-6} M.



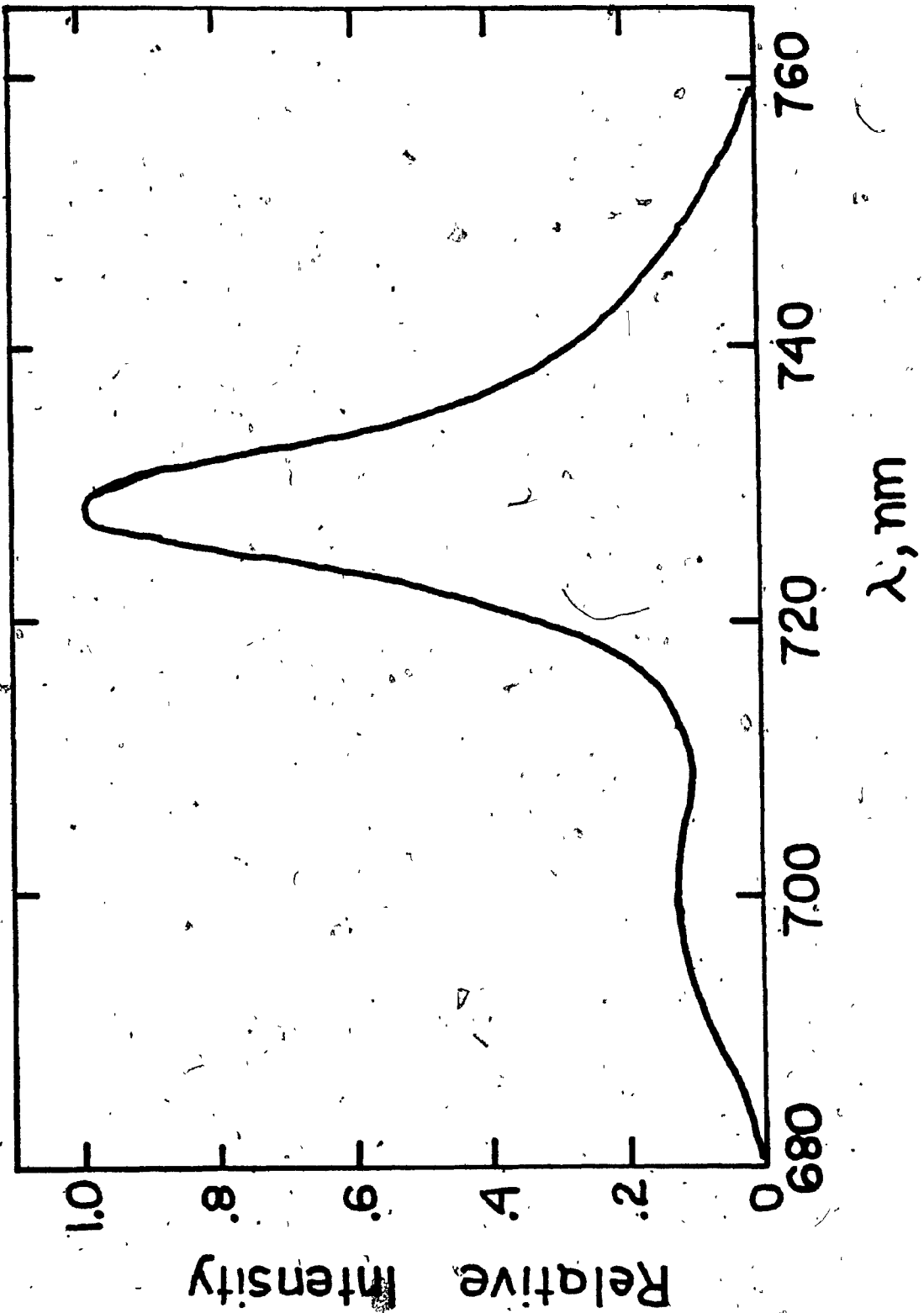
level. A band corresponding to such a transition (${}^2E \rightarrow b{}^2T_1$) is observed at $16.9 \times 10^3 \text{ cm}^{-1}$ (590 nm). The relative insensitivity of this transition to ligand substitution seems to indicate that the doublet manifold ($b{}^2T_1$) is predominantly metal-centered. The remaining two higher-energy bands, red-shifted by the presence of ligand substituents, probably correspond to electronic transitions to doublet states containing some ligand character, and could be described as ${}^2E \rightarrow {}^2$ (LMCT) transitions. Furthermore, analogous to the ground-state absorption spectra, some of the observed features in the 2E excited-state spectra could correspond to vibrational components of the same electronic transition.

The 520-nm band of the $({}^2E)\text{Cr}(\text{phen})_3^{3+}$ absorption spectrum is insensitive to methyl substitution at the 4,7- and 3,4,7,8-positions of the phen ligand framework; however, phenyl groups on the 4,7-positions and the 5-Cl substituent red-shift this band by ca. 20 nm. As for the bpy systems, this band is ascribed to the ${}^2E \rightarrow b{}^2T_1$ transition with the corresponding $a{}^4T_1$ state situated ca. $32 \times 10^3 \text{ cm}^{-1}$ above the ground state. A band at $32.6 \times 10^3 \text{ cm}^{-1}$ (308 nm) is observed in the ground-state spectrum of $\text{Cr}(4,7\text{-Ph}_2\text{phen})_3^{3+}$ which is absent in the free ligand monocation absorption spectrum. The band at $35.2 \times 10^3 \text{ cm}^{-1}$ (283 nm), which is also present in the free ligand monocation spectrum, is attributed to a ligand-centered electronic transition.

3.4.2. Luminescence From $\text{Cr}(\text{NN})_3^{3+}$ Complexes.

The luminescence spectrum of $\text{Cr}(\text{bpy})_3^{3+}$ in aqueous solution at 22°C is shown in Figure 3-7. The two bands at 695 nm and 727 nm (14.4×10^3 and $13.8 \times 10^3 \text{ cm}^{-1}$, respectively) have been previously assigned⁴³ to the 2T_1 and 2E states, respectively. The emission bands represent the O-O transitions ${}^2T_1 \rightarrow {}^4A_2$ and ${}^2E \rightarrow {}^4A_2$ electronic transitions. The

FIGURE 3-7 : Luminescence Spectrum of $\text{Cr}(\text{bpy})_3^{3+}$ in Aqueous Solution
at 22°C.



luminescence spectra of several other $\text{Cr}(\text{NN})_3^{3+}$ complexes in aqueous solution have been recorded and are shown to be very similar to that of $\text{Cr}(\text{bpy})_3^{3+}$; the phosphorescence maxima are noted in Table 3-3. The data reveal that the emission bands are only slightly sensitive to the nature of the ligand substituents, such that the energy of the low-energy transition (${}^2\text{E} \rightarrow {}^4\text{A}_2$) varies in the order $\text{bpy} > 4,4'\text{-Me}_2\text{bpy} > 4,4'\text{-Ph}_2\text{bpy}$ for the bipyridyl complexes. For the phenanthroline complexes, the energy of the ${}^2\text{E}$ state decreases in the order $\text{phen} \approx 5\text{-Clphen} \geq 5\text{-Brphen} \geq 5\text{-Mephen} \geq 5\text{-Phphen} \geq 5,6\text{-Me}_2\text{phen} \geq 4,7\text{-Me}_2\text{phen} > 3,4,7,8\text{-Me}_4\text{phen} > 4,7\text{-Ph}_2\text{phen}$. Phenyl substitution on either the bpy or phen framework red-shifts the ${}^2\text{E}$ maxima by ca. 14 nm. Inasmuch as the lifetimes of the ${}^2\text{T}_1$ and ${}^2\text{E}$ excited states are identical, they are considered to be in thermal equilibrium, and may thus be denoted as (${}^2\text{T}_1/{}^2\text{E}$) in the absence of environmental effects. Moreover, Maestri and coworkers³⁸ have found that the relative yield of ${}^2\text{E}$ phosphorescence at 727 nm from $\text{Cr}(\text{bpy})_3^{3+}$ is the same for both ligand-centered (312 nm) and metal-centered (450 nm) excitation; this indicates that relaxation to the ${}^4\text{A}_2$ ground state occurs with unitary efficiency. The results presented later in this thesis confirm this assertion, as the ${}^2\text{E}$ luminescence intensity remains constant over the excitation wavelengths 313 - 480 nm.

A comparison of the emission spectra of $\text{Ru}(\text{NN})_3^{2+}$ and $\text{Cr}(\text{NN})_3^{3+}$ complexes reveals that the energies of the emission bands from the $\text{Ru}(\text{II})$ complexes in fluid media (formally ${}^3\text{CT}$) are not markedly dependent on the nature of the ligand substituent;⁴⁴ however, methyl and phenyl substitution at the 4,7-positions of the phen ligand of $\text{Ru}(\text{II})$ complexes do red-shift the emission maximum.

TABLE 3-3: Luminescence Spectra for Several $\text{Cr}(\text{NN})_3^{3+}$ Complexes in Aqueous Solution at Room-temperature.

(NN)	$^2T_1, \times 10^{-3} \text{ cm}^{-1} (\text{nm})$	$^2E, \times 10^{-3} \text{ cm}^{-1} (\text{nm})$
bpy	14.4 (695)	13.7 ⁴ (727)
4,4'-Me ₂ bpy	14.3 (700)	13.6 ⁸ (731)
4,4'-Ph ₂ npy	14.0 (714)	13.4 ⁷ (742)
phen	14.3 (700)	13.7 ⁴ (727)
5-Clphen	14.3 (700)	13.7 ⁴ (728)
5-Brphen	14.3 (700)	13.7 (730)
5-Mephen	14.3 (700)	13.7 (730)
5,6-Me ₂ phen	14.3 (700)	13.6 ⁶ (732)
4,7-Me ₂ phen	14.2 (704)	13.6 ² (734)
3,4,7,8-Me ₄ phen	14.1 (709)	13.5 ⁷ (737)
5-Phphen	14.3 (700)	13.7 (730)
4,7-Ph ₂ phen	14.0 (714)	13.4 ⁶ (743)

3.5. EXCITED-STATE LIFETIMES OF $Cr(NN)_3^{3+}$ COMPLEXES.

For any excited state "i" which decays chemically or physically via "n" first-order (or pseudo-first-order) processes, the actual lifetime τ_i of that excited state is given by

$$\tau_i = \frac{1}{\sum_n k_{i,n}} \quad (3-5)$$

where $k_{i,n}$ represents the sum of all the rate constants corresponding to the decay processes. The actual lifetime represents the time it takes to reduce the number of molecules in that excited state to 1/e of its initial value. The inherent lifetime, on the other hand, represents the lifetime of an excited state where that excited state decays via only one deactivation pathway "a" (e.g., radiative decay), as defined in (3-6).

$$\tau_{i,a} = 1 / k_{i,a} \quad (3-6)$$

The actual and inherent lifetimes of excited states are related by equation (3-7), which reduces to (3-8) when $\prod_j k_j \tau_j$ equals unity. A unitary

$$\tau_i = \frac{\phi_a \tau_{i,a}}{\prod_j k_j \tau_j} \quad (3-7)$$

$$\tau_i = \phi_a \tau_{i,a} \quad (3-8)$$

value of the denominator in (3-7) is attained when the excited state "i" is the only one directly reached by absorption, or when the conversion of that state directly reached by absorption to the excited state "i" occurs with unitary efficiency. In equations (3-7) and (3-8), ϕ_a represents the quantum yield of luminescence for the particular deactivation process "a".

Figure 3-8 gives a schematic representation of the chemical and physical processes which are of interest in the photochemistry of Cr(III) complexes, including non-radiative (nr), radiative (rad), reactive (rx), intersystem (isc) and back-intersystem (bisc) crossing processes.

3.5.0. Quartet State Lifetimes.

The actual lifetime of the lowest quartet excited state, 4T_2 , of $\text{Cr}(\text{NN})_3^{3+}$ complex ions is defined by

$${}^4\tau = \frac{1}{{}^4k_{\text{rad}} + {}^4k_{\text{nr}} + {}^4k_{\text{isc}} + {}^4k_{\text{rx}}} \quad (3-9)$$

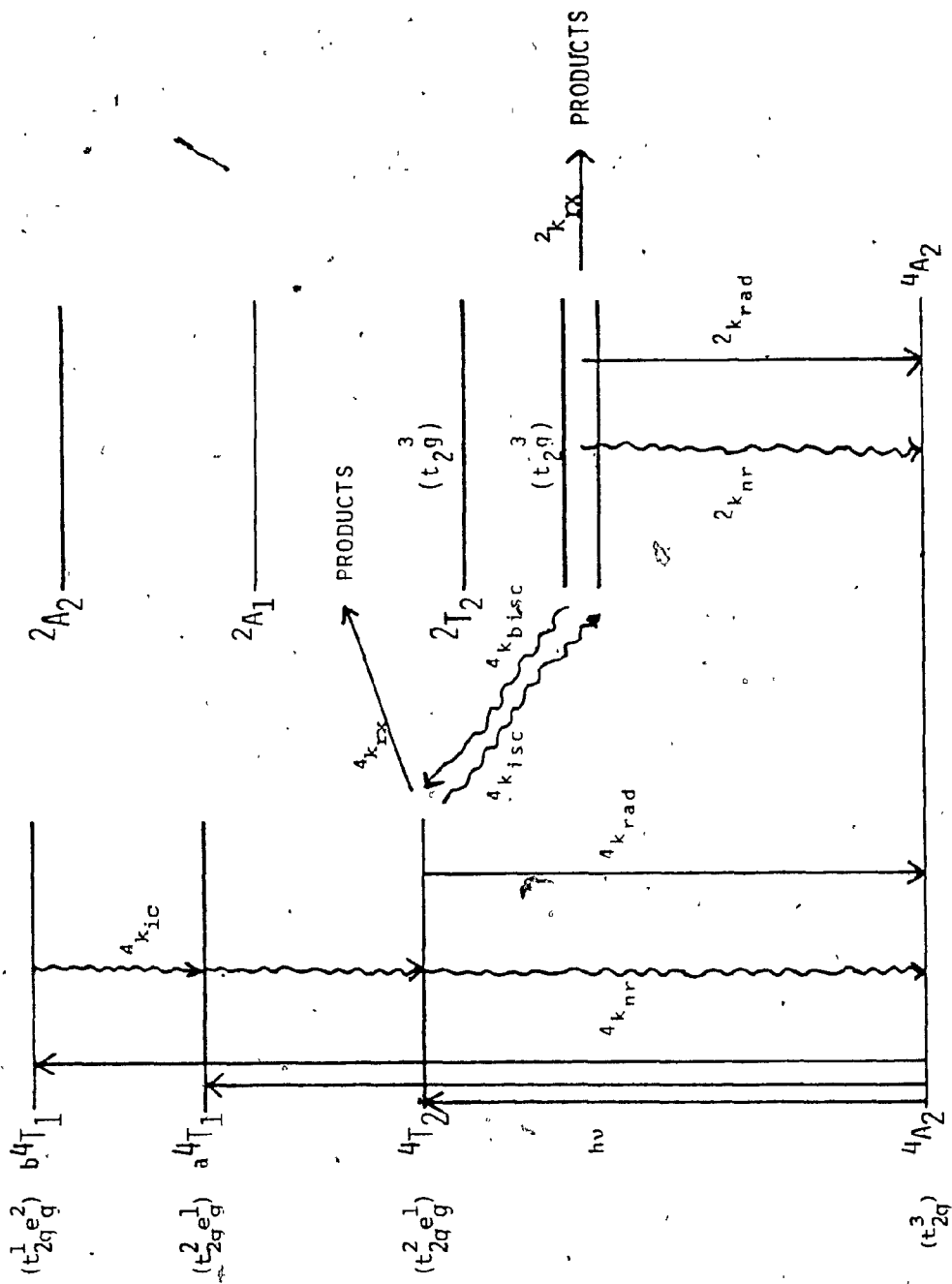
Presently, direct measurement of ${}^4\tau$ for $\text{Cr}(\text{NN})_3^{3+}$ complexes has not been obtained directly, although fluorescence from some Cr(III) species in rigid and room-temperature media has been observed. Recent investigations^{45,46} have assigned a 10 psec lifetime to the $({}^4T_2)\text{Cr}(\text{bpy})_3^{3+}$ species, estimated by populating the 4T_2 state with a 3.2 nsec pulsed tunable laser Raman spectrometer, and subsequently analysing the Raman shifts assigned to the 4A_2 , 2E and 4T_2 states.

3.5.1. Doublet State Lifetimes and Substituent Effects.

The actual (or observed) lifetime of the 2E excited state, ${}^2\tau_{\text{obs}}$, of the $\text{Cr}(\text{NN})_3^{3+}$ complex ion in the absence of quenching is the reciprocal of the sum of all the rate constants k_i which depopulate the

FIGURE 3-8 : Schematic Energy-level Diagram of Chemical and Physical Processes Important to Chromium(III) Complexes.





2E state (from equation 3-5), as given by equation (3-10), (cf. Figure 3-8).

$${}^2\tau_{\text{obs}} = \frac{1}{{}^2k_{\text{nr}} + {}^2k_{\text{rx}} + {}^2k_{\text{rad}} + {}^2k_{\text{bisc}}} \quad (3-10)$$

The 2E excited-state lifetimes, extrapolated to infinite substrate dilution, have been determined for $\text{Cr}(\text{NN})_3^{3+}$ species in oxygen-free 1M HCl at 22°C and are summarized in Table 3-4. The lifetimes reported were obtained by excited-state emission and absorption decay techniques. Also included in Table 3-4 are the 3CT excited-state lifetimes of some analogous $\text{Ru}(\text{NN})_3^{2+}$ complexes in oxygen-free water at 25°C, as determined by Lin et al.⁴⁴ - The $(^2E)\text{Cr}(\text{NN})_3^{3+}$ species are strikingly long-lived in fluid media at room temperature when compared to the analogous $\text{Ru}(\text{II})$ complexes. For both $\text{Ru}(\text{II})$ and $\text{Cr}(\text{III})$ complexes, emission lifetimes are longer for the phen systems than for the bpy systems; furthermore, methyl and phenyl substitution on the phen rings causes an increase in the emission lifetime for both $\text{Cr}(\text{III})$ and $\text{Ru}(\text{II})$ complexes. On the other hand, whereas methyl substitution on the bpy ligand in $\text{Ru}(\text{II})$ complexes decreases the τ_0 value, an increase in τ_0 is observed for the corresponding $\text{Cr}(\text{III})$ complex. A significant decrease in τ_0 for the $\text{Cr}(\text{III})$ complexes occurs for halo-substitution on the phen framework, while τ_0 remains essentially constant for the $\text{Ru}(\text{II})$ analogues when compared to the unsubstituted $\text{M}(\text{phen})_3^{n+}$ complex.

The variation of τ_0 for the $\text{Cr}(\text{NN})_3^{3+}$ complexes can be rationalized in terms of the ligand acting as both an oscillating perturbation dipole

TABLE 3-4: Lifetimes of $(^2E)Cr(NN)_3^{3+}$ and $(^3CT)Ru(NN)_3^{2+}$.

NN	$2 \tau_{O^+}$, msec ^a	$2 \tau_{O^+}$, msec ^b	$3 \tau_{O^+}$, μ sec ^c
	Cr(III)	Cr(III)	Ru(II)
bpy	0.073	0.063	0.060
4,4'-Me ₂ bpy	0.20 ^d	0.23	0.33
4,4'-Ph ₂ bpy	0.17	0.14	0.67
5-Clphen	0.18	0.13	0.94
5-Brphen	0.18	—	1.04
phen	0.33	0.27	0.92
5-Mephen	0.42	—	1.33
5,6-Me ₂ phen	0.42 ^d	—	1.81
4,7-Me ₂ phen	0.57 ^d	0.34	1.74
3,4,7,8-Me ₄ phen	0.64 ^d	0.47	1.39
5-Phphen	0.22 ^d	—	1.29
4,7-Ph ₂ phen	0.57 ^d	0.37	4.68

^a Extrapolated values to infinite substrate dilution in deaerated 1 M HCl at 22°C; from emission lifetime experiments. ^b In deaerated solutions, 23-24°C, 1 M HCl; from absorption decay of transient from flash photolysis. ^c In deaerated H₂O at 25°C, from reference 44. ^d Solution also contains 4% v/v CH₃CN.

and an energy acceptor. The more vibrationally-rigid phen complexes would be expected to show a decrease in non-radiative decay ($^2k_{nr}$) in comparison with analogous bpy complexes, with a consequential increase in the 2E lifetimes. Indeed, this is observed (see Table 3-4), except in the cases where NN = 5-Clphen, 5-Brphen and 5-Phphen where the τ_0 value decreases with respect to NN = phen. The halo substituents provide an increased dipole perturbation which would increase $^2k_{nr}$ and necessarily decrease the 2E lifetime. Phenyl and methyl substitution on the polypyridyl ligand decrease the perturbation dipole, probably through their effect on the critical ligand vibrational modes. The 2E lifetime of the 5-Phphen is expected to be greater than that of the phen complex.

At first glance, the variance in behavior between the lifetimes of the $(^2E)Cr(NN)_3^{3+}$ and $(^3CT)Ru(NN)_3^{2+}$ complexes might be attributed to the different orbital parentages of the respective excited states; that is, MLCT for Ru(II) and MC for the Cr(III) complexes. However, it would be premature to attribute the differences solely to this feature. In addition to the comparison of the Ru(II) and Cr(III) polypyridyl complexes, the phosphorescence lifetimes of $Cr(NN)_3^{3+}$ are significantly longer than those of other chromium(III) complexes; some illustrative examples are given in Table 3-5. The shorter 2E lifetimes of Cr(III) complexes containing ligands such as NH_3 or (en) may be attributed to their capability of forming hydrogen bonds in aqueous solution, thereby enhancing vibrational coupling between the complex and bulk solvent. Such is not the case for Cr(III) polypyridyl complexes, for which the ligands provide a pseudo-hydrophobic environment. The lack of an isotope effect on the lifetimes of $Cr(bpy)_3^{3+}$ and $Cr(phen)_3^{3+}$ ⁴⁷ indicate the absence of direct

TABLE 3-5 : Phosphorescence Lifetimes of Some Chromium(III) Complexes in Fluid Media.^a

COMPLEX	LIFETIME, (μ sec)
$\text{Cr}(\text{bpy})_3^{3+}$	73
$\text{Cr}(\text{phen})_3^{3+}$	330
$\text{Cr}(\text{NH}_3)_6^{3+}$	2.2
$\text{Cr}(\text{en})_3^{3+}$	1.85
$\text{Cr}(\text{CN})_6^{3-}$	0.14
$\text{Cr}(\text{NCS})_6^{3-}$	0.01

^a from Table I in reference 48.

vibrational coupling between the complex and bulk solvent. Also, the dipole perturbation present in complexes containing the (CN) and (SCN) ligands would certainly predict short lifetimes.

The 2E state reacts, in aqueous solution, with water (${}^2k_{rx}$) in competition with radiative (${}^2k_{rad}$) and non-radiative (${}^2k_{nr}$) decay back to the 4A_2 ground-state species. Depopulation via back-intersystem crossing to the 4T_2 state appears to us to be unimportant inasmuch as the energy gap between the 2E and 4T_2 states (ca. 22 kcal, $7.7 \times 10^3 \text{ cm}^{-1}$)³⁸ is large. Additionally, the luminescence quantum yield, ${}^2\phi_{rad}$, has been determined^{38,48} to be less than 10^{-3} for $\text{Cr}(\text{bpy})_3^{3+}$, so that ${}^2k_{rad}$ is insignificant when compared to the non-radiative and reactive decay modes. ${}^2\phi_{rad}$ is given by equation (3-11); for small values of ${}^2\phi_{rad}$, ${}^2k_{rad}$

$${}^2\phi_{rad} = {}^4\eta_{isc} \frac{{}^2k_{rad}}{{}^2k_o} \quad (3-11)$$

will also be small if ${}^4\eta_{isc} = 1$ and ${}^2k_o = {}^2k_{nr} + {}^2k_{rx}$. Therefore, since ${}^2k_{disc}$ and ${}^2k_{rad} \ll ({}^2k_{nr} + {}^2k_{rx})$, the 2E lifetime can more aptly be defined by equation (3-12) in the absence of quenching species.

$${}^2\tau_o = \frac{1}{{}^2k_{nr} + {}^2k_{rx}} \quad (3-12)$$

Inasmuch as the efficiency of the reactive mode, ${}^2\phi_{rx}$, is ca. 0.13 (see Section 3.8.) and the efficiency of the non-radiative pathway (${}^2\eta_{nr} = 1 - {}^2\eta_{rx}$) is ca. 0.87, then ${}^2k_{nr} > ({}^2k_{rad} + {}^2k_{disc} + {}^2k_{rx})$. Thus, the non-radiative deactivation pathway (${}^2k_{nr}$) from the 2E state is the

predominant factor responsible for the lifetime of that state in the absence of environmental effects.

3.5.2. Pressure Effects on Doublet-state Lifetimes of $\text{Cr}(\text{bpy})_3^{3+}$.

Kirk and Porter⁶² have recently investigated the effect of pressure on the luminescence lifetimes of $\text{Cr}(\text{bpy})_3^{3+}$. Their results indicate that ${}^2\tau_{\text{obs}}$ decreases slightly from $71 \pm 2 \mu\text{sec}$ at 1.013×10^{-3} kbar (= 1 atm) to $64 \pm 2 \mu\text{sec}$ at 2.3 kbar (= 2270 atm) in aqueous solution at 16 - 18°C.⁶² Employing equation (3-13), where τ_0^{P} and τ^{P} are the ${}^2\text{E}$ lifetimes at atmospheric pressure and applied pressure (p), respectively, gives

$$\Delta V^\ddagger = \frac{RT}{P-1} \ln \frac{\tau_0^{\text{P}}}{\tau^{\text{P}}} \quad (3-13)$$

the apparent activation volume of -0.9 ± 0.2 ml/mole for degassed solutions at 16 - 18°C.⁶² This value, being negative is diagnostic of an associative mechanism of a water nucleophile with a cationic complex.⁶³

Although these results support an associative mechanism for the photoaquation of $\text{Cr}(\text{bpy})_3^{3+}$, the sensitivity of this technique as a test of mechanism may be questioned. First of all, one might question the variation in ${}^2\tau_{\text{obs}}$ (71 vs 64 sec) determined at pressures of 1 and 2270 atm., respectively, as to whether this constitutes a significant decrease with such a large increase in pressure. Also, the authors⁶² do not report whether or not the compressibility coefficient of activation, $\Delta\beta^\ddagger$, is taken into account in using equation (3-13). The magnitude of $\Delta\beta^\ddagger$ for the $\text{Cr}(\text{bpy})_3^{3+}$ ion could be substantial, and the use of equation (3-14)^{63,64} is therefore required. Lastly, it was not determined⁶² whether ΔV^\ddagger itself

is pressure-dependent.

$$-RT \ln \frac{\tau_p}{\tau_o} = \Delta V^\ddagger P + \Delta \beta^\ddagger P^2/2 \quad (3-14)$$

3.6. SOLUTION MEDIUM EFFECTS ON DOUBLET-STATE LIFETIMES OF $\text{Cr}(\text{NN})_3^{3+}$.

As the investigation into the nature of the $(^2\text{E})\text{Cr}(\text{NN})_3^{3+}$ species progressed, it was discovered that the ^2E lifetimes are significantly affected by the surrounding medium. The results indicate that the ^2E lifetime is found to be sensitive to the nature of the solvent, the pH, the substrate concentration, and the presence of added anions:

3.6.0. Solvent Effects.

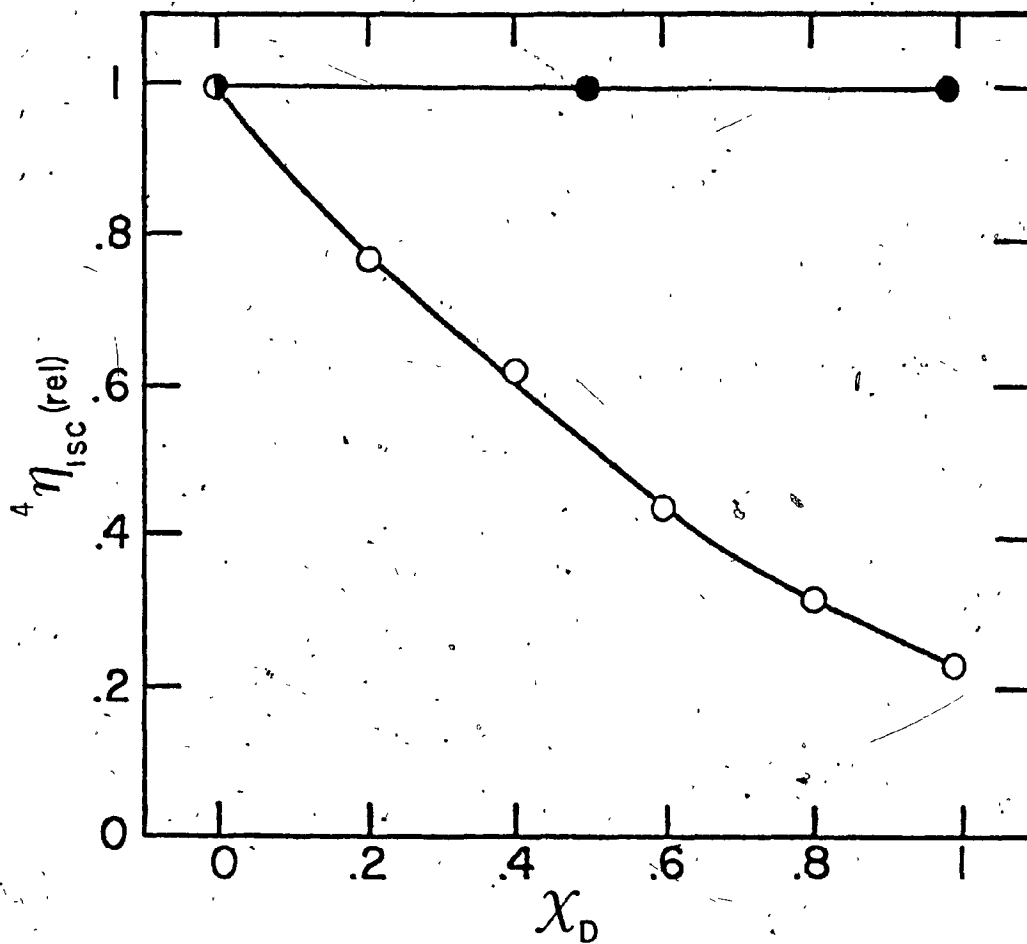
Earlier studies⁴⁹ on the lifetimes of $(^2\text{E})\text{Cr}(\text{bpy})_3^{3+}$ and $(^2\text{E})\text{Cr}(\text{phen})_3^{3+}$ in various neat solvents reported the insensitivity of $^2\tau_{\text{obs}}$ to changes in solvent. More recent investigations in this laboratory have shown that this is not the case. Henry⁵⁰ reported that there was no alteration of the $(^2\text{E})\text{Cr}(\text{bpy})_3^{3+}$ lifetime upon changes in solvent polarity. That the lifetime remained constant in water, acetonitrile, methanol, dimethylformamide and ethylene glycol would indicate that changes in solvent polarity do not effect sufficient perturbation to alter the rate of non-radiative decay, within experimental error. However, Van Houten and Porter⁵¹ noted the $(^2\text{E})\text{Cr}(\text{bpy})_3^{3+}$ lifetime in neat, oxygen-free dimethylformamide to be $3 \pm 1 \mu\text{sec}$ (vs $63 \mu\text{sec}$ in H_2O). Our results show that the $(^2\text{E})\text{Cr}(\text{bpy})_3^{3+}$ lifetime is $17 \mu\text{sec}$ in neat air-equilibrated acetonitrile, as compared with ca. $55 \mu\text{sec}$ in air-equilibrated water. The effect of changing solvent (H_2O vs D_2O) on phosphorescence intensity and lifetime of $(^2\text{E})\text{Cr}(\text{NN})_3^{3+}$ has been investigated by Sriram et al.⁴⁷

A diminution in the luminescence I from $({}^2E)Cr(bpy)_3^{3+}$ was observed upon altering the solvent from H_2O to D_2O , while the 2E emission-lifetime remained unchanged. In contrast, both the luminescence intensity and lifetime of $({}^2E)Cr(phen)_3^{3+}$ remain constant in D_2O and H_2O . These observations led to the study of $Cr(bpy)_3^{3+}$ and $Cr(phen)_3^{3+}$ in several H_2O/D_2O mixtures.

The luminescence intensity I reflects the population of the $({}^2E/{}^2T_1)$ manifold, and is proportional to the quantum yield of luminescence from that manifold, ${}^2\phi_{rad}$. The lifetime of $({}^2E)Cr(NN)_3^{3+}$ reflects the competing modes of deactivation of the 2E state, as in equation (3-10). The constancy of ${}^2\tau_{obs}$ for both complexes was attributed⁴⁷ to the independency of the non-radiative deactivation pathway with changes in solvent isotopic composition. The observed diminution in I , and thus in ${}^2\phi_{rad}$ for the bpy complex as the mole fraction D_2O (χ_D) increased suggested that the 4T_2 state (the precursor of 2E) may be sensitive to the isotopic nature of the solvent. The observed decrease in the quantum yield of luminescence was attributed⁴⁷ to a decrease in ${}^4\eta_{isc}$ with increasing χ_D for the bpy complex, with ${}^4\eta_{isc}$ remaining constant with changing χ_D for the phen complex, as revealed in Figure 3-9. If ${}^2k_{rad}$ were responsible for the change in ${}^2\phi_{rad}$, one expects a dependence of ${}^2k_{rad}$ on the refractive index of the medium; since n_D^{20} for H_2O and D_2O are virtually the same, ${}^2k_{rad}$ was believed⁴⁷ to have negligible effect on ${}^2\phi_{rad}$. Thus, the relative values of ${}^4\eta_{isc}$ will be equal to ${}^2\phi_{rad}(rel)$, inasmuch as ${}^4\eta_{isc} = 1$ for $Cr(bpy)_3^{3+}$ in H_2O .⁵²

The ${}^4T_2 \rightarrow {}^2E$ intersystem crossing efficiency, ${}^4\eta_{isc}$, is given in equation (3-83); in H_2O , ${}^4k_{isc} > {}^4k_{nr}$, but in D_2O ${}^4k_{isc} < {}^4k_{nr}$. Thus, the relative values of ${}^4k_{isc}$ and ${}^4k_{nr}$ are altered as χ_D is increased.

FIGURE 3-9 : Values of ${}^4\eta_{isc}$ (relative to $\chi_D = 0.0$) vs χ_D
for $\text{Cr}(\text{bpy})_3^{3+}$ (○) and $\text{Cr}(\text{phen})_3^{3+}$ (●) at 22°C.^a



^a Reproduced from reference 47.

Analysis of the data gave $^4k_{nr}/^4k_{isc} \approx 4$ in pure D_2O , and $^4k_{nr}/^4k_{isc} \leq 0.1$ in pure H_2O ; furthermore, the ratio of $^4k_{nr}(D_2O)/^4k_{nr}(H_2O)$ ranges from ca. 10 to 100. Thus, the effect is deuterium-favored and affects the non-radiative deactivation pathway from the 4T_2 state, $^4k_{nr}$. This was rationalized⁴⁷ in terms of D_2O being more structured than H_2O , the 4T_2 state being highly distorted and thereby able to accommodate solvent molecules in the interligand pockets with the result that non-radiative deactivation of 4T_2 is entropically more favored in D_2O than in H_2O . The invariance in I , $^2\phi_{rad}$ and $^4\eta_{isc}$ with changing χ_D for the $Cr(phen)_3^{3+}$ complex ion suggests that $^4k_{nr}$ is less sensitive toward solvent isotope composition than in the bpy complex, presumably due to the greater rigidity of the phen ligand framework which would argue for less tightly bound solvent molecules in the interligand pockets and consequential decrease in the entropic effect.

3.6.1. Effect of Added Anions.

Whereas quenching causes the 2E lifetimes of $Cr(NN)_3^{3+}$ to decrease upon addition of increasing amounts of quencher, prolongation of the 2E lifetime can be observed in the presence of high concentrations of added anions. For such studies, the anions do not quench the 2E states, or, if they do, any quenching effect is overwhelmed by the prolongation effect. Early studies on $(^2E)Cr(bpy)_3^{3+}$ revealed⁵⁰ that high concentrations ($>1 M$) of ClO_4^- , Cl^- , HSO_4^- and NO_3^- caused a significant increase in the 2E lifetime, while the emission band maxima and intensity remain unchanged. Furthermore, added ClO_4^- was found⁵⁰ to decrease the quantum yield of photoaquation of $Cr(bpy)_3^{3+}$, $^4+2\phi_{rx}$. The effect on $^2\tau_{obs}$ in the presence of added ClO_4^- was rationalized⁵⁰ in terms of a decrease in both $^2k_{nr}$ and $^2k_{rx}$, with a greater effect on $^2k_{rx}$. The effect on $^2k_{nr}$

would then arise from extensive ion-pairing and placement of ions in the $\text{Cr}(\text{bpy})_3^{3+}$ interligand pockets, thereby decreasing the vibrational freedom of the ligands and the efficiency of electronic-to-vibrational energy transfer processes. The presence of anions in the interligand pockets as well as in the solvation sphere will ultimately curb access to the chromium(III) core by water molecule(s), resulting in a reduction in the value of $^2k_{rx}$ and $^2k_{nr}$. Additionally, the vibrational freedom is expected to be further reduced on going from the $\text{Cr}(\text{bpy})_3^{3+}$ cation to the more vibrationally-rigid $\text{Cr}(\text{phen})_3^{3+}$ cation, an expectation borne out by Henry⁵⁰ and in this work.

3.6.2. Anion-induced Ground-state Quenching.

It has become critically important to investigate solution medium effects on excited-state lifetimes. Prolongation of the 2E lifetimes of $\text{Cr}(\text{NN})_3^{3+}$ complexes is an interesting phenomenon inasmuch as it enhances the potential reactivity of these excited states.

One of the earlier observations made during the course of this investigation was that the 2E lifetimes of $\text{Cr}(\text{NN})_3^{3+}$ is dependent on substrate concentration in the presence of 1 M hydrochloric acid and 1 M sodium chloride. In fact, the data in Table 3-6 reveal that $^2\tau_{\text{obs}}$ decreases by an order of magnitude as $[\text{Cr}(\text{phen})_3^{3+}]$ is increased from 1×10^{-5} M to 1×10^{-2} M; the data are plotted in Figure 3-10. From equation (3-15) and the data in Table 3-6, a linear plot of $^2k_{\text{obs}}$ vs $[\text{Cr}(\text{phen})_3^{3+}]$

$$^2k_{\text{obs}} = \frac{1}{2 \tau_{\text{obs}}} \quad (3-15)$$

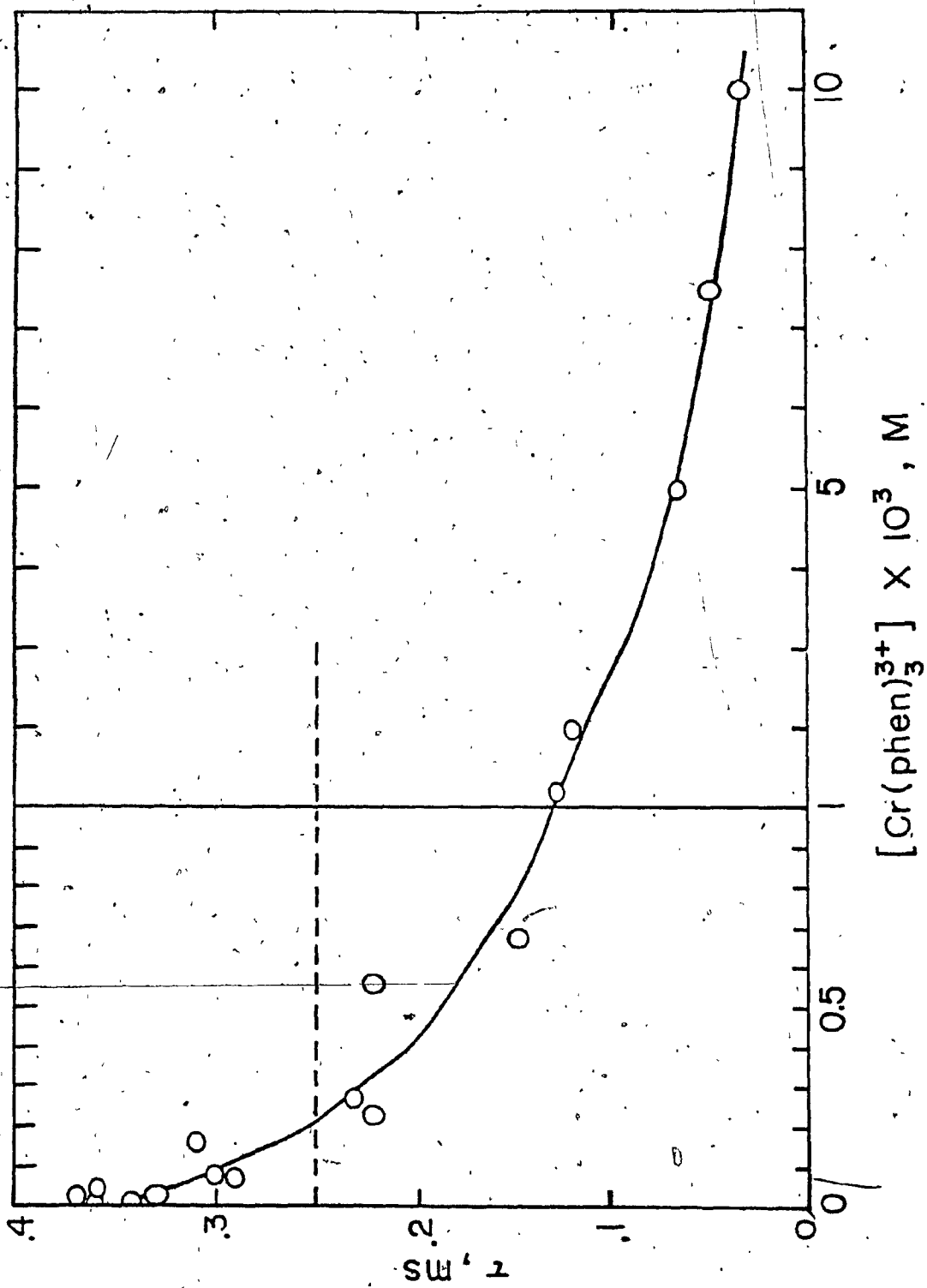
reveals a slope of $2.3 \times 10^6 \text{ M}^{-1} \text{ sec}^{-1}$ and an intercept of $3.0 \times 10^3 \text{ sec}^{-1}$,

TABLE 3-6 : Lifetime of $(^2E)Cr(phen)_3^{3+}$ in Deaerated Aqueous 1 M HCl Solutions at 22° C.

$[Cr(phen)_3^{3+}], M$	$2\tau, msec^a$	$[Cr(phen)_3^{3+}], M$	$2\tau, msec^a$
9.2×10^{-6}	0.36	2.7×10^{-4}	0.23
1.2×10^{-5}	0.34	5.6×10^{-4}	0.22
2.3×10^{-5}	0.37	6.7×10^{-4}	0.15
2.7×10^{-5}	0.33	1.2×10^{-3}	0.13
4.4×10^{-5}	0.36	2.0×10^{-3}	0.12
6.9×10^{-5}	0.29	5.0×10^{-3}	0.067
8.1×10^{-5}	0.30	7.5×10^{-3}	0.050
1.6×10^{-4}	0.31	1.0×10^{-2}	0.037
2.3×10^{-4}	0.22		

^a Each value represents the average of three-ten individual runs.

FIGURE 3-10 : Lifetime of $(^2\text{E})\text{Cr}(\text{phen})_3^{3+}$ as a Function of [Substrate] in Argon-purged Aqueous Solutions at 22°C : — , 1.0 M HCl; each point represents the average of 3-10 individual experiments; - - -, neat H_2O ; the line represents the average of 10 individual experiments performed at different [substrate].



as shown in Figure 3-11. In the absence of HCl, the average value (from ten individual determinations) of ${}^2\tau_{\text{obs}}$ is 0.25 (± 0.03) msec in the range $1.2 \times 10^{-5} \text{ M} \leq [\text{Cr}(\text{phen})_3^{3+}] \leq 1.2 \times 10^{-3} \text{ M}$. It was not possible to determine ${}^2\tau_{\text{obs}}$ for $[\text{Cr}(\text{phen})_3^{3+}] > 1.5 \times 10^{-3} \text{ M}$ in neat H_2O , owing to substrate solubility restrictions. Furthermore, this phenomenon was observed for $\text{Cr}(\text{phen})_3^{3+}$ in both 1 M NaCl and 1 M HCl , and to the same extent in both media. In contrast, ${}^2\tau_{\text{obs}}$ values for the ${}^2\text{E}$ lifetime of $\text{Cr}(\text{bpy})_3^{3+}$ were virtually indistinguishable in 1 M HCl and neat H_2O : ${}^2\tau_{\text{obs}} = 0.073 (\pm 0.008) \text{ msec}$ in 1 M HCl and $0.068 (\pm 0.008) \text{ msec}$ in neat H_2O over the range $1 \times 10^{-5} \text{ M} \leq [\text{Cr}(\text{bpy})_3^{3+}] \leq 2.5 \times 10^{-3} \text{ M}$. However, this quenching phenomenon can be observed for $\text{Cr}(\text{bpy})_3^{3+}$ in a 5 M HCl medium, for which the data in Table 3-7 are obtained, and plotted in Figure 3-12. The linear quenching plot, similar to that in Figure 3-11 for $\text{Cr}(\text{phen})_3^{3+}$ in 1 M HCl , is given in Figure 3-13. The plot yields a slope of $1.3 \times 10^6 \text{ M}^{-1} \text{ sec}^{-1}$ and an intercept of $1.0 \times 10^4 \text{ sec}^{-1}$. To insure that the observed phenomenon was indeed real, and not due to some adventitious impurities, different samples of recrystallized Cr(III) complex ions, analytical reagent grade acid, and purified water were employed; these alterations had no effect on the observed results. Also, the suggestion that excess free ligand present in the $\text{Cr}(\text{NN})_3^{3+}$ samples was responsible for the observed quenching was eliminated in two ways: i) the excellent elemental analyses of the $[\text{Cr}(\text{NN})_3](\text{ClO}_4)_3 \cdot x\text{H}_2\text{O}$ samples (see Section 2.1.4.) do not indicate excess ligand present; ii) the addition of $\sim 1 \times 10^{-3} \text{ M}$ 1,10-phenanthroline to $5 \times 10^{-5} \text{ M}$ $\text{Cr}(\text{phen})_3^{3+}$ in 1 M HCl , and $\sim 5 \times 10^{-3} \text{ M}$ 2,2'-bipyridine to $5 \times 10^{-5} \text{ M}$ $\text{Cr}(\text{bpy})_3^{3+}$ in 5 M HCl , did not quench the ${}^2\text{E}$ luminescence.

The quenching phenomenon depicted in Tables 3-6 and 3-7 and Figures

FIGURE 3-11 : Quenching Plot of the Data for $(^2E)Cr(phen)_3^{3+}$ in Argon-purged 1 M HCl Solutions at 22°C; points at [Substrate] $< 2 \times 10^{-4}$ M cannot be shown owing to scale used. Correlation Coefficient of Least-Squares Plot of all the Points = 0.995.

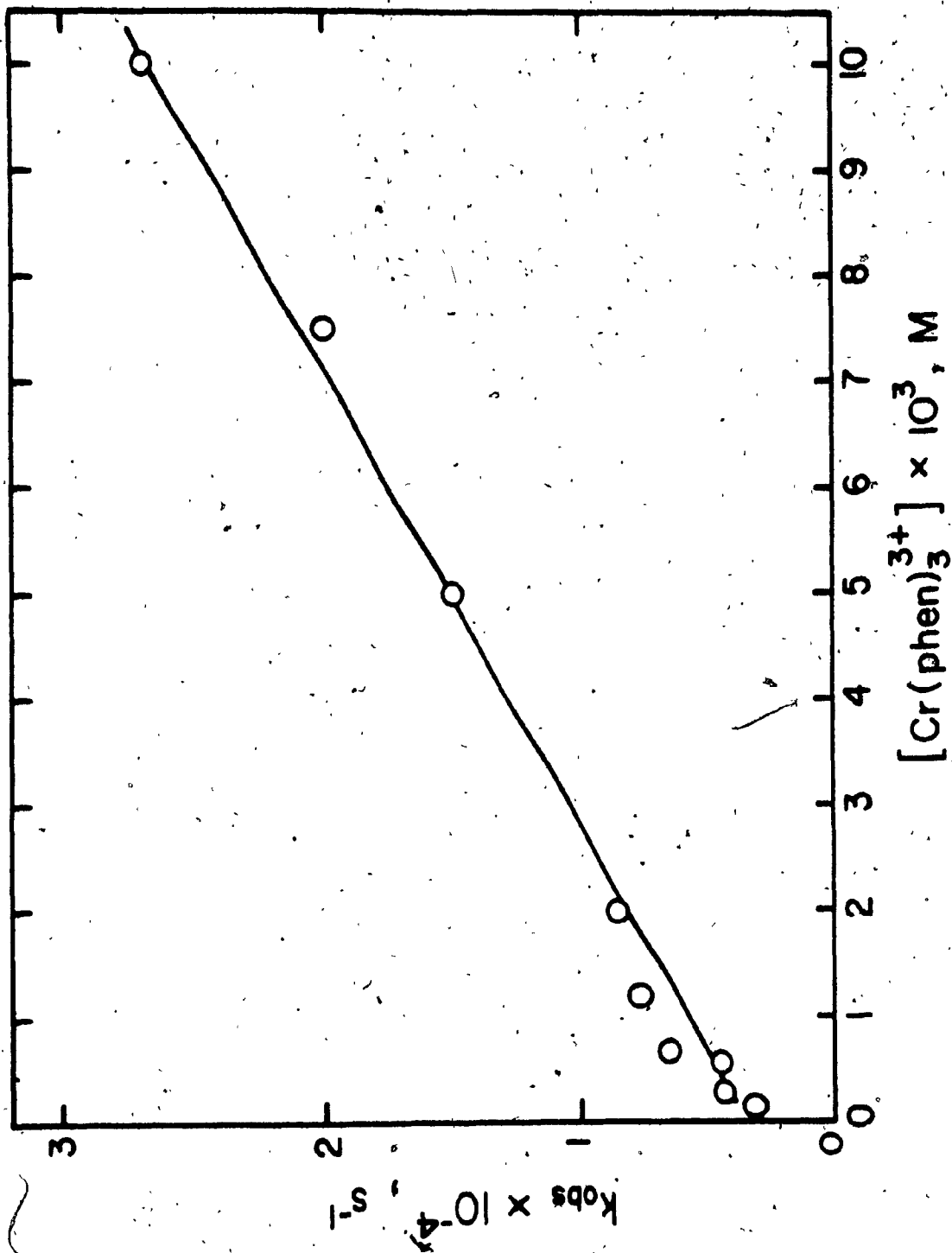


TABLE 3-7 : Lifetime of $(^2E)Cr(bpy)_3^{3+}$ in Deaerated Aqueous 5 M HCl Solutions at 22° C.

$[Cr(bpy)_3^{3+}], M$	$\tau, msec^a$	$[Cr(bpy)_3^{3+}], M$	$\tau, msec^a$
1.2×10^{-5}	0.11	9.4×10^{-4}	0.084
2.8×10^{-5}	0.10	1.0×10^{-3}	0.078
4.6×10^{-5}	0.11	1.2×10^{-3}	0.081
4.7×10^{-5}	0.12	1.5×10^{-3}	0.082
5.7×10^{-5}	0.11	1.8×10^{-3}	0.077
9.4×10^{-5}	0.11	3.6×10^{-3}	0.060
1.0×10^{-4}	0.11	4.8×10^{-3}	0.073
2.0×10^{-4}	0.096	6.0×10^{-3}	0.047
2.8×10^{-4}	0.093	1.0×10^{-2}	0.041
4.7×10^{-4}	0.085	1.1×10^{-2}	0.044
6.0×10^{-4}	0.087	1.2×10^{-2}	0.042
9.0×10^{-4}	0.086		

^a Each value represents the average of three-ten individual runs.

FIGURE 3-12 : Lifetime of $(^2\text{E})\text{Cr}(\text{bpy})_3^{3+}$ as a Function of [Substrate] in Argon-purged Solutions at 22°C : —, 5 M HCl; each point represents the average of 3-10 individual experiments; - - -, neat H_2O ; the line represents the average of 10 individual experiments performed at different [substrate].

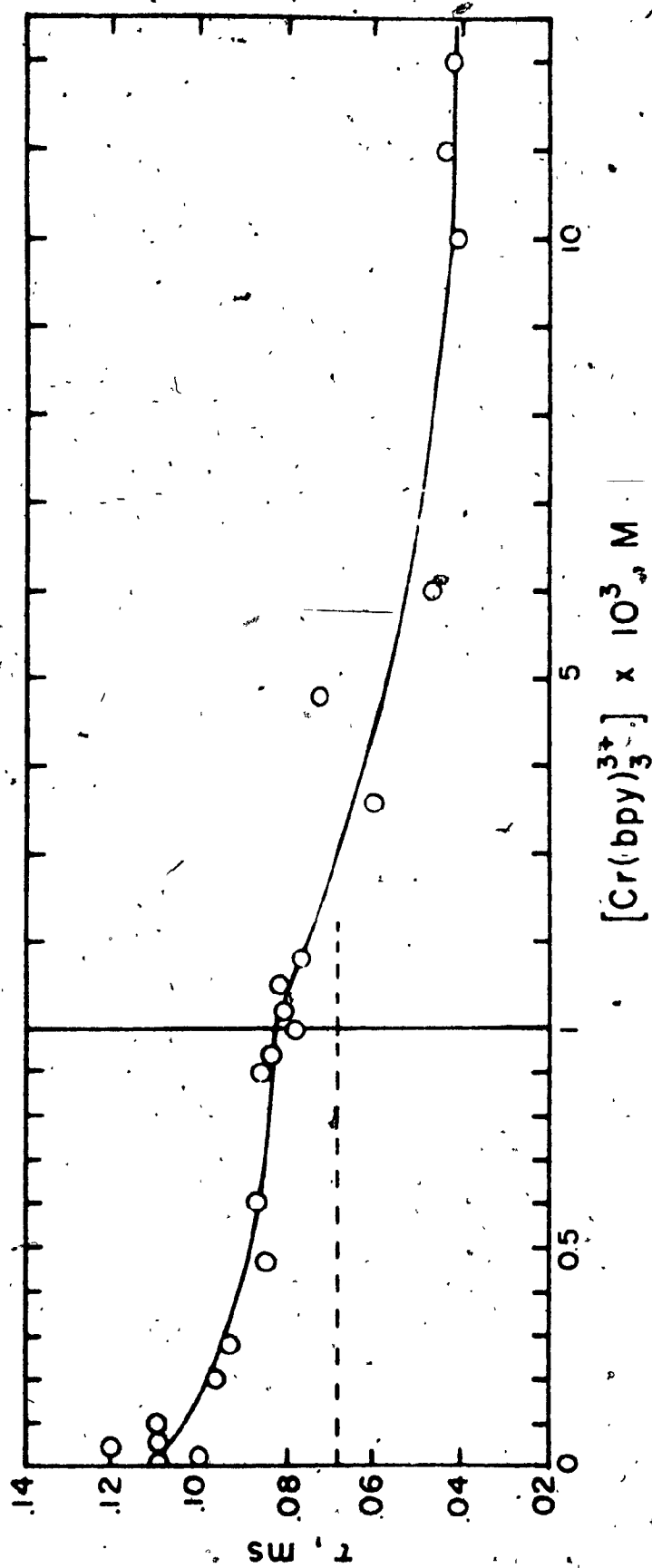
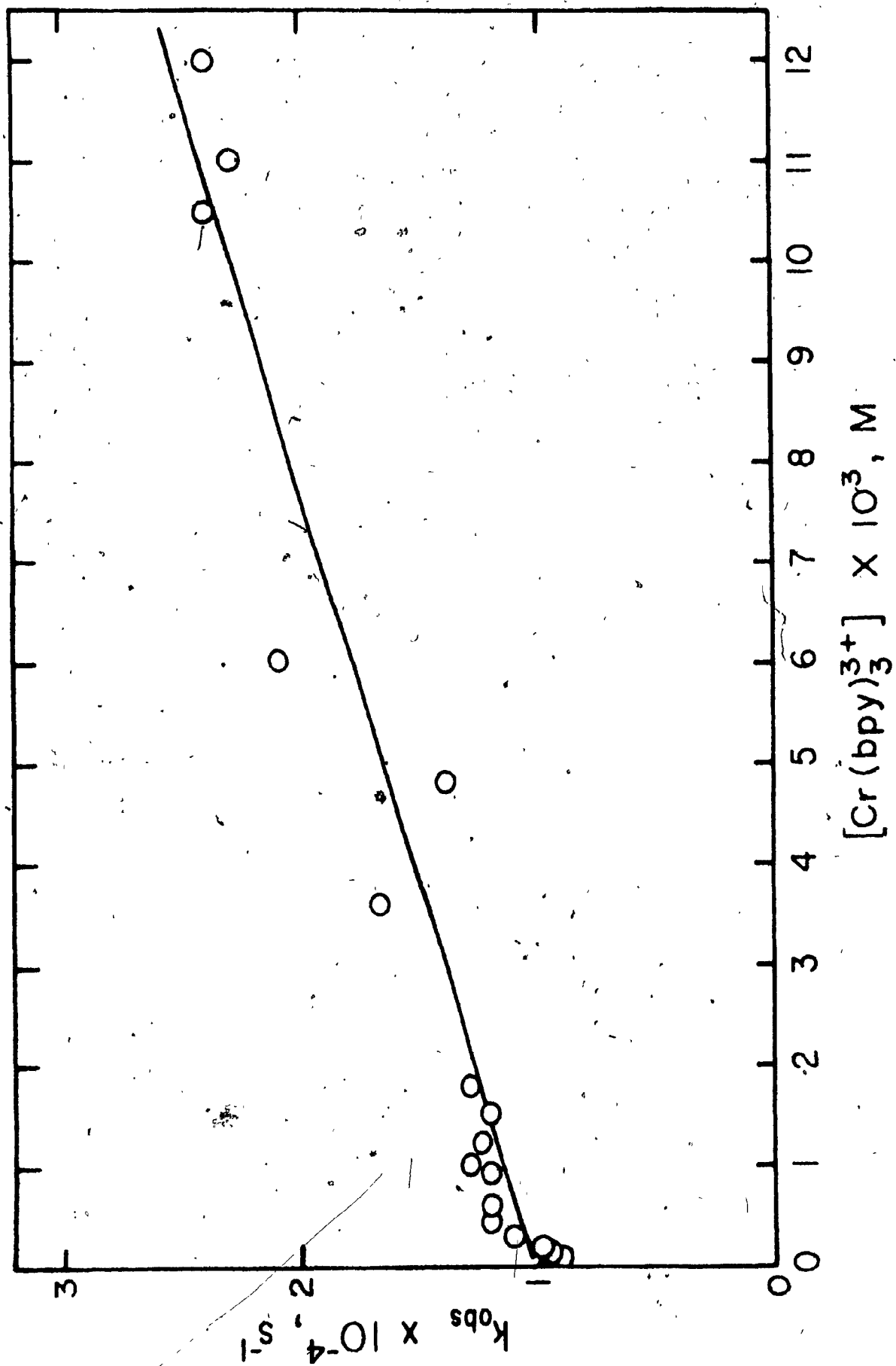


FIGURE 3-13 : Quenching Plot of the Data for $(^2E)Cr(bpy)_3^{3+}$ in Argon-purged 5 M HCl Solutions at 22°C; points at [substrate] $< 2 \times 10^{-4}$ M cannot be shown owing to the scale used. Correlation Coefficient of Least-squares plot of all the points = 0.962.



3-11 and 3-13 may be described by equation (3-16), where 2k_0 is the

$$1/\tau_{\text{obs}} = {}^2k_{\text{obs}} = {}^2k_0 + {}^2k_{\text{gsq}}[\text{Cr}(\text{NN})_3^{3+}] \quad (3-16)$$

first-order rate constant for the decay of the 2E state at infinite $\text{Cr}(\text{NN})_3^{3+}$ dilution, and ${}^2k_{\text{gsq}}$ is the second-order rate constant for the quenching of the 2E state by the ground-state $\text{Cr}(\text{NN})_3^{3+}$ species. Thus, the plots of ${}^2k_{\text{obs}}$ vs $[\text{Cr}(\text{NN})_3^{3+}]$ (Figures 3-10 and 3-12) yield a slope = ${}^2k_{\text{gsq}}$ and an intercept = 2k_0 . Since this concentration quenching phenomenon was not observed in the absence of Cl^- , it becomes clear that this phenomenon is mediated by the Cl^- anion. However, it is noteworthy that the presence of this anion changed neither the absorption spectra of $({}^4A_2)\text{Cr}(\text{NN})_3^{3+}$ nor the wavelength profiles of the $({}^2E)\text{Cr}(\text{NN})_3^{3+}$ emission spectra. At constant $[\text{Cr}(\text{NN})_3^{3+}]$, the presence of Cl^- did cause a change in 2E emission intensity commensurate with the change in τ_{obs} .

It has been established⁵³ that ion-pairing between $\text{Fe}(\text{bpy})_3^{2+}$ or $\text{Fe}(\text{phen})_3^{2+}$ and Cl^- is quite extensive. It would be expected that ion-pairing between $({}^4A_2)\text{Cr}(\text{NN})_3^{3+}$ or $({}^2E)\text{Cr}(\text{NN})_3^{3+}$ and Cl^- would be even more extensive owing to the higher charge on the chromium(III) center, though it is not a necessary condition that the presence of ion-pairing cause a shift in absorption or emission spectrum. In fact it has previously been shown by us and others⁵⁰ that ion-pairing results in $({}^2E)\text{Cr}(\text{NN})_3^{3+}$ lifetime prolongation. If one compares the τ_{obs} values in the limit of infinite $[\text{Cr}(\text{NN})_3^{3+}]$ dilution (i.e., $\tau_0 = 1/{}^2k_0$), in the presence and absence of Cl^- , this lifetime prolongation phenomenon is clearly evident. Table 3-8 gives the rate constants 2k_0 and ${}^2k_{\text{gsq}}$, and τ_0 for the ground-state quenching phenomenon observed for $\text{Cr}(\text{bpy})_3^{3+}$ in 5 M HCl and

TABLE 3-8 : Rate Constants in the Ground-state Quenching of $(^2T_1/{}^2E)Cr(NN)_3^{3+}$ a

	* Cr(III)	* Cr(III) ··· Cl ⁻	$2k_0, \text{sec}^{-1} ({}^2\tau_0, \text{msec})$	$2k_0, \text{sec}^{-1} ({}^2\tau_0, \text{msec})$	$2k_{\text{gsq}}, \text{M}^{-1}\text{sec}^{-1}$
Cr(bpy) ₃ ³⁺	$1.4 \times 10^4 (0.068)$			$1.0 \times 10^4 (0.10)$	1.3×10^6 b
Cr(phen) ₃ ³⁺	$4.0 \times 10^3 (0.25)$			$3.0 \times 10^3 (0.33)$	2.3×10^6 c

a $22 \pm 1^\circ\text{C}$, deaerated aqueous solutions.

b 5 M HCl.

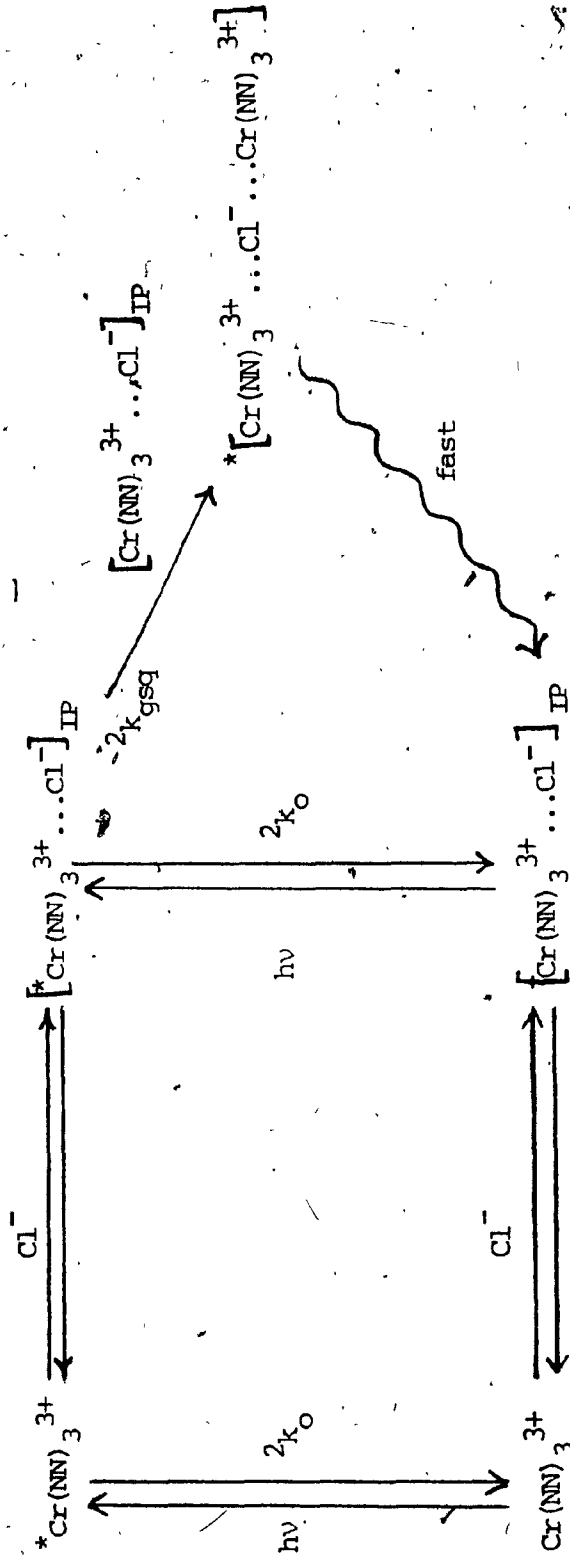
c 1 M HCl.

$\text{Cr}(\text{phen})_3^{3+}$ in 1 M HCl. The fact that this phenomenon was not observed for $\text{Cr}(\text{bpy})_3^{3+}$ in 1 M HCl can be attributed to the failure of this medium to decrease 2k_0 sufficiently for the quenching to be observed outside the experimental error envelope (ca. 10-15%).

In view of the fact that ion-pairing causes a reduction in the overall positive charges of the ground- and excited-state complexes with concomitant reduction of the mutual electrostatic repulsion,⁵³ it appears that the $^2k_{\text{gsq}}$ values reflect the encounter of ion-paired ground-state $[\text{Cr}(\text{NN})_3^{3+} \cdots \text{Cl}^-]$ and ion-paired excited-state $[\text{Cr}(\text{NN})_3^{3+} \cdots \text{Cl}^-]^*$ species. Furthermore, the $^2k_{\text{gsq}}$ values are virtually the same in the presence of Cl^- (see Table 3-8) for $\text{Cr}(\text{bpy})_3^{3+}$ in 5 M HCl and $\text{Cr}(\text{phen})_3^{3+}$ in 1 M HCl; in the absence of Cl^- , $^2k_{\text{gsq}}$ may well be many orders of magnitude lower such that no quenching is observable. Then, the quenching reaction proceeds via collision-induced, non-radiative deactivation of the excited-state $[\text{Cr}(\text{NN})_3^{3+} \cdots \text{Cl}^-]^*$ species. An electron transfer quenching pathway is energetically unfavorable. Scheme 3-1 illustrates an "ion-bridged excimer" resulting from the encounter between $[\text{Cr}(\text{NN})_3^{3+} \cdots \text{Cl}^-]^*$ and $[\text{Cr}(\text{NN})_3^{3+} \cdots \text{Cl}^-]$; that is, the formation of the excited-state species $^*[\text{Cr}(\text{NN})_3^{3+} \cdots \text{Cl}^- \cdots \text{Cr}(\text{NN})_3^{3+}]$. Excimer formation is not an uncommon phenomenon for aromatic molecules, and is manifested in lowered excited-state lifetimes with increasing ground-state substrate concentration.⁵⁴ No emission was observed that could be assigned to the "ion-bridged excimer", and thereby we do not know its excited-state lifetime; however, it is expected to be very short due to rapid non-radiative deactivation through the coupling of the vibrational modes of the aggregate species.

Since the initial observation of ground-state quenching for the bpy and phen complex ions in Cl^- media, the investigation was extended to

Scheme 3-1



several $\text{Cr}(\text{NN})_3^{3+}$ complexes and it was found that this phenomenon is indeed present. Figure 3-14 depicts the variation in $1/\tau_{\text{obs}}^2 (= {}^2k_{\text{obs}})$ with $\text{Cr}(\text{NN})_3^{3+}$ concentration in 1 M HCl for (NN) = 5-Phphen, 5-Clphen, and phen for comparative purposes. Similar plots were obtained for (NN) = 5-Brphen, 5-Mephen, 5,6-Me₂phen, 4,7-Me₂phen, 4,7-Ph₂phen and 3,4,7,8-Me₄phen in 1 M HCl, and for (NN) = 4,4'-Me₂bpy and 4,4'-Ph₂bpy in 5 M HCl. Values of ${}^2k_{\text{gsq}}$ and ${}^2k_{\text{O}}$ obtained from these plots are given in Table 3-9. The data show that ground-state quenching in the presence of 1 M Cl⁻ is observed for all the phen complexes, while 5 M Cl⁻ is required for observation of this phenomenon in the bpy complexes. The lowest values of ${}^2k_{\text{gsq}}$ are those for the unsubstituted bpy and phen complex ions; an increase of substituents on the ligand framework increases the ${}^2k_{\text{gsq}}$ value. It would appear that substituents on the ligand increase the size of the reacting species, which, in turn, enhances collisional interaction between the anion-associated ground- and excited-state species. It may well be that this ground-state quenching of excited-state quenching of excited-state cationic coordination complexes mediated by anions in fluid media at room temperature is a general phenomenon, and that its observability depends on low values of ${}^2k_{\text{O}}$ and high values of ${}^2k_{\text{gsq}}$.

Two consequences of this investigation are noteworthy. First, it becomes imperative that all experimental conditions (i.e., substrate concentration, solution medium, temperature, etc.) be reported explicitly. Secondly, concerning $\text{Cr}(\text{NN})_3^{3+}$ in particular, now that we are aware of this phenomenon, it will be necessary to account for it and, where required, subtract its contribution from the overall photochemistry.

Previous results of anion effects on the ${}^2\text{E}$ lifetimes of $\text{Cr}(\text{NN})_3^{3+}$ complex ions prompted further studies of this phenomenon. Henry and

FIGURE 3-14 : Plot of $1/\tau^2$ for $\text{Cr}(\text{NN})_3^{3+}$ as a Function of [Substrate] in Argon-purged 1 M HCl Solution at 22°C: (O), 5-Phphen in 4% v/v CH_3CN ; (\square), 5-Clphen; (\bullet), phen.

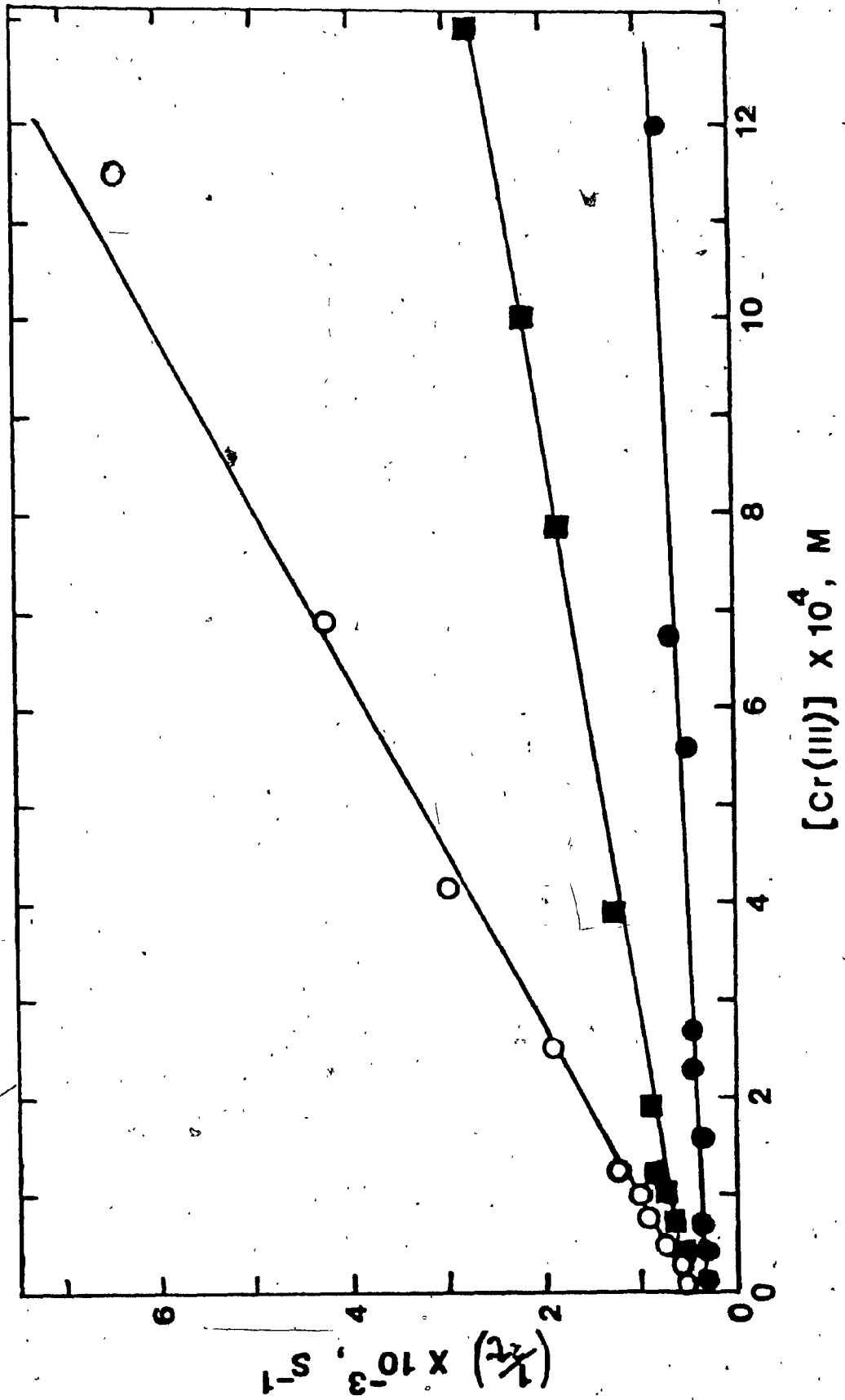


TABLE 3-9 : Ground-state Quenching Parameters for $\text{Cr}(\text{NN})_3^{3+}$ at 22 °C.^a

NN	$k_{\text{gsq}}^2, \text{M}^{-1} \text{sec}^{-1}$	τ_0^2, msec
bpy	1.3×10^6 ^b	0.10 ^b
4,4'-Me ₂ bpy	2.0×10^6 ^{b,c}	0.31 ^{b,c}
		0.20
4,4'-Ph ₂ bpy	1.4×10^8 ^c	0.17 ^c
	1.0×10^8 ^{b,c}	0.19 ^{b,c}
phen	3.0×10^6 ^b	0.32 ^b
	2.3×10^6	0.33
5-Clphen	1.7×10^7	0.18
5-Brphen	5.4×10^7 ^c	0.18 ^c
5-Mephen	5.0×10^6	0.42
5-Phphen	5.7×10^7 ^c	0.22 ^c
5,6-Me ₂ phen	7.5×10^6 ^c	0.42 ^c
4,7-Me ₂ phen	1.0×10^7 ^c	0.57 ^c
4,7-Ph ₂ phen	7.4×10^7 ^c	0.57 ^c
3,4,7,8-Me ₄ phen	1.5×10^7 ^c	0.64 ^c

^a In deaerated 1 M HCl solutions at 22°C, unless otherwise noted.

^b 5.0 M HCl.

^c Solution contains 4% v/v CH₃CN.

Hoffman⁴⁹ reported an increase in ${}^2\tau$ for $\text{Cr}(\text{bpy})_3^{3+}$ in aqueous solution in the presence of high concentrations of inorganic salts. The prolongation was observed for ClO_4^- , HSO_4^- , Cl^- and NO_3^- by flash photolysis studies. This lifetime prolongation was attributed to a decrease in ${}^2k_{\text{rx}}$ and ${}^2k_{\text{nr}}$. In light of these observations and the necessity to cite specific experimental conditions in order to obtain the magnitude of the ground-state quenching phenomenon observed in the presence of Cl^- , further studies were carried out to determine the general applicability of this phenomenon for $\text{Cr}(\text{bpy})_3^{3+}$ and $\text{Cr}(\text{phen})_3^{3+}$ in aqueous, argon-purged solutions at 22°C. Thus, effects of various anions X^- , including Br^- , BrO_3^- , NO_3^- , SCN^- , I^- , HSO_4^- and F^- , on ${}^2\tau_{\text{obs}}$ as a function of $[\text{Cr}(\text{NN})_3^{3+}]$ were investigated. The results obtained in 1 M Br^- , NO_3^- , BrO_3^- , HSO_4^- and 0.5 M F^- parallel those found in 1 M Cl^- ; that is, ${}^2\tau_{\text{obs}}$ decreases with increasing $[\text{Cr}(\text{phen})_3^{3+}]$ and remains essentially constant for varying $[\text{Cr}(\text{bpy})_3^{3+}]$. Further, the behavior may be described by equation (3-16) where 2k_0 and ${}^2k_{\text{gsq}}$ are similarly defined. These rate constants for $\text{Cr}(\text{phen})_3^{3+}$ and $\text{Cr}(\text{bpy})_3^{3+}$ in the various media are collected in Table 3-10. The results obtained for $\text{X}^- = \text{I}^-$ and SCN^- reveal that these two anions completely quench the (${}^2T_1/{}^2E$) phosphorescence from both $\text{Cr}(\text{phen})_3^{3+}$ and $\text{Cr}(\text{bpy})_3^{3+}$. Results for 1 M F^- were not obtained due to solubility limitations of NaF in water.

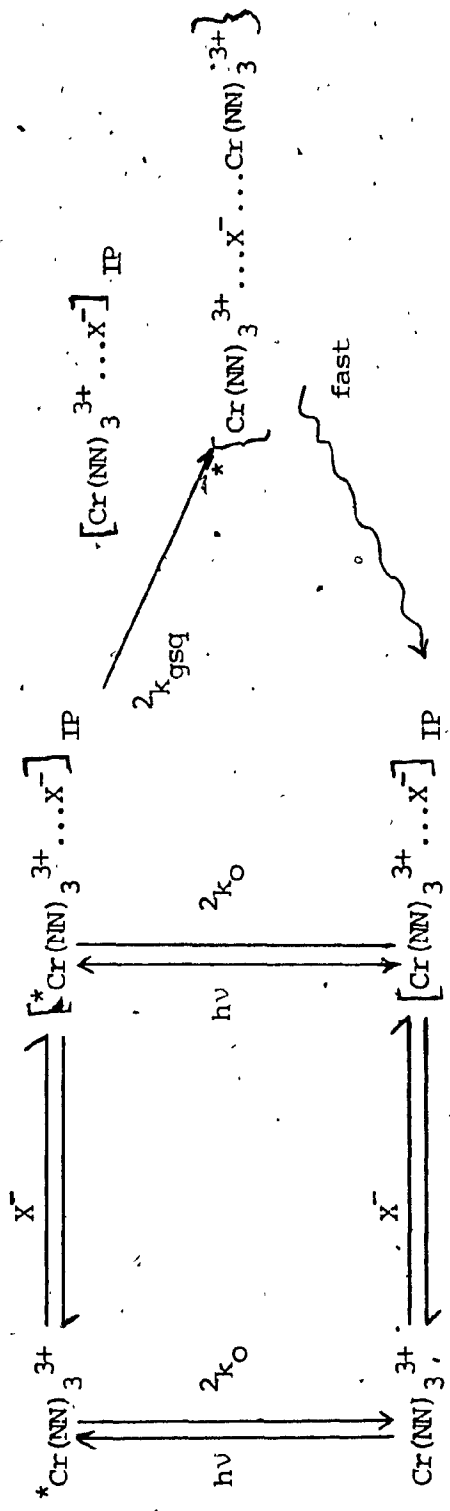
The results presented in Table 3-10 suggest that it is not necessary to invoke a quenching mechanism different from that in Scheme 3-1 for the Cl^- -mediated ground-state quenching effect. Thus, Scheme 3-2 presents the general mechanism for the anion-mediated ground-state quenching phenomenon for $\text{X}^- = \text{Cl}^-$, Br^- , F^- , BrO_3^- , NO_3^- and HSO_4^- . The lack of observable ground-state quenching for $\text{Cr}(\text{bpy})_3^{3+}$ in the various 1 M X^- media

TABLE 3-10: Medium Dependence of Lifetimes of $(^2T_1/{}^2E)Cr(bpy)_3^{3+}$ and $(^2T_1/{}^2E)Cr(phen)_3^{3+}$ in Argon-purged Solutions at 22°C.

Medium ^a	$2\tau_{obs}$ (msec)	$2k_{obs} \times 10^{-4}$ (sec ⁻¹)	$2\tau_{O'}$ (msec)	$2k_O \times 10^{-3}$ (sec ⁻¹)	$2k_{gsq} \times 10^{-6}$ (M ⁻¹ sec ⁻¹)
HClO ₄	--	--	0.49	2.02 ± 0.01^c	4.65 ± 0.32^c
KNO ₃	0.079	1.3	0.29	3.50 ± 0.05	4.13 ± 0.14
NaBr	0.072	1.4	0.30	3.33 ± 0.05	3.29 ± 0.04
NaBrO ₃	0.068	1.5	0.25	3.96 ± 0.04	2.96 ± 0.15
HCl ^b	0.073	1.4	0.33	3.0	2.3
Na ₂ SO ₄	0.076	1.3	0.26	3.78 ± 0.08	2.85 ± 0.20
H ₂ SO ₄	0.094	1.1	0.36	2.79 ± 0.02	2.09 ± 0.11
H ₂ O ^b	0.068	1.5	0.25	4.0 ± 0.4	--
NaF ^d	0.050	2.0	0.19	5.3 ± 0.2	2.5 ± 0.6

^a Concentration, 1.0 M. ^b From Table 3-9. ^c Standard error. ^d Concentration, 0.5 M.

Scheme 3-2



is similarly attributed to the failure of the medium to sufficiently decrease 2k_0 .

Once the encounter complex $[({}^2T_1/{}^2E)Cr(NN)_3^{3+} \cdots X^-]_{IP}$ is formed, the possibility that excited-state electron-transfer and/or energy-transfer quenching occurs must be entertained. Examination of the appropriate redox potentials for $({}^2T_1/{}^2E)Cr(NN)_3^{3+/2+}$ and X^-/X^\cdot couples presented in Table 3-11 eliminates the assignment of an excited-state electron transfer mechanism for all X^- species except I^- and SCN^- , inasmuch as the energetics are unfavorable. An excited-state reductive electron transfer mechanism is assigned (see Section 3.8.) to the quenching of $({}^2T_1/{}^2E)Cr(NN)_3^{3+}$ complexes by I^- , for which ${}^2k_q = 1.4 \times 10^9 \text{ M}^{-1} \text{ sec}^{-1}$ for $NN = \text{bpy}$ and ${}^2k_q = 2.1 \times 10^9 \text{ M}^{-1} \text{ sec}^{-1}$ for $NN = \text{phen}$. Kane-Maguire⁵⁵ have reported the quenching of phosphorescence intensity and photoracemization quantum yield (quenchable component) of $Cr(\text{phen})_3^{3+}$ by SCN^- , as have Bolletta and coworkers³⁹ for the 2E absorption decay of the phen complex. An excited-state energy transfer quenching mechanism is also deemed unlikely if a comparison of the transition energies of the $Cr(NN)_3^{3+}$ and X^- species involved is made; these energies are presented in Table 3-12 for this purpose. Inasmuch as there is insignificant overlap between the absorption or emission spectra of $Cr(NN)_3^{3+}$ and the absorption spectra of the X^- species, an energy transfer mechanism is not favored.

It is therefore believed that the ground-state quenching phenomenon is a general one observed for $Cr(NN)_3^{3+}$ complex ions, and that this phenomenon is mediated by the presence of anions, X^- .

TABLE 3-11 : Redox Potentials (vs NHE) of $^*Cr(NN)_3^{3+/2+}$ and X/X^- Couples in Fluid Media.

X/X^-	E^0, V
$^*Cr(bpy)_3^{3+} / Cr(bpy)_3^{2+}$	+1.44 ^a
$^*Cr(phen)_3^{3+} / Cr(phen)_3^{2+}$	+1.42 ^a
F/F^-	+3.6 ^b
Cl/Cl^-	+2.6 ^c
Br/Br^-	+2.0 ^c
SO_4^- / SO_4^{2-}	+3.4 ^d
NO_3^- / NO_3^-	+1.9 ^c
SCN/SCN^-	+1.62 ^e
I/I^-	+1.42 ^c

^a From Table 3-14 of this work. ^b B.M. Berdinikov and N.M. Bazhim, Zh. Fiz. Khim., 44, 712 (1970). ^c Reference 57. ^d Reference 58.

^e G. Nord, B. Pedersen, and O. Farver, Inorg. Chem., 17, 2233 (1978).

TABLE 3-12 : Absorption Spectral Properties of $\text{Cr}(\text{phen})_3^{3+}$,
 $\text{Cr}(\text{bpy})_3^{3+}$ and X / X^- Couples.

Species	λ_{max} , nm ^a
$(^4\text{A}_2 \rightarrow ^4\text{T}_2)\text{Cr}(\text{NN})_3^{3+}$	400 ^b
$(^4\text{A}_2 \rightarrow ^2\text{T}_1/^2\text{E})\text{Cr}(\text{NN})_3^{3+}$	695, 727 ^c
ClO_4^-	180
Cl^-	175
Br^-	199
HSO_4^-	200
SO_4^{2-}	175
NO_3^-	303
SCN^-	222
I^-	227
BrO_3^-	200

^a From reference 61, unless otherwise noted. ^b From Table 3-1.

^c From Table 3-3.

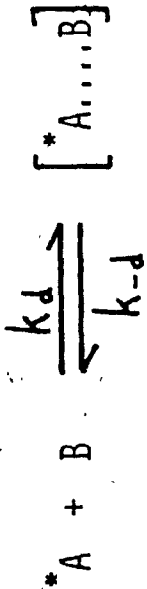
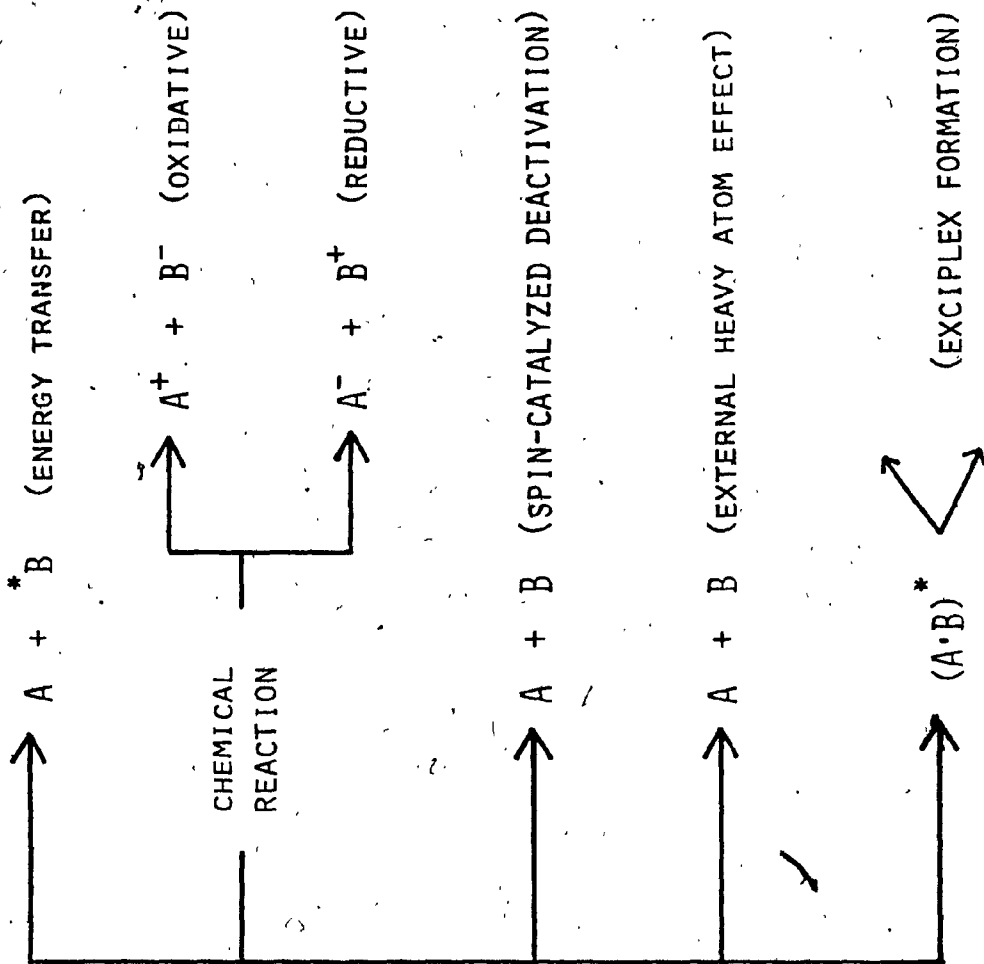
3.7. EXCITED-STATE BIMOLECULAR QUENCHING REACTIONS OF $\text{Cr}(\text{NN})_3^{3+}$

Excited-state quenching provides a unique method for obtaining photochemical and photophysical information, and for elucidating the roles of the various excited-state deactivation pathways. Insofar as chromium(III) polypyridyl complexes are concerned, the object is to ascertain the relative importance of the $^4\text{T}_2$ and $^2\text{T}_1/{}^2\text{E}$ excited states, as well as the importance of each deactivation pathway within each of these excited-state configurations. Balzani *et al.*⁶⁵ have thoroughly reviewed the available data up to 1975 on excited-state quenching processes, and more recently⁵⁶ have included a detailed kinetic analysis of the quenching processes of excited-state transition metal complexes.

When spin and energy requirements are satisfied, excited-state quenching processes between organic species are usually diffusion-controlled.⁶⁵⁻⁶⁸ However, this generality is not applicable to transition metal complexes, for which the quenching efficiency in the collision encounter is greatly affected by the nature of the ligands,⁶⁹⁻⁷³ and by the charge and geometry of the complex.^{69,74-78} Investigations of quenching processes of excited-state transition metal polypyridyls provide insight into the excited-state reactivities of these complexes.

Several distinct mechanisms exist for excited-state bimolecular quenching,^{54,66,67} of which the most relevant to transition metal complexes include the following: electronic energy transfer, electron transfer, spin-catalysed deactivation, excimer or exciplex formation, and the external heavy-atom effect. These quenching processes are illustrated in Scheme 3-3. The participation of each of these pathways in the quenching process has been discussed⁶⁵ with particular emphasis on the various factors which determine their occurrence and relative importance. The most

Scheme 3-3



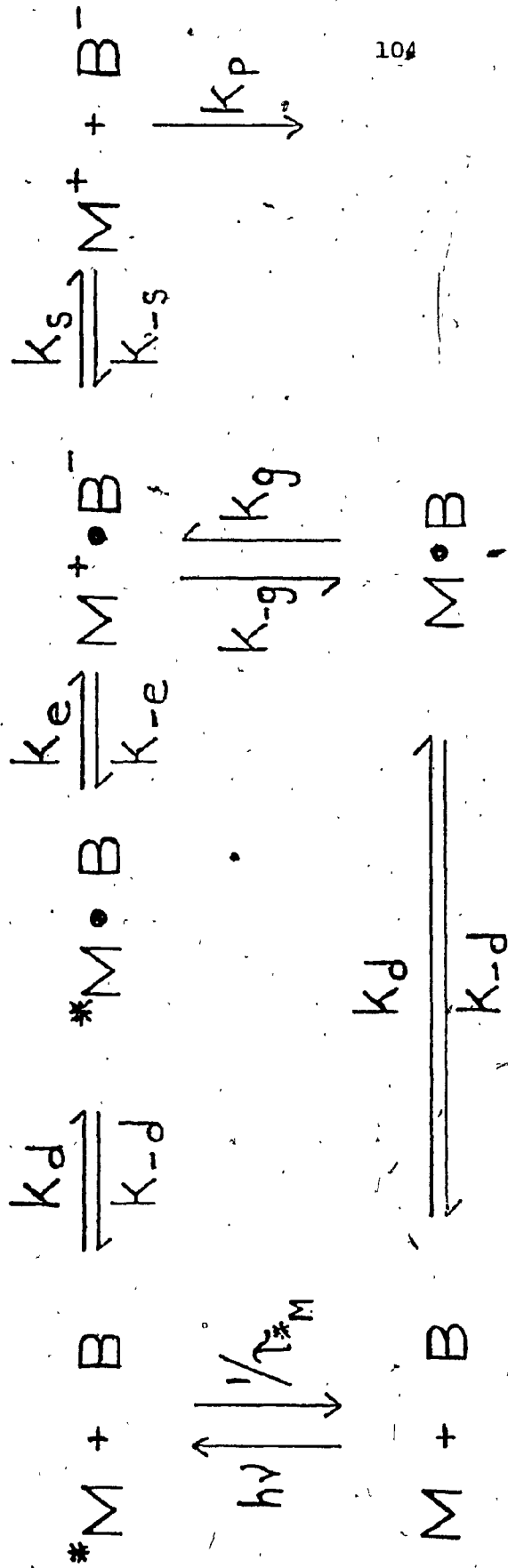
common quenching pathways for transition metal polypyridyl complexes are the energy transfer and electron transfer paths.

3.7.0. *Bimolecular Electron Transfer.*

Transition metal complexes can undergo redox reactions via either outer-sphere or inner-sphere pathways. Since excited-state lifetimes of these complexes in fluid media are usually small, bimolecular processes involving these excited states must be near the diffusion-controlled limit so that they can compete with intra-molecular deactivation processes. It seems unlikely that an inner-sphere redox pathway could occur at a rate competitive with the deactivation of the excited state, inasmuch as ligand substitution processes are relatively slow. On the contrary, an outer-sphere redox pathway forms an activated complex in which the number and type of ligands on the two reactants remain unchanged. This pathway may be very fast, and can thereby compete with excited-state deactivation. The rates of electron transfer quenching processes are governed by both "intrinsic" (self-exchange rates of the reactants) and "extrinsic" (overall free energy change of the reaction)⁶⁵ factors. The nature of the complex will undoubtedly have an effect on the quenching process. With respect to chromium(III) polypyridyl complex ions, the shielding of the chromium(III) core by the hydrophobic ligand sphere, for example, should affect the interaction between the metal-centered excited states and quencher species. Furthermore, since the energy of the 2E state varies only slightly with changes in the ligand field strength, the effect of structure on the quenching process can be examined by varying the ligand sphere.

An electron transfer quenching process for the transition metal complex M is depicted in Scheme 3-4. The electronically-excited species *M

Scheme 3-4



is expected to be both a better reductant and a better oxidant than its corresponding ground-state species M, since excitation of an electron from a low-energy (bonding) orbital to a higher-energy (antibonding) orbital reduces the ionization potential and increases the electron affinity of a molecule. The rate constant for the electron-transfer quenching process in Scheme 3-4, k_q , is given by equations (3-18) and (3-19),⁶⁵

$$k_q = \frac{k_d}{1 + \frac{k_{-d}}{k_d} + \frac{k_{-d}k_e}{k_x k_e}} \quad (3-18)$$

$$k_q = \frac{k_d}{1 + \frac{k_{-d}}{z} \left[\exp \frac{\Delta G_e^\ddagger}{RT} + \frac{\Delta G_e^0}{RT} \right]} \quad (3-19)$$

where the latter equation relates k_q to the free energy of activation, ΔG_e^\ddagger , for the electron transfer step. For equations (3-18) and (3-19), $k_{-g} = k_x$ when the k_p pathway is negligible; as well, when the k_{-s} path is negligible, $(k_{-g} + k_s) = k_x$.⁶⁵ Equation (3-19) may be used to estimate the dependence of k_q on the overall free energy change, ΔG_e^0 , if the free energy of activation for the electron transfer step can be related to the overall free energy change.

To relate ΔG_e^\ddagger to ΔG_e^0 , two relationships have been developed: Marcus^{79,80} has provided the classical relationship (3-20), while Rehm and Weller^{81,82} have proposed the empirical relationship (3-21), where

$$\Delta G_e^\ddagger = \left(\frac{\lambda}{4}\right) + \left(\frac{\Delta G_e^0}{\lambda}\right)^2 \quad (3-20)$$

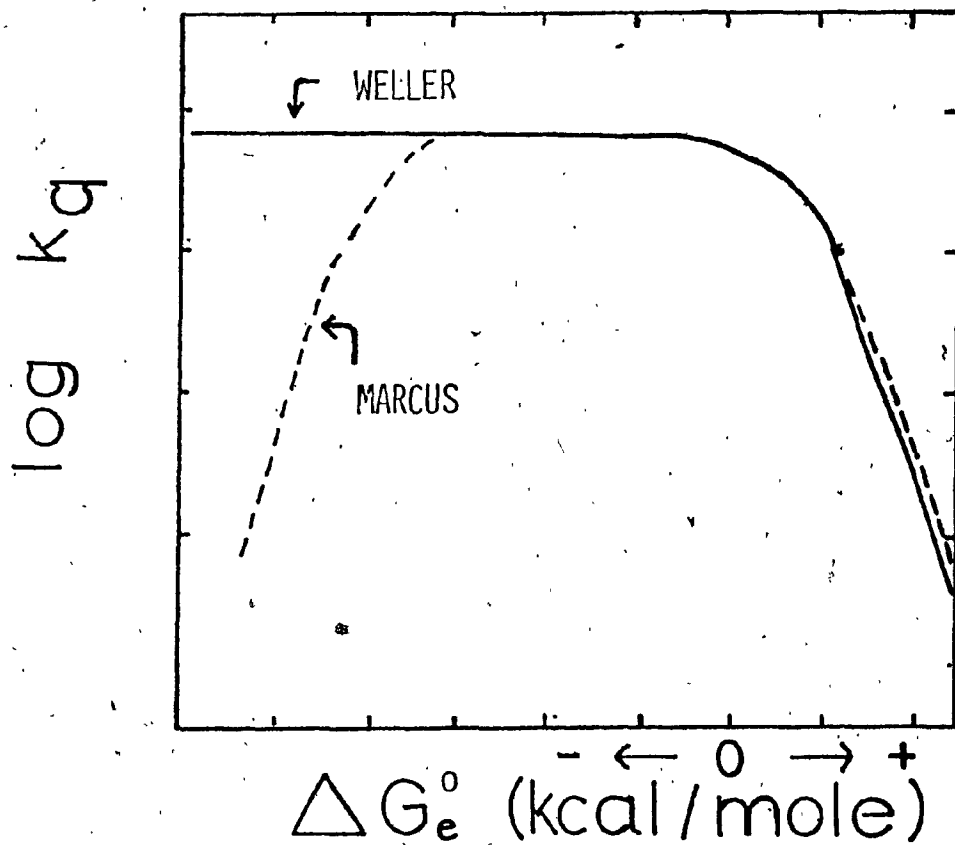
$$\Delta G_e^\ddagger = \left[\left(\frac{\Delta G_e^0}{2}\right)^2 + \left(\frac{\lambda}{4}\right)^2 \right]^{1/2} \quad (3-21)$$

λ is a reorganizational parameter. A detailed kinetic analysis and critical review of these two relationships has been presented by Balzani and coworkers.^{56,65}

The dependence of the quenching rate constant k_q on the overall free energy ΔG_e^0 (equation 3-19) as predicted by the Marcus and Rehm-Weller theories is illustrated in Figure 3-15; it is clear that for positive and slightly negative values of ΔG_e^0 , the dependence of $\log k_q$ on ΔG_e^0 is virtually identical. However, in the region where ΔG_e^0 becomes increasingly negative, the Marcus theory (equation 3-20) reveals a dramatic decrease in k_q (commonly referred to as the Marcus inverted region); in contrast, the Rehm-Weller theory (equation 3-21) predicts that k_q reaches a plateau value under these conditions. Evidence for adherence to the Marcus behavior has only been found in the quenching of $(^3\text{CT})\text{Ru}(\text{bpy})_3^{2+}$ for which there is a small decrease in k_q with increasing endoergic character of the quenching reaction (i.e., with increasing negativity of ΔG_e^0).⁸³

Often an electron transfer process does not yield products different from the reactants; this is usually indicative of a rapid, reverse thermal electron-transfer reaction to yield reactants. In such a case, the electron transfer quenching rate constant in equation (3-18) is described as equation (3-22). One method utilized to confirm the existence of an

FIGURE 3-15 : Dependence of $\log k_q$ on ΔG_e° Calculated From Equation (3-19) (see text) where ΔG_e° is Given by the Marcus and Rehm-Weller Relationships.

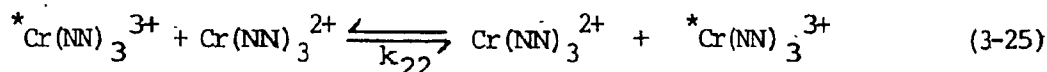
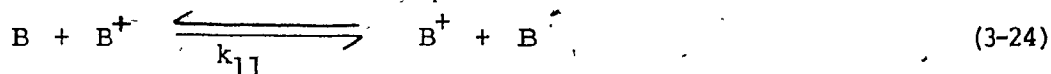


$$k_q = \frac{k_d}{1 + \frac{k_d}{k_e} + \frac{k_d k_{-e}}{k_g k_e}} \quad (3-22)$$

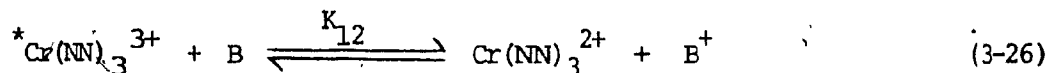
electron transfer quenching pathway emanates from the relationship (3-23)

$$k_q = k_{12} = (k_{11} k_{22} K_{12} f_{12})^{1/2} \quad (3-23)$$

given by Marcus^{84,85} for electron transfer reactions, where $\log f_{12} = (\log K_{12})^2 / [4 \log (k_{11} k_{22} / Z^2)]$, and k_{11} and k_{22} are the rate constants for the self-exchange reactions (3-24) and (3-25), respectively.



K_{12} is the equilibrium constant for the cross-reaction (3-26), and Z is



the collision number usually taken as $10^{11} M^{-1} sec^{-1}$. Also,

$$k_{12} = 0.5 \log k_{11} k_{22} + 0.5 (1 + \alpha) \log K_{12} \quad (3-27)$$

where $\alpha = (\log K_{12}) / 4 \log (k_{11} k_{22} / Z^2)$.⁶⁵ A linear plot of $\log k_q$ ($= \log k_{12}$) vs $(1 + \alpha) \log K_{12}$ suggests electron transfer quenching. If

k_{11} is known, then the value of k_{22} can be estimated by fitting the experimental data assuming various k_{22} values. $\log K_{12}$ is a measure of the driving force for electron transfer, and varies as ΔE° . Creutz and Sutin⁸³ have predicted that electron transfer rates should begin to decrease at sufficiently high driving forces; however, concrete evidence for this prediction is still lacking.

Turning now to the actual investigations of excited-state electron transfer quenching reactions, it is evident that transition metal polypyridyl complexes are suitable candidates as they provide a wide range of excited-state properties. These properties can be varied by altering the metal center, altering the type of ligand, or simply by the addition of substituents to the polypyridyl ligand framework. It is this "excited-state tuning" which allows the excited-state complex to serve as both a better oxidant and reductant, an attribute not possible for the metal ion or the free polypyridyl molecule alone. These properties are illustrated in Table 3-13 for some well-known transition metal polypyridyl complexes.

Where the Stokes shift between the ground-state absorption and the excited-state emission is very small, and the changes in shape, size and solvation between the two states are also small, the entropic differences between the ground and excited states may be neglected. Assuming such negligible differences, and that the excited-state energy is all available as free energy for the excited-state redox processes, the excited-state redox potentials are obtained from the redox potentials of the corresponding ground state and the spectroscopic excited-state energy.⁵⁶ For the chromium(III) polypyridyl complex ions, excited-state redox potentials are estimated according to equations (3-28) and (3-29), where

TABLE 3-13 : Excited-state Identification, Lifetimes, Energies and Redox Potentials
For Various $M(NN)_3^{n+}$ Complexes in Fluid Media.^a

COMPLEX ^b	Lowest Excited State	τ , (μ sec)	$E^{O-O}(M-M)^C$ (eV)	$E(M^+/M)^d$ (V)	$E(M^*/M^+)^d$ (V)
Ru(bpy) ₃ ²⁺	³ CT	0.62	2.12	-0.86	+0.84
Ru(phen) ₃ ²⁺	³ CT	0.50	2.18	-0.89	+0.75
Os(bpy) ₃ ³⁺	³ CT	0.019	1.85 (MeOH)	-1.02	+0.67
Ir(bpy) ₃ ³⁺	³ LC	2.4 (MeOH)	2.81 (MeOH)	-0.64	+2.05
Cr(bpy) ₃ ³⁺	² MC	.77	1.71	> -0.1	+1.46
Cr(phen) ₃ ³⁺	² MC	270	1.71	---	+1.46

^a In aqueous solution at room-temperature, unless otherwise noted; from reference 56.

^b CT = charge-transfer; LC = ligand-centered; MC = metal-centered.

^c energy, in eV, of the zero-zero transition.

^d excited-state reduction potential, vs NHE.

$$E^{\circ}(\text{Cr}^{4+}/^{*}\text{Cr}^{3+}) = E^{\circ}(\text{Cr}^{4+}/\text{Cr}^{3+}) - E^{\circ-\circ}(\text{Cr}^{3+}/^{*}\text{Cr}^{3+}) \quad (3-28)$$

$$E^{\circ}(^{*}\text{Cr}^{3+}/\text{Cr}^{2+}) = E^{\circ}(\text{Cr}^{3+}/\text{Cr}^{2+}) - E^{\circ-\circ}(\text{Cr}^{3+}/^{*}\text{Cr}^{3+}) \quad (3-29)$$

$E^{\circ-\circ}(\text{Cr}^{3+}/^{*}\text{Cr}^{3+})$ is the one-electron potential corresponding to the zero-zero spectroscopic energy of the 2E excited state. The reduction potentials of the 2E states of several $\text{Cr}(\text{NN})_3^{3+}$ complexes from the excitation energy ($\Delta G^* \sim 1.7$ eV) and ground-state reduction potentials⁸⁶⁻⁹⁰ have been evaluated and are summarized in Table 3-14, along with the corresponding ground-state potentials. The validity of this procedure has been verified in the case of the MLCT state of $\text{Ru}(\text{bpy})_3^{2+}$,⁹¹ for which the estimated value of -0.89 V for $E^{\circ}(\text{Ru}^{3+}/^{*}\text{Ru}^{2+})$ ⁴⁴ is in accord with the value of -0.81 V for the $\text{Ru}(\text{bpy})_3^{3+}/^{*}\text{Ru}(\text{bpy})_3^{2+}$ couple in acetonitrile;⁹² this was taken⁹¹ as good evidence that the entropic difference between the ground state and the luminescent state of $\text{Ru}(\text{bpy})_3^{2+}$ is small. For some of the $\text{Cr}(\text{NN})_3^{3+}$ complexes cited in Table 3-14, Ballardini and coworkers⁹³ have experimentally verified the estimation of the redox potentials of the various polypyridyl complexes using a series of amine and methoxy benzene quenchers of graded potential. A comparison of the ground-state and excited-state redox potentials in Table 3-14 reveals that the excited-state species are indeed better oxidants than their respective ground-state species. Furthermore, the $({}^2E)\text{Cr}(\text{NN})_3^{3+}$ complex ions are also more powerful oxidants than are the MLCT states of the analogous $\text{Ru}(\text{II})$ and $\text{Os}(\text{II})$ complexes.^{44,93,94} The reduction potentials of the chromium(III) complexes parallel those of the corresponding $\text{Ru}(\text{II})$ complexes,⁴⁴ with the chromium potentials approximately 1.5 V more negative. The reduction potentials for the 2E excited states of $\text{Cr}(\text{NN})_3^{3+}$ are also about 1.7 V

TABLE 3-14 : Formal Reduction Potentials of Cr(NN)₃ⁿ⁺ Complexes at 25 °C.^a

NN	$E^{\circ}(\text{Cr}^{3+}/\text{Cr}^{2+})$ (V)	$E^{\circ}(\text{Cr}^{3+}/\text{Cr}^{2+})$ (V)
bpy	-0.26	+1.44
4,4'-Me ₂ bpy	-0.45	+1.25
4,4'-Ph ₂ bpy	(-0.28) ^b	(+1.39) ^c
5-Clphen	-0.17	+1.53
5-Brphen	-0.15	+1.55
phen	-0.28	+1.42
5-Mephen	-0.30	+1.39
5,6-Me ₂ phen	-0.29 ^d	+1.40 ^c
4,7-Me ₂ phen	-0.45	+1.23
3,4,7,8-Me ₄ phen	(-0.57) ^b	(1.11) ^c
5-Phphen	-0.21 ^d	+1.49 ^c
4,7-Ph ₂ phen	(-0.26) ^b	(+1.41) ^c

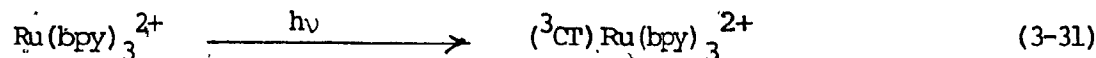
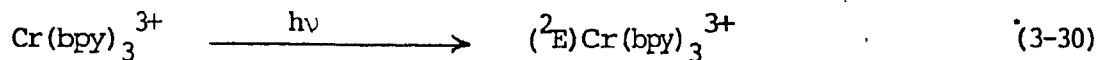
^a Vs. NHE, in 1.0 M LiCl, reference 83, unless otherwise noted. ^b Calculated by interpolation from $\log k_{12}$ vs. $\log k_{12}$ of Cr(phen)₃^{3+/2+} as -0.28 V, and using E° values for the appropriate Cr^{3+/2+} couple in Table IV of reference 91.

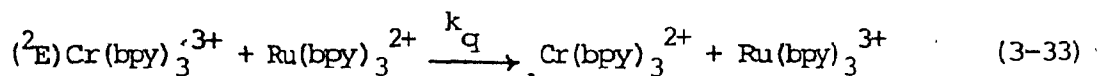
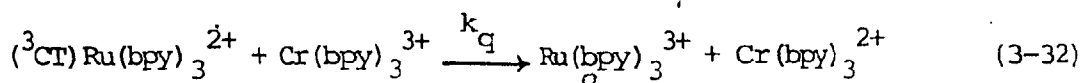
more positive than the corresponding ground-state reduction potentials. This uniform shift of the excited-state reduction potential is due to the similarity in the wavelengths for maximum emission in the $\text{Cr}(\text{NN})_3^{3+}$ species.

Chromium(III) polypyridyl complexes are thus good candidates for studies in bimolecular excited-state redox reactions inasmuch as the ${}^2\text{E}$ states are sufficiently long-lived (see Table 3-4) to be capable of bimolecular reaction, they are photostable in acidic media, and they exhibit an efficient emission⁴³ which is easily monitored.

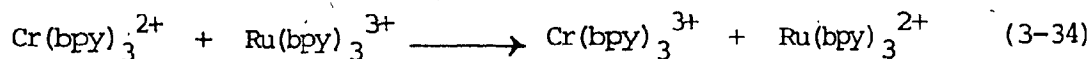
a. The $\text{Cr}(\text{bpy})_3^{3+}/\text{Ru}(\text{bpy})_3^{2+}$ System.

The first evidence of electron transfer quenching of $({}^2\text{E})\text{Cr}(\text{NN})_3^{3+}$ involved the $\text{Cr}(\text{bpy})_3^{3+}/\text{Ru}(\text{bpy})_3^{2+}$ couple. Quenching via energy transfer is unfavorable inasmuch as the energies of $({}^2\text{E})\text{Cr}(\text{bpy})_3^{3+}$ and $({}^3\text{CT})\text{Ru}(\text{bpy})_3^{2+}$ are 13800 and 17100 cm^{-1} , respectively.⁹⁵ Flash photolysis experiments on the $\text{Cr}^{3+}/\text{Ru}^{2+}$ system in acidic solution have shown⁹⁵ that $\text{Cr}(\text{bpy})_3^{2+}$ is observed as a transient product. However, $\text{Cr}(\text{bpy})_3^{3+}$ is also known to be an efficient quencher of $({}^3\text{CT})\text{Ru}(\text{bpy})_3^{2+}$.⁹⁵ Addition of iodide ion, a selective ${}^2\text{E}$ quencher, to the reaction resulted in partial disappearance of $\text{Cr}(\text{bpy})_3^{2+}$. Since complete scavenging of $({}^2\text{E})\text{Cr}(\text{bpy})_3^{3+}$ yielded partial disappearance of $\text{Cr}(\text{bpy})_3^{2+}$, it was concluded⁹⁵ that the following reactions occur for this couple.





The electron transfer rate constants have been evaluated at $k_q = 3.3 \times 10^9 \text{ M}^{-1} \text{ sec}^{-1}$ and $4.0 \times 10^8 \text{ M}^{-1} \text{ sec}^{-1}$ for reactions (3-32) and (3-33), respectively.⁹⁵ From the second-order decay of the $\text{Cr}(\text{bpy})_3^{2+}$ transient absorption, the rate constant for the reverse thermal reaction between $\text{Cr}(\text{bpy})_3^{2+}$ and $\text{Ru}(\text{bpy})_3^{3+}$ (equation 3-34) is $2.6 \times 10^9 \text{ M}^{-1} \text{ sec}^{-1}$.⁹⁵



b. The $\text{Cr}(\text{bpy})_3^{3+}$ /organic molecules Systems.

Quenching of $({}^2\text{E})\text{Cr}(\text{bpy})_3^{3+}$ by a series of aliphatic and aromatic amines and methoxy benzenes has been studied by flash photolysis techniques; these studies have shown that the quenching process results in the formation of a one-electron oxidation product of the quencher species.⁹³ Those quenchers examined and the corresponding k_q values are given in Table 3-15. Plots of $\log k_q$ vs ΔG_e^0 show no decrease in k_q as ΔG_e^0 becomes increasingly negative,⁹³ as predicted by the Marcus relationship. However, a comparison of the relationships between k_q and ΔG_e^0 for the aliphatic and aromatic amine quenchers reveals that the reorganizational energy λ is greater for the aliphatic amines since the electron to be transferred is more localized in the aliphatic species than in the aromatic species, thus requiring a greater geometrical perturbation upon oxidation.⁹³ Also, owing to this greater electron localization, steric factors should cause a decrease in the quenching rate

TABLE 3-15 : Electron Transfer Rate Constants (2k_q) for Quenching of $^*Cr(NN)_3^{3+}$ Complexes.

NN	QUENCHER	2k_q ($M^{-1}sec^{-1}$)	Mechanism	Reference
bpy	Fe ²⁺	1.6×10^7 a	reductive	86
bpy	Fe ²⁺	3.7×10^7 b	reductive	this work
4,4'-Me ₂ bpy	Fe ²⁺	0.082×10^7 a	reductive	86
4,4'-Me ₂ bpy	Fe ²⁺	0.22×10^7 b	reductive	this work
4,4'-Ph ₂ bpy	Fe ²⁺	2.0×10^7 b	reductive	this work
5-Clphen	Fe ²⁺	4.8×10^7 a	reductive	86
5-Clphen	Fe ²⁺	1.2×10^8 b	reductive	this work
5-Brphen	Fe ²⁺	8.4×10^7 b	reductive	this work
phen	Fe ²⁺	1.5×10^7 a	reductive	86
phen	Fe ²⁺	3.2×10^7 b	reductive	this work
5-Mephen	Fe ²⁺	1.0×10^7 a	reductive	86
5-Mephen	Fe ²⁺	3.4×10^7 b	reductive	this work
5,6-Me ₂ phen	Fe ²⁺	2.6×10^7 b	reductive	this work
4,7-Me ₂ phen	Fe ²⁺	0.089×10^7 a	reductive	86
4,7-Me ₂ phen	Fe ²⁺	0.60×10^7 a	reductive	this work

Table 3-15, cont'd.

NN	QUENCHER	$2k_q$ ($M^{-1} \text{ sec}^{-1}$)	Mechanism	Reference
3,4,7,8-Me ₄ phen	Fe ²⁺	0.092×10^7 b	reductive	this work
5-Phphen	Fe ²⁺	4.5×10^7 b	reductive	this work
4,7-Ph ₂ phen	Fe ²⁺	2.5×10^7 b	reductive	this work
bpy	4-aminodiphenylamine	9.4×10^9 c	reductive	93
bpy	N,N,N',N'-tetramethylbenzidine	10.5×10^9 c	reductive	93
bpy	N,N'-diphenyl-p-phenylenediamine	7.2×10^9 c	reductive	93
bpy	benzidine	8.7×10^9 c	reductive	93
bpy	-naphthylamine	7.2×10^9 c	reductive	93
bpy	-naphthylamine	8.2×10^9 c	reductive	93
bpy	N,N'-diethylaniline	6.4×10^9 c	reductive	93
bpy	diphenylamine	9.1×10^9 c	reductive	93
bpy	triphenylamine	7.3×10^9 c	reductive	93
bpy	tributylamine	0.69×10^9 c	reductive	93
bpy	triethylamine	0.74×10^9 c	reductive	93
bpy	N,N'-Me ₂ -benzylamine	0.25×10^9 c	reductive	93
bpy	N-methylaniline	11×10^9 c	reductive	93

TABLE 3-15, cont'd.

NN	QUENCHER	2k_q ($M^{-1} \text{sec}^{-1}$)	Mechanism	Reference
bpy	dicyclohexylamine	0.20×10^9 c	reductive	93
bpy	1,2,4-(OMe) ₃ benzene	2.8×10^9 c	reductive	93
bpy	dibutylamine	0.16×10^9 c	reductive	93
bpy	dipropylamine	0.15×10^9 c	reductive	93
bpy	aniline	9.90×10^9 c	reductive	93
bpy	diethylamine	0.089×10^9 c	reductive	93
bpy	1,4-(OMe) ₂ benzene	1.1×10^9 c	reductive	93
bpy	dibenzylamine	0.010×10^9 c	reductive	93
bpy	1,2,3-(OMe) ₃ benzene	0.043×10^9 c	reductive	93
bpy	1,2-(OMe) ₂ benzene	0.24×10^9 c	reductive	93
bpy	tert-butylamine	0.014×10^9 c	reductive	93
bpy	1,3,5-(OMe) ₃ benzene	0.019×10^9 c	reductive	93
bpy	Iodide ion	14×10^8 b	reductive	this work
4,4'-Me ₂ bpy	Iodide ion	0.40×10^8 b	reductive	this work
4,4'-Ph ₂ bpy	Iodide ion	22×10^8 b	reductive	this work
5-Clphen	Iodide ion	80×10^8 b	reductive	this work

TABLE 3-15, cont'd.

NN	QUENCHER	2k_q ($M^{-1} \text{ sec}^{-1}$)	Mechanism	Reference
phen	Iodide ion	21×10^8 b	reductive	this work
4,7-Me ₂ phen	Iodide ion	1.5×10^8 b	reductive	this work
3,4,7,8-Me ₄ phen	Iodide ion	0.47×10^8 b	reductive	this work
4,7-Ph ₂ phen	Iodide ion	59×10^8 b	reductive	this work
bpy	Mo(CN) ₈ ⁴⁻	52×10^8 d	reductive	97
bpy	Fe(CN) ₆ ⁴⁻	49×10^8 d	reductive	97
bpy	Ru(CN) ₆ ⁴⁻	55×10^8 d	reductive	97
bpy	Ni(CN) ₄ ²⁻	14×10^8 d	reductive	97
bpy	Ru(bpy) ₃ ²⁺	6.1×10^8 a	reductive	86
bpy	Ru(bpy) ₃ ²⁺	4.0×10^8 e	reductive	96
4,4'-Me ₂ bpy	Ru(bpy) ₃ ²⁺	2.0×10^8 a	reductive	86
phen	Ru(bpy) ₃ ²⁺	8.3×10^8 a	reductive	86
bpy	Ru(4,4'-Me ₂ bpy) ₃ ²⁺	11×10^8 a	reductive	86
bpy	Ru(3,4,7,8-Me ₄ phen) ₃ ²⁺	13×10^8 a	reductive	86
bpy	Ru(4,7-Me ₂ phen) ₃ ²⁺	11×10^8 a	reductive	86
phen	Ru(4,7-Me ₂ phen) ₃ ²⁺	14×10^8 a	reductive	86

TABLE 3-15, cont'd.

NN	QUENCHER	k_q ($M^{-1} \text{ sec}^{-1}$)	Mechanism	Reference
bpy	$\text{Ru}(5\text{-Mephen})_3^{2+}$	9.9×10^8 a	reductive	86
4,7-Me ₂ phen	$\text{Ru}(5\text{-Mephen})_3^{2+}$	11×10^8 a	reductive	86
bpy	$\text{Ru}(\text{phen})_3^{2+}$	9.1×10^8 a	reductive	86
bpy	$\text{Ru}(5\text{-Clphen})_3^{2+}$	6.1×10^8 a	reductive	86
phen	$\text{Ru}(5\text{-Clphen})_3^{2+}$	8.1×10^8 a	reductive	86
5-Mephen	$\text{Ru}(5\text{-Clphen})_3^{2+}$	8.4×10^8 a	reductive	86
bpy	$\text{Ru}(5\text{-NO}_2\text{phen})_3^{2+}$	1.8×10^8 a	reductive	86
phen	$\text{Ru}(5\text{-NO}_2\text{phen})_3^{2+}$	2.6×10^8 a	reductive	86
bpy	$\text{Os}(\text{bpy})_3^{2+}$	15×10^8 a	reductive	86
phen	$\text{Os}(\text{bpy})_3^{2+}$	15×10^8 a	reductive	86
bpy	$\text{Ru}(\text{bpy})_3^{3+}$	0.06×10^8 a	oxidative ?	86
bpy	$\text{Os}(\text{bpy})_3^{3+}$	0.01×10^8 a	oxidative ?	86
bpy	$\text{Fe}(\text{CN})_6^{3-}$	2.6×10^8 d	oxidative ?	97
bpy	$\text{Co}(\text{CN})_6^{3-}$	0.002×10^8 d	oxidative ?	97

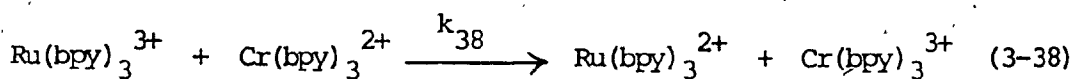
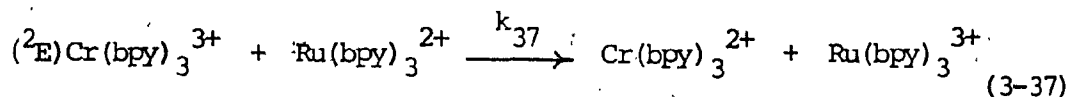
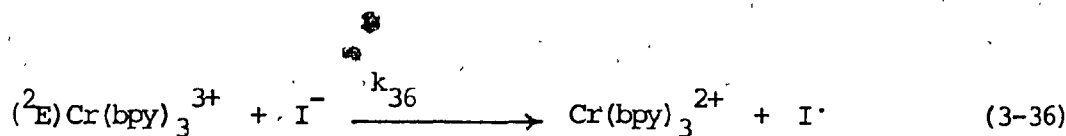
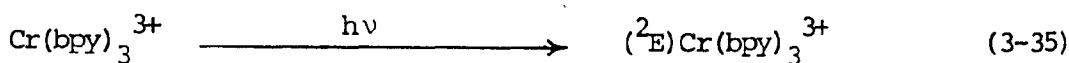
a In 1 M H₂SO₄, at 25°C. b In 1 M HCl, at 25°C. c In 0.02 M TEAP in acetonitrile, at 22°C.

d In water, 0.5 M NaCl, at ca. 20°C. e In water, $\mu = 0.2$, at 25°C.

constant of the aliphatic amines as compared to that for the aromatic amines, as was experimentally observed.⁹³

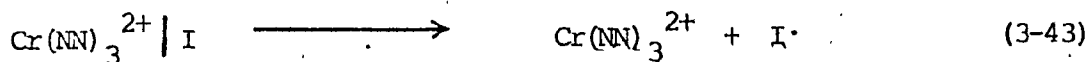
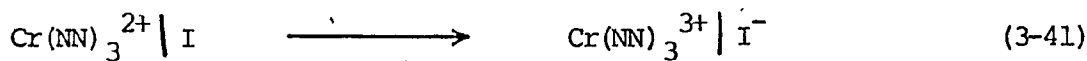
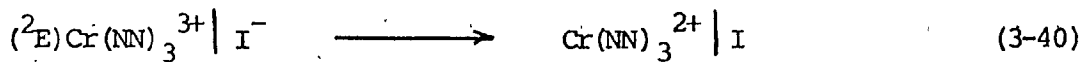
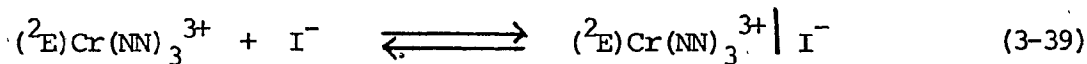
c. The $\text{Cr}(\text{NN})_3^{3+}$ /iodide ion Systems.

Flash photolysis experiments carried out in the presence of iodide ion, which selectively quenches the ${}^2T_1/{}^2E$ state of $\text{Cr}(\text{bpy})_3^{3+}$, unequivocally demonstrates⁹⁵ that reductive electron transfer occurs via



where $k_{36} = 1.4 \times 10^9 \text{ M}^{-1} \text{ sec}^{-1}$, $k_{37} = 4.0 \times 10^8 \text{ M}^{-1} \text{ sec}^{-1}$,⁹⁶ and $k_{38} = 2.6 \times 10^9 \text{ M}^{-1} \text{ sec}^{-1}$.⁹⁵ The products of reaction (3-37) are not observed because of the rapid thermal back electron transfer reaction (3-38). Reactions (3-36) and (3-37) demonstrate that the 2E state of $\text{Cr}(\text{bpy})_3^{3+}$ is a strong oxidizing agent. Table 3-15 shows the rate constants for reductive electron transfer quenching (reaction 3-36) by the iodide ion for several $\text{Cr}(\text{NN})_3^{3+}$ complex ions, as determined by lifetime quenching experiments in 1 M HCl at 25°C. The data reveal that the rate constant k_q varies from $4 \times 10^7 \text{ M}^{-1} \text{ sec}^{-1}$ for $({}^2E)\text{Cr}(4,4'\text{-Me}_2\text{bpy})_3^{3+}$ and $({}^2E)\text{Cr}(3,4,7,8\text{-Me}_4\text{phen})_3^{3+}$ to $8 \times 10^9 \text{ M}^{-1} \text{ sec}^{-1}$ for $({}^2E)\text{Cr}(5\text{-Clphen})_3^{3+}$ under these

experimental conditions. It should be noted that the reduction potential for the $I \cdot / I^-$ couple in aqueous solution has been estimated⁵⁷ as 1.40 V. Thus, the reaction of $(^2E)Cr(NN)_3^{3+}$ with I^- can be viewed as occurring via reactions (3-39) to (3-43). In the flash photolysis of $Cr(bpy)_3^{3+}$ in the presence of I^- , the 2E absorption is rapidly quenched but absorptions due to $Cr(bpy)_3^{2+}$ (λ_{max} 560 nm)⁸ or I_2^- (λ_{max} 380 nm) were not detected. Evidently, I atoms never escape the solvent cages and $k_{41} \gg k_{43}$.



d. The $Cr(bpy)_3^{3+}/M(CN)_x^{n+}$ Systems.

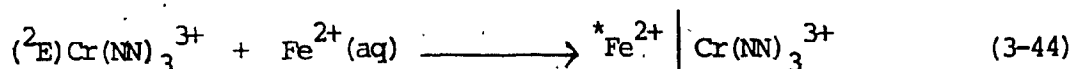
Luminescence quenching of $(^2E)Cr(bpy)_3^{3+}$ by various transition metal cyanide complexes has been studied by Juris et al.⁹⁷ It was concluded that quenching of $(^2E)Cr(bpy)_3^{3+}$ occurs via reductive electron transfer with $Mo(CN)_8^{4-}$, $Fe(CN)_6^{4-}$, $Ru(CN)_6^{4-}$, and $Ni(CN)_4^{2-}$; via oxidative electron transfer with $Fe(CN)_6^{3-}$ and $Co(CN)_6^{3-}$; and via energy transfer with $Cr(CN)_6^{3-}$. Discrimination between the possible quenching pathways may not be based solely on experimental observation of reduced or oxidized products, since a thermal reverse electron transfer reaction

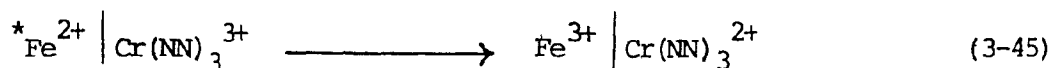
so often occurs (vide infra): nor can it be solely based on the experimentally-obtained k_q values. But, inferences on the operable mechanism may be obtained from relationships between k_q and thermodynamic quantities which determine the driving force for the reaction, including the excited-state energy for energy transfer processes, and the redox potentials of the excited-state and quencher species for oxidative and reductive electron transfer processes.

e. The $\text{Cr}(\text{NN})_3^{3+}/\text{Fe}^{2+}(\text{aq})$ Systems.

$\text{Cr}(\text{bpy})_3^{2+}$ has been used for many years as a reducing agent in inorganic ground-state electron transfer reactions. Interest in the properties of chromium(II) polypyridyl complexes has increased in recent years due to the observation by us and others^{86,95} that $\text{Cr}(\text{NN})_3^{2+}$ can be generated photochemically from the reductive quenching of $(^2\text{E})\text{Cr}(\text{NN})_3^{3+}$. As part of the systematic understanding of the competitive modes of energy partitioning in excited states, this study focused on the formation of $\text{Cr}(\text{NN})_3^{2+}$ by the reductive quenching of $(^2\text{E})\text{Cr}(\text{NN})_3^{3+}$ with $\text{Fe}^{2+}(\text{aq})$ and by direct reduction of $\text{Cr}(\text{NN})_3^{3+}$ with radiation-generated free radicals.

$\text{Fe}^{2+}(\text{aq})$ is an efficient quencher of $(^2\text{E})\text{Cr}(\text{bpy})_3^{3+}$. At pH 3, flash photolysis of a solution containing $\text{Cr}(\text{bpy})_3^{3+}$ and FeSO_4 produced a transient absorption (maxima at 470 and 560 nm)^{86,95} closely resembling the spectrum of $\text{Cr}(\text{bpy})_3^{2+}$.⁸ The formation of $\text{Cr}(\text{bpy})_3^{2+}$ clearly indicates a reductive electron transfer mechanism for the quenching of $(^2\text{E})\text{Cr}(\text{bpy})_3^{3+}$ by $\text{Fe}^{2+}(\text{aq})$. Additionally, Brunschwig and Sutin⁸⁶ have advanced the possibility that the observed electron transfer products could be produced if an energy transfer step occurred prior to the electron transfer step,





The availability of low-lying excited states of $\text{Fe}^{2+}(\text{aq})$ at $10.4 \times 10^3 \text{ cm}^{-1}$ ($^5\text{T}_{2g}$) and ca. $14.4 \times 10^3 \text{ cm}^{-1}$ (probably $^3\text{T}_{1g}$)⁶⁰ above the $^1\text{A}_{1g}$ ground state renders direct energy transfer energetically feasible.

Furthermore, reaction (3-45) is thermodynamically allowed insofar as the reduction potentials of the $^5\text{T}_{2g}$ and $^3\text{T}_{1g}$ Fe^{2+} excited states are ~ -0.5 and $\sim +1.0$ V, respectively. For such a pathway to be feasible, reaction (3-45) would necessarily have to be faster than an electron transfer process involving the encounter complex from reaction (3-44); i.e., faster than reaction (3-46). The involvement of an energy transfer

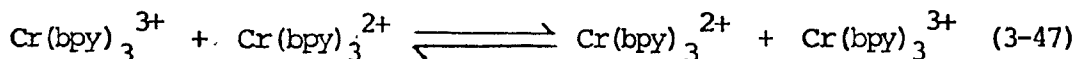


was thus thought⁸⁶ to be improbable inasmuch as reaction (3-45) would likely require more reorganizational energy than reaction (3-46); and also, the orbital symmetry for reaction (3-45) would be less favorable than for reaction (3-46). In reaction (3-46), an electron is transferred from a t_{2g} (bonding) orbital on the Fe^{2+} to a t_{2g} (bonding orbital on Cr^{3+} ; whereas in reaction (3-45), the electron is transferred from an anti-bonding orbital of $*\text{Fe}^{2+}$ to a bonding orbital on Cr^{3+} .

The rate constants (k_q) for the quenching of several $\text{Cr}(\text{NN})_3^{3+}$ complex ions by $\text{Fe}^{2+}(\text{aq})$ in air-equilibrated, aqueous solution (1.0 M HCl) at 25°C have been measured by the luminescence intensity quenching technique and by flash photolysis. Linear Stern-Volmer plots of I_0/I vs $[\text{Fe}^{2+}]$ were obtained in all cases. The k_q values obtained are included in Table 3-15. Additional support for an electron transfer quenching

pathway is the observed dependence of k_q on $\text{Cr}^{3+}/\text{Cr}^{2+}$ reduction potentials. Thus, the plot of $\log k_q$ vs ΔE^f shown in Figure 3-16, where $\Delta E^f = E^f(\text{Cr}(\text{NN})_3^{3+/2+}) - E^f(\text{Cr}(\text{phen})_3^{3+/2+})$ or $E^f(\text{Cr}(\text{NN})_3^{3+/2+}) - E^f(\text{Cr}(\text{bpy})_3^{3+/2+})$, is linear; and the strongest oxidants (5-Clphen and 5-Brphen complexes) give the highest rate constants. Such a dependence has been previously taken as evidence for an electron transfer pathway in the quenching of the MCT states of $\text{Ru}(\text{NN})_3^{2+}$ by $\text{Eu}(\text{III})^{44}$ and $\text{Eu}(\text{II})^{98}$. Furthermore, the excited-state redox potentials, $E^O(\text{Cr}^{3+}/\text{Cr}^{2+})$, also reveal that the strongest oxidant has the highest k_q value (cf. Table 3-14).

Having established a reductive electron transfer quenching mechanism, the quenching data obtained for the (2E) states of the closely related $\text{Cr}(\text{NN})_3^{3+}$ complexes can now be applied to the Marcus theory of electron transfer reactions.^{84,85} Application of the Marcus theory for outer-sphere electron transfer processes in the form of equations (3-23) and (3-27) has afforded the estimation of the self-exchange rate constant k_{22} for reaction (3-25). Further, the determination of k_{22} for this reaction allows the comparison between the excited-state reaction (reaction 3-25) and the ground-state reaction (3-47), inasmuch as the ground and

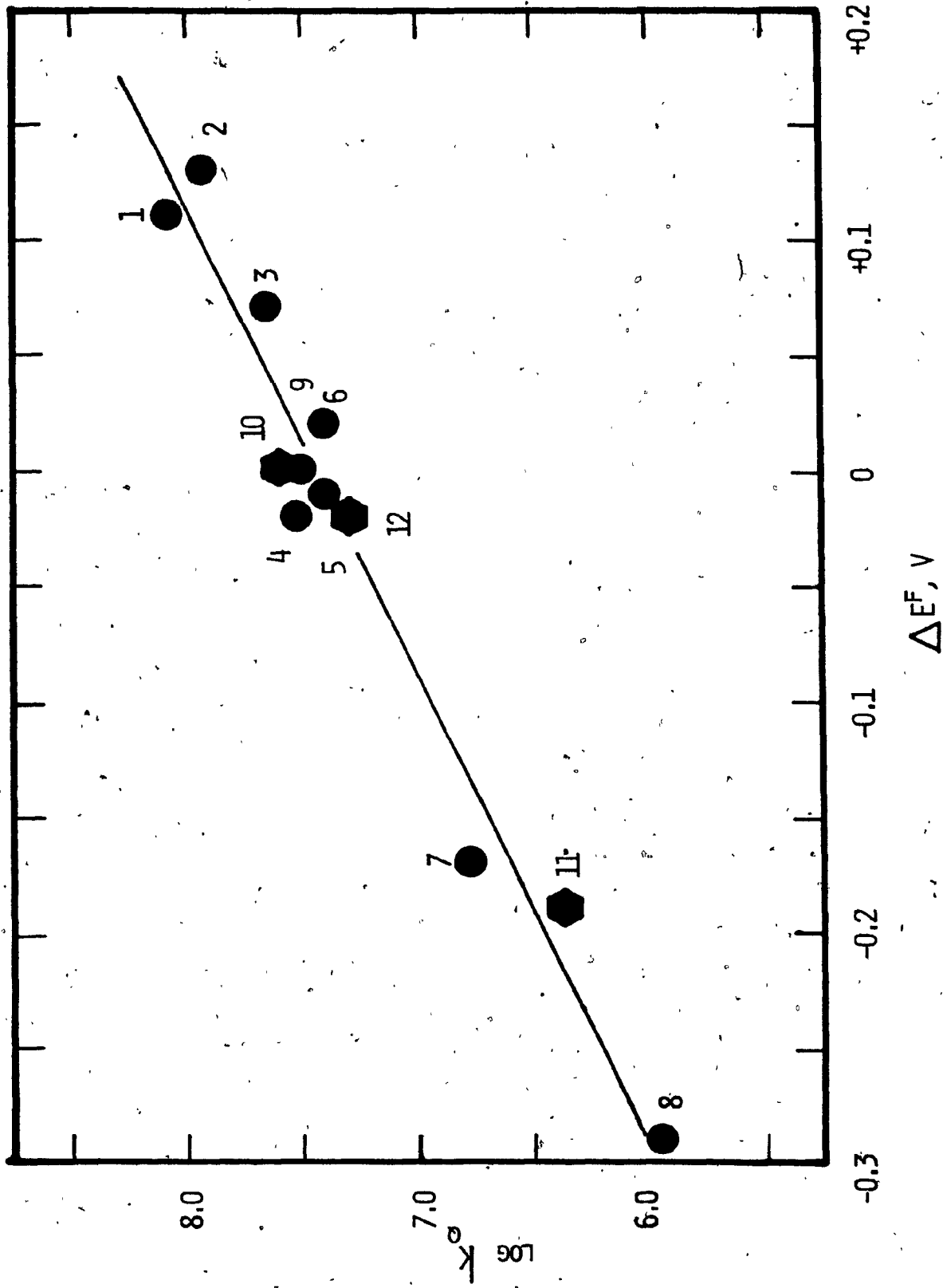


excited states may differ in shape, size and/or dipole moment. The difference between the two should be reflected in the reorganizational energy parameter λ (see equations 3-20 and 3-21). Since the Stokes shift between the ground-state absorption and excited-state emission is related to the nuclear coordinates of these states, it is also expected that the

FIGURE 3-16 : Plot of $\log k_q$ vs ΔE^f (see text) for Reductive
Electron Transfer Quenching of $({}^2T_1/{}^2E)Cr(NN)_3^{3+}$

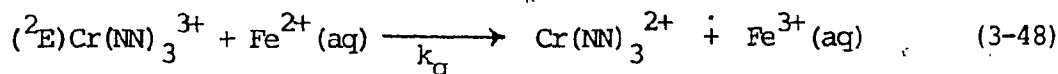
by $Fe^{2+}(aq)$;

- 1 5-Clphen[†]
- 2 5-Brphen
- 3 5-Phphen
- 4 5-Mephen
- 5 5,6-Me₂phen
- 6 4,7-Ph₂phen
- 7 4,7-Me₂phen
- 8 3,4,7,8-Me₄phen
- 9 phen
- 10 bpy
- 11 4,4'-Me₂bpy
- 12 4,4'-Ph₂bpy

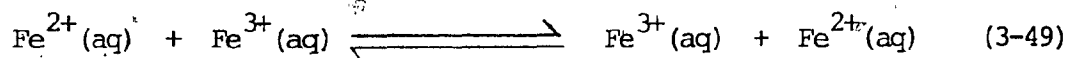


Stokes shift is related to the difference in λ between the ground and excited states. Hence, an observed Stokes shift of zero, as is the case for $\text{Cr}(\text{NN})_3^{3+}$ complex ions, would necessarily imply similar reorganizational energies for the two states.

Several groups^{86,99,100} including ours have recently estimated the self-exchange rate constant for reaction (3-25), based on Marcus theory. Both Brunschwig and Sutin⁸⁶ and our group have determined the self-exchange rate using $\text{Fe}^{2+}(\text{aq})$ as the quencher species, as per reaction (3-48).



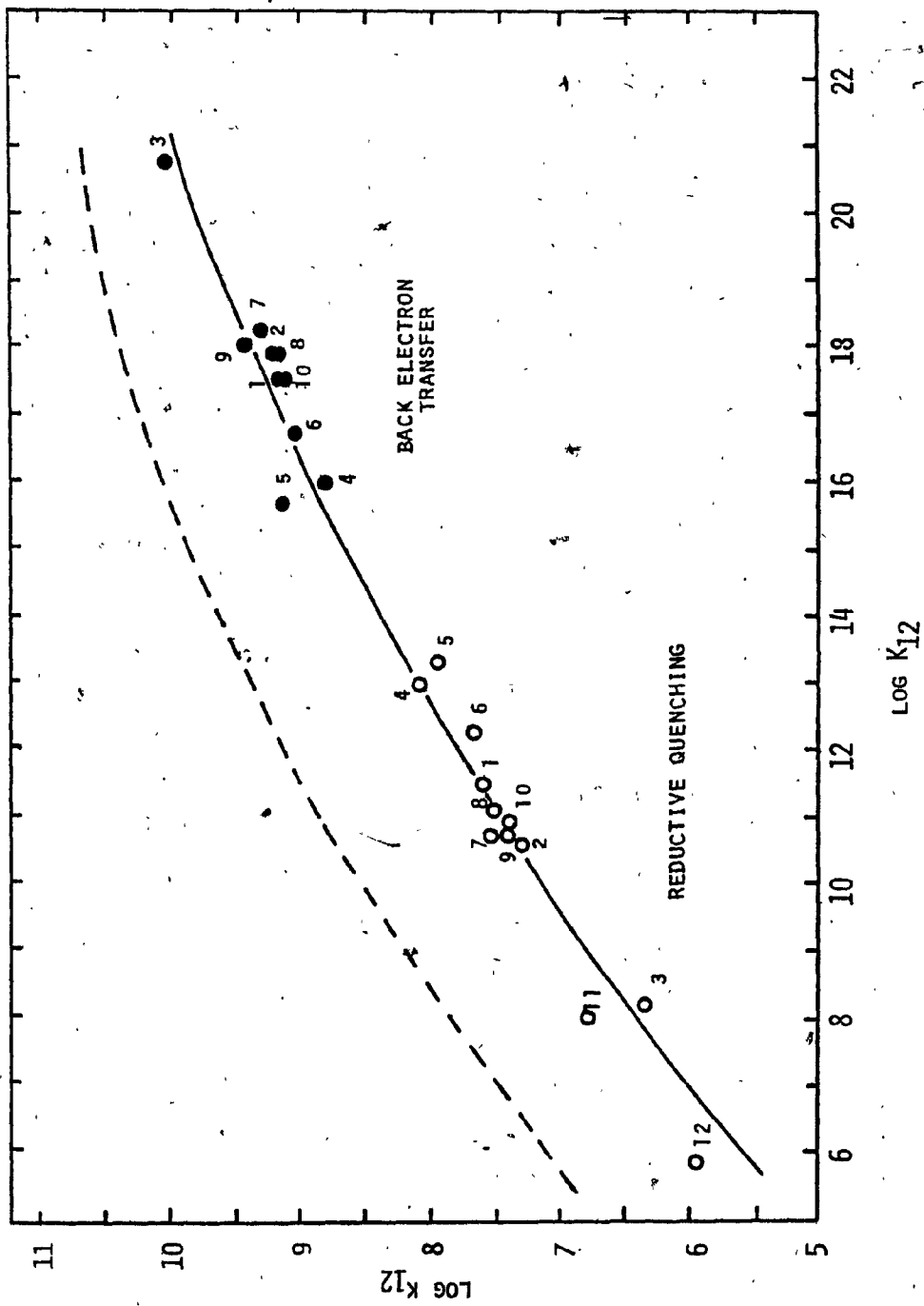
The corresponding self-exchange reactions are noted in reactions (3-25) and (3-49), with k_{22} and k_{11} as the self-exchange rate constants, respectively. Taking $k_{11} = 4.0 \text{ M}^{-1} \text{ sec}^{-1}$,¹⁰¹ an "apparent" k_{22} of $\sim 10^5 \text{ M}^{-1}$



sec^{-1} was obtained from the intercept of the $\log k_{12}$ vs $\log K_{12}$ plot shown in Figure 3-17. Our previous estimation of $k_{22} \sim 10^7 \text{ M}^{-1} \text{ sec}^{-1}$ did not incorporate the α term in equation (3-27). The linear relationship between $\log k_{12}$ and $\log K_{12}$ further supports the formulation of an electron transfer quenching process. In a related study, Brunschwig and Sutin⁸⁶ estimated $k_{22} \sim 1 \times 10^8 \text{ M}^{-1} \text{ sec}^{-1}$ in $1 \text{ M H}_2\text{SO}_4$ at 25°C for the $\text{Cr}(\text{NN})_3^{3+}/\text{Fe}^{2+}(\text{aq})$ system. Some controversy arose surrounding this value, owing to the experimental evaluation of an intercept = 1.7 from the $\log k_{12}$ vs $\log K_{12}$ plot, which yields $k_{\text{ex}} \approx 600 \text{ M}^{-1} \text{ sec}^{-1}$. The six orders of magnitude discrepancy between the experimental and theoretically estimated

FIGURE 3-17 : $\log k_q$ vs $\log K_{12}$ Plot (●) for the Quenching of (${}^2T_1/{}^2E$)- $\text{Cr}(\text{NN})_3^{3+}$ by $\text{Fe}^{2+}(\text{aq})$ in Air-equilibrated 1 M HCl Aqueous Solutions; (○) $\log k_{12}$ vs $\log K_{12}$ Plot for the Reduction $\text{Fe}^{3+}(\text{aq})$ by $\text{Cr}(\text{NN})_3^{2+}$ Transients.

The dashed line is the calculated curve for $k_{22} \approx 10^8 \text{ M}^{-1} \text{ sec}^{-1}$ and the solid line is the calculated curve for $k_{22} \approx 10^5 \text{ M}^{-1} \text{ sec}^{-1}$. The numbers indicate the following NN: (1) bpy, (2) 4,4'-Ph₂bpy, (3) 4,4'-Me₂bpy, (4) 5-Cl-phen, (5) 5-Brphen, (6) 5-Phphen, (7) 5-Mephen, (8) phen, (9) 5,6-Me₂phen, (10) 4,7-Ph₂phen, and (11) 4,7-Me₂phen.

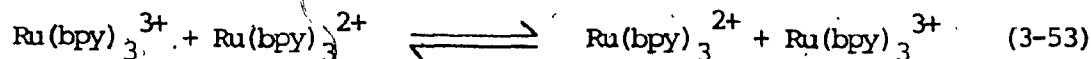
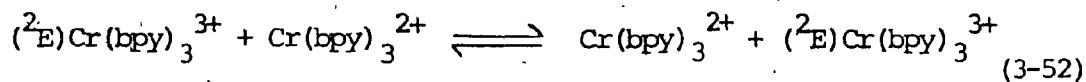
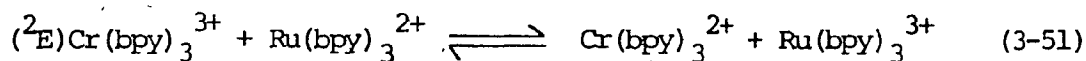


values was explained⁸⁶ in terms of the non-adiabaticity of reaction (3-48), while the self-exchange reactions (3-25) and (3-49) are probably adiabatic. Thus, the Marcus relationship in equation (3-23) was modified to include a term for the probability of electron transfer in the activated complex;¹⁰²

$$k_{12}^* = p_{12} (k_{11} k_{22} K_{12} f_{12} / p_{11} p_{22})^{1/2} \quad (3-50)$$

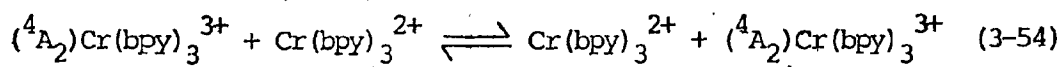
where p are the respective probabilities of electron transfer in the activated complexes. Equation (3-50) reduces to equation (3-23) when all reactions are adiabatic; that is, when $p_{12} = p_{11} = p_{22} = 1$. If, as is believed to be the case here, reaction (3-48) is non-adiabatic, then $p_{11} = p_{22} = 1$ and $p_{12} \ll 1$, and a plot of $\log k_{12}$ vs $\log K_{12}$ yields an intercept from which $k_{22} p_{12}^2$, (rather than k_{22}), is evaluated. Thus, the uncorrected intercept will yield a k_{22} value that is p_{12}^2 lower than expected. Under these assumptions, $k_{22} \sim 10^8 - 10^9 \text{ M}^{-1} \text{ sec}^{-1}$ seems plausible.⁸⁶

Endicott and Ferraudi¹⁰⁰ have estimated k_{22} for the $(^2\text{E})\text{Cr}(\text{bpy})_3^{3+} / \text{Cr}(\text{bpy})_3^{2+}$ couple to be $\sim 3 \times 10^5 \text{ M}^{-1} \text{ sec}^{-1}$, based on data for the $\text{Ru}(\text{bpy})_3^{2+} / (^2\text{E})\text{Cr}(\text{bpy})_3^{3+}$ cross-reaction (3-51), and self-exchange reactions (3-52) and (3-53) for which $k_{11} = 4 \times 10^9 \text{ M}^{-1} \text{ sec}^{-1}$ ^{44,83} for (3-53).



On the other hand, Brunshwig and Sutin⁸⁶ estimated $k_{22} \sim 1 \times 10^8 \text{ M}^{-1} \text{ sec}^{-1}$ from a series of $\text{Ru}(\text{NN})_3^{2+} / ({}^2\text{E})\text{Cr}(\text{NN})_3^{3+}$ reactions in which the ligands NN on both Cr(III) and Ru(II) were varied.

The self-exchange rate constant for the ground-state reaction (3-47) was estimated by Sutin⁸⁶ to be ca. $10^8 - 10^9 \text{ M}^{-1} \text{ sec}^{-1}$; whereas Ferraudi and Endicott⁹⁹ have reported $k_{\text{ex}} \approx 4 \times 10^9 \text{ M}^{-1} \text{ sec}^{-1}$ for reaction (3-54)



from flash photolysis studies of $\text{Cr}(\text{bpy})_3^{3+}$ in the presence of $\text{Cr}(4,7\text{-Me}_2\text{-phen})_3^{3+}$ in methanolic solutions at 25°C. These results on the evaluation of self-exchange reaction rate constants are important in that they demonstrate the similarities in the ground-state and excited-state self-exchange reactions. This is not unexpected in view of the fact that the reactants in both reaction (3-25) and (3-54) have the same size and charges, and the ${}^4\text{A}_2$ and ${}^2\text{E}$ states are virtually undistorted with respect to each other, thereby indicating that the work terms and solvent reorganization barriers for the two reactions will be the same. These similarities then appear to suggest that the ground- and excited-state reactions can only differ with respect to their inner-sphere barriers to electron transfer, $\Delta G_{\text{in}}^\ddagger$.⁸⁶ For metal-centered states, the differences in these barriers have been approximated⁸⁶ by equation (3-55), where f is a

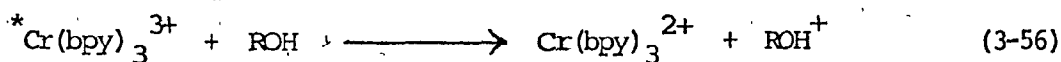
$$\begin{aligned} \Delta(\Delta G_{\text{in}}^\ddagger) &= {}^* \Delta G_{\text{in}}^\ddagger - \Delta G_{\text{in}}^\ddagger \\ &= \frac{3f_2}{(f_2+f_3)} \left[(f_3^* - f_3) a_2^2 + \left(\frac{E_s}{6} \frac{a_3^* + a_3 + 2a_2}{a_3^* + a_3} \right) \right] \end{aligned} \quad (3-55)$$

breathing force constant, "a" is the Cr-N bond length, and subscripts 2 and 3 denote the charge on the complex. The $3f_2/(f_2+f_3)$ term is expected¹⁰³ to be small inasmuch as the 4A_2 and 2E states of $\text{Cr}(\text{NN})_3^{3+}$ have the same electron configuration. The second term in equation (3-55) has five possible fates. These include: (i) $E_S = 0$; that is, $(a_3^* - a_3) = 0$; (ii) $a_3^* > a_3$ and $a_2 > 1/2(a_3^* + a_3)$; (iii) $a_3^* > a_3$ but $a_2 < 1/2(a_3^* + a_3)$; (iv) $a_3^* < a_3$ and $a_2 > 1/2(a_3^* + a_3)$; and (v) $a_3^* < a_3$ but $a_2 < 1/2(a_3^* + a_3)$. Fate (i) implies that $\Delta(\Delta G_{\text{in}}^\ddagger) = 0$ and the inner-sphere barriers for the ground- and excited-state self-exchange reactions are the same. Fates (ii) and (v) imply that $^* \Delta G_{\text{in}}^\ddagger < \Delta G_{\text{in}}^\ddagger$, while fates (iii) and (iv) indicate that $^* \Delta G_{\text{in}}^\ddagger > \Delta G_{\text{in}}^\ddagger$. The fate observed depends on whether the excited-state Cr-N bonds expand or compress, compared to the ground-state Cr-N bonds. For the $\text{Cr}(\text{NN})_3^{3+}/\text{Cr}(\text{NN})_3^{2+}$ system, it is expected that only the number of t_{2g} electrons changes, and thus the Cr-N bond lengths do not change appreciably. Thus, fate (i) is thought most likely; that is, $(a_3^* - a_3) = 0$, and therefore $\Delta(\Delta G_{\text{in}}^\ddagger) = 0$ and inner-sphere barriers are the same for the ground- and excited-state reactions. This reasoning then leads to the suggestion that the exchange rate for the two reactions should be the same, as was observed.

Involvement of the 4T_2 state in the excited-state exchange reaction has been suggested.⁹⁹ However, the lifetime of the $(^4T_2)\text{Cr}(\text{bpy})_3^{3+}$ has been estimated to be of the order of 10^{-11} sec;⁴⁵ thus, this state cannot be involved in reaction (3-25) since $a_3^* > a_3$, and because its lifetime is too short to be involved in bimolecular reactions. The other possibility is the 2T_1 excited state, in thermal equilibrium with the 2E state. Although the 2T_1 and 2E states have the same overall t_{2g}^3 orbital configuration, the 2T_1 state differs in that the spin density of one of the t_{2g}

orbitals is drastically reduced; (α, α, β) for the 2E state and ($\alpha, \alpha\beta, _$) for the 2T_1 state. In our studies of the ligand labilization of $({}^2E)\text{-Cr}(\text{bpy})_3^{3+}$, it was concluded that the 2T_1 state was the reactive entity due to the vacant t_{2g} orbital situated in the vicinity of the interligand pockets. However, if the 2T_1 state were the sole contributor to reaction (3-25), and to the extent that the overall rate constant for this reaction is $\sim 10^8 - 10^9 \text{ M}^{-1} \text{ sec}^{-1}$, taking into account the population of the 2T_1 state, k_{ex} is expected to be $\sim 10^9 - 10^{10} \text{ M}^{-1} \text{ sec}^{-1}$. Unfortunately, the presently available data and the uncertainties inherent in the Marcus relationships for electron transfer processes preclude a delineation as to the reactive state in the self-exchange reaction (3-25) involving the ${}^2T_1/{}^2E$ pair.

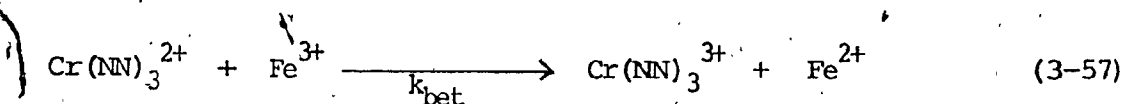
It is interesting to note that the 2E excited state does not appear to be implicated in the reductive quenching of ${}^* \text{Cr}(\text{bpy})_3^{3+}$ in alcoholic media,⁹⁹ reaction (3-56). This suggestion was attributed to observations



that both the $({}^2E)\text{Cr}(\text{bpy})_3^{3+}$ transient and $\text{Cr}(\text{bpy})_3^{2+}$ were detected in aqueous alkaline and alcoholic media, and that the $({}^2E)\text{Cr}(\text{bpy})_3^{3+}$ lifetime was relatively independent of solution medium while the yield of $({}^2E)\text{Cr}(\text{bpy})_3^{3+}$ was medium-dependent. It was further suggested⁹⁹ that the solvent-dependent process leading to the chromium(II) species is a prompt, upper-state process that occurs in competition with excited-state relaxation to form the $({}^2E)\text{Cr}(\text{bpy})_3^{3+}$ transient species. Thus, Ferraudi and Endicott⁹⁹ implicate the involvement of either 4T_2 or 2T_2 or some higher excited state in reaction (3-56). It is worth noting at

this point that 2E lifetimes are not independent of solution medium.

As mentioned previously, net electron transfer products are not always observed owing to the rapid thermal reverse electron transfer process. To this extent, it is important to determine the rate of this back reaction and compare it to the forward excited-state electron transfer process. The rate constants, k_q and k_{bet} , have been determined for the $Cr(NN)_3^{3+}/Fe^{2+}$ (aq) system, as depicted in reactions (3-48) and (3-57).



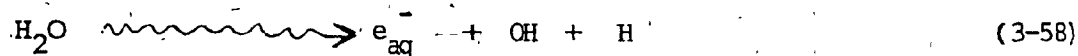
The quenching mechanism in (3-48) has previously been assigned to reductive electron transfer, and the rate constants k_q are given in Table 3-16 for the various $Cr(NN)_3^{3+}$ complex ions investigated. The rate constants for the back electron transfer reaction (3-57), k_{bet} , were obtained by flash photolysis experiments from the second-order decay of $Cr(NN)_3^{2+}$ according to reaction (3-57); $Cr(NN)_3^{2+}$ and Fe^{3+} (aq) are generated in equimolar amounts in reaction (3-48). For the 4,7-Me₂phen and 3,4,7,8-Me₄phen complexes, the low k_q values ($\sim 10^6 M^{-1} sec^{-1}$) for reaction (3-48) required rather large Fe^{2+} (aq) quencher concentrations in order to completely quench $({}^2E)Cr(NN)_3^{3+}$. Unfortunately, the concentration of Fe^{3+} impurity in the $Fe(NH_4)_2(SO_4)_2$ used showed pseudo-first-order kinetics, too rapid to be followed within the time resolution of the flash photolysis apparatus ($\sim 30 \mu sec$). In order to study the back reaction for these two complex ions, it was necessary to generate $Cr(NN)_3^{2+}$ via the reduction of $Cr(NN)_3^{3+}$ by the $\alpha-(CH_3)_2COH$ radical at pH ~ 1 . The pulse radiolysis of aqueous acidic solutions of 2-propanol results in the decomposition of the solvent according to the following stoichiometry.

TABLE 3-16 : Electron Transfer Rate Constants (k_q) and Thermal Back Electron Transfer Rate Constants (k_{bet}) for the Cr(NN) $_3^{3+}$ Fe $^{2+}$ (aq) Systems at 22 - 24°C.^a

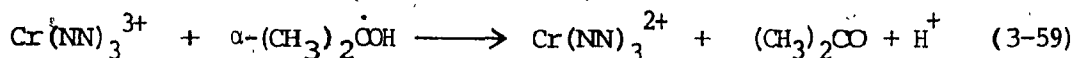
NN	$k_q \times 10^{-7}$, (M $^{-1}$ sec $^{-1}$)	$k_{bet} \times 10^{-9}$, (M $^{-1}$ sec $^{-1}$)
bpy	3.7	1.44 \pm 0.04
4,4'-Me $_2$ bpy	0.22	10.6 \pm 0.6
4,4'-Ph $_2$ bpy	2.0	1.6 \pm 0.2
5-Clphen	12	0.61 \pm 0.08
5-Brphen	8.4	1.4 \pm 0.4
phen	3.2	1.3 \pm 0.3
5-Mephen	3.4	2.0 \pm 0.7
5,6-Me $_2$ phen	2.6	2.7 \pm 1.0
4,7-Me $_2$ phen	0.60	(7) ^b
3,4,7,8,-Me $_4$ phen	0.092	(18) ^b
5-Phphen	4.5	1.9 \pm 0.6
4,7-Ph $_2$ phen	2.5	1.4 \pm 0.4

TABLE 3-16, cont'd.

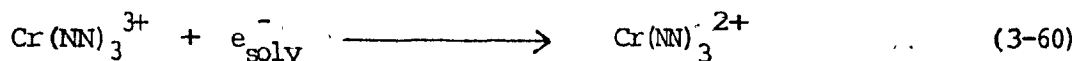
a In 1 M HCl, 22-24°C. b The experimental k_{bet} value was obtained at pH 1 and $\mu = 0.15$; the k_{bet} value is estimated from the appropriate $E^{\circ}(\text{Cr}^{3+}/2^{+})$ value and the data at $\mu = 1.0$.



In the presence of acid, e_{aq}^- is efficiently scavenged by H^+ , yielding H atoms. The presence of 2-propanol allows for reaction between H and OH to form α - $(\text{CH}_3)_2\dot{\text{C}}\text{OH}$ and β - $(\text{CH}_3)_2\dot{\text{C}}\text{OH}$ radicals. The α -radical is a rather good reducing agent ($E^0 = -1.2 \text{ V vs NHE}$)⁵⁷ and can reduce $\text{Cr}(\text{NN})_3^{3+}$ to $\text{Cr}(\text{NN})_3^{2+}$ via reaction (3-59). Also, the e_{solv}^- species is capable



of reducing $\text{Cr}(\text{NN})_3^{3+}$ to $\text{Cr}(\text{NN})_3^{2+}$, as per reaction (3-60). The rate



constants k_{bet} for the back electron transfer reaction (3-57) are included in Table 3-16 for various $\text{Cr}(\text{NN})_3^{2+}$ complex ions. It is observed in Table 3-16 that the values of k_{bet} span the range of $10^8 - 10^{10} \text{ M}^{-1} \text{ sec}^{-1}$, with the slowest rate afforded by the 5-Clphen complex and the fastest by the 3,4,7,8-Me₄phen complex.

The data for k_{bet} can also be treated by the Marcus relationships (3-18) to (3-20), (3-23) and (3-27). The plot of $\log k_{\text{bet}}$ vs $\log K_{12}$, shown in Figure 3-17 by the closed circles, yields an "apparent" self-exchange rate constant for reaction (3-54) of $\sim 10^5 \text{ M}^{-1} \text{ sec}^{-1}$, with the actual value of $10^8 - 10^9 \text{ M}^{-1} \text{ sec}^{-1}$. Ferraudi and Endicott's⁹⁹ value of $\sim 4 \times 10^9 \text{ M}^{-1} \text{ sec}^{-1}$ for $\text{Cr}(\text{bpy})_3^{3+}$ in 90% methanol at 25°C may reflect the different solution media used and the errors intrinsic in the techniques employed. It must be noted that for very similar conditions of

solution medium, temperature and ionic strength, the rate of excited-state self-exchange reaction (3-25) is identical with the corresponding rate of the ground-state self-exchange reaction (3-54).

The kinetics of formation of $\text{Cr}(\text{NN})_3^{2+}$ via reactions (3-59) or (3-60) have been evaluated; the values of the rate constants k for these reactions are included in Table 3-17 along with the wavelength at which formation of $\text{Cr}(\text{NN})_3^{2+}$ was monitored. The 3,4,7,8-Me₄phen complex was too insoluble in aqueous and methanolic media to afford the Cr(II) spectrum. From the fact that e_{solv}^- and $(\text{CH}_3)_2\text{COH}^\cdot$ were scavenged quantitatively and rapidly, the values of the extinction coefficients (ϵ) of the absorption bands of $\text{Cr}(\text{NN})_3^{2+}$ were obtainable as a function of wavelength. The absorption spectra (300 - 750 nm) of the $\text{Cr}(\text{NN})_3^{2+}$ complexes obtained from the reduction of $\text{Cr}(\text{NN})_3^{3+}$ by e_{solv}^- or $\alpha\text{-(CH}_3)_2\text{COH}^\cdot$ are presented in Figures 3-18a - j. Additionally, $\text{Cr}(\text{NN})_3^{2+}$ can be generated by the reductive quenching of $(^2\text{E})\text{Cr}(\text{NN})_3^{3+}$ by $\text{Fe}^{2+}(\text{aq})$ in flash photolysis experiments. The $\text{Cr}(\text{NN})_3^{2+}$ spectra recorded 50 μsec after the flash upon complete quenching of $(^2\text{E})\text{Cr}(\text{NN})_3^{3+}$ by $\text{Fe}^{2+}(\text{aq})$ are also included in Figures 3-18a - j. A comparison of the $\text{Cr}(\text{NN})_3^{2+}$ spectra obtained by the two techniques shows reasonable coincidence. The $\text{Cr}(\text{NN})_3^{2+}$ absorption band maxima and ϵ values are summarized in Table 3-18.

The absorption spectrum of $\text{Cr}(\text{bpy})_3^{2+}$ has been reported by König and Herzog;⁸ their spectrum is reproduced in Figure 3-18a and is compared with that obtained here. At $\lambda > 310$ nm, the bands have been assigned as arising from ligand-to-metal charge-transfer (LMCT) transitions on the basis of intensity, while at $\lambda < 310$ nm, the spectrum was thought to arise from intra-ligand (IL) transitions.⁸ Interestingly, despite the band intensities ($\log \epsilon \approx 3 - 4$), the band maxima at 310 - 830 nm could

TABLE 3-17 : Rate Constants (k) and Monitoring Wavelength for the Formation of $\text{Cr}(\text{NN})_3^{2+}$

$\text{Cr}(\text{NN})_3^{2+}$	$k \times 10^{-9}, (\text{M}^{-1} \text{sec}^{-1})$ (reducing agent + $\text{Cr}(\text{III})$)	Monitoring Wavelength, (nm) ^a
bpy	---	---
4,4'-Me ₂ bpy	2; $(\text{CH}_3)_2\dot{\text{C}}\text{OH}$	480
4,4'-Ph ₂ bpy	100; e ⁻ _{solv}	600
5-Clphen	2.8; $(\text{CH}_3)_2\dot{\text{C}}\text{OH}$	400
5-Brphen	3.8; $(\text{CH}_3)_2\dot{\text{C}}\text{OH}$	420
5-Phphen	50 - 80; e ⁻ _{solv}	---
5-Mephen	3.1; $(\text{CH}_3)_2\dot{\text{C}}\text{OH}$	400
phen	4.1; $(\text{CH}_3)_2\dot{\text{C}}\text{OH}$	480
5,6-Me ₂ phen	3.6; $(\text{CH}_3)_2\dot{\text{C}}\text{OH}$	420
4,7-Ph ₂ phen	82; e ⁻ _{solv}	575
4,7-Me ₂ phen	81; e ⁻ _{solv}	575

^a Wavelength at which kinetics were monitored.

FIGURE 3-18 a : Absorption Spectra of $\text{Cr}(\text{bpy})_3^{2+}$ (reference 102),
dashed line, O, (this work), and of the $\text{Cr}(4,4'\text{-Me}_2\text{bpy})_3^{2+}$ (●—●) Transient Obtained by Reduc-
tion of the Corresponding Cr(III) Complex ($53 \mu\text{M}$)
with $(\text{CH}_3)_2\dot{\text{C}}\text{OH}$ at pH ca. 1 in Argon-purged
Solutions Containing 0.26 M 2-propanol and 0.05 M
 H_2SO_4 Dose/pulse = 1.30 krad; $G(\text{Cr}^{\text{II}}) = 5.5$.

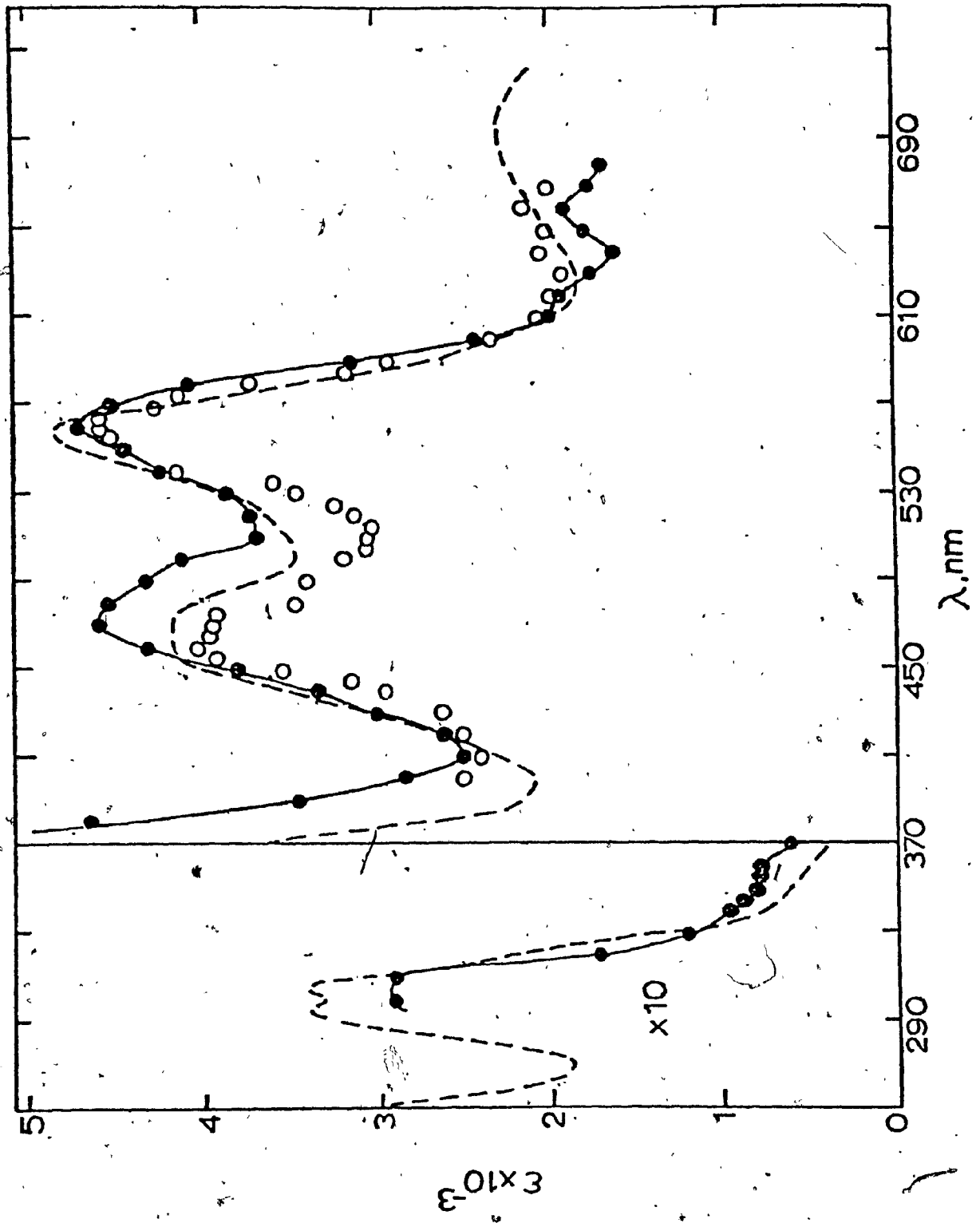


FIGURE 3-18 b : Absorption Spectra of the $\text{Cr}(4,4'\text{-Ph}_2\text{bpy})_3^{2+}$ Transient:
○—○ by Flash Photolysis Methods in N_2 -purged 1 M
HCl Aqueous Solutions Containing 5% v/v MeOH ; ●—●
by Pulse Radiolysis Methods in Which the Cr(III) Species
(45 μM) were Reduced by e_{solv}^- at Natural pH in Argon-
purged Methanolic Solutions. Dose/pulse 1.47 krad;
 $G(\text{Cr}^{\text{II}}) = 1.5$.

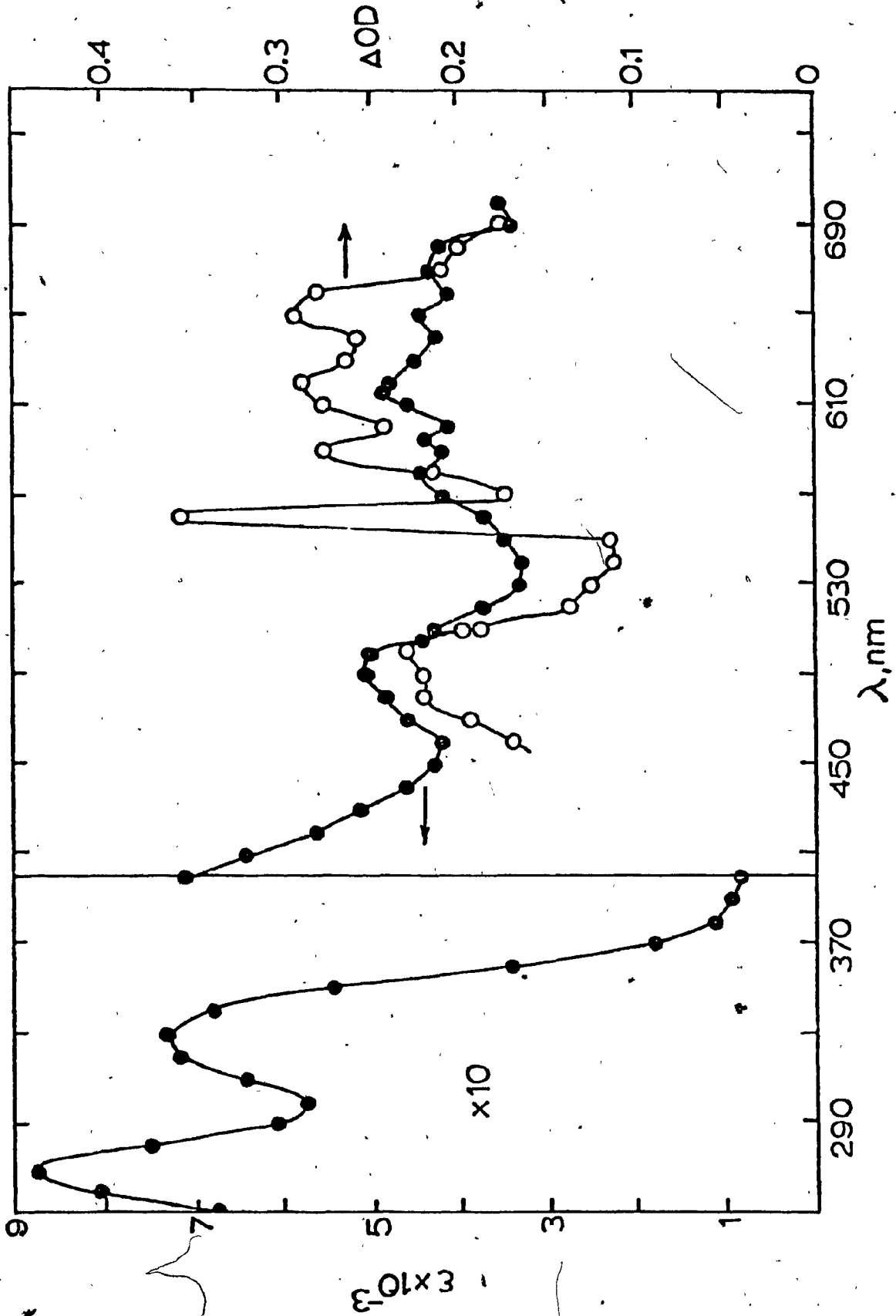


FIGURE 3-18 c : Absorption Spectra of $\text{Cr}(\text{phen})_3^{2+}$: $\text{O} \text{---} \text{O}$ by Flash
Photolysis in N_2 -purged 1 M HCl Aqueous Solutions;
 $\bullet \text{---} \bullet$ by Pulse Radiolysis Methods by Reduction of
the Cr(III) Species ($52 \mu\text{M}$) with $(\text{CH}_3)_2\dot{\text{C}}\text{OH}$ at pH ca.
2 in Argon-purged Aqueous Solutions Containing 0.26 M
2-propanol and 0.01 M HClO_4 . Dose/pulse = 1.27 krad;
 $G(\text{Cr}^{\text{II}}) = 4.6$.

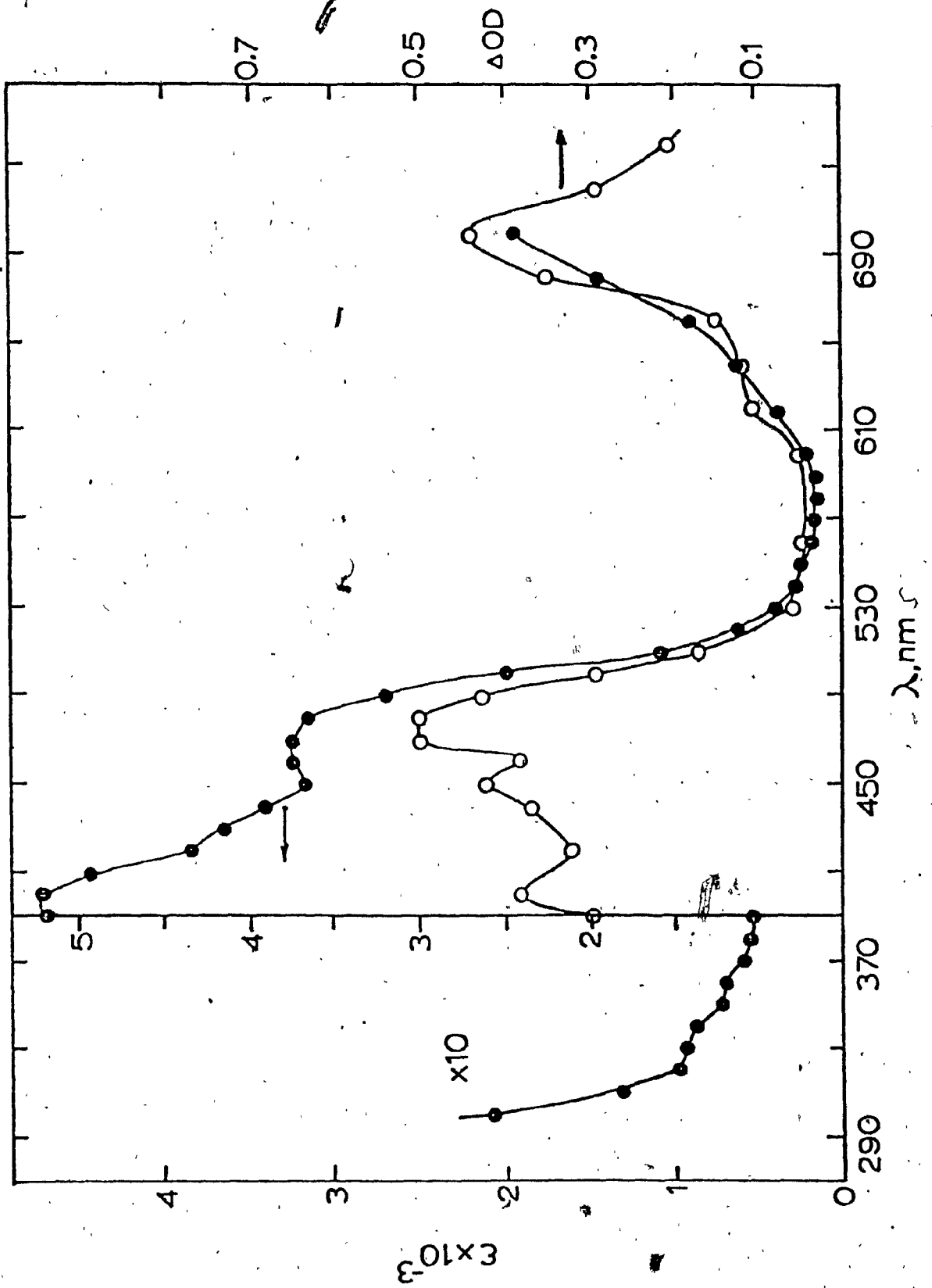


FIGURE 3-18 d : Absorption Spectra of the $\text{Cr}(\text{5-Clphen})_3^{2+}$ Ion: $\text{O} \text{---} \text{O}$
by Flash Photolysis in N_2 -purged 1 M HCl Aqueous
Solutions; $\bullet \text{---} \bullet$ by Pulse Radiolysis by Reduction
of Cr(III) Species (50 μM) with $(\text{CH}_3)_2\text{COH}$ at pH ca. 1
in Argon-purged Solutions Containing 0.9 M 2-propanol
and 0.1 M HClO_4 . Dose/pulse = 1.8 krad; $G(\text{Cr}^{\text{II}}) = 4.8$.

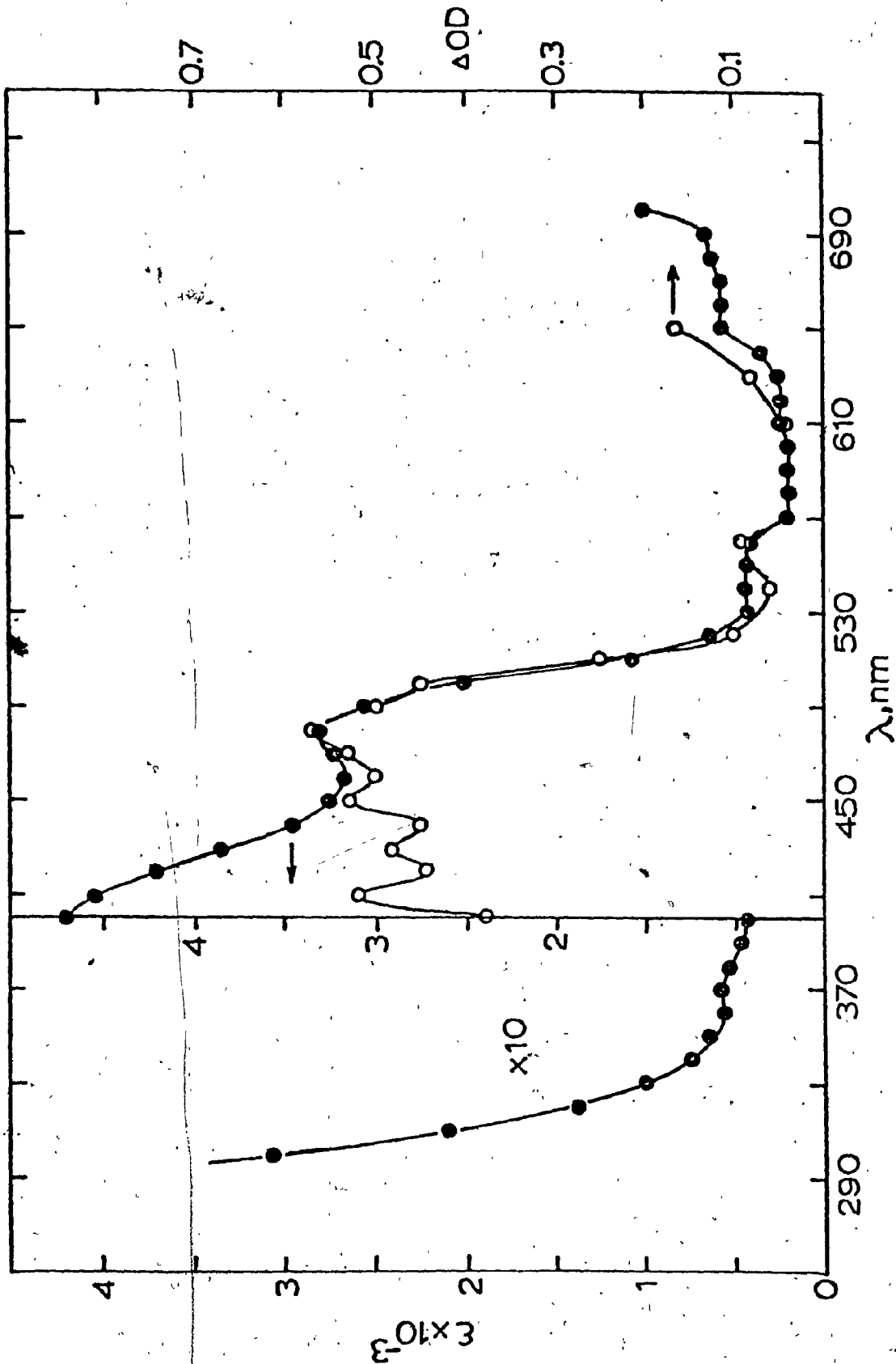


FIGURE 3-18 e : Absorption Spectra of $\text{Cr}(\text{5-Brphen})_3^{2+}$ ions: $\text{O} \text{---} \text{O}$ by Flash Photolysis in N_2 -purged Aqueous 1 M HCl Solutions: $\bullet \text{---} \bullet$ by Pulse Radiolysis by Reduction of Cr(III) Species ($39 \mu\text{M}$) with $(\text{CH}_3)_2\dot{\text{C}}\text{OH}$ at pH ca. 1 in Argon-purged Aqueous Solutions Containing 0.52 M 2-propanol and 0.05 M H_2SO_4 . Dose/pulse = 0.54 krad; $G(\text{Cr}^{\text{II}}) = 5.1$.

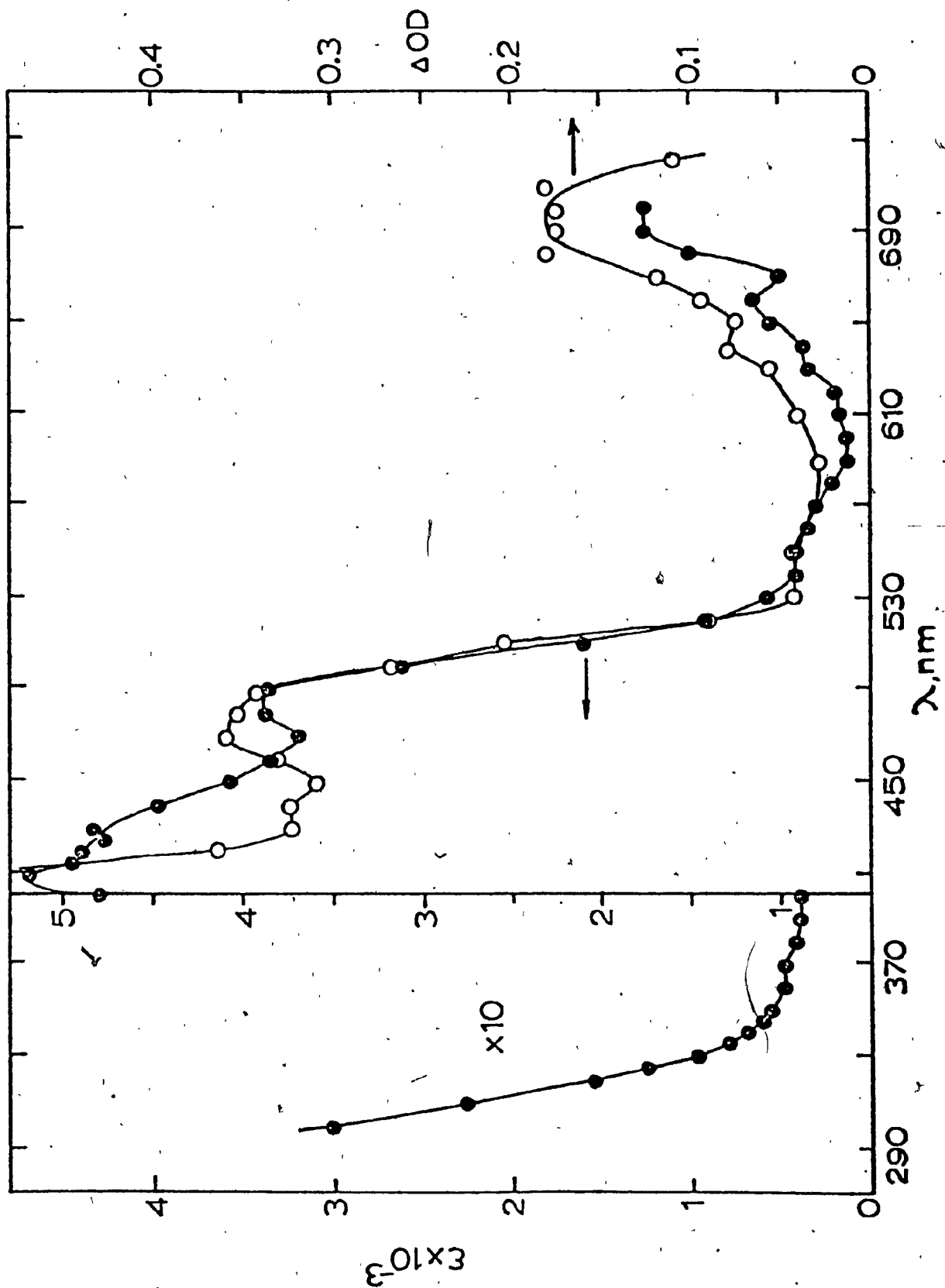


FIGURE 3-18 f : Absorption Spectra of $\text{Cr}(\text{5-Mephen})_3^{2+}$: $\text{O} \text{---} \text{O}$ by Flash
Photolysis Techniques in N_2 -purged Aqueous 1 M HCl
Solutions; $\bullet \text{---} \bullet$ by Pulse Radiolysis Techniques by
Reduction of Cr(III) Species ($52 \mu\text{M}$) with $(\text{CH}_3)_2\dot{\text{C}}\text{OH}$
at pH ca. 1 in Argon-purged Aqueous Solutions Containing
 0.26 M 2-propanol and 0.05 M H_2SO_4 . Dose/pulse = 0.57
krad; $G(\text{Cr}^{\text{II}}) = 5.2$.

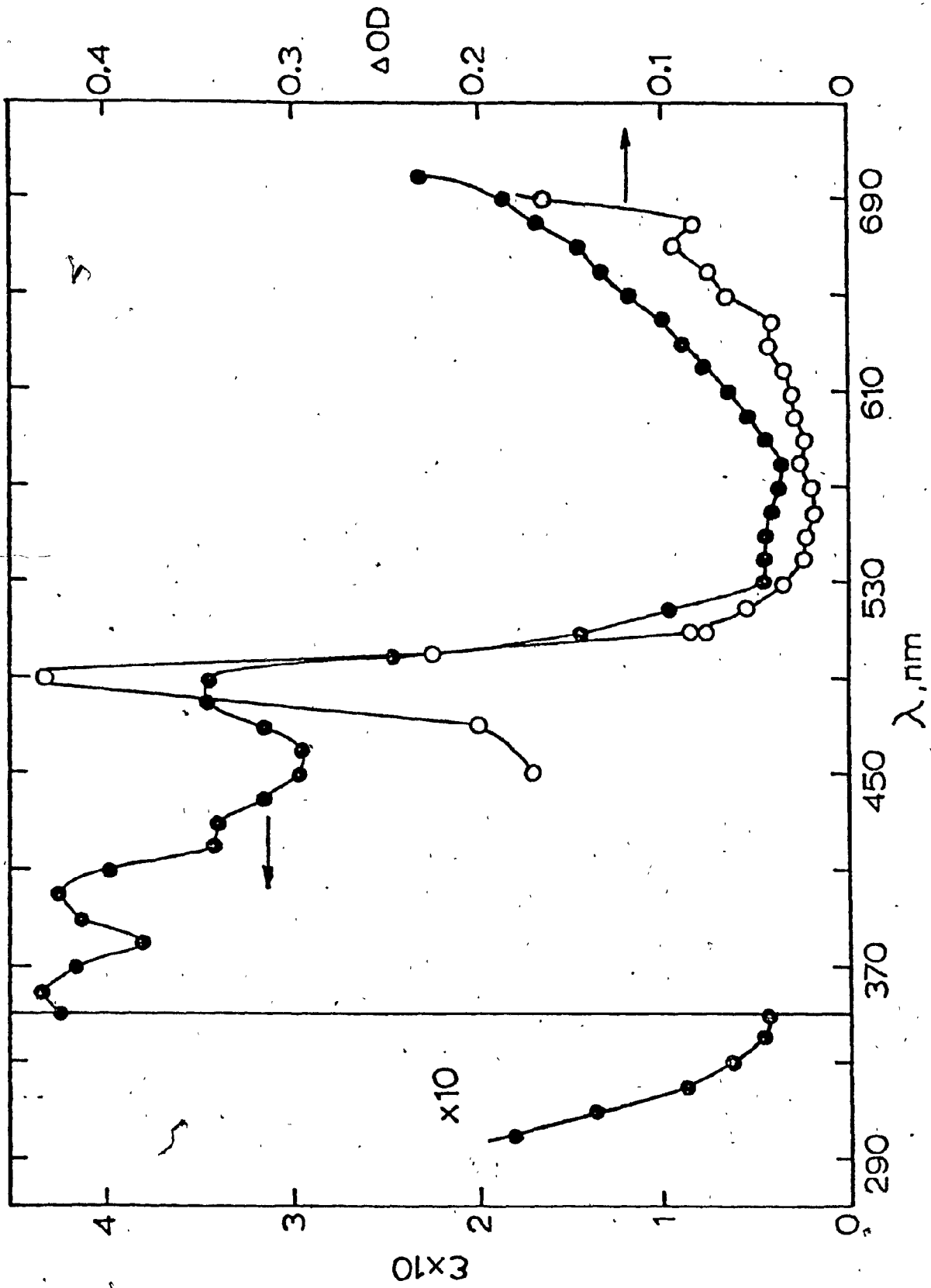


FIGURE 3-18 g : Absorption Spectra of the $\text{Cr}(\text{5-Phphen})_3^{2+}$ Species:
O—O by Flash Photolysis in N_2 -purged 1 M HCl Aqueous
Solutions Containing 1% v/v MeOH; ●—● by Pulse
Radiolysis Methods by Reduction of the Cr(III) Species
(49 μM) with e_{solv}^- in Argon-purged Methanolic Solutions
at Natural pH. Dose/pulse = 1.20 krad; $G(\text{Cr}^{\text{II}}) = 2.$

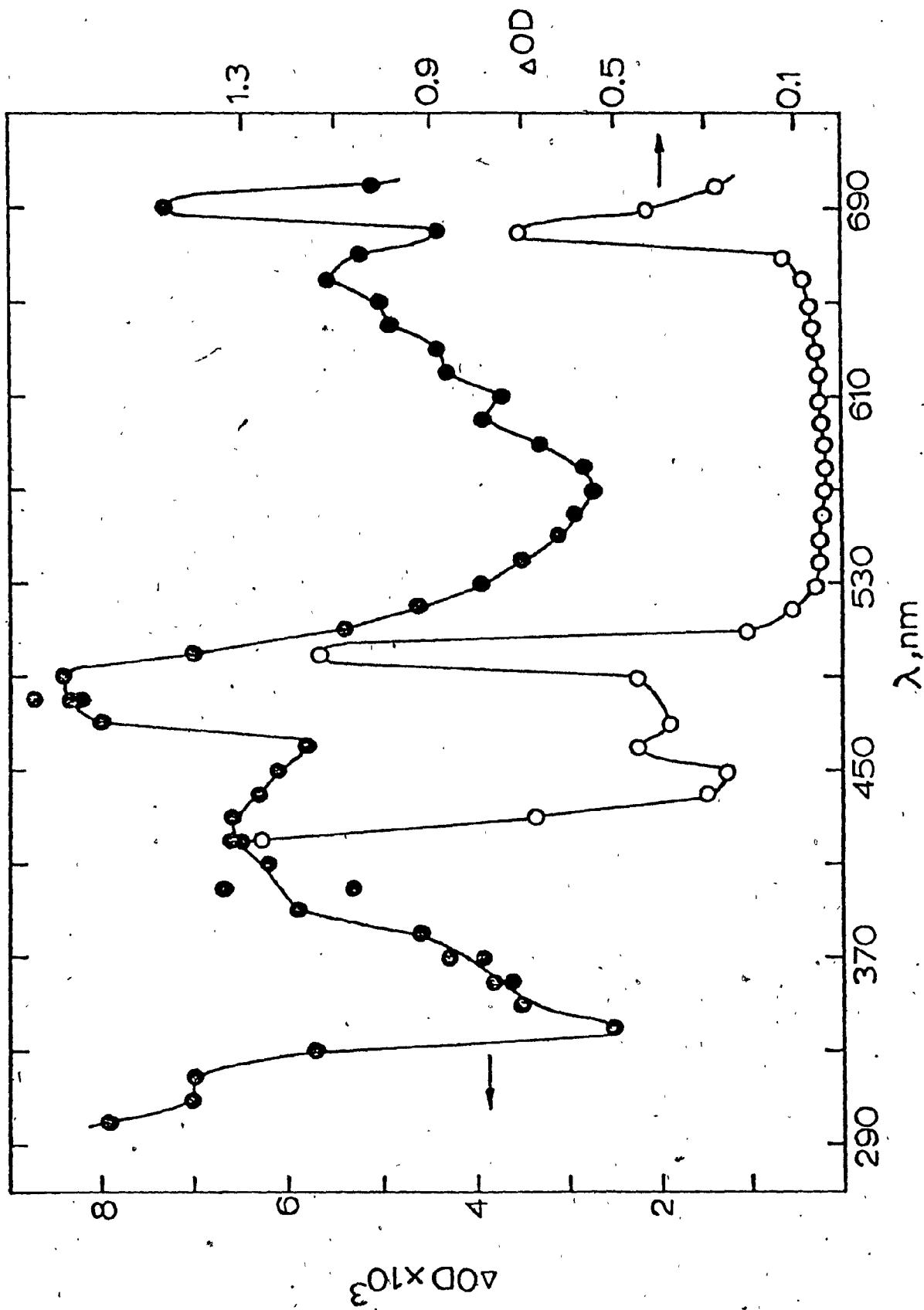


FIGURE 3-18 h : Absorption Spectra of the $\text{Cr}(5,6\text{-Me}_2\text{phen})_3^{2+}$ Ion:
O—O by Flash Photolysis in N_2 -purged Aqueous 1 M
HCl Solutions; ●—● by Pulse Radiolysis Methods by
Reduction of Cr(III) Species ($53 \mu\text{M}$) with $(\text{CH}_3)_2\dot{\text{C}}\text{OH}$
at pH ca. 1 in Argon-purged Aqueous Solutions Contain-
ing 0.26 M 2-propanol, and 0.05 M H_2SO_4 . Dose/pulse =
1.37 krad; $G(\text{Cr}^{\text{II}}) = 4.9$.

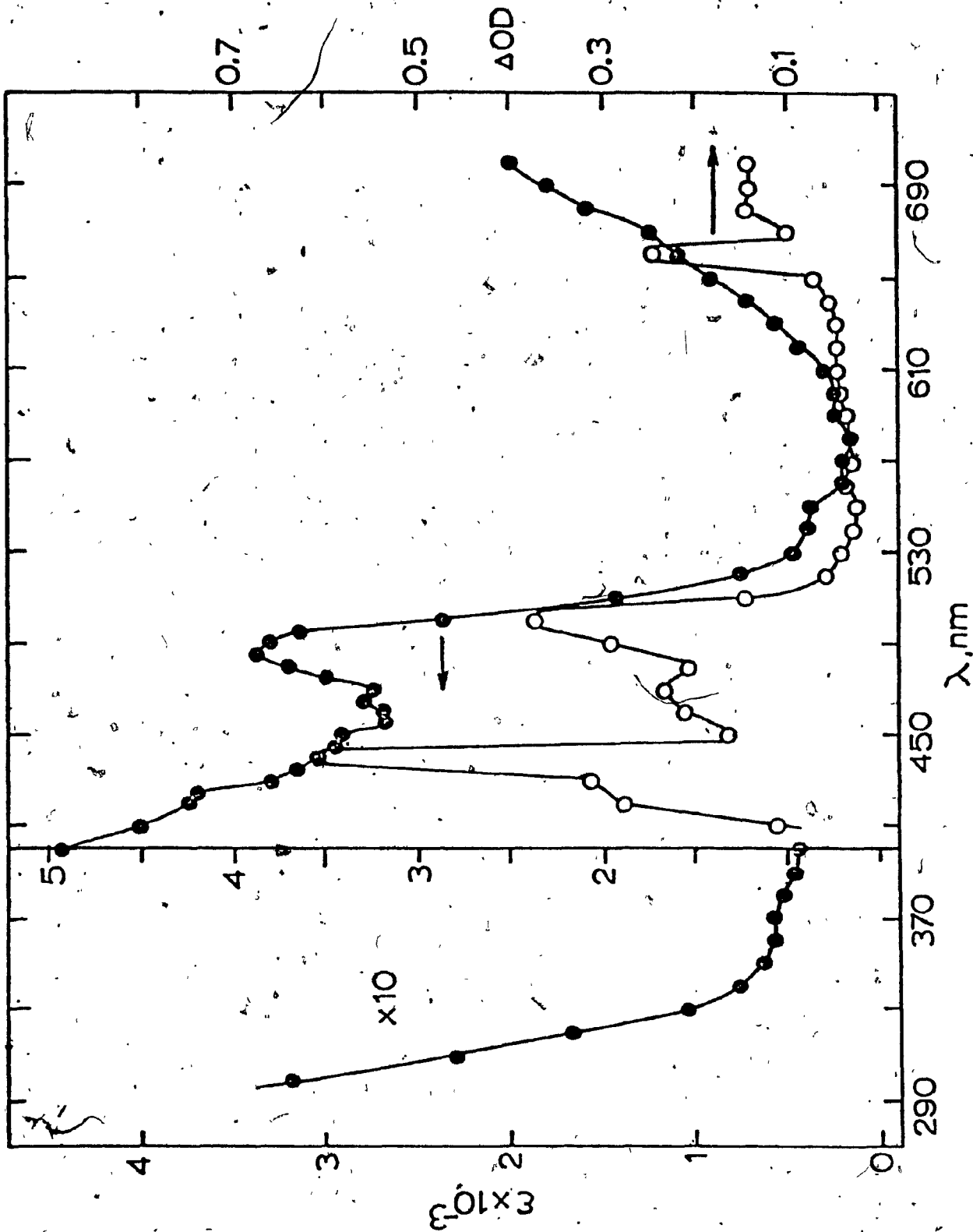


FIGURE 3-18 i : Absorption Spectrum of $\text{Cr}(4,7\text{-Me}_2\text{phen})_3^{2+}$ Species
Obtained by Pulse Radiolysis Techniques by Reduction of the
of the Corresponding Cr(III) Species ($54 \mu\text{M}$) with
 e_{solv}^- in Argon-purged Methanolic Solutions at Natural
pH. Dose/pulse = 1.67 krad; $G(\text{Cr}^{\text{II}}) = 1.8$.

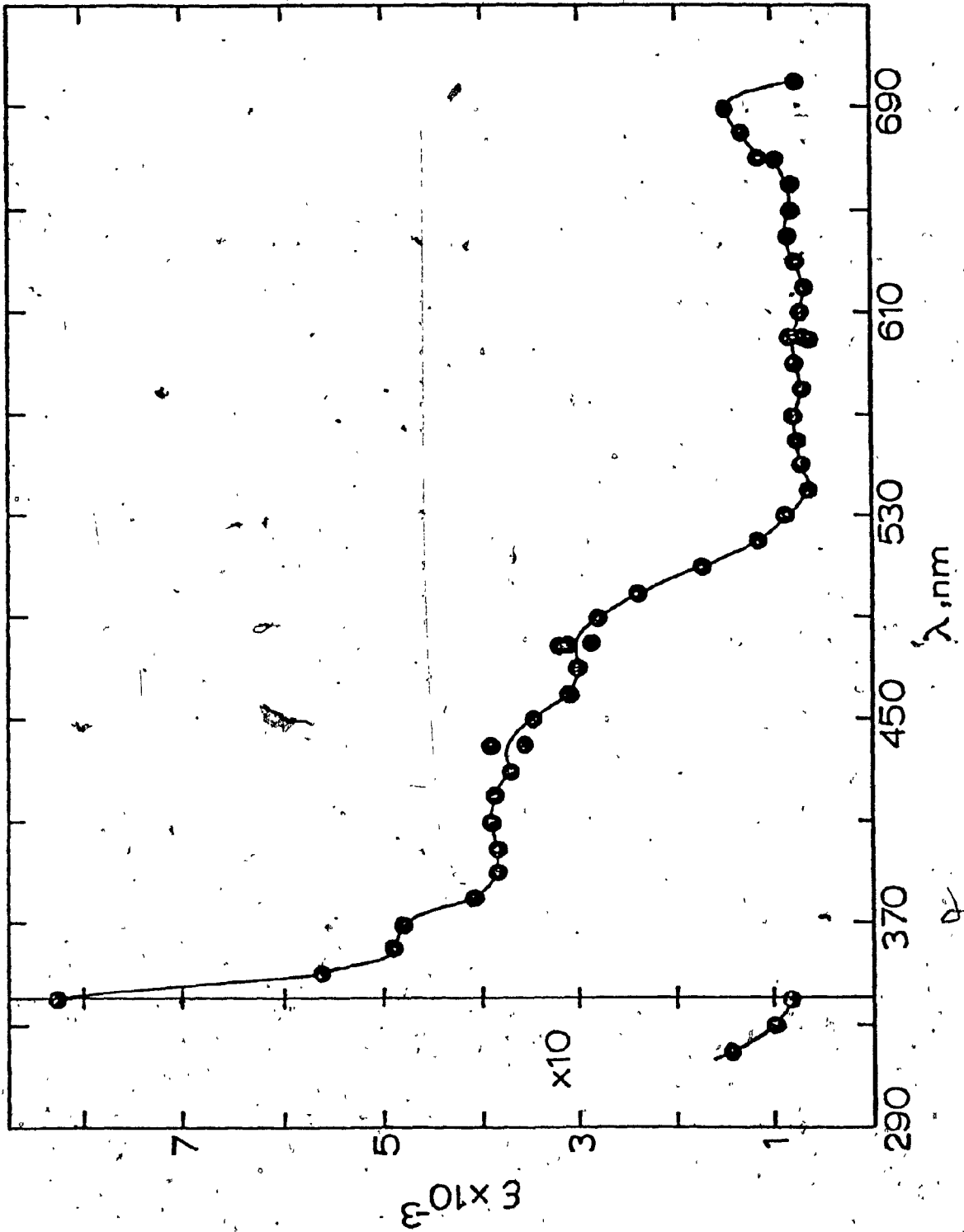


FIGURE 3-18 j : Absorption Spectra of the $\text{Cr}(4,7\text{-Ph}_2\text{phen})_3^{2+}$ Transient:
○—○ by Flash Photolysis in N_2 -purged 1 M HCl Aqueous
Solutions Containing 5% v/v MeOH; ●—● by Pulse
Radiolysis Methods by Reductions of the Cr(III) Species
(48 μM) with e_{solv}^- in Argon-purged Methanolic Solutions
at Natural pH. Dose/pulse = 1.67 krad; $G(\text{Cr}^{\text{II}}) = 1.9$.

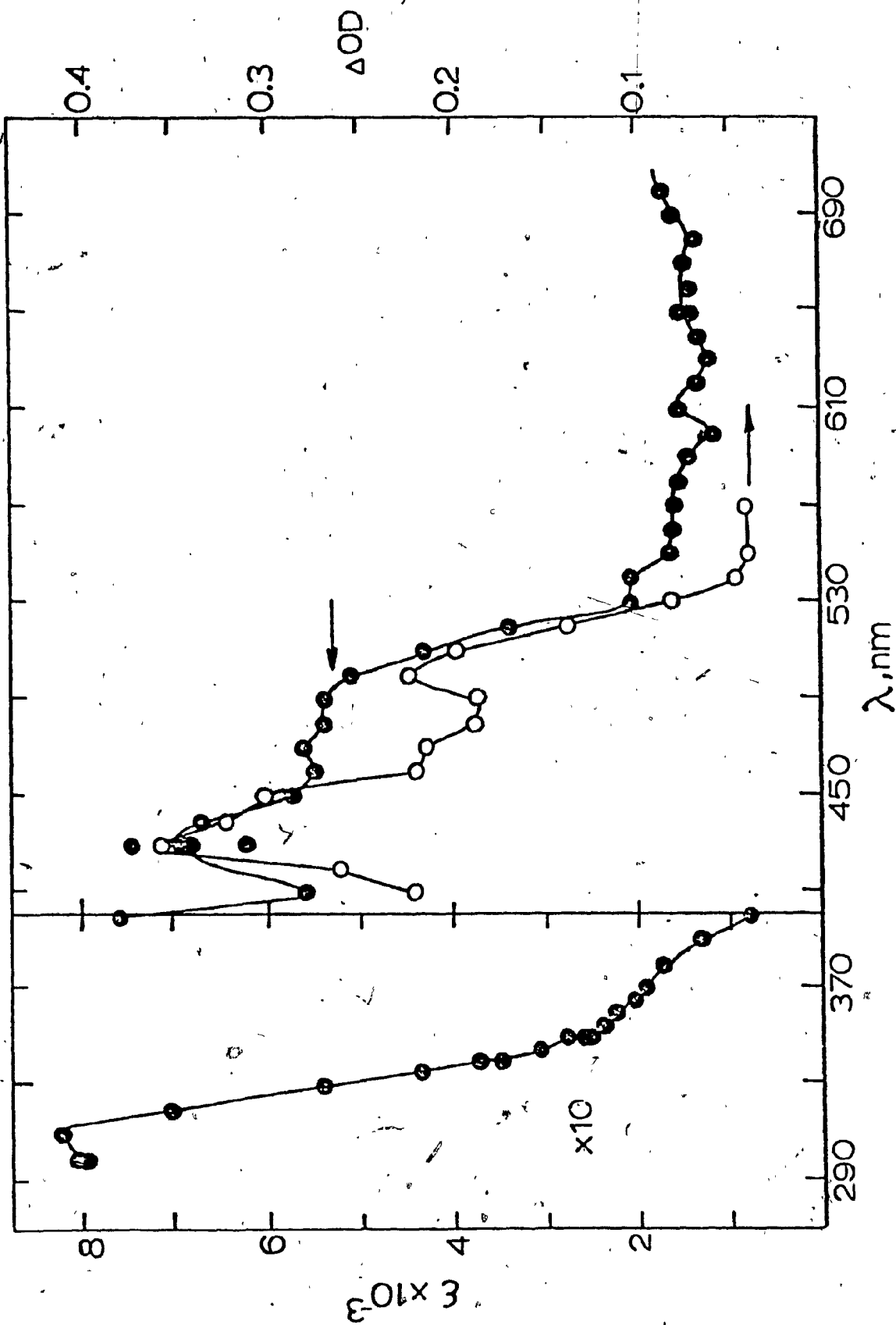
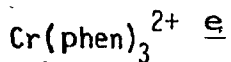


TABLE 3-18 : Absorption Spectra of Cr(NN)₃²⁺ Transients.

Complex Ion	λ^* , nm	$10^{-3}\epsilon$ (M ⁻¹ cm ⁻¹)	Tentative Assignments ^b
Cr(bpy) ₃ ²⁺ ^a	287	25.0	NN + NN*
	308	30.5	NN + NN*
	326	7.2	t ₂ ⁴ + t ₂ ² e ² (?)
	339	5.2	³ T ₁ + ³ T ₂ (b)+CT
	360	4.7	+ ³ T ₁ (b)+CT
	463(465) ^a	4.2(3.9) ^a	+ ³ E(b)+CT
	- (490) ^a	- (3.4) ^a	+ ³ A ₁ +CT
	562	4.9(4.6) ^a	+ ³ A ₂ +CT
	690	2.3	+ ³ T ₁ (a)+ ³ T ₂ (a)+CT
	830	1.7	+ ³ E(a)+CT
	Cr(4,4'-Me ₂ bpy) ₃ ²⁺ ^c	305	29.0
360		8.0	³ T ₁ + ³ T ₁ (b)+ ³ T ₂ (b)+CT
470		4.6	+ ³ E(b)+CT
495		4.2	+ ³ A ₁ +CT
560		4.5	+ ³ A ₂ +CT
620		2.0	+ ³ T ₂ (a)+CT
660		1.8	+ ³ T ₁ (a)+CT
Cr(4,4'-Ph ₂ bpy) ₃ ²⁺ ^d		270	87.5
	330	73.1	NN + NN*
	410	6.4	³ T ₁ + ³ T ₁ (b)+ ³ T ₂ (b)+CT (?)
	470	4.6	
	485	4.9	+ ³ E(b)+CT
	515	4.0	+ ³ A ₁ +CT
	575	4.4	+ ³ A ₂ +CT
	595	4.4	
	620	4.8	
	650	4.5	+ ³ T ₂ (a)+CT
	670	4.4	+ ³ T ₁ (a)+CT

TABLE 3-18, continued

161

335(330)^f 8.9

360 6.7

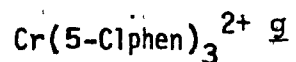
400(415)^f 4.6

430 3.6

470(475)^f 3.2550(550)^f 0.73

620 0.88

700 2.5



370 5.8

410 4.5

480 3.3

550 0.95

610 0.74

650 1.1

680 1.1



370 4.9

410 5.2

430 4.8

485 3.9

560 0.85

610 0.66

630 0.83

660 1.1

695 1.7



360 4.3

400 4.2

430 3.4

485 3.5

550 0.45

630 0.89

660 1.3

680 1.8

 ${}^3T_1 \rightarrow {}^3T_2(b)+CT$ $\rightarrow {}^3T_1(b)+CT$ $\rightarrow {}^3E(b)+CT$ $\rightarrow {}^3A_1$ $\rightarrow {}^3A_2$ $\rightarrow {}^3T_1(a)+{}^3T_2(a)+CT$ ${}^3T_1 \rightarrow {}^3T_2(b)+CT$ $\rightarrow {}^3T_1(b)+CT$ $\rightarrow {}^3E(b)+CT$ $\rightarrow {}^3A_1$ $\rightarrow {}^3A_2+CT$ $\rightarrow {}^3T_2(a)+CT$ ${}^3T_1 \rightarrow {}^3T_2(b)+CT$ $\rightarrow {}^3T_1(b)+CT$ $\rightarrow {}^3E(b)+CT$ $\rightarrow {}^3A_1$ $\rightarrow {}^3A_2+CT$ $\rightarrow {}^3T_2(a)+CT$ ${}^3T_1 \rightarrow {}^3T_2(b)+CT$ $\rightarrow {}^3T_1(b)+CT$ $\rightarrow {}^3E(b)+CT$ $\rightarrow {}^3A_1$ $\rightarrow {}^3A_2+CT$ $\rightarrow {}^3T_2(a)+CT$

Table 3-18, continued

$\text{Cr}(\text{5-Phphen})_3^{2+ \underline{d}}$	~360	(6.4)	3T_1	+ ${}^3T_2(\text{b})+\text{CT}$ + ${}^3T_1(\text{b})+\text{CT}$ + ${}^3E(\text{b})+\text{CT}$ + ${}^3A_1+\text{CT}$ + ${}^3A_2+\text{CT}$ + ${}^3T_2(\text{a})+\text{CT}$
	~390	(4.4)		
	~430	(2.7)		
	~480	(2.6)		
	~600	(0.99)		
	~620	(1.1)		
	~640	(1.2)		
	~660	(1.4)		
	~690	(1.8)		
$\text{Cr}(\text{5,6-Me}_2\text{phen})_3^{2+}$	370	5.9	3T_1	+ ${}^3T_2(\text{b})+\text{CT}$ + ${}^3T_1(\text{b})+\text{CT}$ + ${}^3E(\text{b})+\text{CT}$ + 3A_1 + ${}^3A_2+\text{CT}$
	420	4.3		
	445	3.4		
	470	3.2		
	485	3.9		
	545	0.88		
	570	0.70		
	590	0.74		
	660	1.6		
$\text{Cr}(\text{4,7-Me}_2\text{phen})_3^{2+ \underline{d}}$	370	4.8	3T_1	+ ${}^3T_2(\text{b})+\text{CT}$ + ${}^3T_1(\text{b})+\text{CT}$ + ${}^3E(\text{b})+\text{CT}$ + 3A_1 + 3A_2 + ${}^3T_2(\text{a})$ + ${}^3T_1(\text{a})+\text{CT}$
	410	3.9		
	440	3.7		
	480	3.0		
	565	0.75		
	600	0.68		
	640	0.83		
	690	1.5		
	$\text{Cr}(\text{4,7-Ph}_2\text{phen})_3^{2+ \underline{d}}$	310		
380		17.0		
430		6.8		
470		5.6		
490		5.4		
540		2.1		
570		1.6		
610		1.5		
660		1.4		

Table 3-18, continued

- a This work.
- b See text and equation (3-61).
- c In 0.05 M H_2SO_4 , 1 M 2-propanol, argon-purged solutions; 70 μ sec after the pulse.
- d In methanol, natural pH, argon-purged solutions; 1 μ sec after the pulse.
- e In 0.01 M HClO_4 , 0.26 M 2-propanol, argon-purged solutions; 20 μ sec after the pulse.
- f From references 104 and 105.
- g In 0.01 M HClO_4 , 0.9 M 2-propanol, argon-purged solutions; 40 μ sec after the pulse.
- h In 0.05 M HClO_4 , 0.52 M 2-propanol, argon-purged solutions; 25 μ sec after the pulse.

be reasonably accounted for in terms of simple ligand field theory by employing octahedral microsymmetry yielding $\Delta = 17,370 \text{ cm}^{-1}$ and the Racah parameter $B = 604 \text{ cm}^{-1}$. Alternatively, the $\text{Cr}(\text{bpy})_3^{2+}$ spectrum has also been described in terms of absorption to excited states possessing a configuration admixture of metal-to-ligand charge-transfer (MLCT) character, coupled with $\pi-\pi^*$ excited states of the three bidentate NN ligands.^{104,105}

The spectrum of $\text{Cr}(4,4'\text{-Me}_2\text{bpy})_3^{2+}$ is nearly identical with that of $\text{Cr}(\text{bpy})_3^{2+}$, with the prominent band at 470 nm slightly red shifted by 10 nm upon methyl substitution; the intraligand $\pi-\pi^*$ transition in the $4,4'\text{-Me}_2\text{bpy}$ complex occurs at 300 nm. Complexation of the $4,4'\text{-Ph}_2\text{bpy}$ ligand with $\text{Cr}(\text{II})$ red-shifts the internal ligand transitions by ca. 15-20 nm, nearly the same shift observed in the spectrum of $\text{Cr}(4,4'\text{-Ph}_2\text{bpy})_3^{3+}$. The visible spectrum of $\text{Cr}(4,4'\text{-Ph}_2\text{bpy})_3^{2+}$ is unlike that of the bpy analogue in that several narrow bands are evident at $\lambda > 450 \text{ nm}$.

To the extent that $\text{Cr}(\text{NN})_3^{2+}$ are low-spin d^4 complexes (3T_1 ground state in O_h microsymmetry)¹⁰⁶ the spin-allowed band maxima may be estimated by second-order perturbation theory using the equations (3-61) given by König and Herzog.⁸ With the assumption that $C \approx 4B$, the energy maxima for the transitions are as follows:

$$\begin{aligned}
 {}^3T_1 &\rightarrow {}^3E_a(a), \Delta - 2B + 64B^2/\Delta - 5.33B; \\
 {}^3T_1 &\rightarrow {}^3T_1(a), \Delta + .52B^2/\Delta - 4.70B; \\
 {}^3T_1 &\rightarrow {}^3T_2(a), \Delta + 2B + 52B^2/\Delta - 6.25B; \\
 {}^3T_1 &\rightarrow {}^3A_1, \Delta - B + 64B^2/\Delta; \\
 {}^3T_1 &\rightarrow {}^3A_2, \Delta + 3B - 80B^2/\Delta;
 \end{aligned}
 \tag{3-61}$$

$$\begin{aligned}
 {}^3T_1 &\rightarrow {}^3T_2(b), & \Delta &+ 14B - 12B^2 / \Delta + 6.25B; \\
 {}^3T_1 &\rightarrow {}^3E(b), & \Delta &+ B + 46B^2 / \Delta + 5.33B; \\
 {}^3T_1 &\rightarrow {}^3T_1(b), & \Delta &+ 16B - 36B^2 / \Delta + 4.70B.
 \end{aligned}
 \tag{3-61}$$

In the case of the analogous $\text{Cr}(\text{NN})_3^{3+}$ complexes, it was previously indicated that the ligand field parameter Δ was nearly the same for the three bpy complexes (ca. $23.6 \times 10^3 \text{ cm}^{-1}$). Using the empirical relationship¹⁰⁷ in (3-62), where $g_{\text{ion}} = 17.4 \times 10^3 \text{ cm}^{-1}$, a value of $f_{\text{bpy}} =$

$$\Delta = f_{\text{ligand}} g_{\text{ion}} \tag{3-62}$$

1.36 is obtained, in good agreement with the value of 1.33 given by Jorgensen.¹⁰⁷ A Δ value = $16.9 \times 10^3 \text{ cm}^{-1}$ for the $\text{Cr}(\text{II})$ bipyridine complexes is predicted if a value of $g_{\text{ion}} = 12.4 \times 10^3 \text{ cm}^{-1}$ for low-spin $\text{Cr}(\text{II})$ ⁶⁰ is employed.

Tentative assignments for these bipyridyl complexes are presented in Table 3-18, and were based on a comparison between experimental band maxima and calculated energies by using the above relationships (3-61), with the assumption that the Racah parameter B is constant in this series. The assignments for $\text{Cr}(\text{bpy})_3^{2+}$ are based on those by König and Herzog,⁸ except that the ${}^3T_1 \rightarrow {}^3T_1(b)$ and ${}^3T_1 \rightarrow {}^3T_2(b)$ transitions are assigned to the bands at 360 and 339 nm, respectively. In the $\text{Cr}(4,4'\text{-Me}_2\text{bpy})_3^{2+}$ spectrum, these two transitions occur at ca. 360 nm and are not resolved, due to the very intense intraligand transition at 305 nm. It is interesting, however, that the ${}^3T_1 \rightarrow {}^3T_1(a)$ and ${}^3T_1 \rightarrow {}^3T_2(a)$ transitions

are resolved in this spectrum, but are not resolved in the bpy analogue. In the $\text{Cr}(4,4'\text{-Ph}_2\text{bpy})_3^{2+}$ spectrum, the very intense bands at 270 and 330 nm are ascribed to intraligand $\pi - \pi^*$ transitions on the basis of intensity and by comparison with the spectrum of the protonated form of the free ligand which has bands at 260 and 312 nm.¹⁰⁸ The much richer spectrum of the diphenyl complex is probably due to vibrational components or to transitions predominantly charge-transfer in nature. The low-energy ${}^3T_1 \rightarrow {}^3E(a)$ transition is expected to occur at $\lambda > 700$ nm in the $\text{Cr}(4,4'\text{-Me}_2\text{bpy})_3^{2+}$ and $\text{Cr}(4,4'\text{-Ph}_2\text{bpy})_3^{2+}$ spectra.

Unlike the spectra of the bpy complexes, those of the Cr(II) phen complexes reveal relatively weak, barely discernable bands at ca. 520 - 650 nm. It is likely that transitions in this region have little or no charge-transfer character. At $\lambda < 520$ nm and $\lambda > 650$ nm, intense bands were observed, and, therefore, must be, to a large extent, charge transfer in nature.

From the absorption spectra of the various Cr(III) phen complexes, the value of Δ may be estimated; and assuming a value of $g(\text{Cr(III)}) = 17.4 \times 10^3 \text{ cm}^{-1}$,¹⁰⁷ values for f_{ligand} may be calculated from equation (3-62). The f_{ligand} values thus obtained are collected in Table 3-19. The f value of 1.34 for the phen, 4,7-Me₂phen, and 3,4,7,8-Me₄phen complexes is in excellent agreement with the value of 1.34 reported for phen by Jorgensen.¹⁰⁷ Employing a value for $g(\text{Cr(II)}) = 12.4 \times 10^3 \text{ cm}^{-1}$,⁶⁰ the values of Δ for Cr(NN)_3^{2+} were calculated and tabulated in Table 3-19. To estimate the energy maxima on the basis of ligand field considerations, (using 3-61), the assumption has been made that the value of the Racah parameter B ($\sim 600 \text{ cm}^{-1}$) for these phen complexes is nearly the same as that of the bpy complexes. This assumption is not unreasonable since the

TABLE 3-19 : Calculated Values of f_{ligand} and $\Delta(\text{Cr(III)})$ and $\Delta(\text{Cr(II)})$.

Cr(III)^{3+}	f_{ligand}^a	$\Delta(\text{Cr(III)})$ (cm^{-1})	$\Delta(\text{Cr(II)})$ (cm^{-1})
4,7-Me ₂ phen	1.34	$\sim 23.4 \times 10^3$	16.6×10^3
3,4,7,8-Me ₄ phen	1.34	$\sim 23.4 \times 10^3$	16.6×10^3
phen	1.34	$\sim 23.4 \times 10^3$	16.6×10^3
5-Clphen	1.27	22.2×10^3	15.7×10^3
4,7-Ph ₂ phen	1.23	21.6×10^3	15.3×10^3
5-Brphen	1.27	$\sim 22 \times 10^3$	$\sim 15.7 \times 10^3$
5-Mephen	1.27	$\sim 22 \times 10^3$	15.7×10^3
5-Phphen	1.23	$\sim 21.3 \times 10^3$	15.3×10^3
5,6-Me ₂ phen	1.23	$\sim 21.3 \times 10^3$	15.3×10^3

^a Calculated according to equation (3-62), using $g_{\text{ion}} = 17.4 \times 10^3 \text{ cm}^{-1}$.

B values for $\text{Ni}(\text{bpy})_3^{2+}$ and $\text{Ni}(\text{phen})_3^{2+}$ are nearly identical (898 and 908 cm^{-1} , respectively).⁹ The tentative assignments in Table 3-18 have been based on such estimates.

The analysis indicates that the ${}^3T_1 \rightarrow {}^3T_1(b)$ and ${}^3T_1 \rightarrow {}^3T_2(b)$ transitions should be degenerate in all of the spectra of the phen complexes. This is not generally observed (cf. Table 3-18). Furthermore, the transitions to the ${}^3E(a)$ excited states are not seen in the $\text{Cr}(\text{phen})_3^{2+}$ spectrum, which may be attributed to the band maxima lying at $\lambda > 700$ nm. The ${}^3T_1 \rightarrow {}^3T_1(a)$ and ${}^3T_1 \rightarrow {}^3E(a)$ transitions are expected at $\lambda > 700$ nm in the spectra of the 5-Clphen, 5-Brphen and 5-Phphen complexes; the extra bands at $\sim 400 - 560$ nm have not been assigned. In general, substituents at the 5-phen position red-shift the corresponding transitions in the parent phen complex by ca. 20 - 40 nm; the 5-Brphen and 5-Phphen substituents effect a larger red shift.

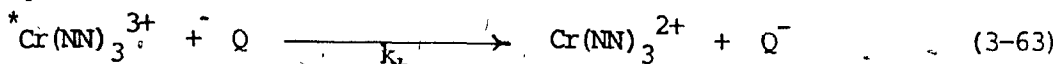
Methyl and phenyl substituents at the 5,6- and 4,7-positions on the phen ring system also red shift the transitions of $\text{Cr}(\text{phen})_3^{2+}$. Phenyl substituents at the 4,7-positions and 5,6-dimethyl substituents are particularly effective, to the extent that the ${}^3T_1 \rightarrow {}^3T_2(a)$, ${}^3T_1 \rightarrow {}^3T_1(a)$ and ${}^3T_1 \rightarrow {}^3E(a)$ transitions occur at $\lambda > 700$ nm. Additional unassigned bands are also evident in the spectra of these disubstituted phen complexes. It is likely that these bands also possess d-d character and the rich spectra probably originate from transitions between states of the trigonal symmetry, D_3 , of the complexes.

This comprehensive examination of the $\text{Cr}(\text{NN})_3^{3+}/\text{Fe}^{2+}$ system and the characterization of the $\text{Cr}(\text{NN})_3^{2+}$ species produced contributes to the overall knowledge of chromium(III) polypyridyl photochemistry in several ways. First of all, it has been shown that the excited-state ${}^* \text{Cr}(\text{NN})_3^{3+}$

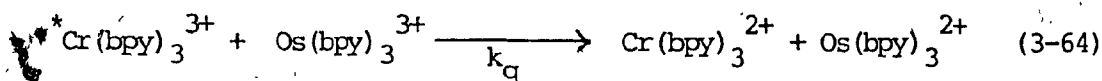
species is quenched by $\text{Fe}^{2+}(\text{aq})$ via a reductive electron transfer process for which the quenching constants vary over two orders of magnitude (cf. Table 3-16). Furthermore, insofar as reaction (3-48) or its analogue involving other reductive quenchers is of potential importance in solar energy conversion schemes, knowledge of the rate constants for the thermal back electron transfer reaction as a function of ligand structure and kinetic parameters is necessary and important. Also, the absorption spectra of $\text{Cr}(\text{NN})_3^{2+}$, generated by flash photolysis in the presence of quencher or by pulse radiolysis, have been recorded and characterized. Finally, examination of the $\text{Cr}(\text{NN})_3^{3+}/\text{Fe}^{2+}$ system has afforded rate constants for both the ground-state (3-54) and excited-state (3-25) self-exchange reactions of $\text{Cr}(\text{NN})_3^{3+}$. To a first approximation, the work terms and solvent reorganization barriers for reactions (3-25) and (3-54) are expected to be the same for the following reasons: i) the $^*\text{Cr}(\text{NN})_3^{3+}$ and $(^4\text{A}_2)\text{Cr}(\text{NN})_3^{3+}$ complexes involved in these reactions both have the same charge, +3; ii) $^*\text{Cr}(\text{NN})_3^{3+}$ and $(^4\text{A}_2)\text{Cr}(\text{NN})_3^{3+}$ are isogeometric inasmuch as the Stokes shift between the $^2\text{E} \leftrightarrow ^4\text{A}_2$ emission⁵⁴ and absorption⁸ bands is zero and their orbital population is identical, t_{2g}^3 , although different in spin. Consequently, if both the ground-state and excited-state self-exchange reactions are adiabatic, they can only differ in their inner-sphere barriers, $\Delta G_{\text{in}}^{\ddagger}$, for which it has been shown that $\Delta G_{\text{in}}^{\ddagger} \approx ^*\Delta G_{\text{in}}^{\ddagger}$; and the rates for reactions (3-25) and (3-54) are thus the same.

f. Other $\text{Cr}(\text{NN})_3^{3+}$ /quencher Systems.

Quenching of $\text{Cr}(\text{NN})_3^{3+}$ excited states by quencher species Q capable of oxidizing chromium(III) to chromium(IV), as in reaction (3-63), has revealed some inconclusive results regarding the operable



quenching mechanism. The strong oxidants $\text{Ru}(\text{NN})_3^{3+}$ and $\text{Os}(\text{NN})_3^{3+}$ have been utilized⁸⁶ to effect oxidative quenching of ${}^* \text{Cr}(\text{NN})_3^{3+}$. $\text{Os}(\text{bpy})_3^{3+}$ was found to be an extremely inefficient quencher species, such that only an upper limit ($k_q < 1 \times 10^6 \text{ M}^{-1} \text{ sec}^{-1}$) could be assigned⁸⁶ for the reaction (3-64). However, $\text{Ru}(\text{bpy})_3^{3+}$ was found⁸⁶ to be an efficient



quencher of ${}^* \text{Cr}(\text{bpy})_3^{3+}$, with $k_q = 6 \times 10^6 \text{ M}^{-1} \text{ sec}^{-1}$ in $1 \text{ M H}_2\text{SO}_4$ at 25°C . If electron transfer quenching occurs with the $\text{Ru}(\text{III})$ and $\text{Os}(\text{III})$ polypyridyl complexes, it is anticipated that $\text{Ru}(\text{bpy})_3^{3+}$ will be the more effective quencher owing to the more favorable driving force for reaction (3-65), compared to reaction (3-64), $+1.25 \text{ V}$ vs $+0.82 \text{ V}$ ⁸⁶ respectively. An energy transfer quenching pathway (see Section 3.8.1.) should not be discounted for these two $\text{M}(\text{NN})_3^{3+}$ quencher complexes inasmuch as the $\text{Ru}(\text{III})$ complex has an absorption band at 674 nm ⁹² which is in close proximity to the emission band at 695 nm of $\text{Cr}(\text{bpy})_3^{3+}$; and both the $\text{Ru}(\text{III})$ and $\text{Os}(\text{III})$ complexes have spin-forbidden bands at longer wavelengths (lower energy) which may be close to, or overlap with, the 727-nm emission band of $\text{Cr}(\text{bpy})_3^{3+}$. Inconclusive results were also obtained¹⁰¹ using $\text{Fe}(\text{CN})_6^{3-}$ and $\text{Co}(\text{CN})_6^{3-}$ as potential oxidative quenchers of $({}^2\text{E})\text{Cr}(\text{bpy})_3^{3+}$.

The importance of electron transfer quenching studies lies therefore in the identification of products of the process, the identity and characterization of the excited state which gives rise to the oxidized or reduced products, and the comparison of the corresponding ground-state and

excited-state self-exchange reactions.

3.7.1. Bimolecular Energy Transfer.

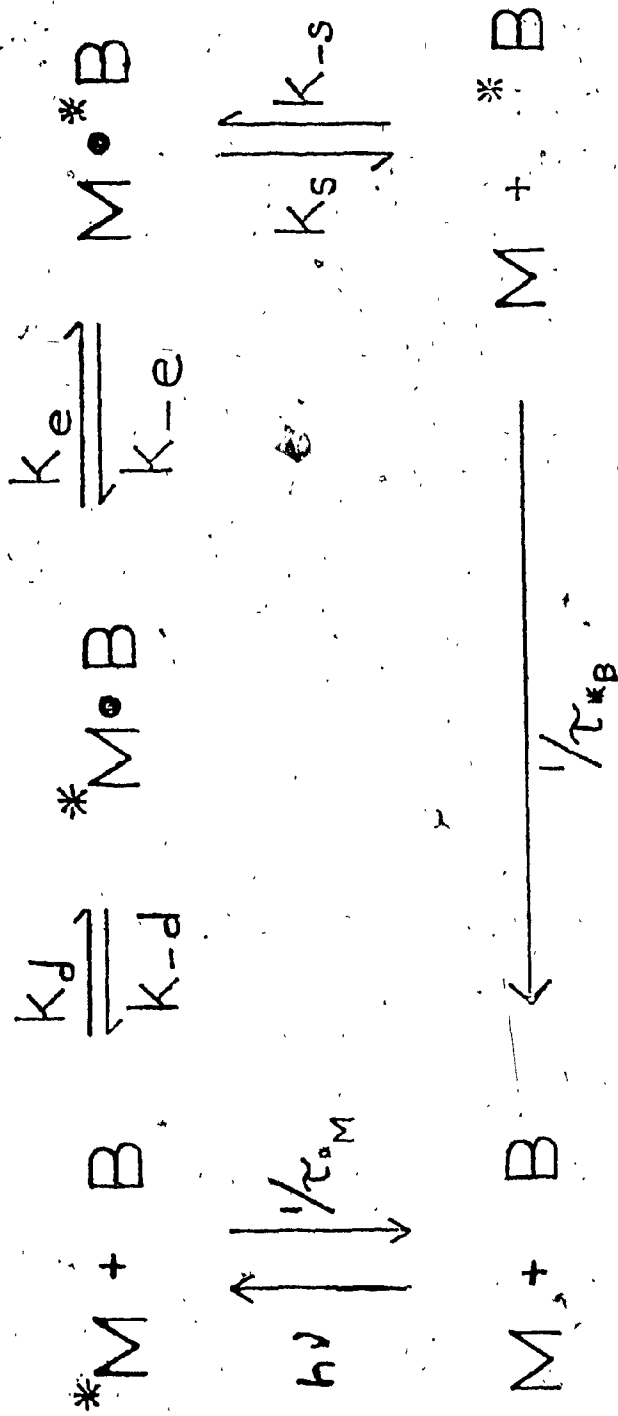
Bimolecular energy transfer quenching is an intermolecular transfer of electronic energy from a donor species M^* to an acceptor species A. This intermolecular transfer of energy allows for selective population and depopulation of specific excited states. Scheme 3-5 depicts such an energy transfer pathway for M^* and A. The energy transfer process may occur via two types of interactions: (i) a dipole-dipole interaction which takes place over an intermolecular distance much greater than the molecular diameter. This type of interaction is important only for spin- and symmetry-allowed transitions in the donor and acceptor species. Thus, in transition metal complexes, the dipole-dipole interaction will not make a significant contribution to excited-state energy transfer. (ii) An exchange interaction, on the other hand, requires a collisional encounter between M^* and A, and thus, is dependent on the energy of the excited-state species M^* . Scheme 3-5 depicts such a collisional energy transfer process.

Using Scheme 3-5 and analogous assumptions in deriving expression (3-18) for electron transfer quenching processes, Balzani and Bolletta¹⁰⁹ have shown that the rate constant for energy transfer quenching, k_q , is

$$k_q = \frac{k_d}{1 + \frac{k_{-d}}{k_e} + \frac{k_{-d}k_{-e}}{k_s k_e}} \quad (3-65)$$

where $1/\tau(^*A) \gg k_{-s}[M]$, and k_e and k_{-e} are the rate constants for the energy transfer step, and $k_{-d} = k_s$. Furthermore, k_q is related to the

Scheme 3-5



overall free energy changes and free energy of activation of the energy transfer step by the equivalent of equation (3-19). The overall free energy change for the energy transfer process is given by equation (3-66)

$$\Delta G_e^0 = -E^{0-0}(*M,M) + E^{0-0}(*A,A) + \text{constant} \quad (3-66)$$

wherein E^{0-0} refers to the zero-zero excited-state energy, and the constant term accounts for differences in partition functions and in the entropies of the ground and excited states. This constant is usually small, and considered negligible in most cases.¹⁰⁹ When a homogeneous series of donors $*M$ is quenched by a single quencher A , equation (3-66) reduces to (3-67). At low values of $E^{0-0}(*M,M)$, equations (3-19) and

$$\Delta G_e^0 = -E^{0-0}(*M,M) + \text{constant} \quad (3-67)$$

(3-67) predict that $\log k_q$ will increase linearly with $E^{0-0}(*M,M)$ with a slope of $1/2.303RT$; at high values of $E^{0-0}(*M,M)$, $\log k_q$ becomes equal to $\log k_d$ (plateau) as depicted in Figure 3-15. k_d is the rate constant for diffusion, and it is expected that the upper limit for k_q for an energy transfer process should be that of a diffusion-controlled reaction.

To ascertain that excited-state quenching occurs via an energy transfer process from the donor to the acceptor species, there must be some experimental and/or theoretical evidence to support such a contention. Luminescence from the excited-state acceptor species $*A$ is the experimental evidence required for an energy transfer assignment; however, if the acceptor species undergoes a sensitized chemical reaction, it cannot be assumed automatically that energy transfer has occurred, as the observed

phenomenon may well be due to chemical interaction between the excited-state donor species and the ground-state acceptor species. Alternatively, a catalytic effect on the reactivity of the ground-state acceptor species may take place. Clear-cut evidence (i.e., sensitized emission) for an energy transfer pathway is seldom encountered with transition metal complexes. However, such a pathway has been proposed on the basis of various tenets, including: i) the magnitude of k_q values relative to the diffusion-controlled rate constant k_d ; ii) correlation of the k_q values with the energies of the excited-state species; iii) comparison of analogous ground-state reactions; iv) the sensitivity of k_q towards excited-state redox potentials; and v) comparison of the spectroscopic energies and redox potentials of the donor and acceptor species.

Turning then to experimental investigations of Cr(III) energy transfer quenching, it must be noted that a donor species having excited-state energies greater than the lowest excited-state (2E for $\text{Cr}(\text{NN})_3^{3+}$) of the donor, but less than the energies of the 4T excited states, can populate the (${}^2E/{}^2T_1$) (and perhaps 2T_2) excited states of Cr(III). Similarly, if an acceptor species possesses excited-state energies less than the energy of the 2E state of $\text{Cr}(\text{NN})_3^{3+}$, energy transfer from the 2E state to the acceptor species is possible.

a. The $\text{Cr}(\text{NN})_3^{3+}/\text{Cr}(\text{CN})_6^{3-}$ Systems.

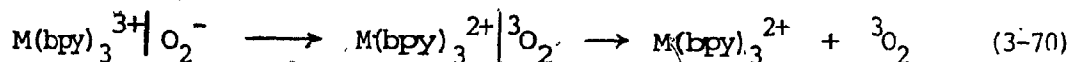
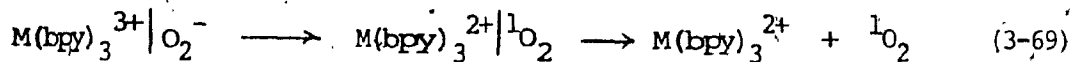
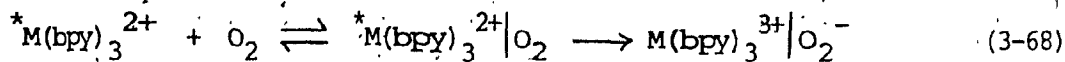
Sensitized emission has been observed for the ${}^* \text{Cr}(\text{bpy})_3^{3+}/\text{Cr}(\text{CN})_6^{3-}$ and ${}^* \text{Cr}(\text{phen})_3^{3+}/\text{Cr}(\text{CN})_6^{3-}$ donor/acceptor couples in $\text{H}_2\text{O}/\text{DMF}$ solutions.⁵² An electron transfer quenching pathway is thermodynamically unfavorable for these two couples, while an energy transfer pathway is both spin- and thermodynamically-allowed. A more recent investigation of the $\text{Cr}(\text{bpy})_3^{3+}/\text{Cr}(\text{CN})_6^{3-}$ couple by Juris and coworkers⁹⁷ in aqueous

solution at 20°C confirms an energy transfer path. A comparison of the quenching rate constants k_q for $M(\text{bpy})_3^{n+}/\text{Cr}(\text{CN})_6^{3-}$ couples (where $M = \text{Ru}(\text{II}), \text{Os}(\text{II})$ and $\text{Cr}(\text{III})$) revealed that k_q increases in the order $\text{Ru}(\text{II}) < \text{Os}(\text{II}) < \text{Cr}(\text{III})$.⁹⁷ An energy transfer mechanism should be more favorable for the $^*\text{Cr}(\text{bpy})_3^{3+}$ complex ion owing to its higher ionic charge and to the absence of excited-state distortion relative to the $^*\text{Os}(\text{bpy})_3^{2+}$ and $^*\text{Ru}(\text{bpy})_3^{2+}$ ions. On the other hand, the metal-centered nature of $^*\text{Cr}(\text{bpy})_3^{3+}$ does not favor an energy transfer pathway inasmuch as there is expected to be less favorable overlap between the $^*\text{Cr}(\text{bpy})_3^{3+}$ and $\text{Cr}(\text{CN})_6^{3-}$ orbitals.¹¹⁰ However, the greater value of k_q for the $\text{Cr}(\text{III})$ complex suggests that ionic charge and/or excited-state distortion play major roles in energy transfer processes.

b. The $\text{Cr}(\text{NN})_3^{3+}/\text{O}_2$ Systems.

Quenching of excited triplet states of organic molecules by molecular oxygen has been extensively investigated;¹¹¹⁻¹¹⁴ in contrast, only recently have there been studies focused on the interaction between excited-state transition metal complexes and molecular oxygen.^{44,66,91,115-117} Assigning a mechanistic pathway to oxygen quenching has been the subject of much discussion.^{44,117}

The quenching of several $^*\text{Cr}(\text{NN})_3^{3+}$ complex ions by molecular oxygen in 1 M HCl has been investigated in this work by the lifetime quenching technique and by Brunschwig and Sutin,⁸⁶ and an energy transfer quenching pathway has been assigned. Lin and Sutin⁹¹ have suggested that oxygen quenching of $^*\text{Ru}(\text{bpy})_3^{2+}$ and $^*\text{Os}(\text{bpy})_3^{2+}$ takes place via an oxidative electron transfer mechanism as per reactions (3-68) to (3-70). Direct



evidence for the electron transfer products has been given by Winterle et al.¹¹⁷ It is anticipated that k_q should be sensitive to the reduction potential of $M(\text{bpy})_3^{3+}$ for an electron transfer process; however, this was not observed.⁴⁴ Moreover, since the k_q values for oxygen quenching of ${}^*Ru(\text{bpy})_3^{2+}$ are very close to k_d , the diffusion-controlled limit, the sensitivity of k_q toward the $M(\text{bpy})_3^{3+}/M(\text{bpy})_3^{2+}$ reduction potential is not expected. Inasmuch as the 2E states of $Cr(\text{NN})_3^{3+}$ are metal-centered and the excited states of $Os(\text{bpy})_3^{2+}$ and $Ru(\text{bpy})_3^{2+}$ are metal-to-ligand charge-transfer, it was important to examine the effects of the orbital nature of the excited state as well as ligand substitution for Cr(III) in comparison with Ru(II).

Quenching rate constants k_q have been evaluated from lifetime quenching experiments for the quenching of several ${}^*Cr(\text{NN})_3^{3+}$ complexes by O_2 . The k_q values so obtained are collected in Table 3-20, along with the spectroscopic energies of the $({}^2E)Cr(\text{NN})_3^{3+}$ species. Also included in Table 3-20 are the k_q values obtained by other research groups for comparative purposes. The data reveal that the k_q values are 2-3 orders of magnitude smaller than the diffusion-controlled limit. As well, they are 1-2 orders of magnitude smaller than the k_q values obtained for oxygen quenching of organic triplets, for which $k_q \sim 3 \times 10^9 \text{ M}^{-1} \text{ sec}^{-1}$ for $10.0 \text{ kK} < E_T < 15.0 \text{ kK}$ and decreases at $E_T > 16.0 \text{ kK}$.¹¹¹ It has been suggested^{63,111} that when the donor triplet energy E_T exceeds the energy of the acceptor

TABLE 3-20 : Energy Transfer Rate Constants (2k_q) for Quenching by Oxygen and Excited-state Energies (E^{O-O}) of ($^2T_1/{}^2E$)Cr(NN) $_3$ Complexes in Fluid Media.

NN	$^2k_q \times 10^{-7}$ ($M^{-1} \text{ sec}^{-1}$) ^a	Reference	$E^{O-O} (M^*M) \times 10^{-3}$ (cm^{-1}) ^b
bpy	1.7	this work	13.74
bpy	2.6	86	
bpy	2.7 ^e	86	
bpy	2.9 ^f	86	
4,4'-Me ₂ bpy	3.4	this work	13.68
4,4'-Me ₂ bpy	4.2	86	
4,4'-Ph ₂ bpy	17	this work	13.47
5-Clphen	3.7	this work	13.74
5-Clphen	3.7	86	
5-Birphen	3.5	this work	13.7
5-Birphen	4.0	86	
phen	2.7	this work	13.74
phen	4.9	86	
phen	5.0 ^f	86	

TABLE 3-20, cont'd.

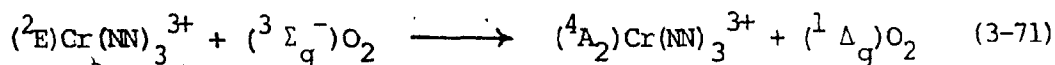
NN	$k_q \times 10^{-7}$ ($M^{-1} \text{ sec}^{-1}$) ^a	Reference	$E^{O-O} (M/M) \times 10^{-3}$ (cm^{-1}) ^b
phen	4.4 ^g	86	13.7 ₄
5-Mephen	5.7	this work	13.7
5-Mephen	6.4	86	
5,6-Me ₂ phen	8.5	this work	13.6 ₆
4,7-Me ₂ phen	19.0	this work	13.6 ₂
4,7-Me ₂ phen	8.8	86	
3,4,7,8-Me ₄ phen	15.0	this work	13.5 ₇
5-Phphen	5.5	this work	13.7
4,7-Ph ₂ phen	31.0	this work	13.4 ₆

^a In 1 M HCl at 25°C, unless otherwise noted. ^b Energies corresponding to the (⁴A₂) → (²E) transition.

^c In water, 0.5 M NaCl, at ca. 25°C. ^d In H₂O/DMF solutions, at ca. 20°C. ^e In 1 M DCl, at 25°C.

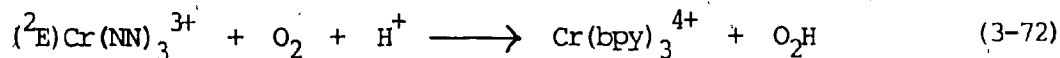
^f In D₂O, at 25°C. ^g In water, at 25°C.

by ca. 1.0 kK, a decrease in the energy transfer rate occurs. Inasmuch as the two lowest excited states of O_2 occur at ~ 12.9 kK ($^1\Sigma_g^+$) and ~ 7.9 kK ($^1\Delta_g$)¹¹⁸ and the energy of (2E)Cr(NN) $_3^{3+}$ is ~ 13.7 kK, energy transfer from (2E)Cr(NN) $_3^{3+}$ to O_2 to form ($^1\Delta_g$) O_2 is energetically feasible (reaction 3-71). The data in Table 3-20 also reveal that k_q is



particularly sensitive to small changes in the energies of the 2E donor states, as revealed in Figure 3-19.

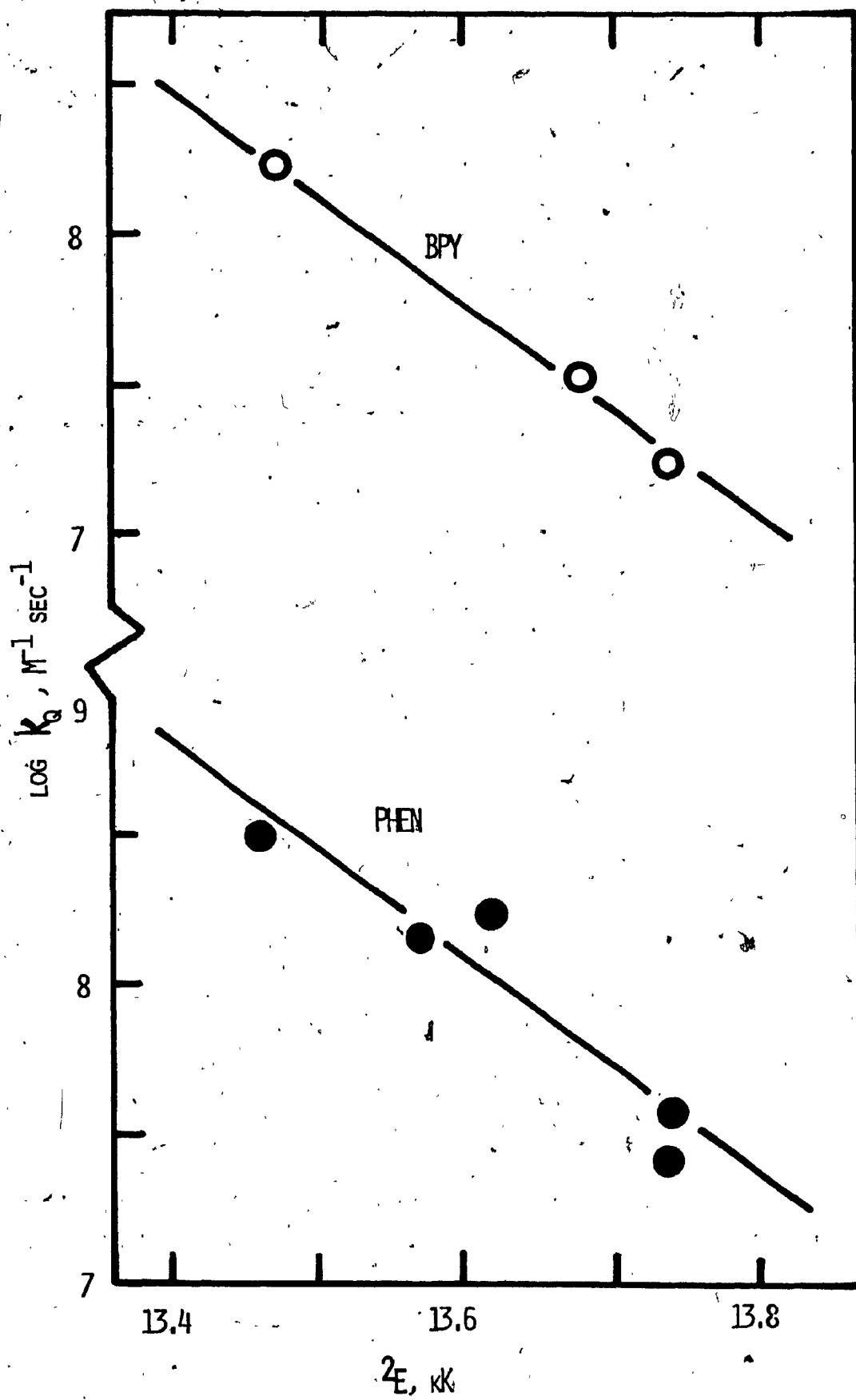
An oxidative electron transfer pathway for oxygen quenching of (2E)Cr(NN) $_3^{3+}$ (reaction 3-72) is believed⁸⁶ inoperable inasmuch as the



Cr(bpy) $_3^{4+}$ /(2E)Cr(bpy) $_3^{3+}$ couple will be more positive than -0.1 V. Moreover, reaction (3-73) will be endoergic in 1.0 M HCl if a reduction potential of -0.33 V for O_2 and a $pK = 4.7$ for O_2H are used.⁸⁶ Thus it would appear highly unlikely that an oxidative electron transfer process, with an unfavorable driving force, will be the dominant quenching pathway.

The results in Table 3-20 and Figure 3-19 show that k_q decreases with increasing donor energy. This trend has been observed¹¹¹ for oxygen quenching of triplet states of aromatic molecules and attributed to the proportionality of energy transfer rate and Franck-Condon-factors of the donor and acceptor species. (However, the Franck-Condon factors for molecular oxygen are very small except for the zero-zero transition, and thus need not be considered). The Franck-Condon factors are a function of the

FIGURE 3-19 : Plots of $\log k_q$ vs the Energy of the 2E States for the
Reaction Between $({}^2E)\text{Cr}(\text{NN})_3^{3+}$ and O_2 ; $\mu = 1.0 \text{ M (HCl)}$,
Aqueous Solutions, 25°C .



difference between the energy of the excited-state donor molecule, *E , and the energy that the oxygen molecule can accept upon excitation, E_{O_2} , ≈ 7.9 kK; that is,

$$\Delta E = {}^*E - E_{O_2} \quad (3-73)$$

where ΔE is essentially the remaining energy of the donor species. The efficiency of the quenching process should decline when the excited-state energy *E exceeds E_{O_2} to a significant degree, in view of Siebrand's¹¹⁹ conclusion that the Franck-Condon factor decreases monotonically with ΔE . In this light, it is interesting to note that while there is no significant change in the energies of the $({}^2E)Cr(NN)_3^{3+}$ species, the k_q values do vary by an order of magnitude (cf. 3-19). This would seem to suggest that Franck-Condon factors do not contribute significantly to the energy transfer pathway proposed here.

Pfeil⁶⁹ has investigated the quenching of various excited-state Cr(III) complexes by molecular oxygen, including $Cr(en)_3^{3+}$, $trans-Cr(NH_3)_2(NCS)_4^-$, $Cr(CN)_6^{3-}$ and $Cr(NCS)_6^{3-}$. His results show that k_q decreases with increasing 2E energy, and this was attributed to the "insulating" effects of the ligands such as ethylenediamine. Pfeil suggested⁶⁹ that the energy transfer process should be promoted by "conducting" ligands like CN^- and NCS^- , and hindered by "insulating" ligands like NH_3 and $NH_2CH_2CH_2NH_2$. With regard to the $Cr_2(NN)_3^{3+}$ complex ions, the variation in k_q with 2E energies cannot be attributed solely to the insulating effects of the polypyridyl ligands; however, the magnitude of k_q , relative to k_d , may arise from the insulating effect of the tight solvation spheres about the highly-charged cation which would retard the rate of O_2

penetration to the distance required for effective quenching.

Balzani and Bolletta¹⁰⁹ have shown that a collisional energy transfer process can successfully be treated within the Marcus and Rehm-Weller concepts of an outer-sphere electron transfer process in excited-state reactions. Thus, equation (3-19) can be written in the form

$$k_q = \frac{k_d}{1 + \frac{k_{-d}}{k_{en}} \exp(\Delta G^\ddagger/RT) + \exp(\Delta G_e^0/RT)} \quad (3-74)$$

for an energy transfer process, where ΔG_e^0 is defined by equation (3-66) and the free energy of activation for the energy transfer step, ΔG^\ddagger , is defined by equation (3-75) for the Weller relationship and equation (3-76) for the Marcus relationship; λ is the reorganizational energy

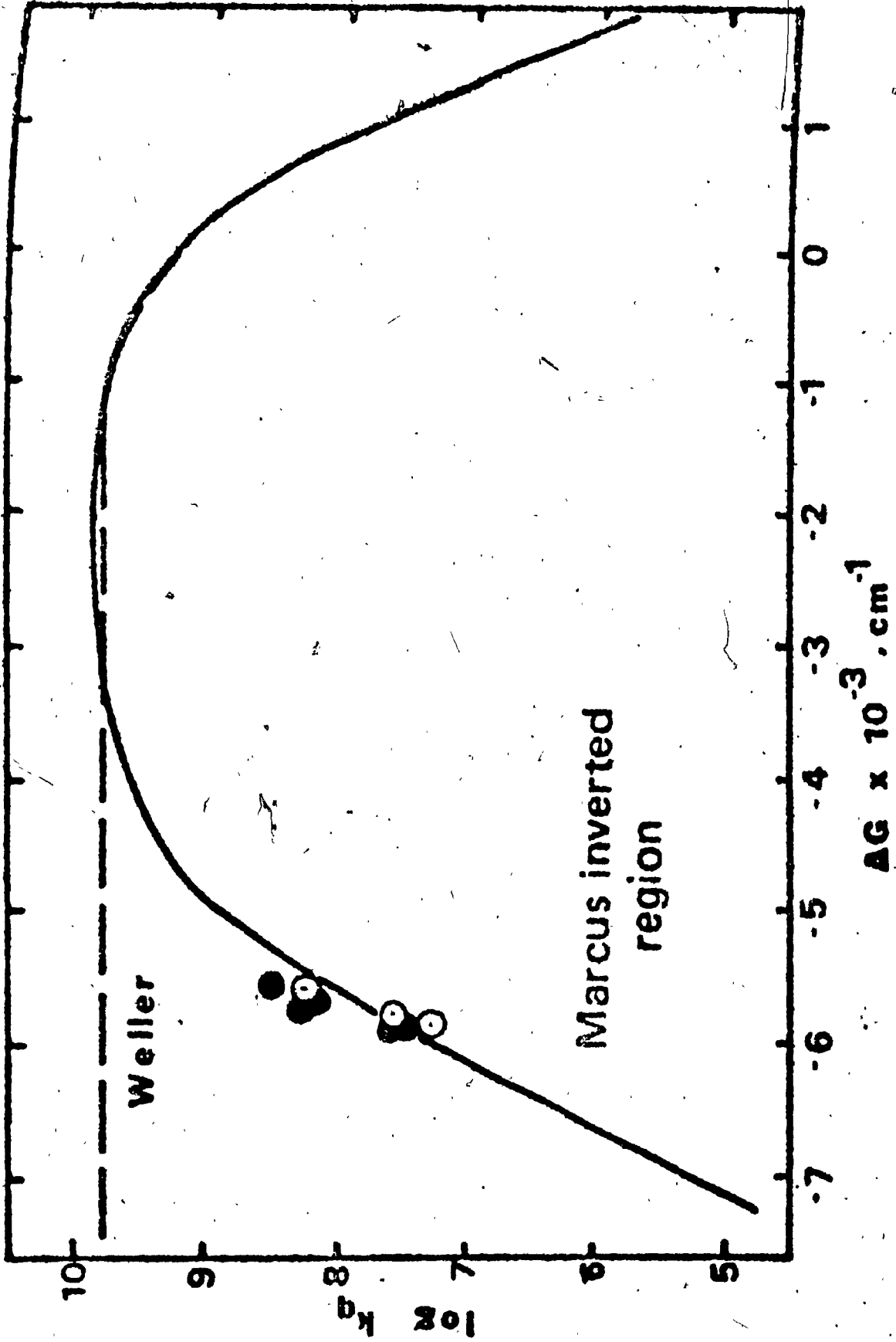
$$\Delta G^\ddagger = \frac{\Delta G_e^0}{2} + \left[\left(\frac{\Delta G_e^0}{2} \right)^2 + \left(\frac{\lambda}{4} \right)^2 \right]^{1/2} \quad (3-75)$$

$$\Delta G^\ddagger = \left(\frac{\lambda}{4} \right) \left(1 + \frac{\Delta G_e^0}{\lambda} \right)^2 \quad (3-76)$$

parameter associated with the energy transfer process. Figure 3-20 depicts the theoretical plot of $\log k_q$ vs the free energy change, ΔG_e^0 , for the Weller and Marcus relationships, assuming a value of $\lambda \sim 6$ kcal/mole which is the value obtained by curve-fitting the experimental k_q values of Table 3-20. Figure 3-20 shows that when $\Delta G_e^0 > -3.0$ kcal,

FIGURE 3-20 : Theoretical Plot of $\log k_q$ vs the Free Energy Change

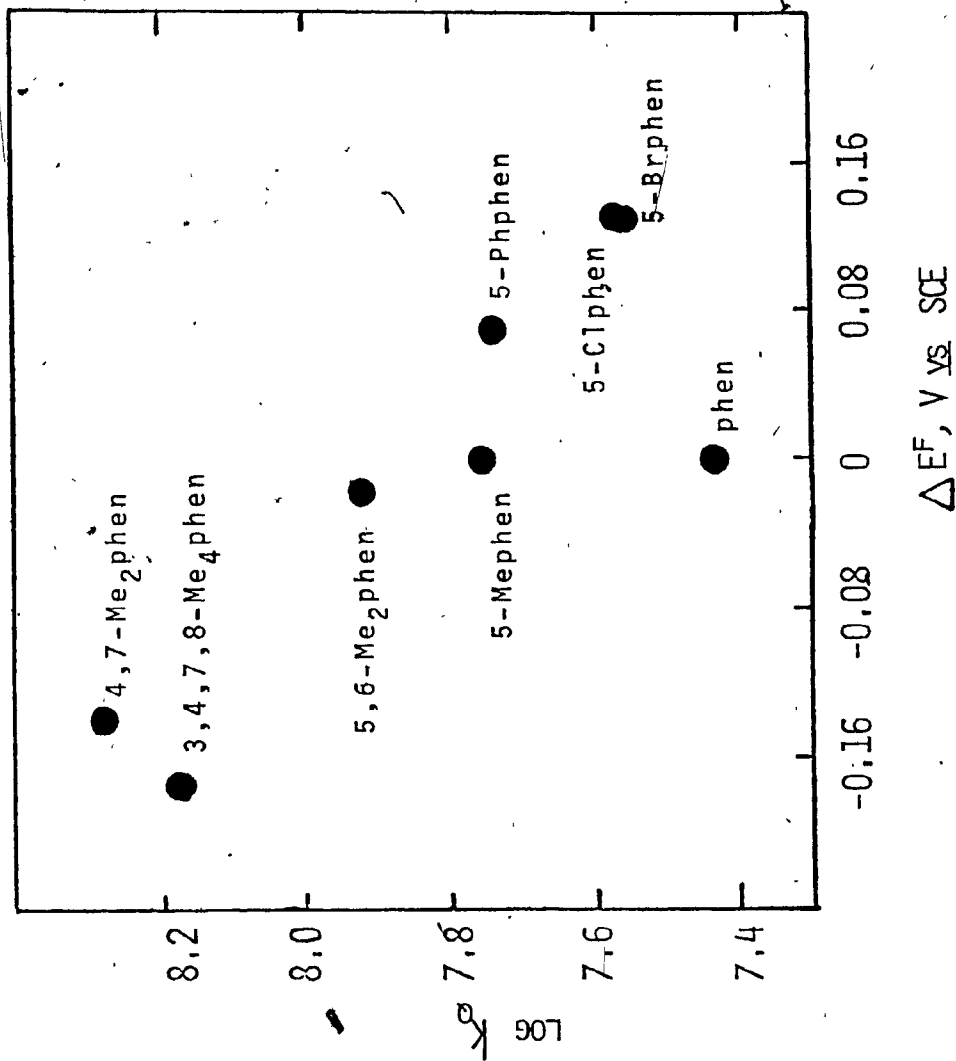
ΔG : (●) represent experimental quenching constants of the phenanthroline complexes; (○) indicate the k_q values for the bipyridyl complexes.



(that is, when the driving force for energy transfer becomes more favorable), the Marcus relationship predicts a dramatic decrease in k_q while the Weller relationship predicts that k_q will attain a plateau value approximately equal to the diffusion-controlled rate constant ($k_q \sim k_d$). Moreover, Figure 3-20 reveals that oxygen quenching of $(^2E)Cr(NN)_3^{3+}$ follows a Marcus-type inverted behavior, analogous to the electron transfer quenching of $(^3CT)Ru(NN)_3^{2+}$ by various complexes for which "vestiges" of the inverted Marcus region were observed.⁸³

It is also apparent from Table 3-20 that the k_q values obtained for oxygen quenching of $(^2E)Cr(NN)_3^{3+}$ exhibit some functionality toward the redox potentials of the Cr(III) complexes. A plot of $\log k_q$ vs ΔE_f is given in Figure 3-21, where $\Delta E_f = E_f(Cr(NN)_3^{3+}/Cr(NN)_3^{2+}) - E_f(Cr(phen)_3^{3+}/Cr(phen)_3^{2+})$ and E_f denotes the formal potential. The Figure illustrates the ligand substituent effects on redox potentials for the substituted phenanthroline complexes, as well as the relationship of k_q to those redox potentials. There appears to be a small but definite dependence of k_q on the redox potentials; such a dependence has previously been attributed to an electron transfer quenching path for the quenching of $(^3CT)Ru(NN)_3^{2+}$ by $Eu(III)$ ⁴⁴ and $Eu(II)$.⁹⁸ The behavior revealed in Figure 3-21 for the $Cr(NN)_3^{3+}$ complex ions does not support a reductive electron transfer pathway inasmuch as the stronger oxidant, $(^2E)Cr(5-Clphen)_3^{3+}$, has one of the smaller quenching constants. In fact, the variations revealed in Figure 3-21 are suggestive of an oxidative electron transfer pathway, though such a path seems unlikely in view of its endo-ergic nature. The dependence on redox potentials is nowhere near as dramatic as that exhibited by the $(^2E)Cr(NN)_3^{3+}/Fe^{2+}$ systems for which quenching does proceed via a reductive electron transfer pathway.

FIGURE 3-21 : Dependence of $\log k_q$ on ΔE^f (see text) for Oxygen
Quenching of $(^2E)Cr(NN)_3^{3+}$ Species.



Analysis of the oxygen quenching data for $(^2E)Cr(NN)_3^{3+}$ complex ions and comparison with MLCT excited states of analogous Ru(II) complex ions lead to the conclusion that reaction of $(^2E)Cr(NN)_3^{3+}$ with molecular oxygen proceeds predominantly via an energy transfer mechanism.

3.8. CHEMICAL REACTIVITY OF $(^2T_1/^2E)Cr(NN)_3^{3+}$ IN AQUEOUS SOLUTION.

Reactive deactivation of electronically-excited states of transition metal complexes may occur via three main pathways: i) substitutional photoreaction, ii) redox photoreaction, and/or iii) ligand photoreaction. Often one is tempted to assume that photosubstitution results from excitation into ligand-field absorption bands, while photo-redox and ligand reactions result from excitation into the charge-transfer and ligand-centered bands, respectively. Assumptions cannot be made a priori since absorption bands of different orbital parentage may overlap, the excited state reached by light absorption may be converted to a lower excited state of a different type (e.g., CT \xrightarrow{ISC} LC), and/or reaction products may vary according to the excited state from which they originate.

The principal factor which determines the chemical reactivity of a ground-state molecule is the electron distribution. As well, excited-state reactivity is also determined to some degree by the electron configuration. According to ligand field theory, a d-d transition redistributes the electrons between orbitals belonging to the metal ion (i.e., between the t_{2g} and e_g orbitals). In an octahedral complex, electronic excitation promotes an electron from a t_{2g} orbital, which points toward the center of the faces of the octahedron, to an e_g orbital, which points in the direction of the ligands. The accumulation of electron density between the metal center and the ligands in the 4T_2 state of Cr(III)

complexes is expected to give rise to ligand repulsion and, thereby, metal-ligand bond labilization. The concomitant decrease in electron density along the edges/faces of the octahedron may favor nucleophilic attack by an incoming ligand. According to molecular orbital theory, a spin-allowed d-d transition results in the promotion of an electron from the non-bonding t_{2g} orbitals to the σ -antibonding e_g orbitals, if one only considers σ bonding. As a result, any vacant t_{2g} orbital would be available to some entering ligand. Thus, ligand-field transitions involve angular movement of electron density, and the photoreaction expected is one of heterolytic fission (i.e., substitution).

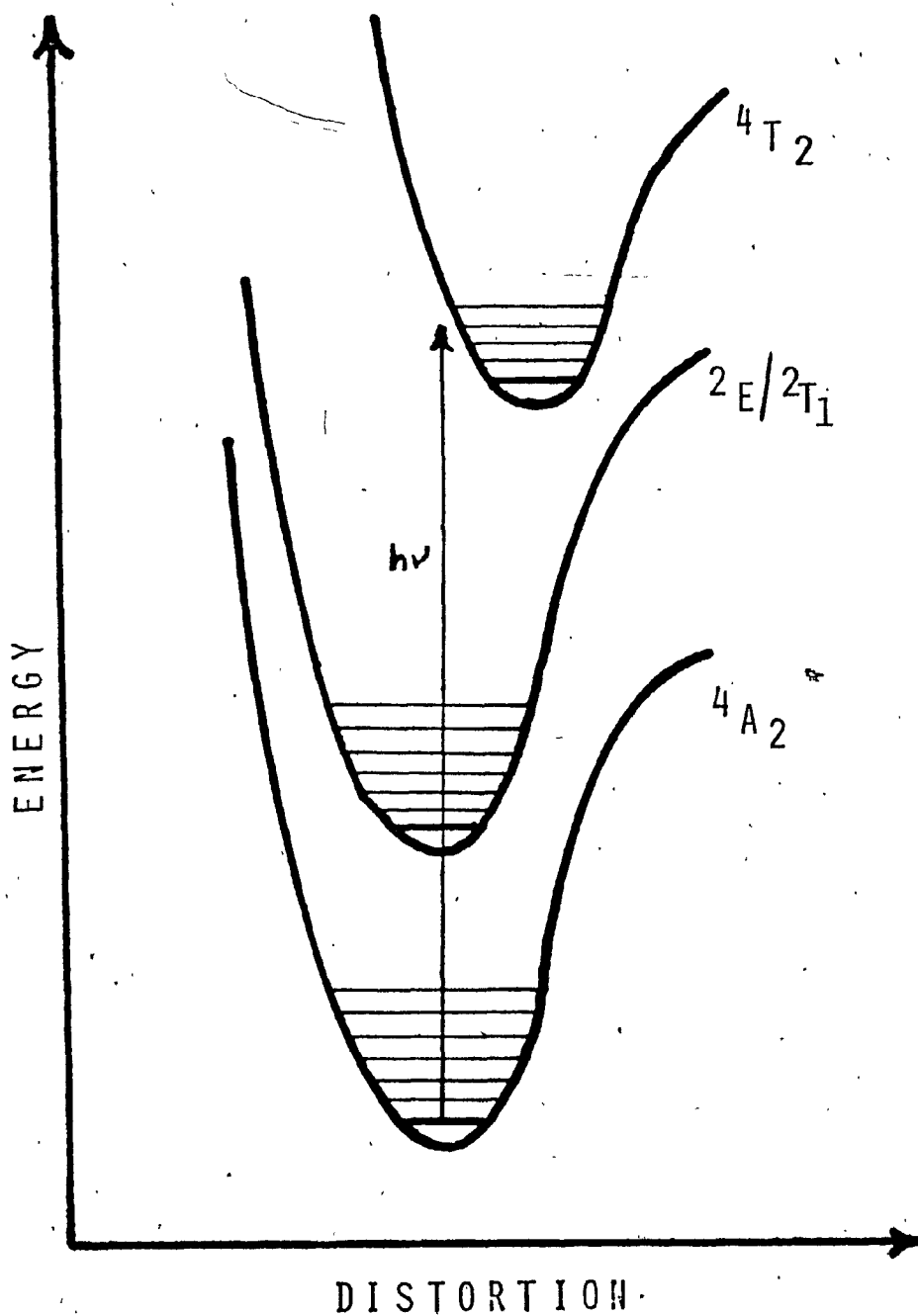
In addition to electron configuration, the geometry and energies of the excited states must be considered. Spectroscopic behavior of Cr(III) complexes reveals that the spin-allowed ${}^4A_2 \longrightarrow {}^4T$ absorption bands are generally broad and structureless, while the spin-forbidden ${}^4A_2 \longrightarrow {}^2E$ bands are sharp. This would indicate that the potential energy surfaces for the spin-forbidden excited states possess virtually the same geometry as the ground state. Luminescence data support this contention, inasmuch as little or no Stokes shift is observed. A potential energy surface diagram (in two dimensions) is given in Figure B-22 for octahedral Cr(III) complexes.

In light of the predicted photoreactivity of Cr(III) excited states and the known ground-state reactivity of $\text{Cr}(\text{NN})_3^{3+}$ in aqueous solution,¹ the photoreactivity of $\text{Cr}(\text{NN})_3^{3+}$ has been investigated in aqueous solution, as well as that of $\text{Cr}(\text{bpy})_3^{3+}$ in a mixed solvent system.

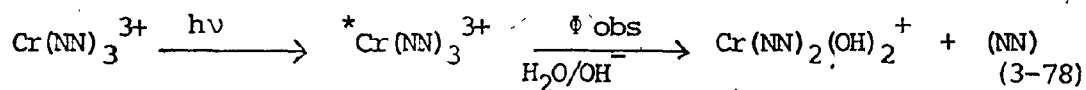
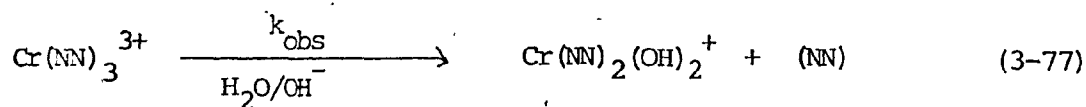
3.8.0. Continuous Photolysis of $\text{Cr}(\text{NN})_3^{3+}$ Complexes.

Continuous photolysis (313 - 464 nm) of aqueous neutral or basic solutions (pH 7 - 10.5) of $\text{Cr}(\text{bpy})_3^{3+}$ and $\text{Cr}(\text{phen})_3^{3+}$ leads to

FIGURE 3-22 : A Potential Energy Surface Diagram (in two dimensions) for Octahedral Cr(III) Complexes. The 2E and 2T_1 states are in thermal equilibrium and are designated as ${}^2E/{}^2T_1$.



substitution by two water (or hydroxyl) molecules for one polypyridyl ligand as well as the formation of free polypyridine, as shown in this work and by others.^{38,49} The spectral changes, formation of free polypyridine and location of isosbestic points mimic those observed¹ for the corresponding thermal reactions. For $\text{Cr}(\text{bpy})_3^{3+}$ at pH 9.6, the absorption spectral changes of continuously photolysed, repeatedly flashed, and thermal solutions were identical, with isosbestic points located at 306, 270, 262 and 254 nm. Similar experiments for $\text{Cr}(\text{phen})_3^{3+}$ locate the isosbestic points at ca. 475, 287, 256, 235 and 222 nm, and these are shown in Figure 3-23. The overall stoichiometric thermal and photochemical reactions are given in reactions (3-77) and (3-78), respectively, for $\text{Cr}(\text{bpy})_3^{3+}$ and $\text{Cr}(\text{phen})_3^{3+}$ in basic aqueous solutions, for which ϕ_{obs} is the observed quantum yield for polypyridine release. The



observed quantum yield, ϕ_{obs} , results from all the processes that eventually lead to the observed products. With reference to Figure 3-24, the quantum yield may be defined in terms of the efficiencies of the intersystem crossing (${}^4\eta_{\text{isc}}$) and reactive (${}^4\phi_{\text{rx}}$, ${}^2\phi_{\text{rx}}$) processes of the ${}^4\text{T}_2$ and ${}^2\text{T}_1/\text{E}$ excited states, as in equation (3-79);

$$\phi_{\text{obs}} = ({}^4\eta_{\text{isc}} {}^2\eta_{\text{rx}}) + {}^4\eta_{\text{rx}} \quad (3-79)$$

FIGURE 3-23 : Spectral Variations upon 365-nm Irradiation of 2.2×10^{-5} M $\text{Cr}(\text{phen})_3^{3+}$ at pH 10.4 and 15°C in 0.008 M Britton-Robinson Buffer and 1.0 M NaCl; Irradiation Times are: A, 0 min; B, 8 min; C, 20 min; D, 40 min; E, 180 min.

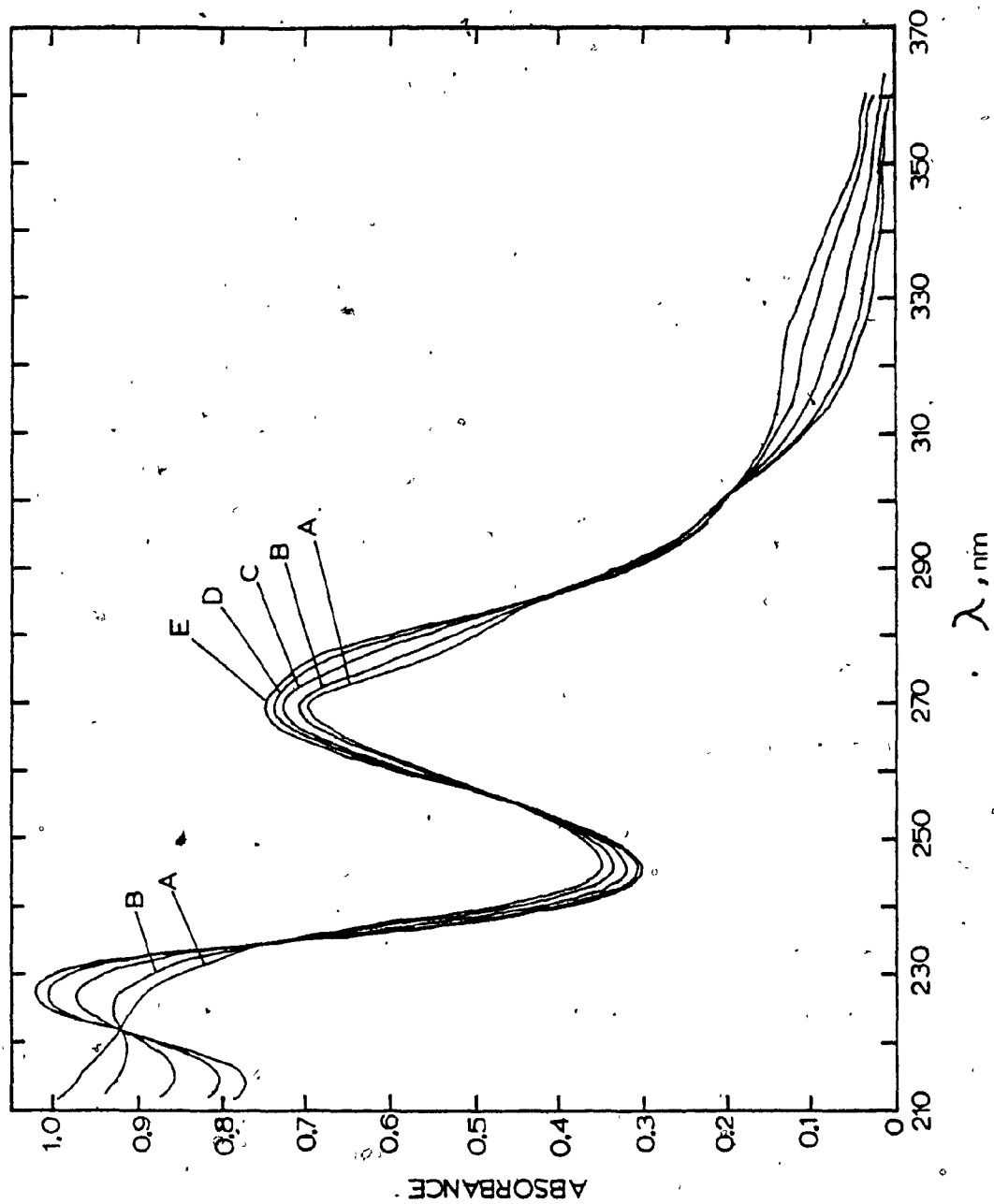
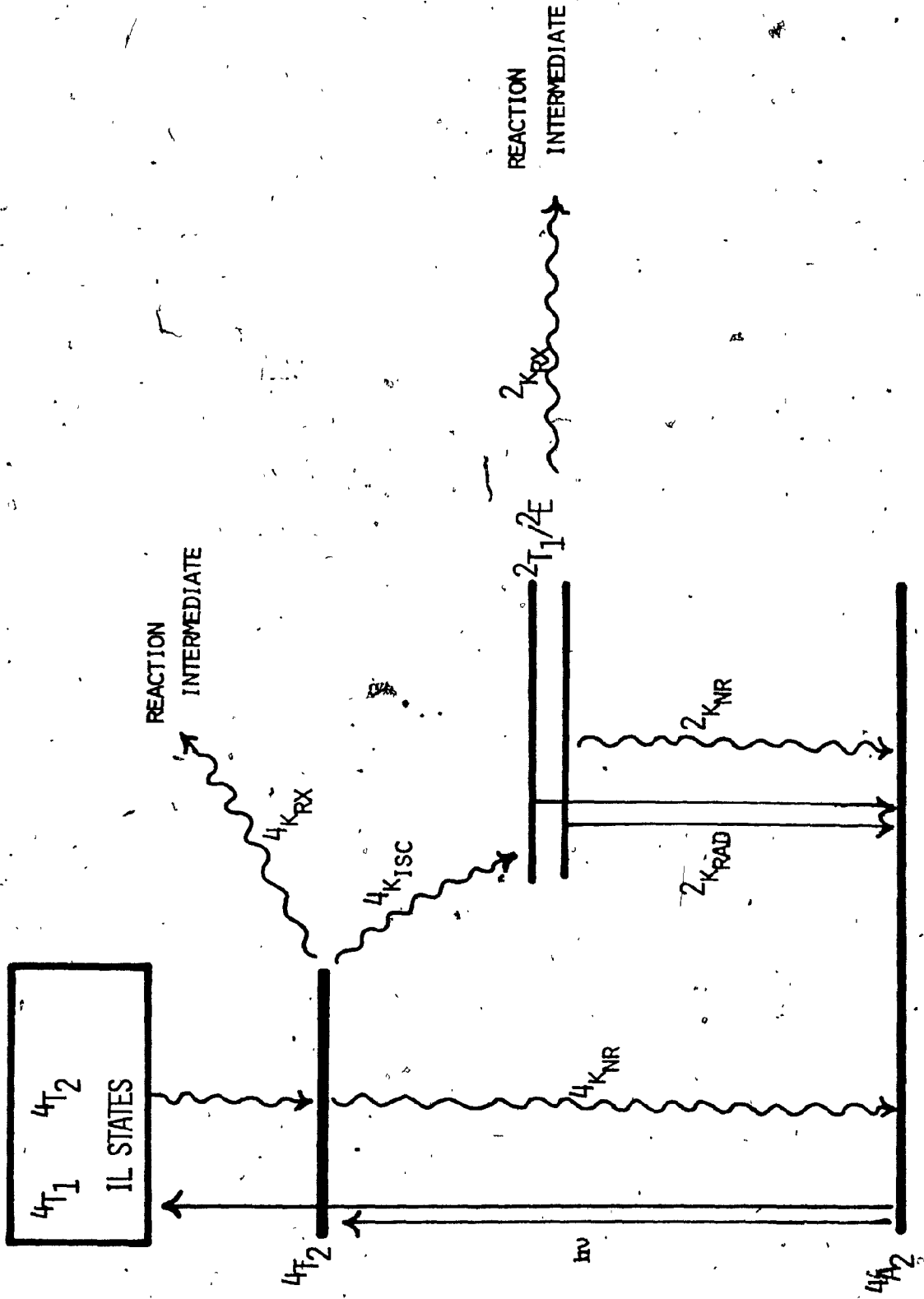


FIGURE 3-24 : Energy-level Diagram for $\text{Cr}(\text{NN})_3^{3+}$ Complexes Depicting
Important Chemical and Physical Processes.



${}^2\eta_{rx}$ is the efficiency of the chemical reaction out of ${}^2T_1/{}^2E$, ${}^4\eta_{rx}$ is the efficiency of chemical reaction out of 4T_2 , and ${}^4\eta_{isc}$ is the efficiency of the ${}^4T_2 \rightsquigarrow {}^2T_1/{}^2E$ intersystem crossing process. These are defined in equations (3-80) to (3-82).

$${}^2\eta_{rx} = \frac{{}^2k_{rx}}{{}^2k_{rx} + {}^2k_{rad} + {}^2k_{nr}} \approx \frac{{}^2k_{rx}}{{}^2k_{rx} + {}^2k_{nr}} = {}^2k_{rx} {}^2\tau \quad (3-80)$$

$${}^4\eta_{rx} = \frac{{}^4k_{rx}}{{}^4k_{rx} + {}^4k_{rad} + {}^4k_{nr} + {}^4k_{isc}} \approx \frac{{}^4k_{rx}}{{}^4k_{isc} + {}^4k_{rx}} \quad (3-81)$$

$${}^4\eta_{isc} = \frac{{}^4k_{isc}}{{}^4k_{isc} + {}^4k_{nr} + {}^4k_{rx}} \approx \frac{{}^4k_{isc}}{{}^4k_{isc} + {}^4k_{nr}} \quad (3-82)$$

Inasmuch as ${}^4\eta_{isc} \sim 1$ (see Section 3.10.0.),

$$\phi_{obs} \approx {}^2\eta_{rx} + {}^4\eta_{rx} \approx {}^{4 \rightarrow 2}\phi_{rx} \quad (3-83)$$

Thus, ϕ_{obs} is the efficiency of chemical reaction out of ${}^2T_1/{}^2E$ and 4T_2 . Studies have shown that ${}^4\eta_{rx} \sim 0.003$ (see Section 3.9.); therefore, the observed quantum yield becomes that in (3-84) if ${}^4\eta_{rx}$ is neglected.

$$\phi_{obs} \approx {}^2\eta_{rx} \approx {}^2\phi_{rx} \quad (3-84)$$

Under conditions where ${}^2\eta_{rx} \sim 0$, the observed quantum yield will be the efficiency of chemical reaction from the 4T_2 state,

$$\phi_{obs} \approx {}^4\eta_{rx} \approx {}^4\phi_{rx} \quad (3-85)$$

The total quantum yield for photoaquation has been evaluated spectrophotometrically for several $Cr(NN)_3^{3+}$ complexes; the data are presented in Table 3-21 for the various complex ions at pH < 6, and pH 9 - 10.5. Among the bpy complexes, ${}^{4+2}\phi_{rx}$ decreases with increasing size of substituent on the bpy ligand framework; and, except for the 5-halo complexes, a similar trend is observed for the phen complexes. For the 5-halo complexes, the increase in ${}^{4+2}\phi_{rx}$ is most likely due to the electron-withdrawing nature of the chloro- and bromo-substituents and to an increase in the hydrophilic environment of the reaction site. For all $Cr(NN)_3^{3+}$ complexes investigated, ${}^{4+2}\phi_{rx}$ is substantially less in acidic media than in basic media, suggesting that the substituted complexes behave analogously to $Cr(bpy)_3^{3+}$ and $Cr(phen)_3^{3+}$.

A critical evaluation of ${}^{4+2}\phi_{rx}$ as a function of pH for $Cr(bpy)_3^{3+}$ and $Cr(phen)_3^{3+}$ has shown that ${}^{4+2}\phi_{rx}$ for the photoreaction and k_{obs} for the thermal aquation reaction exhibit similar pH dependence; the results are shown in Figures 3-25 and 3-26 for the photoaquation of the bpy and phen complexes, and are to be compared with Figures 3-3a and b for the thermal reaction. The results for $Cr(bpy)_3^{3+}$ at 22°C in Figure 3-25 are in agreement with those of Balzani and coworkers³⁸ at 11°C. The similarity of k_{obs} and ${}^{4+2}\phi_{rx}$ vs pH eliminates the possibility that the pH dependence of ${}^{4+2}\phi_{rx}$ is due to acid-base properties of the excited states; furthermore, it suggests that either the ground state reactant is present

TABLE 3-21 : Photoaquation Quantum Yields for Cr(NN)₃³⁺ Complexes at 22°C in Deaerated Solutions.^a

NN	[Cr(NN) ₃ ³⁺] (mM)	ϕ_{rx} (pH)
bpy	1.0	0.13 (9.8)
4,4'-Me ₂ bpy ^b	0.12	0.002 ± 0.001 (5.1)
		0.064 ± 0.013 (9.3)
		0.061 ± 0.001 (10.4)
4,4'-Ph ₂ bpy ^c	0.048	0.011 ± 0.002 (5.1)
		0.024 ± 0.005 (9.3)
		0.018 ± 0.001 (10.4)
phen	1.5	0.0005 (5.1)
		0.005 ± 0.002 (9.2)
		0.006 ± 0.001 (10.4)
5-Clphen	0.14	0.0020 ± 0.0010 (5.1)
		0.010 ± 0.001 (9.2)
		0.013 ± 0.003 (10.4)

TABLE 3-21, cont'd.

NN	$[Cr(NN)_3^{3+}]$ (mM)	$4+2 \phi_{EX}$ (pH)
5-Birphen ^b	0.12	0.0062 ± 0.0002 (5.2), 0.009 ± 0.001 (9.2)
5-Mephen	0.12	0.007 ± 0.001 (10.4) 0.0044 ± 0.0004 (5.2)
5-Phphen ^b	0.072	0.012 ± 0.001 (9.2) 0.012 ± 0.001 (10.4) 0.0033 ± 0.0005 (5.2)
5,6-Me ₂ phen ^b	0.11	0.006 ± 0.001 (9.2) 0.006 ± 0.001 (10.4) 0.0047 ± 0.0002 (5.2)
4,7-Me ₂ phen ^b	0.11	0.006 ± 0.001 (9.3) 0.007 ± 0.001 (10.4) 0.0003 (5.1) 0.004 ± 0.001 (9.3) 0.003 ± 0.001 (10.4)

TABLE 3-21, cont'd.

NN	$[\text{Cr}(\text{NN})_3^{3+}]$ (mM)	$4^{+2} \phi_{\text{rx}}$ (pH)
4,7-Ph ₂ phen ^c	0.034	0.0012 ± 0.0003 (5.1)
		0.0015 ± 0.0001 (9.3)
		0.0013 ± 0.0001 (10.4)
3,4,7,8-Me ₄ phen	0.084	0.0002 (5.1)
		0.0014 ± 0.0002 (9.3)
		0.0018 ± 0.0002 (10.4)

a $\lambda_{\text{exct}} = 313 \text{ nm}$; solution contains 1.0 M NaCl in 0.008 M Britton-Robinson buffer at $[\text{Cr}(\text{NN})_3^{3+}]$ shown.
 $4^{+2} \phi_{\text{rx}}$ is reported as the mean value of 2 - 6 determinations with the error as the deviation from the mean.

b Solution contains 4% v/v CH₃CN. ^c Solution contains 40% MeOH.

FIGURE 3-25 : Dependence of the Quantum Yield of Photoaquation on
pH for $\text{Cr}(\text{bpy})_3^{3+}$ at 22°C in Argon-purged Solutions
Containing 0.008 M Britton-Robinson Buffer and 1.0 M
NaCl.

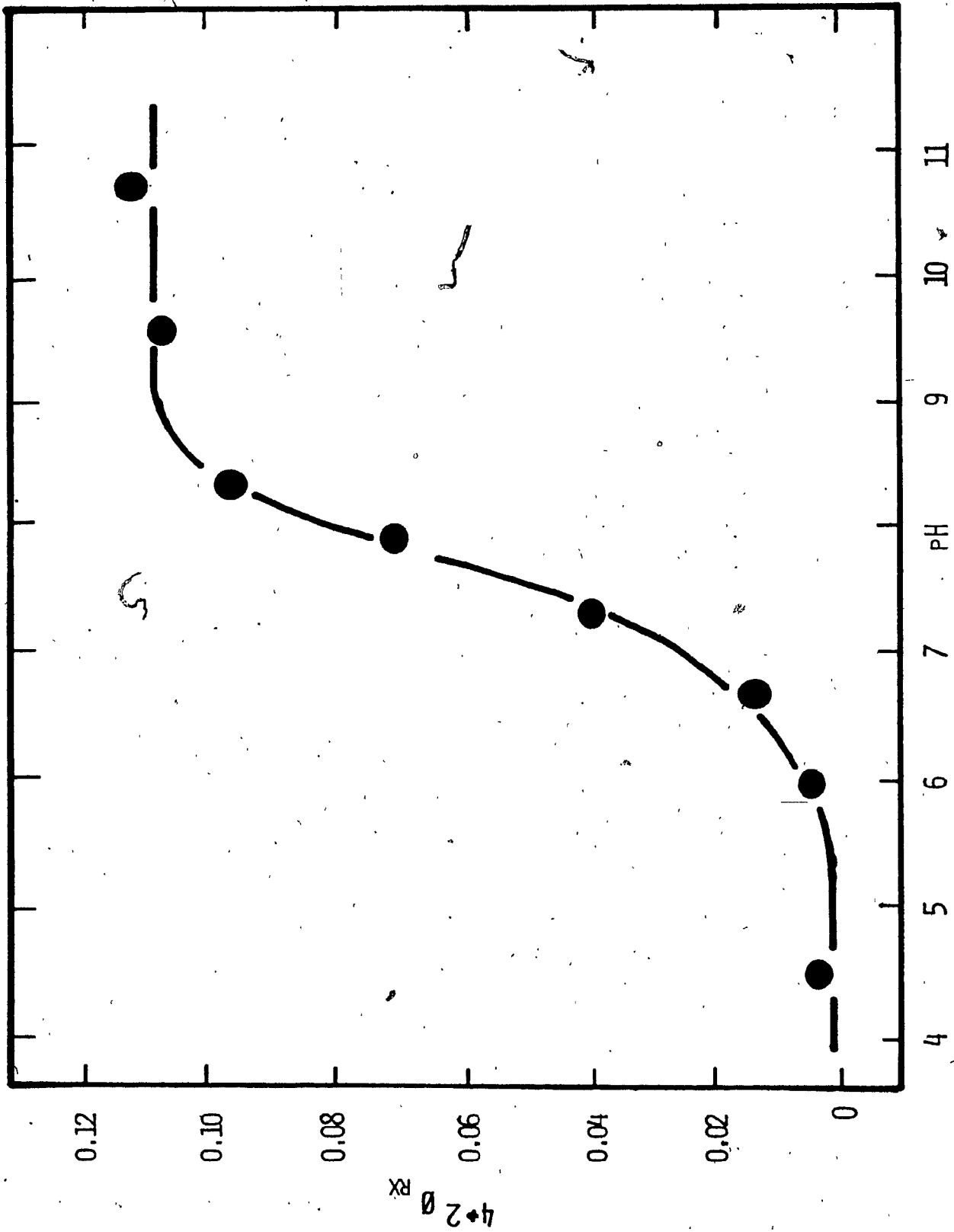
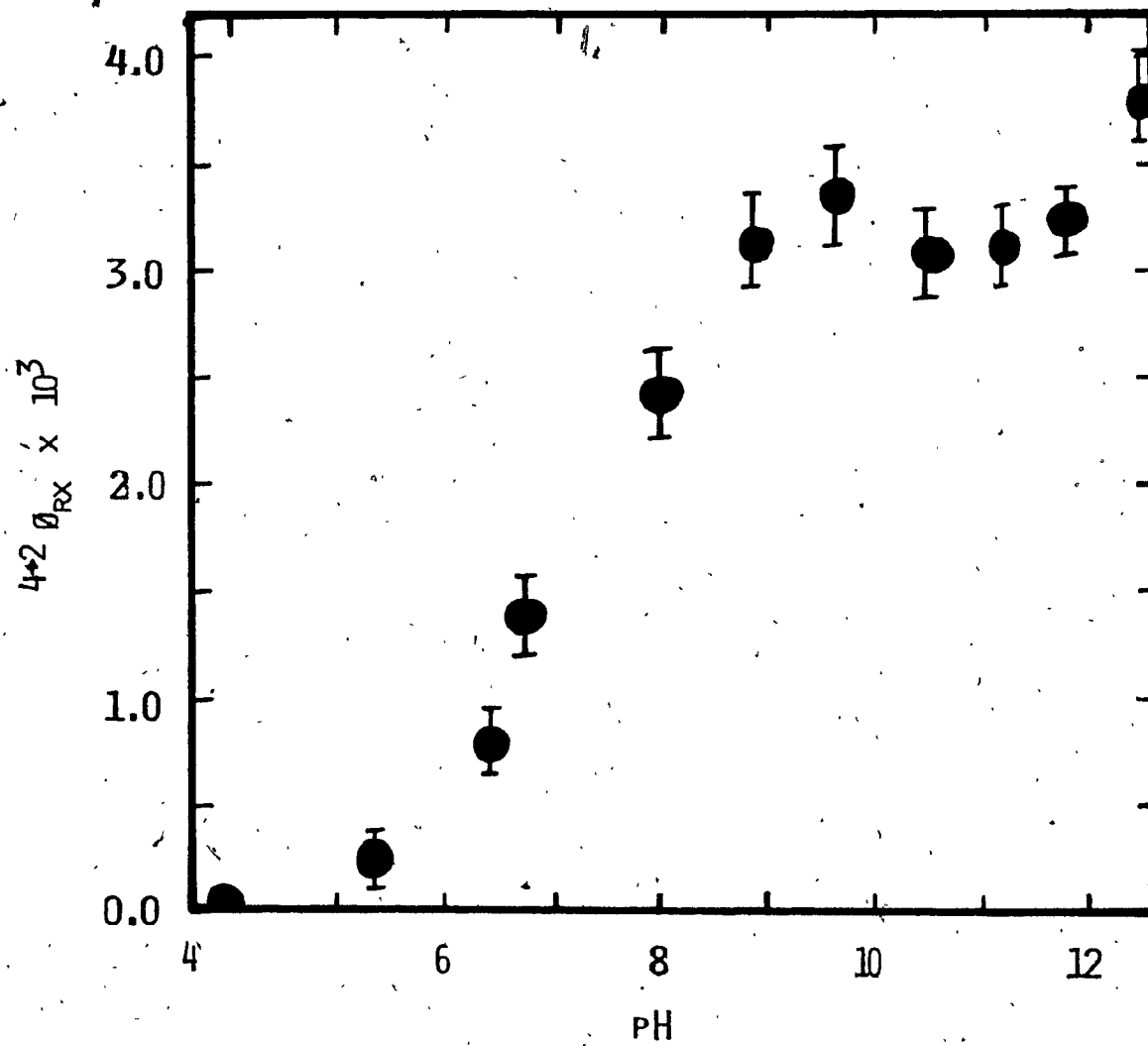


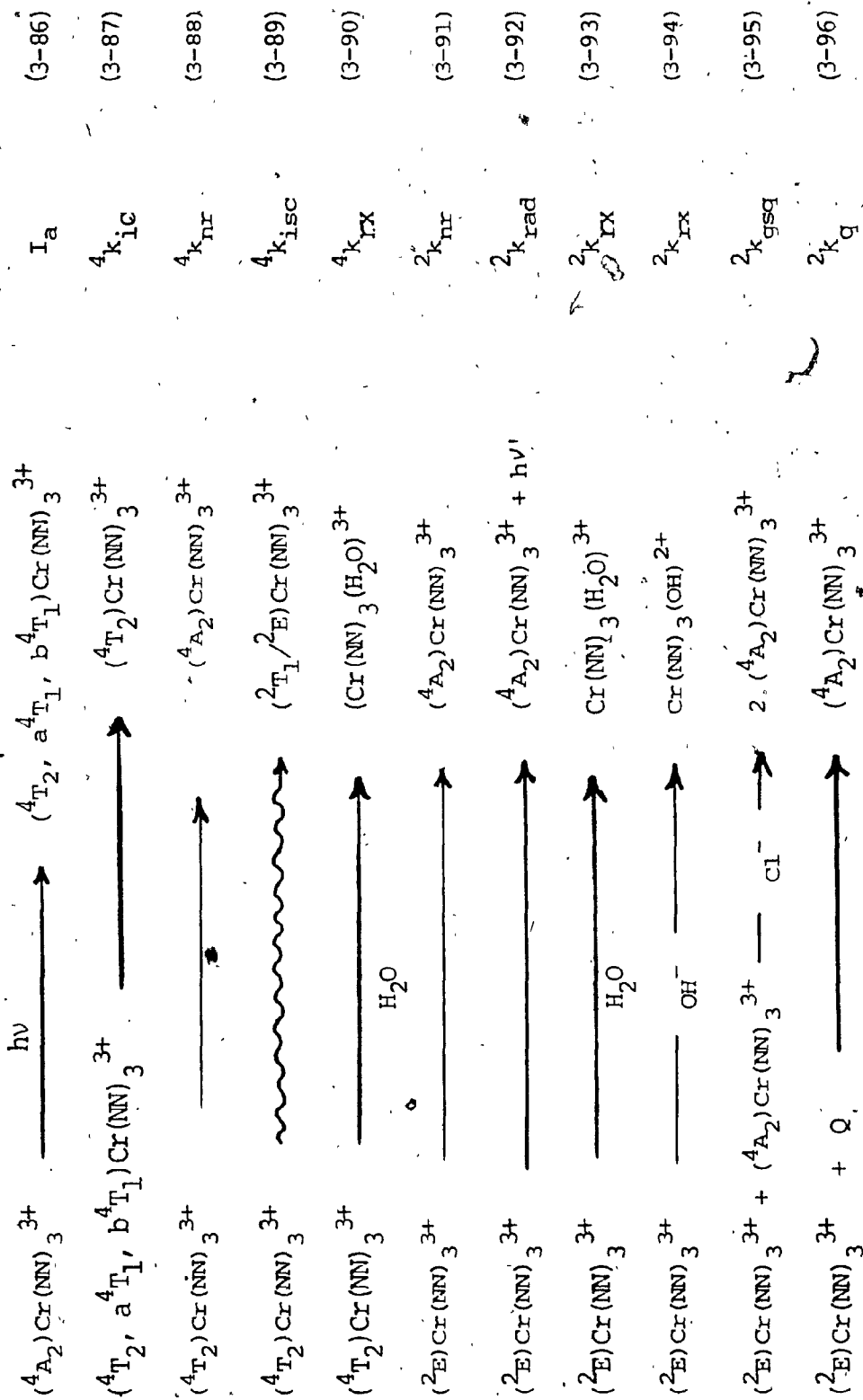
FIGURE 3-26 : Dependence of the Quantum Yield of Photoaquation on pH for $\text{Cr}(\text{phen})_3^{3+}$ at 15°C in Air-equilibrated Solutions Containing 0.008 M Britton-Robinson Buffer and 1.0 M NaCl.



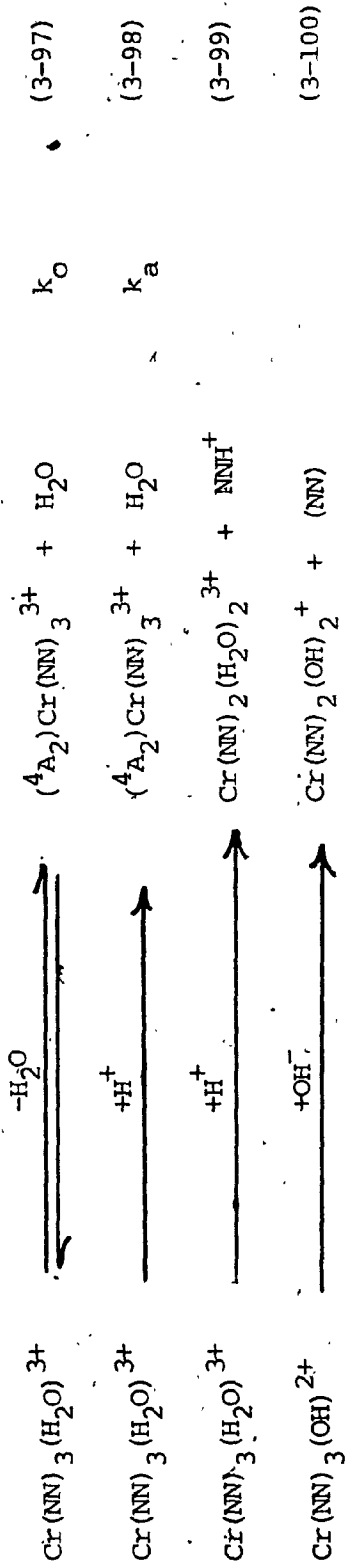
in different acid-base forms in acidic and alkaline media, or that the thermal and photochemical reactions involve common, acid-dependent intermediate species. Whereas both are plausible hypotheses to account for the thermal reaction kinetics, only the hypothesis involving common, pH-dependent chemical intermediate species for the thermal and photoaquation reactions appears valid inasmuch as both the absorption and emission spectra for $\text{Cr}(\text{bpy})_3^{3+}$ and $\text{Cr}(\text{phen})_3^{3+}$ are pH independent. The associative interchange mechanism assigned¹ to the thermal aquation of $\text{Cr}(\text{bpy})_3^{3+}$ and $\text{Cr}(\text{phen})_3^{3+}$ is believed to be equally applicable to the photoaquation reaction. The reaction scheme is outlined in Scheme 3-6 for $\text{Cr}(\text{NN})_3^{3+}$ complex ions (reactions 3-86 to 3-100).

The formation of an intermediate, presumably the seven-coordinate species (reactions 3-93 and 3-94) is evidenced by transient bleaching in acidic media (secondary transient) of $\text{Cr}(\text{bpy})_3^{3+}$.³⁸ Reformation of $(^4A_2)\text{Cr}(\text{NN})_3^{3+}$ from the seven-coordinate intermediate occurs via acid-dependent (reaction 3-98) and acid-independent (reaction 3-97) paths. The acid-dependent pathway involves $\text{Cr}-\text{OH}_2$ bond rupture, assisted by H^+ ; and the acid-independent pathway reflects the relaxation of the seven-coordinate intermediate to form $(^4A_2)\text{Cr}(\text{NN})_3^{3+}$ via direct loss of coordinated water. The acid-dependent path is thought to be the primary reaction leading to the relative stability, both thermal and photochemical, of $\text{Cr}(\text{NN})_3^{3+}$ in acidic solution. Both the acid-independent and -dependent paths are operable in the thermal reaction, for which the reverse of reaction (3-97) is the rate-determining step. In the photochemical reaction, $k_o \sim 10 \text{ sec}^{-1}$ and $k_a = 4 \times 10^5 \text{ M}^{-1} \text{ sec}^{-1}$ for reactions (3-97) and (3-98), respectively, as obtained from ²E absorption spectra. Finally, deprotonation of the seven-coordinate intermediate (reaction 3-101) leads

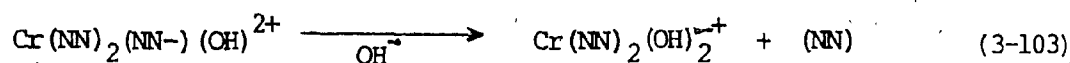
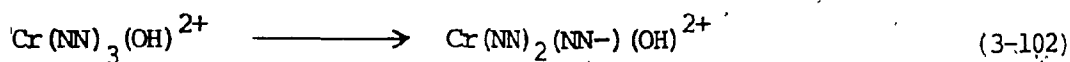
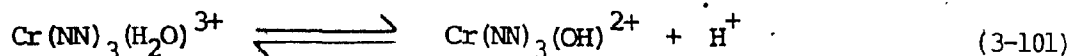
SCHEME 3-6



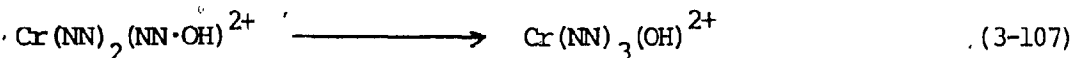
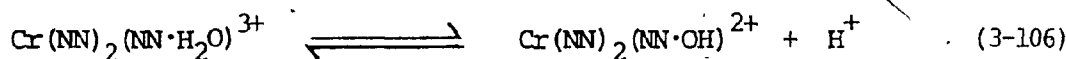
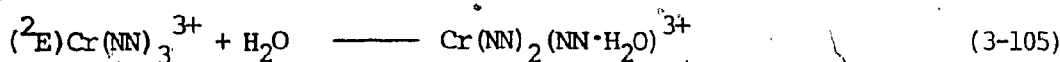
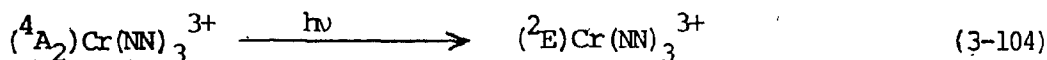
SCHEME 3-6, cont'd.



ultimately, quantitatively and irreversibly to ring-opening (reaction 3-102) and to loss of NN (reaction 3-103).



As suggested previously for the ground-state aquation reaction, a Gillard-type¹¹ covalent-hydrate mechanism is also plausible for the photoaquation reaction, for which reactions (3-104) to (3-107) followed by reactions (3-102) and (3-103) are applicable.



A general kinetic treatment of such a mechanism accounts for the pH dependence of the photoaquation reaction. However, such a mechanism is thought not to be applicable for $\text{Cr}(\text{NN})_3^{3+}$ complex ions for the following reasons. In O_h symmetry, the t_{2g} orbitals are occupied equally in the

2E excited state; but for complexes of lower symmetry, configuration interactions are present. As such, the lowering of symmetry should facilitate direct nucleophilic attack by H_2O on the Cr(III) center. While a covalent-hydrate mechanism would be favored by ligand-to-metal charge-transfer excited configurations since nucleophilic attack occurs on the ligand framework, an associative interchange mechanism involving direct nucleophilic attack on the metal center would be favored by metal-centered excited configurations; that is, direct attack on the $^2E/2T_1$ species. Furthermore, Sandrini and coworkers¹²⁰ have found evidence for direct reaction between the 2E state and hydroxide ion for $\text{trans-Cr(en)}_2(\text{NCS})_2^+$, a complex incapable of photoaquation via a covalent-hydrate pathway. For these reasons, a Gillard-type mechanism is believed to be highly improbable for the Cr(NN)_3^{3+} complexes.

3.8.1. Temperature Dependence of $^{4+2}\phi_{rx}$

Since the same seven-coordinate intermediate, $\text{Cr(NN)}_3(\text{H}_2\text{O})^{3+}$, is believed to be formed from both the 4A_2 and $(^2T_1/2E)$ electronic states via equivalent reaction paths, the Cr(bpy)_3^{3+} and Cr(phen)_3^{3+} complex ions allow a direct comparison of the kinetic parameters of the ground- and excited-state reactivities in aqueous solution.

The observed quantum yield of photoaquation was measured as a function of temperature for Cr(bpy)_3^{3+} and Cr(phen)_3^{3+} at pH 9.5 - 10, employing 313-nm excitation. The values of $^{4+2}\phi_{rx}$ at the various temperatures are shown in Tables 3-22 and 3-23 for the bpy and phen complex ions, respectively. Since the contribution of the unquenchable reaction component is only about 3-4% for Cr(bpy)_3^{3+} , the total quantum yields are used.

Employing the Arrhenius-type equation (3-108), an "apparent" activation energy, E_{app} , can be obtained from the slope ($= -E_{app}/RT$) of a linear

TABLE 3-22 : Quantum Yields of Photoaquation and Doublet-state Rate Constants for $(^2T_1/E)Cr(bpy)_3^{3+}$ as a Function of Temperature in Deaerated Solutions.^a

Temperature, (K)	$4 \rightarrow 2 \phi_{rx}$	$^2k_{O'}$ (sec^{-1})	$^2k_{rx}$ (sec^{-1})	$^2k_{nr}$ (sec^{-1})
279.5	0.089	0.56×10^4	0.5×10^3	0.51×10^4
284.3	0.095	0.77×10^4	0.73×10^3	0.70×10^4
295.3	0.12	1.52×10^4	1.83×10^3	1.34×10^4
301.0	0.127	2.13×10^4	2.70×10^3	1.86×10^4
305.8	0.122	2.79×10^4	3.39×10^3	2.45×10^4
309.5	0.119	3.42×10^4	4.07×10^3	3.01×10^4

^a pH = 9.8, 0.008 M Britton-Robinson Buffer, $\mu = 1.0$ with NaCl, argond-purged solutions.

TABLE 3-23 : Temperature Profile of the Total Photoaquation, Unquenchable Photoaquation and Quenchable Photoaquation Quantum Yields for $\text{Cr}(\text{phen})_3^{3+}$ in Deaerated Solutions. ^a

Temperature, (K)	$\phi_{\text{IX}}^{\text{tot}}$	$4\phi_{\text{IX}}^{\text{b}}$	$2\phi_{\text{IX}}^{\text{c}} = \phi_{\text{IX}}^{\text{tot}} - 4\phi_{\text{IX}}^{\text{b}}$
286.2	0.001 ₉	1.1×10^{-4}	1.8×10^{-3}
295.4	0.003 ₆	2.5×10^{-4}	3.3×10^{-3}
302.2	0.011 ₇	4.3×10^{-4}	1.13×10^{-2}
309.2	0.018 ₁	2.1×10^{-3}	1.6×10^{-2}
314.4	0.046 ₂	1.57×10^{-2}	3.05×10^{-2}

^a In deaerated solutions containing 0.008 M Britton-Robinson buffer, $\mu = 1.0$ (with NaCl), unless otherwise noted; pH = 10.0. ^b Contains 0.05 M iodide ion.

$${}^{4+2}\phi_{\text{rx}} = A e^{-E_{\text{app}}/RT} \quad (3-108)$$

plot of $\ln {}^{4+2}\phi_{\text{rx}}$ vs $1/T$ for the bpy system. Such a plot is linear in the temperature range investigated, and yields $E_{\text{app}} = 1.9$ kcal/mole. However, the E_{app} value so obtained cannot be considered as a direct measure of the true activation energy, since the Arrhenius equation relates a rate constant "k" to the activation energy E_a , and ${}^{4+2}\phi_{\text{rx}}$ reflects a variety of rate constants which contribute to the overall reaction.

The quantum yield of reaction, in terms of rate constants, is given by

$${}^{4+2}\phi_{\text{rx}} = \frac{{}^2k_{\text{rx}}}{{}^2k_{\text{rx}} + {}^2k_{\text{nr}} + {}^2k_{\text{gsq}}[\text{Cr}^{3+}]} = \frac{{}^2k_{\text{rx}}}{{}^2k_{\text{obs}}} \quad (3-109)$$

Then, knowledge of ${}^2k_{\text{obs}}$ ($= {}^2k_{\text{rx}} + {}^2k_{\text{nr}} + {}^2k_{\text{gsq}}[\text{Cr}^{3+}]$) from lifetime studies as a function of temperature enable the evaluation of ${}^2k_{\text{rx}}$ and ${}^2k_{\text{nr}}$, as per equations (3-110) and (3-111). For the $\text{Cr}(\text{bpy})_3^{3+}$ system, one does

$${}^2k_{\text{rx}} = {}^{4+2}\phi_{\text{rx}} {}^2k_{\text{obs}} \quad (3-110)$$

$${}^2k_{\text{nr}} = {}^2k_{\text{obs}} - {}^2k_{\text{rx}} \quad (3-111)$$

not have to consider the contribution to ${}^2k_{\text{obs}}$ from ground-state quenching (${}^2k_{\text{gsq}}$); thus, ${}^{4+2}\phi_{\text{rx}} = {}^2k_{\text{rx}} / ({}^2k_{\text{rx}} + {}^2k_{\text{nr}})$. The values of ${}^2k_{\text{O}}$ have been interpolated from a plot of $\ln {}^2k_{\text{O}}$ vs $1/T$ for the temperature

dependence of the 2E decay of $\text{Cr}(\text{bpy})_3^{3+}$ in deaerated solution at pH 9.8 shown in Figure 3-27. The values of 2k_o so obtained, and the values of ${}^2k_{\text{rx}}$ and ${}^2k_{\text{nr}}$ calculated from equations (3-110) and (3-111) are collected in Table 3-22.

Arrhenius plots of $\ln {}^2k_{\text{rx}}$ and $\ln {}^2k_{\text{nr}}$ vs $1/T$ are shown in Figure 3-28; from the slope of these plots, ${}^2E_a(\text{rx}) = 12.3$ kcal/mole and ${}^2E_a(\text{nr}) = 10.1$ kcal/mole. Furthermore, the slope and intercept of a plot of $\ln ({}^2k_{\text{rx}}/T)$ vs $1/T$ affords the enthalpy and entropy of activation for the "rx" pathway, respectively; ${}^2\Delta H_{\text{rx}}^\ddagger = 11.7$ kcal/mole and ${}^2\Delta S_{\text{rx}}^\ddagger = -4.2$ eu.

A comparison of the activation parameters for the reactions of the 4A_2 and (${}^2T_1/{}^2E$) species with H_2O to form the seven-coordinate intermediate shows that, for the $\text{Cr}(\text{bpy})_3^{3+}$ system at pH 9 - 10.5, the (${}^2T_1/{}^2E$) reaction is about 10^{10} times faster (cf. k_{obs} and ${}^2k_{\text{rx}}$), requires considerably less enthalpy of activation (cf. ΔH_{298}^\ddagger and ${}^2\Delta H_{\text{rx}}^\ddagger$), and exhibits a decrease in entropy in going to the activated complex as does the 4A_2 reaction. It is assumed that the activated complexes formed from the 4A_2 and (${}^2T_1/{}^2E$) reactions have the same geometry since there is no Stokes shift between the ${}^2E \longleftrightarrow {}^4A_2$ absorption and emission bands. Furthermore, since it is a condition of transition state theory that reactants and activated complex be in equilibrium¹²¹ the activated complex from (${}^2T_1/{}^2E$) must be in a state of electronic excitation while that from 4A_2 must be in a ground state. As a first approximation, it is assumed that the spin multiplicities of the activated complexes are the same as the reactants from which they are derived. Then, in going from an excited-state activated complex to the seven-coordinate intermediate, a seven-coordinate excited-state species, ${}^* \text{Cr}(\text{bpy})_3(\text{H}_2\text{O})^{3+}$, is formed, which rapidly deactivates (non-radiatively) to $\text{Cr}(\text{bpy})_3(\text{H}_2\text{O})^{3+}$. The energetics of the

FIGURE 3-27 : Plot of $\ln k_0$ as a Function of Temperature for $\text{Cr}(\text{bpy})_3^{3+}$
at pH 9.8 in Argon-purged Solutions.

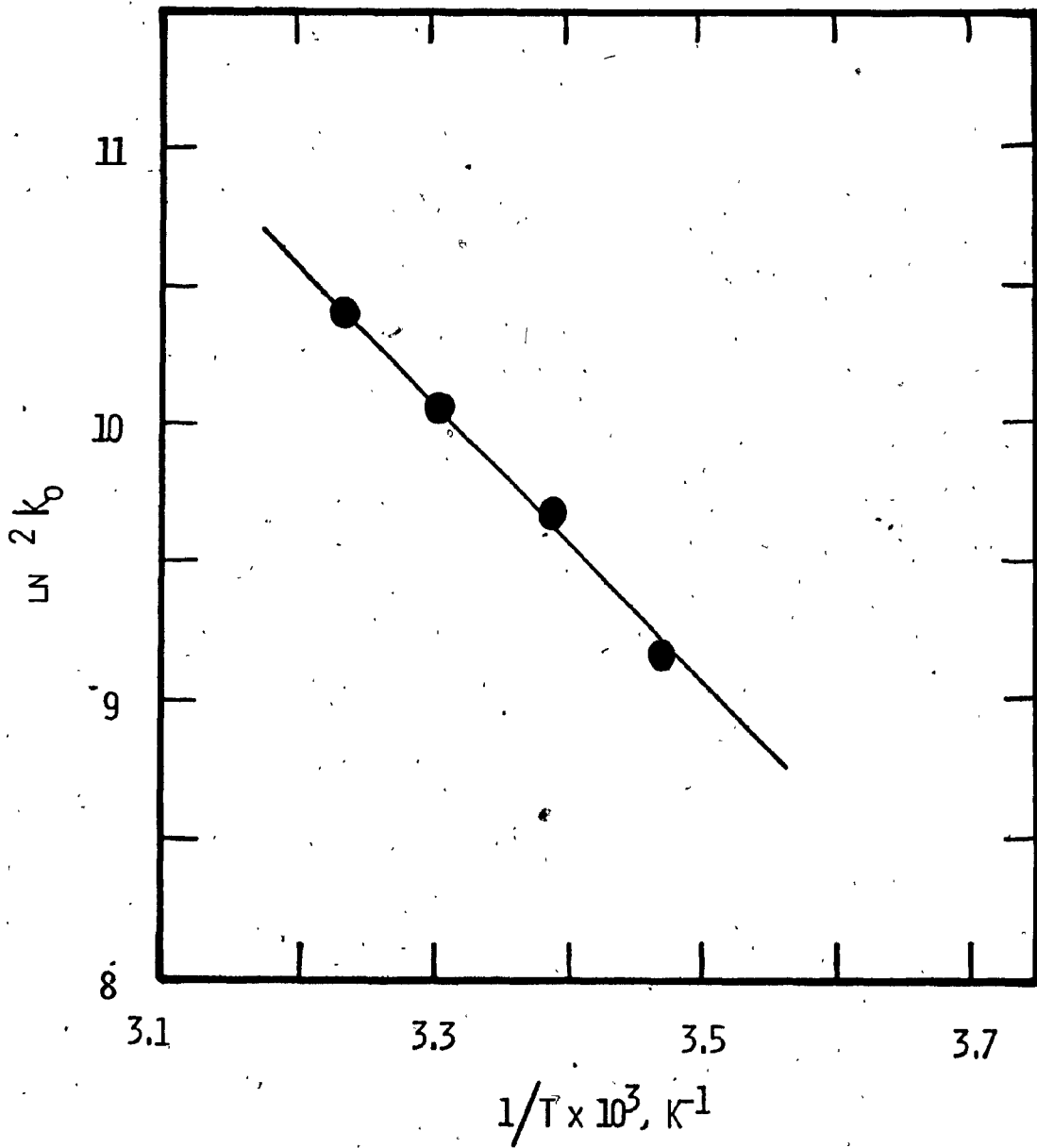
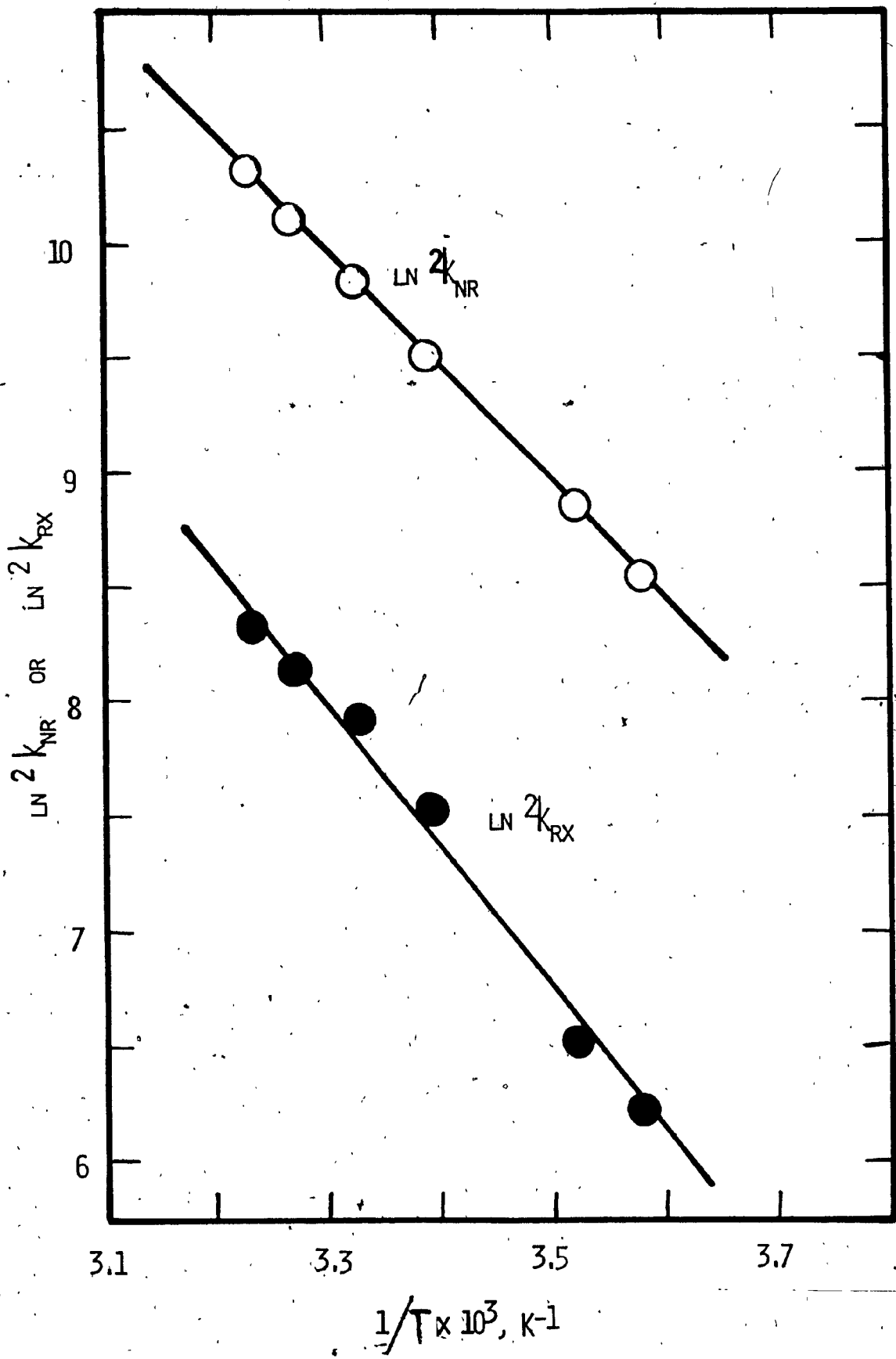


FIGURE 3-28 : Plots of $\ln^2 k_{rx}$ and $\ln^2 k_{nr}$ vs $1/T$ for $\text{Cr}(\text{bpy})_3^{3+}$ at
pH 9.8 in Argon-purged Solutions.



seven-coordinate species are unknown, but their values have no effect on the activation parameters.

In order to accommodate the entering H_2O , the ${}^4\text{A}_2$ and $({}^2\text{T}_1/{}^2\text{E})$ activated complexes must exhibit incipient formation of the Cr-OH_2 bond as well as distortion and loosening of the normally-regular structure of the bpy ligands. The values of the enthalpy of activation for the ${}^4\text{A}_2$ and $({}^2\text{T}_1/{}^2\text{E})$ reactions then reflect the energy spent to loosen the six Cr-N bonds (though not to the same extent) in balance with the energy gained from the formation of the Cr-OH_2 bond. The negative values for the entropy of activation imply that the coalescence of the two microscopic particles is the dominant contributor to the activation entropy.

Owing to the geometric similarities between ${}^4\text{A}_2$ and $({}^2\text{T}_1/{}^2\text{E})$, the enthalpy of activation is expected to be the same for both reactions. However, the lower value for the $({}^2\text{T}_1/{}^2\text{E})$ reaction (by ca. 10 kcal/mole) can be interpreted in terms of the "vacant" t_{2g} orbital of the ${}^2\text{T}_1$ excited-state configuration, which is in thermal equilibrium with the ${}^2\text{E}$ state. This "vacant" orbital can accommodate a Lewis base solvent molecule oriented between the bidentate bpy ligands, and would result in less reorganizational energy being required to form the activated complex, and consequently, a lower enthalpy of activation. The large difference in k_{obs} and ${}^2k_{\text{rx}}$ simply reflects these differences in the activation enthalpies for the ${}^4\text{A}_2$ and $({}^2\text{T}_1/{}^2\text{E})$ reactions.

An analogous investigation of the $\text{Cr}(\text{phen})_3^{3+}$ system at pH 10.0 in deaerated solutions reveals that one must account for both ground-state quenching and the unquenchable reaction component. A temperature dependence study of ${}^{4+2}\phi_{\text{rx}}$ in the range 13-41°C shows an increase in ${}^{4+2}\phi_{\text{rx}}$ with increasing temperature, as revealed in Table 3-23. An Arrhenius-

type plot of $\ln \phi_{rx}^{4+2}$ vs $1/T$ is linear and yields an "apparent" activation energy $E_{app} = 20.2$ kcal/mole. In the presence of, 0.05 M iodide ion, the unquenchable photoaquation quantum yield, ϕ_{rx}^4 , can be measured as a function of temperature; the data obtained is presented in Table 3-23. Furthermore, since the total photoaquation quantum yield may be defined as the sum of the quenchable and unquenchable reaction components, the quantum yield for reaction from $({}^2T_1/{}^2E)$, ϕ_{rx}^2 , can be evaluated from $\phi_{rx}^2 = \phi_{rx}^{4+2} - \phi_{rx}^4$, the values of which are contained in Table 3-23 as well.

A linear Arrhenius-type plot of $\ln \phi_{rx}^2$ vs $1/T$ is obtained and revealed in Figure 3-29, and yields $E_{app} = 18.5$ kcal/mole. However, such a plot is not linear for the temperature dependence of ϕ_{rx}^4 , and one immediately recognizes the variation in the contribution of ϕ_{rx}^4 to ϕ_{rx}^{4+2} with temperature variation ($\phi_{rx}^4 / \phi_{rx}^{4+2}$ increases with increasing temperature). The analysis of the unquenchable reaction component will be discussed in Section 3.9.

The $({}^2T_1/{}^2E)Cr(phen)_3^{3+}$ reaction quantum yield (ϕ_{rx}^2) can be defined in terms of rate constants in a manner similar to that for the bpy system.

$$\phi_{rx}^2 = \frac{k_{rx}^2}{k_{rx}^2 + k_{nr}^2 + k_{gsq}[Cr^{3+}]} = \frac{k_{rx}^2}{k_{obs}^2} \quad (3-112)$$

Inasmuch as ground-state quenching makes a significant contribution to the deactivation of $({}^2T_1/{}^2E)Cr(phen)_3^{3+}$, it was necessary to measure k_{obs}^2 ($= 1/\tau_{obs}^2$) as a function of $[Cr(phen)_3^{3+}]$ at various temperatures; these results are shown in Table 3-24 for the ground-state quenching

FIGURE 3-29 : Arrhenius-type Plot for Temperature Dependences of ${}^{4+2}\phi_{rx}$, ${}^4\phi_{rx}$ and ${}^2\phi_{rx}$ for $\text{Cr}(\text{phen})_3^{3+}$ at pH 10.0 and $\mu = 1.0$.

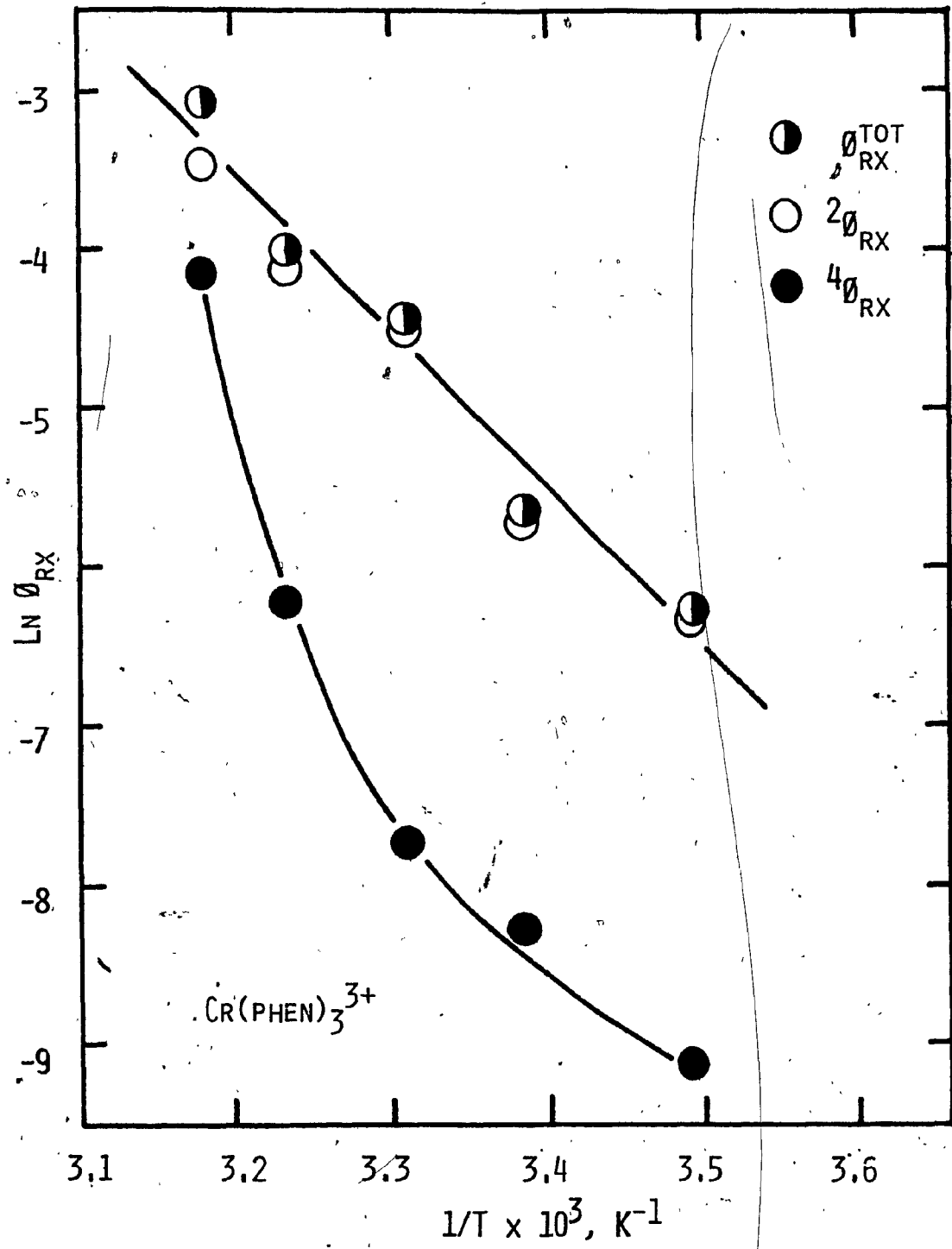


TABLE 3-24 : Temperature Profile of the Ground-state Quenching Phenomenon for $(^2T_1/{}^2E)Cr(phen)_3^{3+}$ at pH 10.0 in Deaerated Solutions. ^a

Temperature, (K)	${}^2k_{O'}$ (sec^{-1})	${}^2k_{gsq'}$ ($M^{-1} sec^{-1}$)	${}^2k_{obs'}$ (sec^{-1}) ^b
286.7	0.24×10^4	4.03×10^7	4.28×10^4
295.2	0.40×10^4	5.41×10^7	5.81×10^4
302.4	0.64×10^4	6.46×10^7	7.10×10^4
309.2	1.04×10^4	8.77×10^7	8.53×10^4
315.0	1.40×10^4	8.77×10^7	10.17×10^4

^a In deaerated solutions at pH = 10.0, containing 0.008 M Britton-Robinson buffer and $\mu = 1.0$ (with NaCl). ${}^2k_{O'}$ and ${}^2k_{gsq'}$ calculated from equation (3-16).

^b Calculated from equation (3-16), for which $[Cr(phen)_3^{3+}] = 1.0 \times 10^{-3} M$.

phenomenon described by equation (3-16). Using a concentration of 1.0×10^{-3} M $\text{Cr}(\text{phen})_3^{3+}$, as employed for measuring ${}^4\text{A}_2$ ϕ_{rx} , the values of ${}^2k_{\text{obs}}$ (see Table 3-24) can be calculated. Employing these calculated values of k_{obs} , ${}^2k_{\text{rx}}$ and ${}^2k_{\text{nr}}$ can be calculated from equations (3-113) and (3-114),

$${}^2k_{\text{rx}} = {}^2\phi_{\text{rx}} {}^2k_{\text{obs}} \quad (3-113)$$

$${}^2k_{\text{nr}} = {}^2k_{\text{obs}} - {}^2k_{\text{rx}} \quad (3-114)$$

respectively, and are collected in Table 3-25. A linear Arrhenius plot of $\ln {}^2k_{\text{rx}}$ vs $1/T$ yields ${}^2E_a(\text{rx}) = 23.9$ kcal/mole (corr. coeff. 0.991); an analogous plot for $\ln {}^2k_{\text{nr}}$ vs $1/T$ yields ${}^2E_a(\text{nr}) = 5.2$ kcal/mole (corr. coeff. 0.999). The entropy and enthalpy of activation for the $({}^2\text{T}_1/{}^2\text{E})$ reaction are obtained from the slope and intercept of a linear plot of $\ln ({}^2k_{\text{rx}}/T)$ vs $1/T$ (corr. coeff. 0.990), yielding ${}^2\Delta H_{\text{rx}}^\ddagger = 23.3$ kcal/mole and ${}^2\Delta S_{\text{rx}}^\ddagger = +31.1$ eu. The activation parameters for the $({}^2\text{T}_1/{}^2\text{E})$ reaction are collected in Table 3-26 for the $\text{Cr}(\text{bpy})_3^{3+}$ and $\text{Cr}(\text{phen})_3^{3+}$ systems under similar experimental conditions.

A comparison of the activation parameters for the ${}^4\text{A}_2$ reaction (Table 3-2) and $({}^2\text{T}_1/{}^2\text{E})$ (Table 3-26) aquation reactions for $\text{Cr}(\text{phen})_3^{3+}$ under similar experimental conditions reveals that i) the $({}^2\text{T}_1/{}^2\text{E})$ reaction is ca. 10^8 times faster than the ${}^4\text{A}_2$ reaction; ii) the $({}^2\text{T}_1/{}^2\text{E})$ reaction requires a considerable increase in entropy in going to the activated complex, in contrast to the ${}^4\text{A}_2$ reaction which undergoes an entropy decrease; and iii) the $({}^2\text{T}_1/{}^2\text{E})$ and ${}^4\text{A}_2$ reactions require similar enthalpies for activation (cf. ΔH_{298} and ${}^2\Delta H_{\text{rx}}^\ddagger$).

TABLE 3-25 : Quantum Yields of Photoaquation and Doublet-state Rate Constants for $(^2T_1/{}^2E)Cr(phen)_3^{3+}$ as a Function of Temperature in Deaerated Solutions.^a

Temperature, (K)	${}^2\phi_{rx}$	${}^2k_{obs}$ (sec^{-1})	${}^2k_{rx}$ ^b (sec^{-1})	${}^2k_{nr}$ ^c (sec^{-1})
286.2	1.8×10^{-3}	4.3×10^4	0.76×10^2	4.27×10^4
295.4	3.3×10^{-3}	5.81×10^4	1.9×10^2	5.79×10^4
302.2	1.13×10^{-2}	7.10×10^4	8.0×10^2	7.02×10^4
309.2	1.6×10^{-2}	8.53×10^4	1.4×10^3	8.39×10^4
314.4	3.05×10^{-2}	10.1×10^4	3.1×10^3	9.86×10^4

^a In deaerated solutions containing 0.008 M Britton-Robinson buffer, $\mu = 1.0$ (with NaCl).

^b Calculated from ${}^2\phi_{rx} = {}^2\phi_{k_{obs}}$. ^c Calculated from ${}^2k_{nr} = {}^2k_{obs} - {}^2k_{rx}$.

TABLE 3-26 : Activation Parameters for the (${}^2T_1/{}^2E$) Reaction of $\text{Cr}(\text{bpy})_3^{3+}$ and $\text{Cr}(\text{phen})_3^{3+}$ in Deaerated Solutions at pH 9.5 - 10.0.

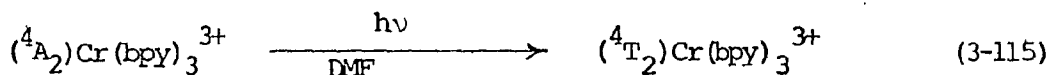
Activation Parameter	$\text{Cr}(\text{bpy})_3^{3+}$	$\text{Cr}(\text{phen})_3^{3+}$
${}^2E_a(\text{nr})$, kcal/mole	10.1	5.2
${}^2E_a(\text{rx})$, kcal/mole	12.3	23.9
${}^2E_{\text{app}}$, kcal/mole	1.9 ^a	18.5 ^b
${}^2\Delta H_{\text{rx}}^{\ddagger}$, kcal/mole	11.7	23.3
${}^2\Delta S_{\text{rx}}^{\ddagger}$, eu	-4.2	+31.3
${}^2k_{\text{rx}}$, sec^{-1} (295K)	1.8×10^3	2×10^2

a From a plot of $\ln \phi_{\text{rx}}^{\text{tot}}$ vs $1/T$. b From a plot of $\ln^2 \phi_{\text{rx}}$ vs $1/T$.

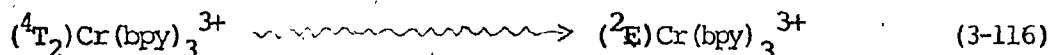
3.8.2. Photolysis in Dimethylformamide.

It is interesting to take note of a recent study by Porter and Van Houten^{5,122} on the photolytic behavior of $\text{Cr}(\text{bpy})_3^{3+}$ in DMF at room temperature. Irradiation of oxygen-free solutions of $\text{Cr}(\text{bpy})_3^{3+}$ in neat DMF gave observations different from those in aqueous solution. The luminescence lifetime and quantum yield of $\text{Cr}(\text{bpy})_3^{3+}$ in DMF are a factor of 15 smaller than in water, while the photochemical quantum yield for the photosolvolytic disappearance of $\text{Cr}(\text{bpy})_3^{3+}$ in DMF is orders of magnitude larger than in water. The overall quantum yield for the photosolvolytic disappearance of $\text{Cr}(\text{bpy})_3^{3+}$ in oxygen-free DMF was estimated¹²² to be of the order of unity.

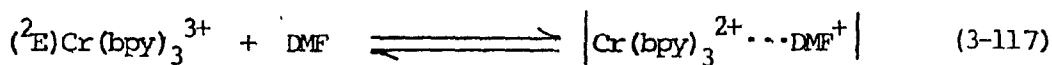
Absorption of radiation ($\lambda = 442 \text{ nm}$) by $\text{Cr}(\text{bpy})_3^{3+}$ in neat DMF populates the ${}^4\text{T}_2$ state (reaction 3-115) with subsequent intersystem crossing



to the ${}^2\text{E}$ excited state (reaction 3-116), presumably also with unitary

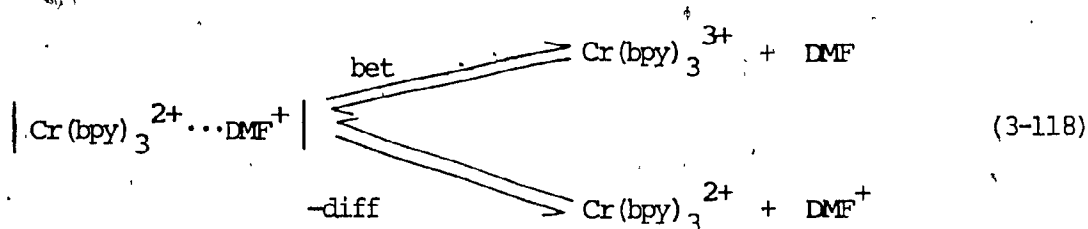


efficiency.¹²² Since $\text{Cr}(\text{bpy})_3^{2+}$ has been observed during photolysis, and $({}^2\text{E})\text{Cr}(\text{bpy})_3^{3+}$ is known to be a strong oxidizing agent, the ${}^2\text{E}$ species undergoes reduction to form a cage pair (reaction 3-117). It may well be



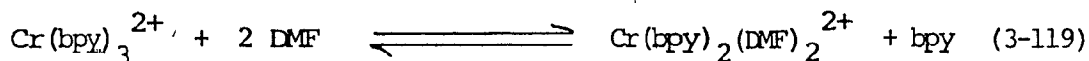
that DMF itself serves as the electron donor, though this remains uncertain.

Subsequently, back-electron transfer (bet) results in overall quenching which occurs in competition with diffusion out (-diff) of the cage pair.

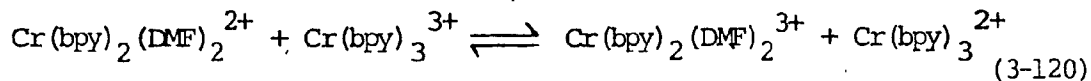


To the extent that the entire reaction is completed in a short time, reaction of $\text{Cr}(\text{bpy})_3^{2+}$ with DMF^+ does not appear¹²² to be important. The quantum yield for $\text{Cr}(\text{bpy})_3^{2+}$ formation was estimated to be ca. 0.006.¹²²

Subsequent solvolysis leads to ligand substitution of one bpy ligand,



and further reaction with $\text{Cr}(\text{bpy})_3^{3+}$ yields $\text{Cr}(\text{bpy})_2(\text{DMF})_2^{3+}$ and $\text{Cr}(\text{bpy})_3^{2+}$.



It was further noted¹²² that if some $\text{Cr}(\text{bpy})_3^{3+}$ remained in the reaction solution, the reverse of reaction (3-119) cannot occur because of competition with reaction (3-120). The equilibrium in reaction (3-119) is established when all the $\text{Cr}(\text{bpy})_3^{3+}$ has been consumed.

The implication of a chromium(II) species in DMF was rationalized¹²² in terms of the formation of a radical ion via oxidation of a DMF molecule in the inner solvation sphere. This radical ion can then escape from the cage pair by self-exchange with molecules in the outer solvent sphere, and

ultimately with the bulk solvent via transfer of an electron from the bulk solvent into the inner solvent sphere. Although $\text{Cr}(\text{bpy})_3^{3+}$ can be reduced to $\text{Cr}(\text{bpy})_3^{2+}$ in DMF and water,¹²² the fate of the Cr(II) species appears to be different in the two solvents. Porter and Van Houten attribute¹²² this difference to the fact that a solvent molecule such as DMF can more efficiently undergo oxidation and escape from the cage pair than could a solute in low concentration, as it would be in aqueous solutions.

3.9. THE UNQUENCHABLE PHOTOREACTION.

3.9.0. $\text{Cr}(\text{bpy})_3^{3+}$.

The continuing controversy in Cr(III) photochemistry surrounding the specific roles played by the excited quartet and doublet states has prompted us to look at the photoaquation of $\text{Cr}(\text{bpy})_3^{3+}$ under conditions such that any direct photoaquation from the (${}^2T_1/{}^2E$) excited manifold is completely quenched. There have been past indications that (4T_2) $\text{Cr}(\text{bpy})_3^{3+}$ is photoreactive, although the mechanistic details of its reactions remained to be elucidated. What has been done in this work is to employ iodide ion to quench (${}^2T_1/{}^2E$) $\text{Cr}(\text{bpy})_3^{3+}$ virtually completely, and then investigate the pH and temperature profiles of the unquenchable photoreaction.

Luminescence lifetime measurements and Stern-Volmer kinetics have shown that iodide ion quenches (${}^2T_1/{}^2E$) phosphorescence of $\text{Cr}(\text{bpy})_3^{3+}$ with a rate constant $k_q = 1.4 \times 10^9 \text{ M}^{-1} \text{ sec}^{-1}$ in aqueous solution (1 M HCl) at 22°C. Furthermore, equation (3-121) can be used to calculate the concentration of I^- required to quench greater than 99.9% of the (${}^2T_1/{}^2E$) emission. For $\text{Cr}(\text{bpy})_3^{3+}$, $\text{I}^- = 9.8 \times 10^{-4} \text{ M}$ is required for $\tau = 0.073 \text{ msec}$ and $k_q = 1.4 \times 10^9 \text{ M}^{-1} \text{ sec}^{-1}$.

$$\frac{I_0}{I} = 1 + k_q \tau [I^-] \quad (3-121)$$

The initial investigation involved the determination of the photoaquation quantum yield of $\text{Cr}(\text{bpy})_3^{3+}$ as a function of the I^- concentration, the results of which are given in Table 3-27 and Figure 3-30; also included are the data obtained for the $\text{Cr}(\text{phen})_3^{3+}$ system. The observation that ϕ_{rx} reaches more or less a plateau value at ca. $0.1 \text{ M } \text{I}^-$ for $\text{Cr}(\text{bpy})_3^{3+}$, which is much greater than that required for complete quenching of $({}^2\text{T}_1/{}^2\text{E})$, indicates that the residual quantum yield of photoreaction occurs from short-lived excited states. Inasmuch as ${}^{4+2}\phi_{\text{rx}} = 0.13$ for $\text{Cr}(\text{bpy})_3^{3+}$ in the absence of I^- , the maximum quantum yield from unquenched $({}^2\text{T}_1/{}^2\text{E})$ would be $\sim 1 \times 10^{-5}$ under conditions where the plateau values of ϕ_{rx} are observed. The unquenchable portion of the quantum yield ($\sim 2 \times 10^{-3}$) constitutes ca. 3% of the total yield under identical conditions of temperature, pH and ionic strength. For the purpose of further discussion, this unquenchable quantum yield will be designated ${}^4\phi_{\text{rx}}$, as the excited states responsible for this reaction component are presumably the short-lived quartet excited states.

a. pH Dependence of ${}^4\phi_{\text{rx}}$.

The pH profile of the unquenchable photoreaction of $\text{Cr}(\text{bpy})_3^{3+}$ was studied under conditions where $\text{I}^- = 0.15 \text{ M}$, the plateau region. The dependence of ${}^4\phi_{\text{rx}}$ on pH is depicted in Figure 3-31; one immediately recognizes the profile similarity between the unquenchable reaction (${}^4\phi_{\text{rx}}$) (Figure 3-31), the $({}^2\text{T}_1/{}^2\text{E})$ reaction (${}^{4+2}\phi_{\text{rx}}$) (Figure 3-25), and the ${}^4\text{A}_2$ reaction (Figure 3-3a). This similarity argues strongly for the existence of a common intermediate which renders the overall

TABLE 3-27a: Photoaquation Quantum Yields for $\text{Cr}(\text{bpy})_3^{3+}$ as a Function of Iodide Ion Concentration at pH ~ 9.6 in Deaerated Solutions at 22°C.^a

$[\text{I}^-], \text{M}$	${}^{4+2} \phi_{rx}$
0.0	0.099 ₆
1.6×10^{-3}	0.003 ₈
0.05	0.002 ₃
0.10	0.001 ₇
0.15	0.001 ₉
0.20	0.001 ₆
0.30	0.001 ₅
0.50	0.000 ₇

TABLE 3-27b: Photoaquation Quantum Yields for $\text{Cr}(\text{phen})_3^{3+}$ as a Function of Iodide Ion Concentration at pH ~ 9.6, in Deaerated Solutions at 22°C.^a

$[\text{I}^-]$, M	ϕ_{rx}
2.0×10^{-4}	0.001 ₁
2.0×10^{-4}	0.001
4.0×10^{-4}	0.001 ₅
0.012	0.0007
0.02	0.0007
0.05	0.0004
0.08	0.0004

^a Experimental error estimated at $\pm 20\%$.

FIGURE 3-30 : Dependence of the Quantum Yield for Photoaquation of $\text{Cr}(\text{bpy})_3^{3+}$ (●) and $\text{Cr}(\text{phen})_3^{3+}$ (○) complexes on I^- Concentration; 22°C ; $\mu = 1.0$, 0.008 M Britton-Robinson Buffer, pH 9-10, argon-purged solutions.

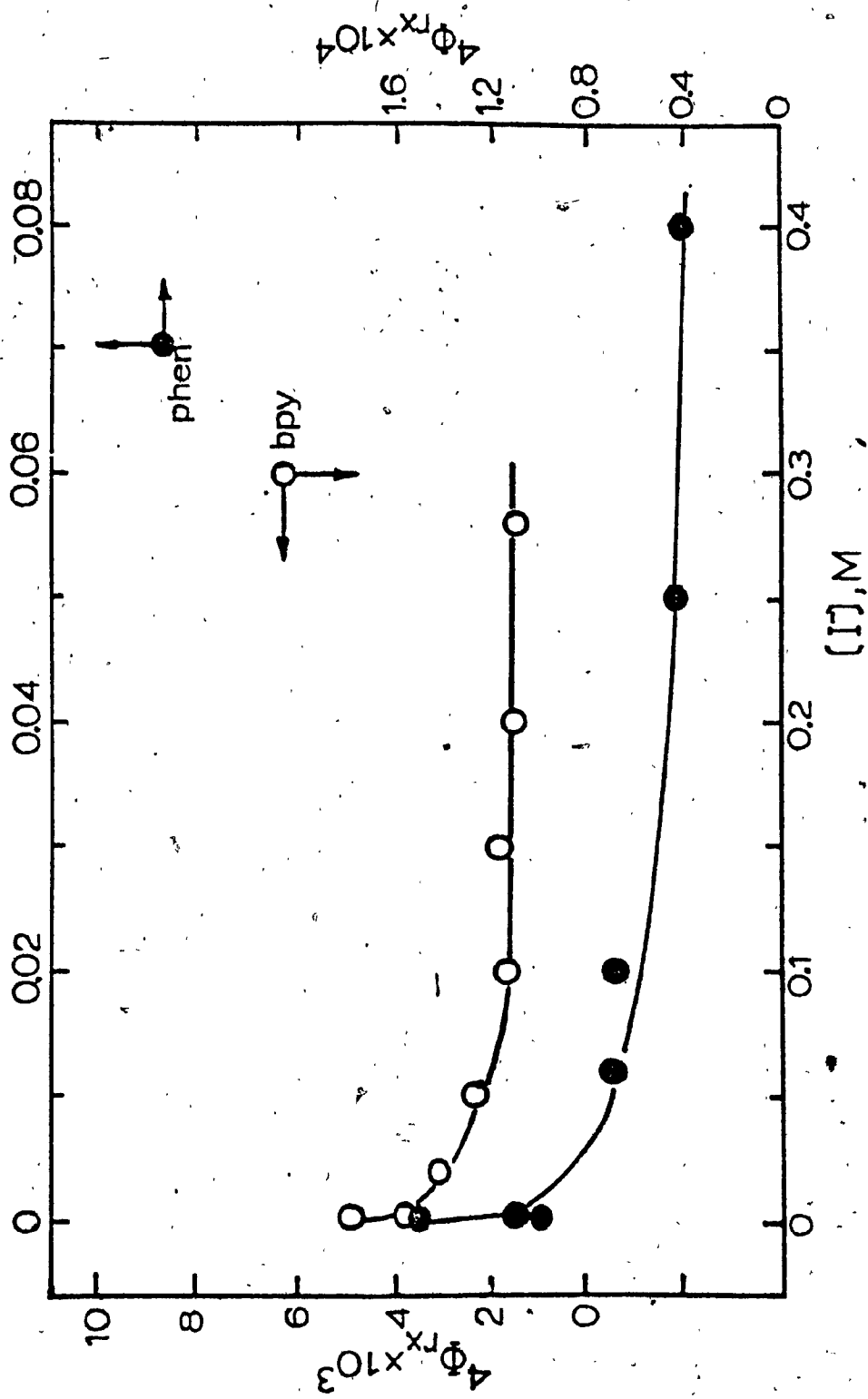
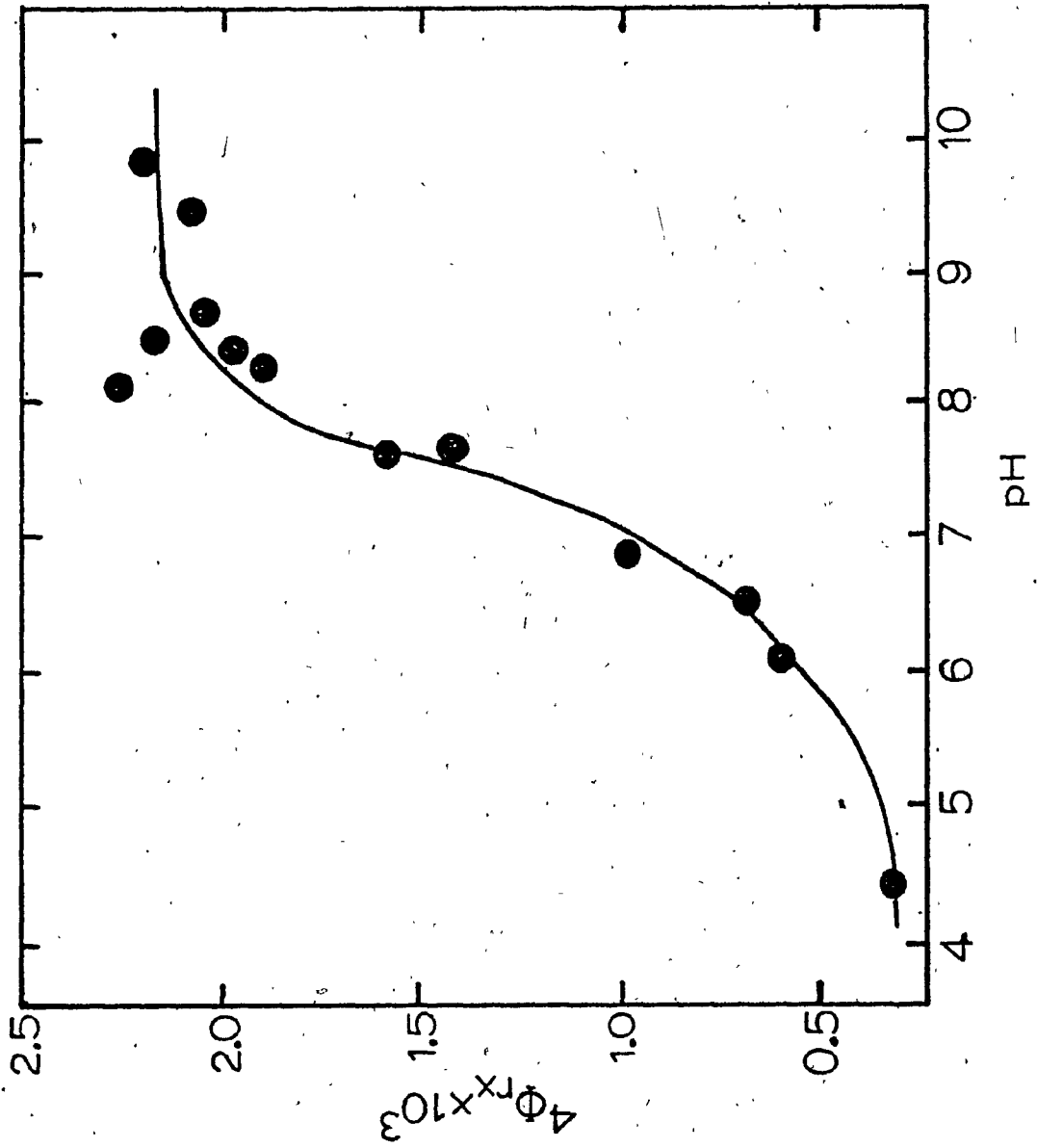


FIGURE 3-31 : $^4\phi_{rx}$ as a Function of pH for $\text{Cr}(\text{bpy})_3^{3+}$ at 22°C ; 313-nm
Photolysis of Argon-purged Solutions of 1.6×10^{-4} M
 $\text{Cr}(\text{bpy})_3^{3+}$ containing 0.008 M Britton-Robinson Buffer,
0.15 M NaI and 0.85 M NaCl, pH 9.6.



aquation reaction efficient in alkaline solution and inefficient in acidic solution. If the common intermediate is $\text{Cr}(\text{bpy})_3(\text{H}_2\text{O})^{3+}$, as suggested for the (${}^2\text{T}_1/{}^2\text{E}$) and ${}^4\text{A}_2$ reactions, then it also must be true that photochemical reactions from the long-lived (${}^2\text{T}_1/{}^2\text{E}$) and short-lived quartet excited states (as well as the thermal reaction from ${}^4\text{A}_2$) are mechanistically indistinguishable except for the efficiencies and temperature dependences of the formation of that seven-coordinate intermediate species.

b. Temperature Dependence of ${}^4\phi_{\text{RX}}$.

The temperature dependence of the unquenchable photoreaction of $\text{Cr}(\text{bpy})_3^{3+}$ was performed in order to compare the energetics of this reaction with those of the (${}^2\text{T}_1/{}^2\text{E}$) and ${}^4\text{A}_2$ reactions. Table 3-28 shows those data obtained for the total photoaquation in the absence of I^- (${}^{4+2}\phi_{\text{RX}}$) and the unquenchable photoaquation in the presence of 0.15 M I^- (${}^4\phi_{\text{RX}}$). A linear plot of $\ln {}^4\phi_{\text{RX}}$ vs $1/T$ (Figure 3-32) yields an "apparent" activation energy $E_{\text{app}} = 9.6$ kcal/mole for the unquenchable reaction; $E_{\text{app}} = 1.9$ kcal/mole for the total photoaquation reaction ($\ln {}^{4+2}\phi_{\text{RX}}$ vs $1/T$).

If the common seven-coordinate intermediate is a ground-state species, then the differences in the temperature dependences of ${}^4\phi_{\text{RX}}$ and ${}^{4+2}\phi_{\text{RX}}$ must arise from reactions leading to the formation of that intermediate, regardless of the origin or subsequent reaction of the intermediate. Those reactions leading to the formation of the intermediate must then involve the interaction of excited-state species with the solvent, or back-intersystem crossing from (${}^2\text{T}_1/{}^2\text{E}$) to ${}^4\text{T}_2$ in competition with other modes of decay. It is important to note here that these quantum yield measurements reflect a number of cumulative steps leading to the final

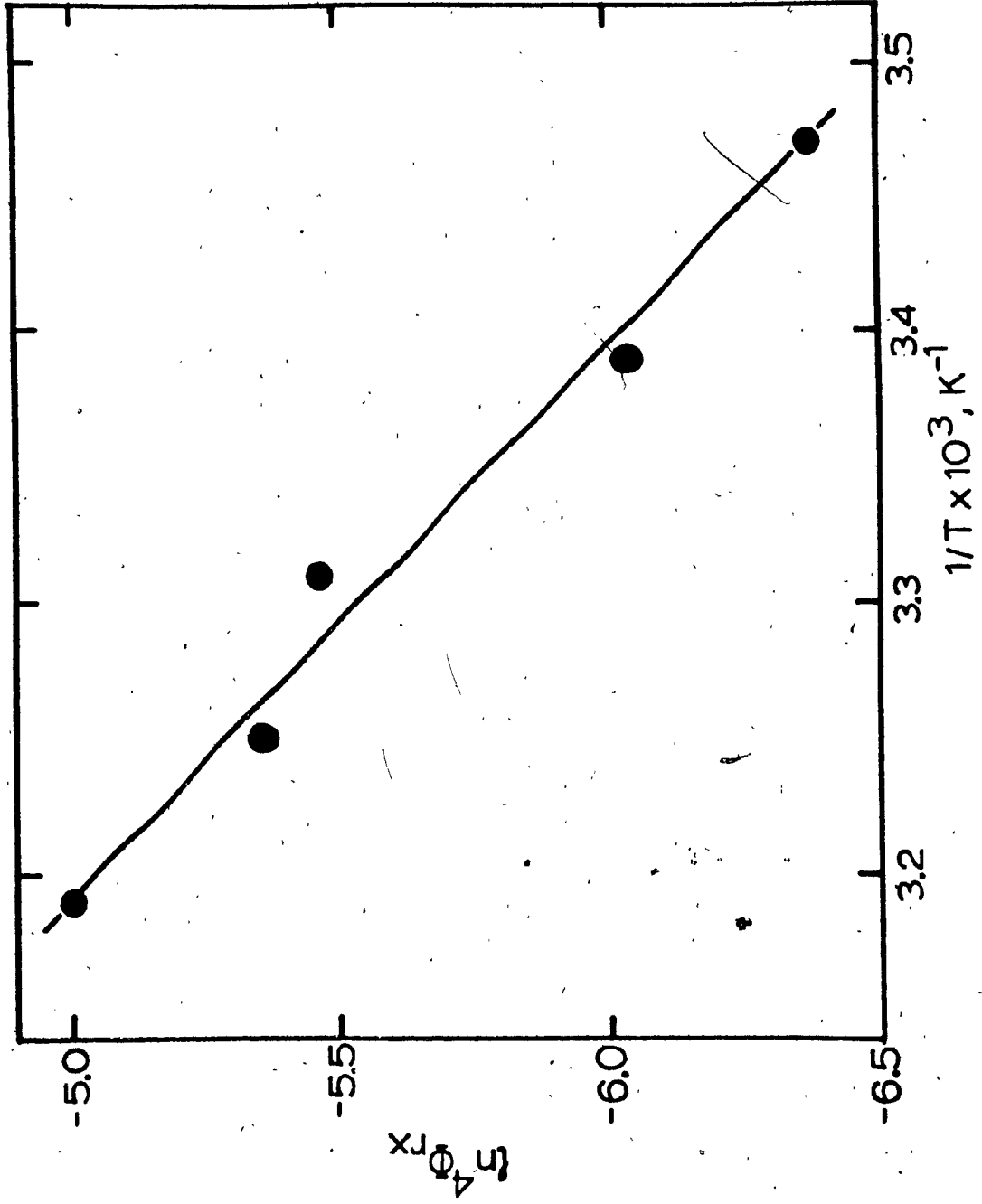
TABLE 3-28 : Quantum Yields of Photoaquation at 313 nm of $\text{Cr}(\text{bpy})_3^{3+}$ as a Function of Temperature.

T, °C	ϕ_{rx}	
	in the absence of I^- ^a	in the presence of I^- ^b
6.3	0.089	—
11.1	0.095	—
15.2	—	1.7×10^{-3}
22.0	—	2.4×10^{-3}
22.1	0.12	—
27.8	0.13	—
28.9	—	4.2×10^{-3}
32.6	0.12	—
34.8	—	4.7×10^{-3}
36.2	0.12	—
40.4	—	6.7×10^{-3}

^a Experimental conditions: 1×10^{-3} M $\text{Cr}(\text{bpy})_3^{3+}$, pH 9.8, 0.008 M Britton-Robinson buffer, 1 M NaCl. Values of ϕ_{rx} represent the average of two to four determinations (std. dev. $\pm 10\%$).

^b Experimental conditions: 1.6×10^{-4} M $\text{Cr}(\text{bpy})_3^{3+}$, pH 9.6, 0.008 M Britton-Robinson buffer, 0.15 M NaI and 0.85 M NaCl. Values of ϕ_{rx} represent the average of two to four determinations (std. dev. $\pm 15\%$).

FIGURE 3-32 : Plot of $\ln \Phi_{RX}^4$ vs $1/T$ for $\text{Cr}(\text{bpy})_3^{3+}$ at 22°C ; 313-nm
Photolysis of Argon-purged Solutions of 1.6×10^{-4} M
 $\text{Cr}(\text{bpy})_3^{3+}$ Containing 0.008 M Britton-Robinson Buffer
0.15 M NaI and 0.85 M NaCl, pH 9.6.



reaction products, and not the temperature dependence of a single step that proceeds quantitatively irrespective of the activation energy of that step. Thus, the temperature dependences of ${}^{4\rightarrow 2}\phi_{RX}$ and ${}^4\phi_{RX}$ must arise from mechanistic steps that are inefficient and in competition with non-productive reactions. One can express the efficiency of any one of the steps leading ultimately to product formation in terms of a ratio of rate constants of the competing reactions; the temperature dependences of these competing reactions then lead to the observed temperature dependences of the quantum yield.

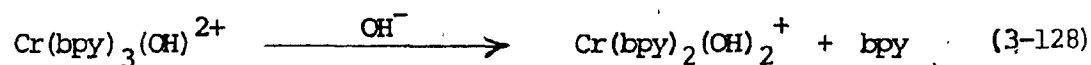
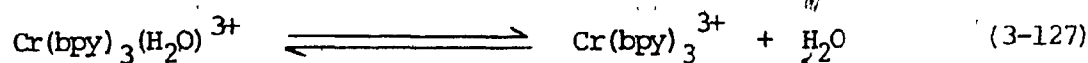
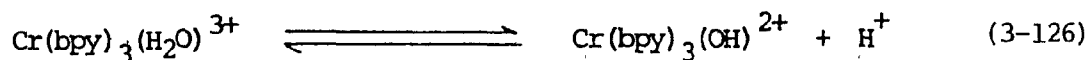
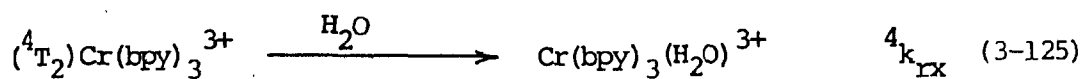
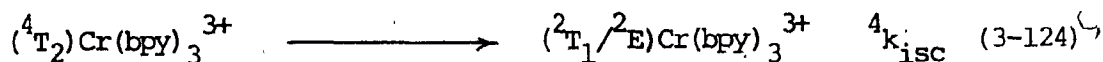
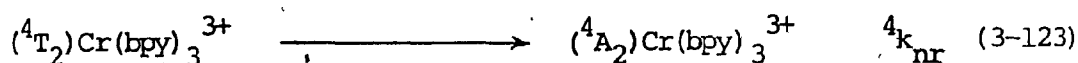
To discern the nature of the excited-state origin of the unquenchable photoaquation reaction of $\text{Cr}(\text{bpy})_3^{3+}$, various models are suggested and examined with respect to their validity to this particular system.

Model I: ${}^4\phi_{RX}$ from the 4T_2 manifold.

This model assumes that the unquenchable reaction component originates from the 4T_2 manifold, which is populated with unitary efficiency from the initially-excited Franck-Condon (${}^4\text{FC}$) states via vibrational relaxation. Furthermore, the 4T_2 state undergoes reaction with the solvent molecule in competition with non-radiative decay to 4A_2 (${}^4k_{NR}$) and inter-system crossing (either prompt or delayed, or both) to the doublet manifold. The pH dependence of ${}^4\phi_{RX}$, as well as ${}^{4\rightarrow 2}\phi_{RX}$ and k_{obs} , represent the titration of the seven-coordinate intermediate $\text{Cr}(\text{bpy})_3(\text{H}_2\text{O})^{3+}$ such that deprotonation to $\text{Cr}(\text{bpy})_3(\text{OH})^{2+}$ is quantitatively accomplished at pH 9.6. It was earlier suggested that $\text{Cr}(\text{bpy})_3(\text{OH})^{2+}$ converts rapidly, quantitatively and irreversibly to $\text{Cr}(\text{bpy})_2(\text{OH})_2^+$ rather than returning to $\text{Cr}(\text{bpy})_3^{3+}$, based on the following reasoning: i) OH^- is a much stronger base than bpy, so that labilization of coordinated OH would be significantly less probable than labilization of one end of coordinated (bpy-);

ii) formation of $\text{Cr}(\text{bpy})_2(\text{OH})_2^+$ occurs within the time frame of the decay of $(^2\text{T}_1/^2\text{E})\text{Cr}(\text{bpy})_3^{3+}$ ($\sim 70 \mu\text{sec}$); iii) direct reaction of $(^2\text{T}_1/^2\text{E})\text{Cr}(\text{bpy})_3^{3+}$ with OH^- , which presumably proceeds via the $\text{Cr}(\text{bpy})_3(\text{OH})^{2+}$ intermediate species, yields a value of the quantum yield that approaches unity at high OH^- concentrations (see Section 3.10.)

Model I is summarized in reactions (3-122) to (3-128).



The quantum yield for reaction occurring exclusively from $^4\text{T}_2$, ${}^4\phi_{\text{rx}}$, is equal to the efficiency of reaction from that state, ${}^4\eta_{\text{rx}}$. Since the efficiency of such reaction can be written in terms of the rate constants of all of the processes which deactivate that state, ${}^4\phi_{\text{rx}}$ is given by

$${}^4\phi_{rx} = {}^4\eta_{rx} = \frac{{}^4k_{rx}}{{}^4k_{rx} + {}^4k_{nr} + {}^4k_{isc}} = \frac{{}^4k_{rx}}{{}^4k_o} \quad (3-129)$$

Since the efficiency of the intersystem crossing process is near unity, and ${}^4\phi_{rx}$ is very small, ${}^4k_{rx}$ and ${}^4k_{nr}$ must be very small compared to ${}^4k_{isc}$; thus, ${}^4\phi_{rx}$ can be approximated by equation (3-130).

$${}^4\phi_{rx} \approx \frac{{}^4k_{rx}}{{}^4k_{isc}} \quad (3-130)$$

${}^4\eta_{isc}$ is defined by equation (3-131).

$${}^4\eta_{isc} = \frac{{}^4k_{isc}}{{}^4k_{rx} + {}^4k_{nr} + {}^4k_{isc}} = \frac{{}^4k_{isc}}{{}^4k_o} \quad (3-131)$$

Equation (3-130) allows for evaluation of ${}^4k_{rx} \approx 10^8 \text{ sec}^{-1}$, if ${}^4k_o (= 1/{}^4\tau)$ is taken to be $\approx 10^{11} \text{ sec}^{-1}$. When compared to ${}^2k_{rx}$ for $\text{Cr}(\text{bpy})_3^{3+}$ (${}^2k_{rx} = 1.6 \times 10^3 \text{ sec}^{-1}$), the factor of $\sim 10^5$ times greater reactivity of 4T_2 can be attributed simply to the fact that the 4T_2 state is distorted with respect to the ground state, whereas the $({}^2T_1/{}^2E)$ states are not. Thus, the distortion present in the 4T_2 excited configuration should facilitate the incoming solvent molecule that is interacting with the vacant t_{2g} orbital oriented into the interligand pockets.

In terms of the classical kinetic relation (3-132), expression (3-130)

may be rewritten as (3-133),

$$k = \frac{\bar{k}T}{h} \exp \frac{\Delta S^\ddagger}{R} \exp \frac{-\Delta H^\ddagger}{RT} \quad (3-132)$$

$${}^4\phi_{rx} = \frac{(\bar{k}T/h) \exp \frac{{}^4\Delta S_{rx}^\ddagger}{R} \exp \frac{-{}^4\Delta H_{rx}^\ddagger}{RT}}{(\bar{k}T/h) \exp \frac{{}^4\Delta S_{isc}^\ddagger}{R} \exp \frac{-{}^4\Delta H_{isc}^\ddagger}{RT}} \quad (3-133)$$

Then, taking natural logarithms, one obtains

$$\ln {}^4\phi_{rx} = \frac{{}^4(\Delta S_{rx}^\ddagger - \Delta S_{isc}^\ddagger)}{R} - \frac{{}^4(\Delta H_{rx}^\ddagger - \Delta H_{isc}^\ddagger)}{RT} \quad (3-134)$$

Thus, a plot of $\ln {}^4\phi_{rx}$ vs $1/T$ has a slope equal to $\frac{{}^4(\Delta H_{rx}^\ddagger - \Delta H_{isc}^\ddagger)}{R}$ and an intercept equal to $\frac{{}^4(\Delta S_{rx}^\ddagger - \Delta S_{isc}^\ddagger)}{R}$. For the data in Table 3-28, a plot of $\ln {}^4\phi_{rx}$ vs $1/T$ yields $\frac{{}^4(\Delta H_{rx}^\ddagger - \Delta H_{isc}^\ddagger)}{R} = 9.6$ kcal/mole and $\frac{{}^4(\Delta S_{rx}^\ddagger - \Delta S_{isc}^\ddagger)}{R} = +21$ eu. $\frac{{}^4\Delta H_{isc}^\ddagger}{R}$ is assumed to be zero, or near zero, inasmuch as rapid intersystem crossing, being isoenergetic crossing from the quartet to the doublet manifolds, occurs in the picosecond time frame. If this is true, then $\frac{{}^4\Delta H_{rx}^\ddagger}{R} = 9.6$ kcal/mole. The large value of $\frac{{}^4\Delta H_{rx}^\ddagger}{R}$ is surprising in view of the greater energy and shorter lifetime of the 4T_2 state when compared with the $({}^2T_1/{}^2E)$ manifold. The large change in geometry that occurs when the system crosses from 4T_2 to $({}^2T_1/{}^2E)$ may well lead to a substantial energy barrier at the crossing point of the potential energy surfaces. A comparison of $\frac{{}^4\Delta H_{rx}^\ddagger}{R}$ and $\frac{{}^2\Delta H_{rx}^\ddagger}{R}$ for $\text{Cr}(\text{bpy})_3^{3+}$ suggests that the photoaquation activation mechanisms, i.e., the formation

of the seven-coordinate intermediate, are the same.

The positive value of ${}^4(\Delta S_{rx}^\ddagger - \Delta S_{isc}^\ddagger)$ indicates that ${}^4\Delta S_{rx}^\ddagger$ is more positive than ${}^4\Delta S_{isc}^\ddagger$ for $\text{Cr}(\text{bpy})_3^{3+}$. If the difference between ${}^4k_{rx}$ and ${}^2k_{rx}$ is attributed to entropy differences, then ${}^4\Delta S_{rx}^\ddagger$ is more positive than ${}^2\Delta S_{rx}^\ddagger$ by ca. 23 eu. The value of ${}^2\Delta S_{rx}^\ddagger = -11$ eu (Section 3.8.1.) leads to the suggestion that the driving force for the rapid reaction from 4T_2 will arise from the positive value of ${}^4\Delta S_{rx}^\ddagger$ of +13 eu. Whereas the activated complex from 4T_2 must possess quartet multiplicity and thereby be distorted relative to the activated complex from $({}^2T_1/{}^2E)$, the distortion will result in structural disorder of the activated complex and a large positive value of ${}^4\Delta S_{rx}^\ddagger$.

Model II: Prompt reaction.

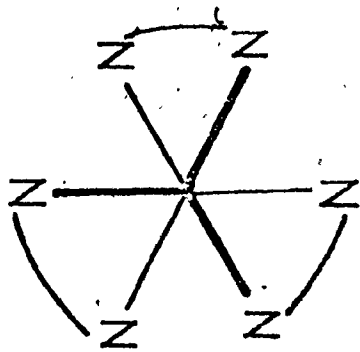
Hollebone and coworkers¹²³ have developed a tensorial model to mechanistically categorize photoreactions of transition metal complexes. Two limiting cases were suggested:¹²³ (1) excited-state decay via random coordinate selection (DERCOS), and (2) excited-state decay on a specific nuclear coordinate (DOSENCO). In the DERCOS limit, reactive excited states have lifetimes which are long compared to vibrational and orientational relaxation, and their decay is inversely dependent on the energy barrier such that the availability of any deactivation pathway depends on the random distribution of normal modes at the effective Boltzmann temperature. Excited-state reactions in the DERCOS limit may be described using transition state theory (which requires a pseudo-equilibrium assumption) and taking into account the luminescence and non-radiative decay processes. In the DOSENCO limit, excited-state reaction may compete with non-radiative deactivation; that is, with vibrational and orientational relaxation. Thus, excited-state decay occurs on a specific nuclear coordinate

so as to emphasize the preferential selection of a small number of allowed non-radiative processes. The DOSENCO limit predicts that excitation of $\text{Cr}(\text{NN})_3^{3+}$ in the quartet manifold is rapidly accompanied by the t_{1u} buckle vibrational mode, which causes facial exposure of the central metal atom (see Figure 3-33). The exposed Cr(III) core on the stretched faces of the octahedron could be subjected to facile nucleophilic attack by the solvent, therein leading to an associative reaction. The time frame for the DOSENCO process makes it competitive with vibrational relaxation down the quartet manifold, and thus predicts that prompt photoreactivity can occur with an efficiency of ${}^{\text{DOS}}\eta_{\text{rx}}$. If it is assumed that the product of the associative DOSENCO reaction behaves the same way as the seven-coordinate intermediate from reaction (3-125), then

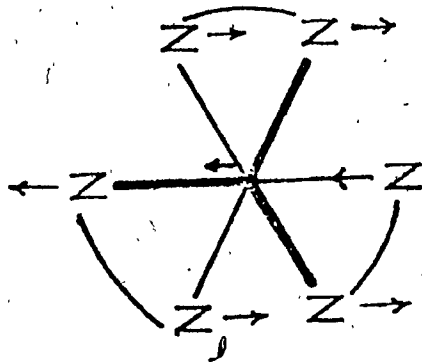
$${}^4\phi_{\text{rx}} = {}^{\text{DOS}}\eta_{\text{rx}} + (1 - {}^{\text{DOS}}\eta_{\text{rx}}) {}^4\eta_{\text{rx}} \quad (3-135)$$

defines ${}^4\phi_{\text{rx}}$ in the presence of I^- , where ${}^4\eta_{\text{rx}}$ is the efficiency of reaction from ${}^4\text{T}_2$. ${}^{\text{DOS}}\eta_{\text{rx}}$ can have values in the range $0 - 10^{-3}$, with corresponding values of ${}^4\eta_{\text{rx}}$ in the range $10^{-3} - 0$, inasmuch as ${}^4\phi_{\text{rx}}$ has been experimentally determined to be ca. 10^{-3} . Thus, ${}^4\phi_{\text{rx}} = {}^{\text{DOS}}\eta_{\text{rx}} + {}^4\eta_{\text{rx}}$. If ${}^4\eta_{\text{rx}}$ is greater than ${}^{\text{DOS}}\eta_{\text{rx}}$, the contribution of prompt photoreaction to the overall quenchable and unquenchable quantum yields is not considered significant. On the other hand, if ${}^4\eta_{\text{rx}} = 0$, then the temperature dependence of ${}^4\phi_{\text{rx}}$ must reflect the dependencies of the very fast DOSENCO associative and vibrational relaxation processes. It seems rather unlikely that such fast intramolecular processes, which involve highly energetic species, would have significant enthalpic barriers. At

FIGURE 3-33: Schematic Representation of the t_{1u} Buckle Vibrational Mode
 Which Accompanies Excitation of $Cr(NN)_3^{3+}$ in the Quartet Manifold.



$4A_2$

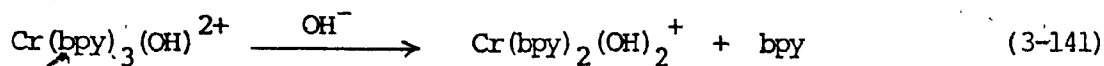
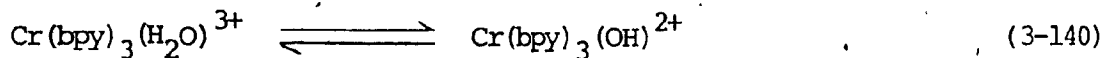
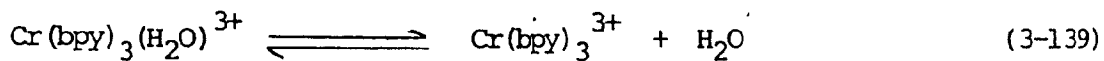
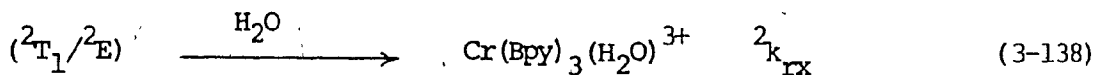
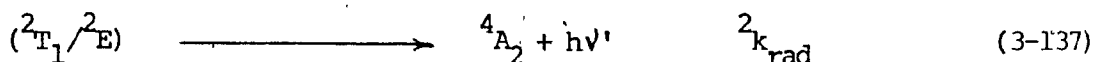
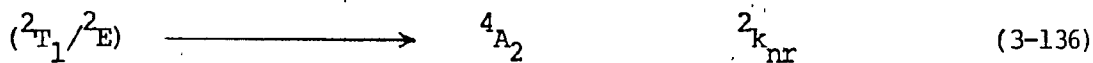


t_{1u} BUCKLE

this time, the temperature dependence of steps after the DOSENCO process cannot be precluded. Suffice it to say that the DOSENCO theory stipulates¹²³ that processes are temperature-independent and wavelength-dependent.

Model III: $4^+ 2\phi_{rx}$ from thermally-equilibrated (${}^2T_1/{}^2E$).

Efficient intersystem crossing, either prompt (pisc) or delayed, from the quartet manifold populates the luminescent (${}^2T_1/{}^2E$) state with a yield that is close to unity. If the quantum yield of photoreaction in the absence of I^- occurs primarily due to reaction of the (${}^2T_1/{}^2E$) states in competition with radiative and non-radiative decay from (${}^2T_1/{}^2E$), then equations (3-136) to (3-141) can be visualized.



The (${}^2T_1/{}^2E$) lifetime is defined as per equation (3-12) for this model.

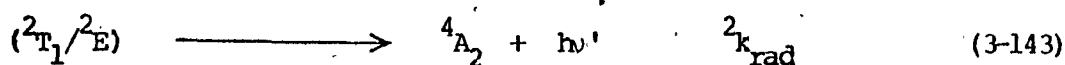
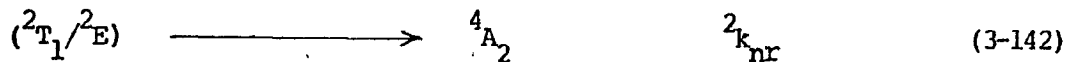
Inasmuch as the quantum yield of luminescence from (${}^2T_1/{}^2E$) is $\sim 10^{-3}$,
 $38,48 \quad {}^2k_{rad} \ll ({}^2k_{nr} + {}^2k_{rx})$. Quantitative formation of the final

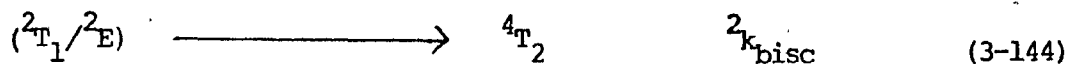
equation product dictates that ${}^{4+2}\phi_{rx}$ is equal to the efficiency of reaction from $({}^2T_1/{}^2E)$, ${}^2\eta_{rx}$, and ${}^2\phi_{rx} = {}^2k_{rx} / ({}^2k_{rx} + {}^2k_{nr})$. The value of ${}^2k_{rx}$ can be extracted from the data of ${}^{4+2}\phi_{rx}$ as a function of temperature, and a plot of $\ln ({}^2k_{rx}/T)$ vs $1/T$ is linear with a slope corresponding to 9.7 kcal/mole and an intercept corresponding to -11 eu, as revealed in Figure 3-28.

Employing the value of ${}^4\Delta H_{rx}^\ddagger \approx 9.6$ kcal/mole, it is clear that the enthalpic barrier of activation toward reaction from 4T_2 and $({}^2T_1/{}^2E)$ could be identical. Furthermore, it seems clear that the large difference in the values of the apparent activation energies (E_{app}) of the quantum yields in the presence (9.6 kcal/mole) and absence (1.9 kcal/mole) of iodide ion may be totally illusory owing to the fact that quantum yields reflect kinetic competitions among reactions with differing temperature coefficients. Though this model may be valid, any conclusions based solely on "apparent" activation energies of quantum yield measurements have limited validity.¹⁶

Model IV: Back-intersystem crossing from $({}^2T_1/{}^2E)$.

The apparent similarities of ${}^4\Delta H_{rx}^\ddagger$ and ${}^2\Delta H_{rx}^\ddagger$ from the 4T_2 and $({}^2T_1/{}^2E)$ states, respectively, immediately raise the question as to whether all the observed photoreaction from $Cr(bpy)_3^{3+}$ occurs from 4T_2 with $({}^2T_1/{}^2E)$ being unreactive. In such a case, $({}^2T_1/{}^2E)$ must engage in non-radiative, radiative and back-intersystem crossing deactivation processes (reactions 3-142 to 3-144), and the system makes repeated passes through the reactive





4T_2 state leading to the observed quantum yield. The inherent lifetime of $({}^2T_1/{}^2E)$ is given by equation (3-12), and the total photoaquation quantum yield is the sum of the immediate reaction from 4T_2 and that resulting from passage of the system through $({}^2T_1/{}^2E)$, with ${}^4\phi_{\text{rx}} \gg {}^4\phi_{\text{isc}}$. Accordingly, the system passes through $({}^2T_1/{}^2E)$ approximately 50 times, with each pass through 4T_2 yielding a contribution to ${}^4\phi_{\text{rx}}$ of $\sim 2 \times 10^{-3}$.

It is important to note here that the non-radiative decay of $({}^2T_1/{}^2E)$ is an essential component of the back-intersystem crossing model. The steady-state population of $({}^2T_1/{}^2E)$ is maintained by the rapid ${}^4T_2 \rightsquigarrow ({}^2T_1/{}^2E)$ intersystem crossing process in competition with the inefficient non-radiative (${}^4k_{\text{nr}}$) and reactive (${}^4k_{\text{rx}}$) decay processes, inasmuch as ${}^4\eta_{\text{isc}} \sim 1$. If the ultimate route of escape of $({}^2T_1/{}^2E)$ is via radiative, non-radiative and reactive pathways from 4T_2 , then the value of the quantum yield of luminescence would approach unity, and this does not appear to be the case for $\text{Cr}(\text{bpy})_3^{3+}$ 38, 48

The back-intersystem crossing model can now be treated using the approximation that during continuous irradiation at 313 nm, the concentrations of 4T_2 and $({}^2T_1/{}^2E)$ reach and remain at a steady-state, so that one can formulate equations (3-145) and (3-146) for the steady-state concentrations of the 4T_2 and $({}^2T_1/{}^2E)$ states, respectively.

$$\frac{d[{}^4T_2]}{dt} = I_a + {}^2k_{\text{bisc}}[{}^2E] - ({}^4k_{\text{rx}} + {}^4k_{\text{isc}} + {}^4k_{\text{nr}})[{}^4T_2] = 0 \quad (3-145)$$

$$[{}^4T_2]_{ss} = \frac{I_a + {}^2k_{bisc}[{}^2E]_{ss}}{{}^4k_{rx} + {}^4k_{isc} + {}^4k_{nr}} = \frac{I_a + {}^2k_{bisc}[{}^2E]_{ss}}{{}^4k_o} \quad (3-145)$$

Similarly,

$$\frac{d[{}^2E]}{dt} = {}^4k_{isc} [{}^4T_2] - {}^2k_{bisc}[{}^2E] - {}^2k_{rad}[{}^2E] - {}^2k_{nr}[{}^2E] = 0 \quad (3-146)$$

$$[{}^2E]_{ss} = \frac{{}^4k_{isc}[{}^4T_2]_{ss}}{{}^2k_{bisc} + {}^2k_{rad} + {}^2k_{nr}} = \frac{{}^4k_{isc}[{}^4T_2]_{ss}}{{}^2k_o}$$

Since ${}^4\eta_{isc} \approx 1$, ${}^4k_{isc} \gg ({}^4k_{nr} + {}^4k_{rx})$, and equation (3-145) becomes

$$[{}^4T_2]_{ss} = \frac{I_a + {}^2k_{bisc}[{}^2E]_{ss}}{{}^4k_{bisc}} \quad (3-147)$$

Then, the combination of equations (3-146) and (3-147) yields the steady-state concentration of the 2E state, $[{}^2E]_{ss}$, given in (3-148), since ${}^2k_{rad}$

$$[{}^2E]_{ss} = \frac{I_a}{{}^2k_{rad} + {}^2k_{nr}} = \frac{I_a}{{}^2k_{nr}} \quad (3-148)$$

$\sim 10^{-3} \text{ sec}^{-1}$ and ${}^2k_{nr} \gg {}^2k_{rad}$. If the quantum yield of luminescence is taken as equal to ${}^2k_{rad} / {}^2k_{nr}$, then a plot of $\ln {}^2\phi_{rad}$ vs $1/T$ should yield a positive slope equal to $(\Delta H_{nr}^\ddagger - \Delta H_{rad}^\ddagger)$; indeed, the slope of such a plot³⁸ yields +8.3 kcal/mole, and since purely radiative decay is

temperature-independent, ${}^2\Delta H_{\text{rad}}^\ddagger = 0$ and ${}^2\Delta H_{\text{nr}}^\ddagger = 8.3$ kcal/mole. The quantum yield for photoaquation, ${}^{4+2}\phi_{\text{rx}}$, represents the yield of product via passage of the system to and from (${}^2T_1/{}^2E$) and is defined by

$${}^{4+2}\phi_{\text{rx}} = \frac{{}^4k_{\text{rx}} [{}^4T_2]_{\text{ss}}}{I_a} \quad (3-149)$$

which assumes that the fate of the 2E state rests nearly entirely on the ${}^2k_{\text{bisc}}$ term; that is, ${}^2k_{\text{bisc}} > ({}^2k_{\text{rx}} + {}^2k_{\text{nr}} + {}^2k_{\text{rad}})$. Equations (3-150) to (3-152) yield an expression for ${}^{4+2}\phi_{\text{rx}}$ in terms of these assumptions.

$${}^{4+2}\phi_{\text{rx}} = {}^4k_{\text{rx}} \frac{1 + {}^2k_{\text{bisc}} [{}^2E]_{\text{ss}} I_a}{{}^4k_{\text{O}}} \quad (3-150)$$

$${}^{4+2}\phi_{\text{rx}} = \frac{{}^4k_{\text{rx}}}{{}^4k_{\text{O}} - {}^4k_{\text{O}} {}^2k_{\text{bisc}} / {}^2k_{\text{O}}} \quad (3-151)$$

Since ${}^4k_{\text{O}} = {}^4k_{\text{isc}} + {}^4k_{\text{nr}} + {}^4k_{\text{rx}} \approx {}^4k_{\text{isc}}$ and ${}^2k_{\text{O}} = {}^2k_{\text{bisc}} + {}^2k_{\text{rad}} + {}^2k_{\text{nr}} \approx {}^2k_{\text{bisc}} + {}^2k_{\text{nr}}$, then

$${}^{4+2}\phi_{\text{rx}} = \frac{{}^4k_{\text{rx}}}{{}^4k_{\text{O}} - \frac{{}^4k_{\text{isc}} {}^2k_{\text{bisc}}}{{}^2k_{\text{bisc}} + {}^2k_{\text{nr}}}} \quad (3-152)$$

If the non-radiative pathway predominates over bisc, such that ${}^2k_{\text{bisc}} \ll$

$^2k_{nr}$, then $^{4+2}\phi_{rx} = ^4k_{rx} / ^4k_o$, which is the same as for $^4\phi_{rx}$ without going through the 2E state. However, if non-radiative decay of ($^2T_1/{}^2E$) were an important process compared to back-intersystem crossing, then $^{4+2}\phi_{rx}$ would approach a value of unity.

Whereas $^{4+2}\phi_{rx}$ for $\text{Cr}(\text{bpy})_3^{3+}$ has an experimentally-determined value (0.13) intermediate between the values of the unquenchable quantum yield ($^4\phi_{rx} \sim 10^{-3}$) and unity, this back-intersystem crossing model requires that the non-radiative and back-intersystem crossing processes compete with each other. Equation (3-153) expresses $^2k_{nr}$ in terms of $^2k_{bisc}$, where X is a fraction that is temperature dependent. Under these conditions,

$$^2k_{nr} = X ^2k_{bisc} \quad (3-153)$$

Then, $^{4+2}\phi_{rx}$ is given by

$$^{4+2}\phi_{rx} = \frac{1 + X}{X} \frac{^4k_{rx}}{^4k_{isc}} \quad (3-154)$$

and since $^4\phi_{rx} = ^4k_{rx} / ^4k_{isc}$,

$$^{4+2}\phi_{rx} = \frac{1 + X}{X} ^4\phi_{rx} \quad (3-155)$$

A comparison of the quenchable and unquenchable quantum yields (Table 3-28) shows that $^4\phi_{rx} / ^{4+2}\phi_{rx} \approx 10^{-2}$ so that $(1 + X) = 1$. Thus, the fraction that is temperature dependent is given by /

$$X = \frac{{}^4\phi_{rx}}{{}^4\phi_{rx}} = \frac{{}^2k_{nr}}{{}^2k_{bisc}} \quad (3-156)$$

where

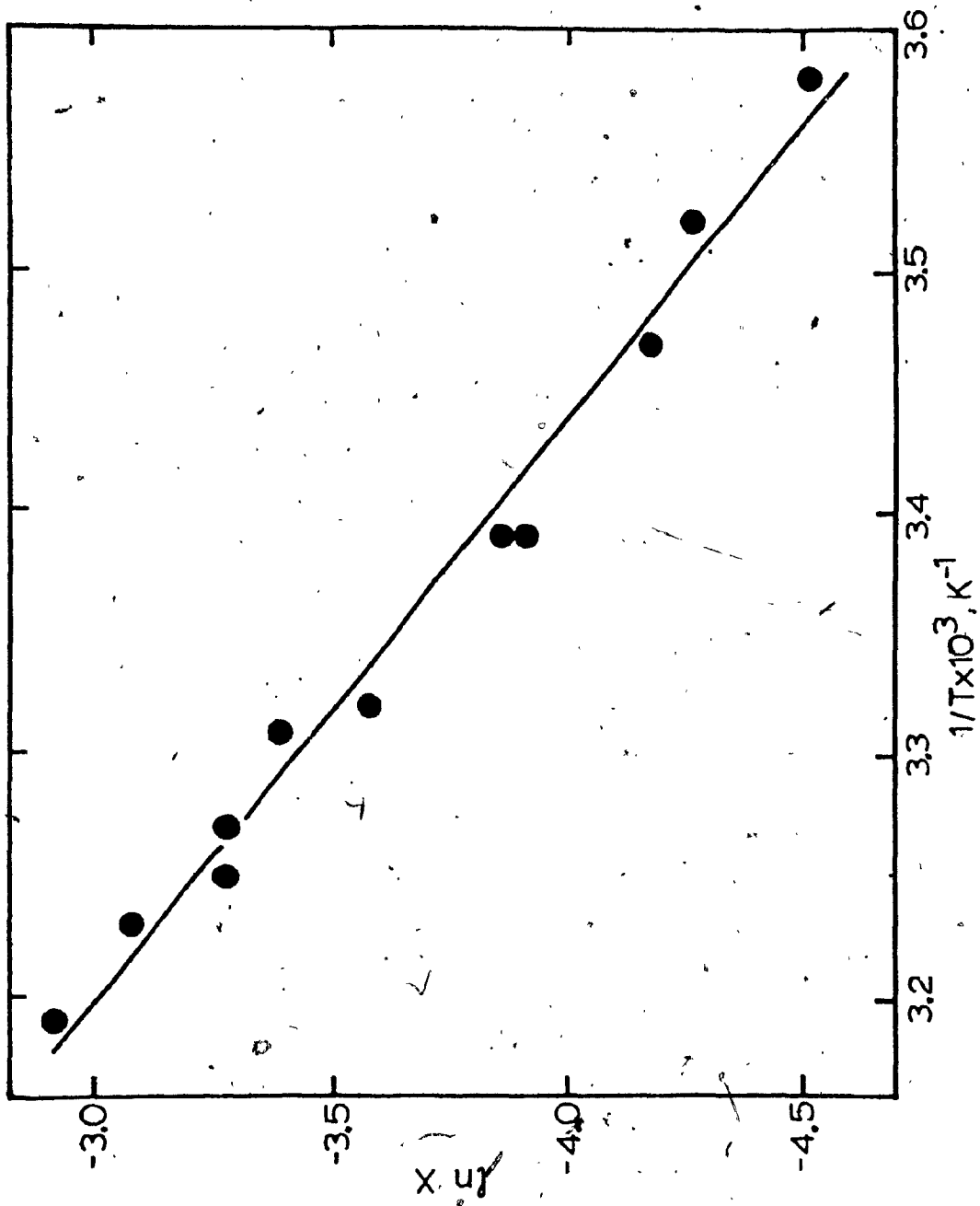
$$\frac{{}^2k_{nr}}{{}^2k_{bisc}} = \frac{\exp\left(\frac{{}^2\Delta S_{nr}^\ddagger}{R}\right) \exp\left(\frac{-2\Delta H_{nr}^\ddagger}{RT}\right)}{\exp\left(\frac{{}^2\Delta S_{bisc}^\ddagger}{R}\right) \exp\left(\frac{-2\Delta H_{bisc}^\ddagger}{RT}\right)} \quad (3-157)$$

Hence, a plot of $\ln X$ vs $1/T$ should be linear with a slope = $-(2\Delta H_{nr}^\ddagger - 2\Delta H_{bisc}^\ddagger) / R$. The data of Table 3-28 and the interpolated data from Figure 3-28 are plotted in Figure 3-34; $(2\Delta H_{nr}^\ddagger - 2\Delta H_{bisc}^\ddagger) = +8.1$ kcal/mole. Inasmuch as $2\Delta H_{nr}^\ddagger$ was noted earlier to be $+8.3$ kcal/mole³⁸ it is concluded that a mechanism which involves only quartet reactivity and back-intersystem crossing from $({}^2T_1/{}^2E)$ can be valid only if $2\Delta H_{bisc}^\ddagger = 0$.

While it is physically possible that there be no physical barrier to $({}^2T_1/{}^2E) \rightsquigarrow {}^4T_2$ conversion, such a requirement places severe restrictions on the relative energies and geometries of the 4T_2 and $({}^2T_1/{}^2E)$ states. In fact, it leads to the possibility that the zeroeth energy level of 4T_2 lies below that of the $({}^2T_1/{}^2E)$, and that fluorescence from 4T_2 , if it exists, lies at longer wavelengths (lower energy) than phosphorescence emission from $({}^2T_1/{}^2E)$. However, experiments designed to test this reveal no fluorescence from $\text{Cr}(\text{bpy})_3^{3+}$ in fluid solution nor at 77K; in fact, no additional luminescence is observed in the 740 - 1100 nm range at 77K.

From the observed quantum yields of the quenchable and unquenchable

FIGURE 3-34 : Plot of $\ln X$ vs $1/T$ (see text), for $\text{Cr}(\text{bpy})_3^{3+}$ at 22°C .



photoaquation of $\text{Cr}(\text{bpy})_3^{3+}$ and the corresponding temperature dependencies for irradiation at 313 nm, it does not appear necessary at this time to invoke any reaction mechanism other than that in which the unquenchable yield arises from the $^4\text{T}_2$ manifold and the quenchable yield comes from the $(^2\text{T}_1/^2\text{E})$ states populated from $^4\text{T}_2$ via rapid, efficient inter-system crossing. This analysis reveals that the back-inter-system crossing model necessitates $^2\Delta\text{H}_{\text{isc}}^\ddagger \sim 0$, which places severe restrictions on the energy and distortion of the $^4\text{T}_2$ state relative to the $^4\text{A}_2$ and $(^2\text{T}_1/^2\text{E})$ states.

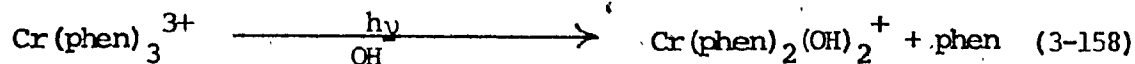
The data and the Model I reveal values for $^4\Delta\text{H}_{\text{rx}}^\ddagger > 9.6$ kcal/mole, $^2\Delta\text{H}_{\text{rx}}^\ddagger = 9.7$ kcal/mole, and $^4\Delta\text{H}_{\text{isc}}^\ddagger \sim 0$; the conclusion is that a similar enthalpic barrier is present for reaction of the solvent with either the $^4\text{T}_2$ or $(^2\text{T}_1/^2\text{E})$ manifolds to form the seven-coordinate intermediate. And, aside from the specific energetics of the $^4\text{T}_2$ and $(^2\text{T}_1/^2\text{E})$ reactions, the activation mechanisms for photoaquation are identical.

The +21 eu value of $^4(\Delta\text{S}_{\text{rx}}^\ddagger - \Delta\text{S}_{\text{isc}}^\ddagger)$ for the $^4\text{T}_2$ reaction implies that $^4\Delta\text{S}_{\text{rx}}^\ddagger$ is more positive than $^4\Delta\text{S}_{\text{isc}}^\ddagger$. The similar negative values of $^2\Delta\text{S}_{\text{rx}}^\ddagger$ and $\Delta\text{S}_{\text{rx}}^\ddagger$ (for reaction from $(^2\text{T}_1/^2\text{E})$ and $^4\text{A}_2$, respectively) indicate that the addition of solvent to the geometrically similar $(^2\text{T}_1/^2\text{E})$ and $^4\text{A}_2$ states forms a common seven-coordinate intermediate. The enhanced reactivity of the $^4\text{T}_2$ state ($^4k_{\text{rx}} \sim 10^8 \text{ sec}^{-1}$) over that of the $(^2\text{T}_1/^2\text{E})$ ($^2k_{\text{rx}} \sim 10^3 \text{ sec}^{-1}$) seemingly arises from differences in $\Delta\text{S}_{\text{rx}}$ from $^4\text{T}_2$ and $(^2\text{T}_1/^2\text{E})$, inasmuch as values of $^4\Delta\text{H}_{\text{rx}}^\ddagger$ and $^2\Delta\text{H}_{\text{rx}}^\ddagger$ are identical. If the rate constant factor is strictly entropic, then $^4\Delta\text{S}_{\text{rx}}^\ddagger$ would be more positive than $^2\Delta\text{S}_{\text{rx}}^\ddagger$ by ca. 23 eu; thus, the driving force for fast $^4\text{T}_2$ reaction would arise from the value of $\Delta\text{S}_{\text{rx}}^\ddagger \approx +13$ eu. Presumably, reaction from $^4\text{T}_2$ involves an interaction with solvent to yield an activated

complex that is more distorted than the separated 4T_2 and solvent reactants. The 4T_2 activated complex must be distorted relative to the (${}^2T_1/{}^2E$) activated complex inasmuch as it must possess quartet multiplicity in order to satisfy an essential condition in transition state theory; this distortion allows for a wide variety of configurations in the activated complex. Intersystem crossing from this distorted quartet state into the doublet manifold would be accompanied by a tightening of the system and a negative value of ${}^4\Delta S_{isc}^\ddagger$; according to the analysis in Model I, ${}^4\Delta S_{isc}^\ddagger \approx -10$ eu.

3.9.1. $Cr(phen)_3^{3+}$.

As with $Cr(bpy)_3^{3+}$, reaction (3-158) is quenched by iodide ion, although the Stern-Volmer plot for the quantum yield is not linear,



as illustrated in Figure 3-35. The observation that ϕ_{rx} approaches a lower limit at high I^- concentrations can be explained by assuming two sources for reaction (3-158); namely, one quenchable by I^- and one which is not quenchable by I^- .

a. Temperature dependence of ${}^4\phi_{rx}$.

The temperature dependence of the unquenchable photoreaction of $Cr(phen)_3^{3+}$ was investigated in order to compare the energetics of this reaction with those of the (${}^2T_1/{}^2E$) and 4A_2 reactions, and also with $Cr(bpy)_3^{3+}$. Table 3-29 shows the data obtained for $[Cr(phen)_3^{3+}] = 1 \times 10^{-3}$ M at pH 10 ($\mu = 1.0$ with NaCl) in the presence of 0.05 M I^- . An Arrhenius-type plot of $\ln \phi_{rx}$ vs $1/T$ is not linear (see Figure 3-36), but reveals two temperature-dependent regions: i) region A (286 - 302K) for

FIGURE 3-35 : Stern-Volmer Plot for Quenching of Φ_{rx} by I^- for $Cr(phen)_3^{3+}$ at pH 10.5 and 15°C; from reference 35. Superscript 0 refers to solutions without iodide ion.

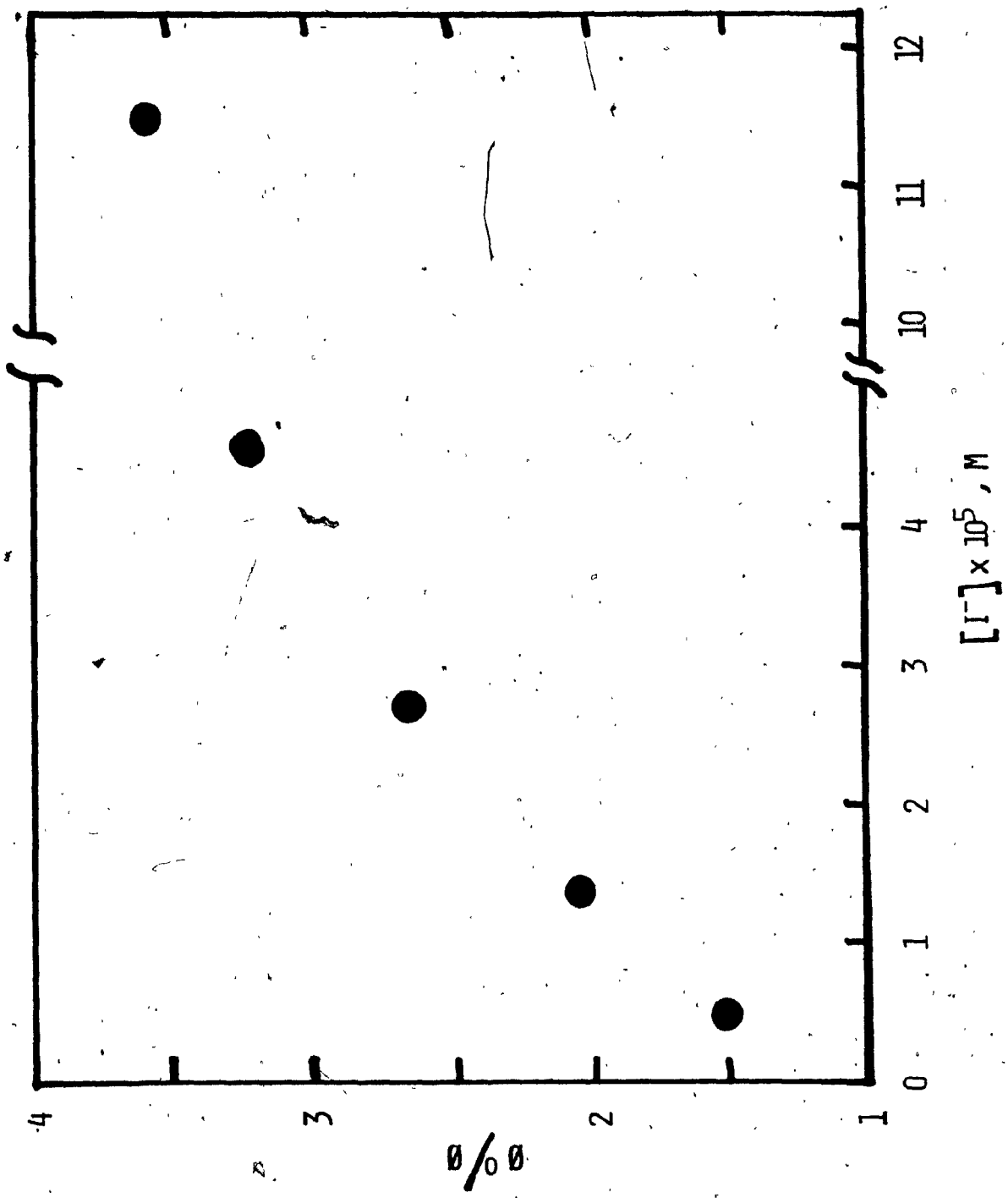
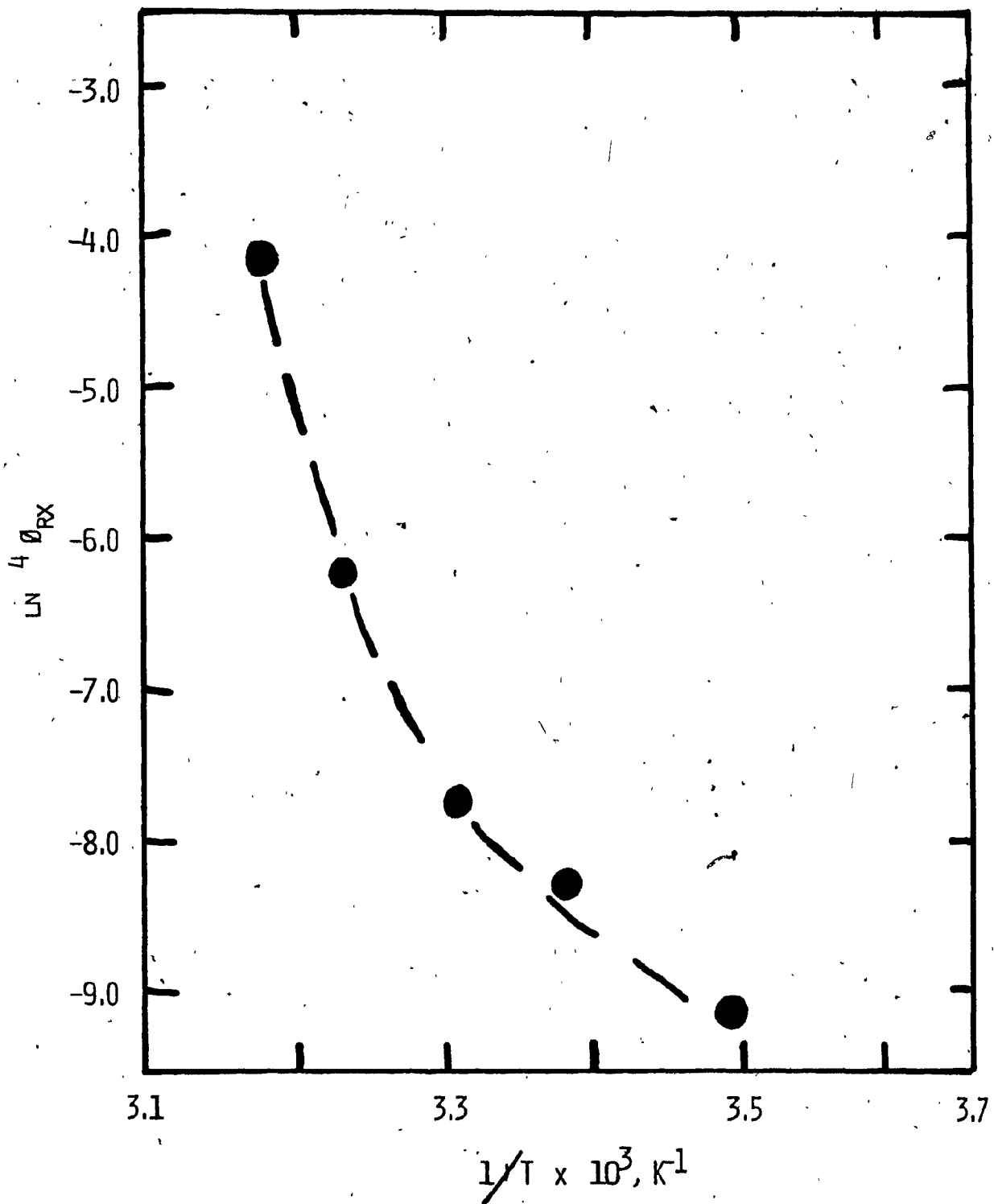


TABLE 3-29 : Temperature Profile of the Photoaquation Quantum Yield and Reactive Decay Rate Constant for the Unquenchable Reaction Component of $\text{Cr}(\text{phen})_3^{3+}$ in Deaerated Solutions.^a

Temperature, (K)	$^4\phi_{\text{rx}}$ ^b	$^4k_{\text{rx}}$ (sec^{-1}) ^c
286.3	1×10^{-4}	1.1×10^7
295.4	2.5×10^{-4}	2.5×10^7
302.2	4.3×10^{-4}	4.3×10^7
309.2	2.1×10^{-3}	20.9×10^7
314.4	1.57×10^{-2}	157×10^7

^a Experimental conditions: 1.0×10^{-3} M $\text{Cr}(\text{bpy})_3^{3+}$, pH 10.0, 0.008 M Britton-Robinson buffer, $\mu = 1.0$ (with NaCl). Solution contains 0.05 M NaI. ^b From Table 3-23. ^c Calculated from $^4k_{\text{rx}} = ^4\phi_{\text{rx}} ^4k_0$, where $^4k_0 = 10^{11} \text{ sec}^{-1}$.

FIGURE 3-36 : Arrhenius-type Plot of $\ln \phi_{rx}$ vs $1/T$ for $\text{Cr}(\text{phen})_3^{3+}$
at pH 10.0 in Argon-purged Solutions.



which an "apparent" activation energy $E_{app} = 15.3$ kcal/mole, and ii) region B for which $E_{app} = 53.8$ kcal/mole. Such non-linearity is not unexpected but is difficult to rationalize, particularly in view of the very large values of E_{app} .

An evaluation of ${}^4k_{rx}$ may be made from equation (3-129); since ${}^4\eta_{isc} \approx 1$, ${}^4k_{isc} > ({}^4k_{rx} + {}^4k_{nr})$, and equation (3-129) yields ${}^4k_o \approx {}^4k_{isc} \approx 1 / {}^4\tau$. If the value of ${}^4\tau$ is taken to be 10^{-11} sec, then

$${}^4k_{rx} = {}^4\phi_{rx} {}^4k_o = {}^4\phi_{rx} (10^{11}) \quad (3-159)$$

Values of ${}^4k_{rx}$ calculated from equation (3-159) are presented in Table 3-29. A plot of $\ln ({}^4k_{rx} / T)$ vs $1/T$ also reveals two regions A and B. Region A affords ${}^4\Delta H_{rx}^\ddagger = +14.5$ kcal/mole and ${}^4\Delta S_{rx}^\ddagger = +24.3$ eu; region B yields ${}^4\Delta H_{rx}^\ddagger = +54$ kcal/mole and ${}^4\Delta S_{rx}^\ddagger = +155$ eu. These very large values are not understood at present.

At this point, some tentative comparisons can be made, which involve only region A of the temperature dependence results of the unquenchable reaction component. Thus, one can compare the activation parameters for the 4A_2 and $({}^2T_1/{}^2E)$ aquation reactions with that of the unquenchable reaction component. This comparison (cf. Tables 3-2 and 3-26) reveals "apparent" activation energies of 23.3, 18.5 and 15.3 kcal/mole for the 4A_2 , $({}^2T_1/{}^2E)^\circ$ and unquenchable reaction component, respectively; enthalpies of activation for the reactive decay of 4A_2 , $({}^2T_1/{}^2E)$ and unquenchable component of 23.3, 23.3, and 14.5 kcal/mole, respectively; and entropies of activation for the reactive deactivation of the 4A_2 , $({}^2T_1/{}^2E)$ and unquenchable component of -8.4, +31.1 and +24.3 eu, respectively. However, no such comparison can be made for region B, where the calculated values of

E_{app} , ${}^4\Delta H_{rx}^\ddagger$ and ${}^4\Delta S_{rx}^\ddagger$ are clearly difficult to rationalize.

The existence of two temperature-dependent regions A and B for the quantum yield of reaction is in agreement with the predicted behavior of such relationships; that is, plots of $\ln \phi_{rx}$ vs $1/T$ are not expected to be linear.¹⁶ Therefore, the "apparent" activation energy will depend on the temperature range chosen for the experiments, and in practice is thought¹⁶ to occur only when $\phi > 0.1$. When $\phi > 0.1$, the $E_a - E_{app}$ difference will attain a large value. Furthermore, when $\phi = 1$, $E_{app} = 0$, regardless of the actual value of E_a . This reasoning assumes that physical deactivation processes exhibit no activation energy; if, in fact, they do, then the situation becomes much more complex. So, at this time it suffices to say that the non-linear relationship expected is observed for $Cr(phen)_3^{3+}$ but not for $Cr(bpy)_3^{3+}$. The inability to observe this phenomenon for the bpy complex may be due to the narrow temperature range investigated.

3.10. EVALUATION OF THE ${}^4T_2 \rightsquigarrow ({}^2T_1/{}^2E)$ INTERSYSTEM CROSSING YIELD.

The nature and extent of participation of the 4T_2 and $({}^2T_1/{}^2E)$ excited-state configurations in chromium(III) photochemistry has stimulated great interest. As concerns such complexes, the identity of the reactive state continues to be a controversial issue. It is generally accepted that part of the photochemistry quenched in parallel with the luminescence from $({}^2T_1/{}^2E)$ states must involve these states. What is not clear very often, however, is whether the quenchable part of the photo-reaction occurs directly from the $({}^2T_1/{}^2E)$ manifold or from the 4T_2 manifold subsequent to back-intersystem crossing. A crucial parameter in elucidating the photochemical mechanism of Cr(III) polypyridyl complexes

is the intersystem crossing yield, ${}^4\eta_{isc}$, defined by equation (3-82).

The increased interest in the relative roles of the quartet and doublet excited states of $\text{Cr}(\text{NN})_3^{3+}$ complex ions was stimulated by the work of Bolletta and coworkers;⁵² these authors reported that the intersystem crossing efficiencies for $\text{Cr}(\text{bpy})_3^{3+}$ and $\text{Cr}(\text{phen})_3^{3+}$ were 0.94 and 0.21, respectively. The method used was based on electronic energy transfer from an emitting donor species (D) to an emitting acceptor species (A). For the two donor/acceptor couples biacetyl/ $\text{Cr}(\text{bpy})_3^{3+}$ in water and $\text{Cr}(\text{phen})_3^{3+}$ / $\text{Cr}(\text{CN})_6^{3-}$ in $\text{H}_2\text{O}/\text{DMF}$, a representative energy level diagram given in Figure 3-37 was used as the basis for determining ${}^4\eta_{isc}$. For both D/A couples, excitation of the donor species D causes a sensitized emission from the acceptor species A. According to Figure 3-37, the emission intensity of the acceptor, E_A^O , and the sensitized emission intensity of the acceptor, E_A^S , are given by

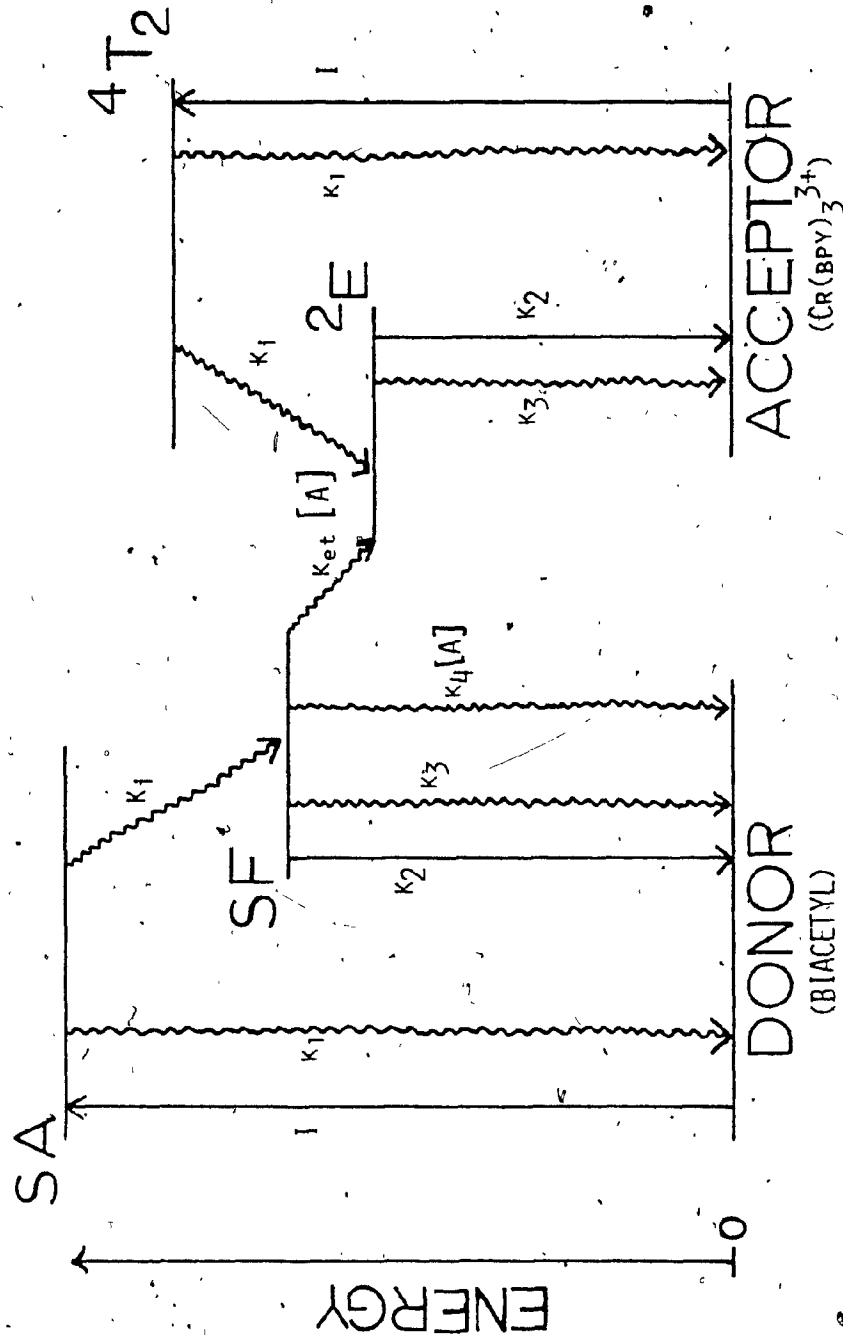
$$E_A^O \propto I_A^O \eta_i^A \eta_2^A \quad (3-160)$$

$$E_A^S \propto I_D \eta_i^D \eta_{et} \eta_2^A \quad (3-161)$$

where I_A^O is the light intensity absorbed by the acceptor solution, and I_D is the light intensity absorbed by the donor in a solution containing known amounts of donor and acceptor species. The efficiency of the intersystem crossing step, η_i , from the spin-allowed state to the spin-forbidden state for the donor and acceptor, respectively, is given by

$$\eta_i^D = k_i^D / (k_i^D + k_1^D) \quad (3-162)$$

FIGURE 3-37 : Simplified Energy Level Diagram of the Biacetyl/Cr(bpy)₃³⁺ Couple used in the Determination of the Intersystem Crossing Efficiency of Cr(bpy)₃³⁺; SA and SF denote spin-allowed and spin-forbidden states, respectively; k₁, k₂, k₃, k₄, k_i and k_{et} refer to the rate constants of non-radiative, radiative, non-radiative, quenching, intersystem crossing and energy transfer processes.



$$\eta_i^A = k_i^A / (k_i^A + k_a^A) \quad (3-163)$$

The efficiency of the emission from the spin-forbidden state of the acceptor is given by

$$\eta_2^A = k_2^A / (k_2^A + k_3^A) \quad (3-164)$$

The energy transfer efficiency from the spin-forbidden donor state to the spin-forbidden acceptor state is

$$\eta_{et} = \frac{k_{et}^D [A]}{k_2^D + k_3^D + (k_{et}^D + k_4^D) [A]} \quad (3-165)$$

Taking $(k_{et}^D + k_4^D) = k_q^D$, equation (3-165) becomes

$$\eta_{et} = \eta_q \eta_{et} \frac{k_q^D [A]}{k_2^D + k_3^D + k_q^D [A]} \frac{k_{et}^D}{k_q^D} \quad (3-166)$$

where η_q represents the quenching efficiency of the spin-forbidden donor state by the ground-state acceptor species, and η_{et} refers to the fraction of quenching events that cause formation of the excited-state acceptor species. Carrying out the emission intensity measurements under the same instrumental conditions, equations (3-160) and (3-161) may be combined to give

$$\frac{E_A^{\circ}}{E_a^s} = \frac{I_A^{\circ} \eta_i^A}{I_D \eta_i^D \eta_q \eta_{et}} \quad (3-167)$$

From the above analysis, it follows that

$$E_A^s = E_A' - \alpha_A E_A^{\circ} \quad (3-168)$$

$$I_D = \alpha_D I_A^{\circ} \quad (3-169)$$

$$\eta_q = 1 - (E_D' / \alpha_D E_D^{\circ}) \quad (3-170)$$

$$\frac{\eta_i^A}{\eta_i^D \eta_{et}} = \frac{E_A^{\circ}}{E_A^s - \alpha_A E_A^{\circ}} \left(\alpha_D - \frac{E_D'}{E_D^{\circ}} \right) = R \quad (3-171)$$

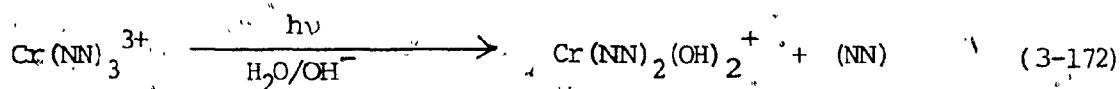
As R in equation (3-171) is an experimentally-determined quantity, the ratio $(\eta_i^A / \eta_i^D \eta_{et})$ can be obtained. Thus, η_i^A can be determined if η_i^D , η_{et} , and R are known. η_i^D for biacetyl in aqueous solution at room temperature was taken⁵² as 0.86 and $\eta_{et} = 1$; the efficiency for isc, η_i^A , for $\text{Cr}(\text{bpy})_3^{3+}$ in the biacetyl/ $\text{Cr}(\text{bpy})_3^{3+}$ couple is 0.94 in water.⁵² A similar analysis on the $\text{Cr}(\text{phen})_3^{3+}/\text{Cr}(\text{CN})_6^{3-}$ couple yielded $\eta_i^D = 0.21$ in $\text{H}_2\text{O}/\text{DMF}$ (1/3, v/v) media at room temperature.⁵²

3.10.0. Evaluating⁴ η_{isc} By Doublet-state Irradiation.

More recently, alteration of solution medium has been shown to have profound effects on the various photochemical and photophysical parameters of the $\text{Cr}(\text{NN})_3^{3+}$ complexes in this work. These include concentration quenching in the presence of added anions and the diminution of

$(^2T_1/{}^2E)$ lifetimes in DMF. As a result, additional experiments have been performed in an effort to determine the intersystem crossing efficiency under identical conditions for $\text{Cr}(\text{NN})_3^{3+}$. Furthermore, such studies are justified in view of expectations that ${}^4\eta_{\text{isc}}$ for the very similar bpy and phen complexes should be nearly the same under similar experimental conditions.

In alkaline solution (pH 9.26), the quantum yield ${}^{4+2}\phi_{\text{rx}}$ for the photoaquation reaction (3-172) reflects the population of the $(^2T_1/{}^2E)$



manifolds and other competitive pathways. For excitation directly into the $(^2T_1/{}^2E)$ manifold, the quantum yield for photoaquation becomes

$${}^2\phi_{\text{rx}} = {}^2k_{\text{rx}} {}^2\tau \quad (3-173)$$

where the lifetime of the doublet state is given by

$${}^2\tau = \frac{1}{({}^2k_{\text{rx}} + {}^2k_{\text{nr}} + {}^2k_{\text{rad}} + {}^2k_{\text{gsq}}[\text{Cr}^{3+}] + {}^2k_{\text{q}}[\text{Q}])} \quad (3-174)$$

For direct excitation into the 4T_2 manifold, the quantum yield for photoaquation is given by

$${}^{4+2}\phi_{\text{rx}} = {}^4\eta_{\text{isc}} {}^2k_{\text{rx}} {}^2\tau \quad (3-175)$$

At this point, the quantum yield of photoaquation from the 4T_2 state,

$^4\phi_{rx}$ is neglected, inasmuch as it accounts for only 3-4% of the total photoaquation quantum yield. Combining equations (3-173) and (3-175),

$$^4\phi_{rx} = \phi_{tot} = 2\phi_{rx} \quad ^4\eta_{isc} \quad (3-176)$$

In order to evaluate $^4\eta_{isc}$ for $Cr(phen)_3^{3+}$ and $Cr(bpy)_3^{3+}$ simultaneously, equation (3-176) may be rewritten in the form of equation (3-177) to

$$\frac{^4\phi_{rx}^P}{^4\phi_{rx}^B} = \frac{\phi_{tot}^P}{\phi_{tot}^B} = \frac{2\phi_{rx}^P \quad ^4\eta_{isc}^P}{2\phi_{rx}^B \quad ^4\eta_{isc}^B} \quad (3-177)$$

compare the $Cr(bpy)_3^{3+}$ (B) and $Cr(phen)_3^{3+}$ (P) systems. In deaerated alkaline solution, $^4\phi_{rx}^P = 0.006$ and $^4\phi_{rx}^B = 0.13$, and $^4\eta_{isc}^B = 1.52$. Thus, the determination of $(\frac{^2\phi_{rx}^P}{^2\phi_{rx}^B})$ under identical photochemical solution medium conditions as those used to evaluate $^4\phi_{rx}^B$ and $^4\phi_{rx}^P$ will afford an estimation of $^4\eta_{isc}^P$.

The experimental procedure used to estimate the value of $^4\eta_{isc}^P$ involved flash photolysis ($\lambda_{max} = 692 \text{ nm}$) equimolar aqueous $Cr(bpy)_3^{3+}$ and $Cr(phen)_3^{3+}$ solutions directly into the ($^2T_1/{}^2E$) manifold, followed by the determination of the concentration of free polypyridine NN released into solution. Under the experimental conditions employed, $[BPY] = 4 \times 10^{-6} \text{ M}$ and $[PHEN] < 3 \times 10^{-7} \text{ M}$ (the limit of detection by the spectrophotometric method used). Furthermore, the quantum yield $^2\phi_{rx}$ may be defined by equation (3-178), where I_a is the incident light intensity and t is the irradiation time.

$${}^2\phi_{rx} = \frac{[NN]}{t} I_a \quad (3-178)$$

Then, for identical concentrations of weakly absorbing $\text{Cr}(\text{bpy})_3^{3+}$ and $\text{Cr}(\text{phen})_3^{3+}$, equations (3-177) and (3-178) combine to yield

$$\frac{{}^{4+2}\phi_{rx}^P}{{}^{4+2}\phi_{rx}^B} = \frac{\phi_{tot}^P}{\phi_{tot}^B} = \frac{[\text{PHEN}]}{[\text{BPY}]} \frac{\epsilon_{\lambda}^B}{\epsilon_{\lambda}^P} \frac{{}^4\eta_{isc}^P}{{}^4\eta_{isc}^B} \quad (3-179)$$

where ϵ_{λ} is the extinction coefficient of $\text{Cr}(\text{NN})_3^{3+}$ at 695 and 727 nm. Inasmuch as the ϵ_{λ} values for $\text{Cr}(\text{phen})_3^{3+}$ at 695 and 727 nm are approximately twice those of $\text{Cr}(\text{bpy})_3^{3+}$,⁸ equation (3-179) yields an estimated value of ${}^4\eta_{isc}^P \approx {}^4\eta_{isc}^B \approx 1$. If ${}^4\eta_{isc}^P$ is taken as ≈ 1 , then $[\text{PHEN}] \approx 4 \times 10^{-7} \text{ M}$; if ${}^4\eta_{isc}^P \approx 0.2$ (as predicted by Bolletta *et al.*,⁵²), then $[\text{PHEN}] \approx 2 \times 10^{-6} \text{ M}$. Since no free PHEN was observed in the photolysed $\text{Cr}(\text{phen})_3^{3+}$ solution, the conclusion that ${}^4\eta_{isc}^B \approx {}^4\eta_{isc}^P \approx 1$ appears valid. This result is consistent with the value of 0.95 suggested by Kane-Maguire and Langford¹²⁴ on oxygen quenching studies of the photo-racemization of optically-active $\text{Cr}(\text{phen})_3^{3+}$. Additionally, the observation that ${}^{4+2}\phi_{rx}^P \approx 0.05 {}^{4+2}\phi_{rx}^B$ is noteworthy, and may be accounted for by the presence of ground-state quenching in 1 M Cl^- media for the $\text{Cr}(\text{phen})_3^{3+}$ complex ion as well as the greater rigidity of the phen vs bpy ligand framework.

3.10.1. Photochemical Evaluation of ${}^4\eta_{isc}$.

The possibility of obtaining an estimation of the efficiency of the ${}^4T_2 \rightsquigarrow ({}^2T_1/{}^2E)$ intersystem crossing process (${}^4\eta_{isc}$) by photochemical means is based on a limiting value of ${}^{4+2}\phi_{rx}$ at high OH^- concentrations. If it is assumed that a seven-coordinate aquo-intermediate is formed via nucleophilic attack of H_2O on the Cr(III) center, followed by deprotonation to give a seven-coordinate hydroxy-intermediate with subsequent reaction with OH^- leading to the observed $Cr(NN)_2(OH)_2^{3+}$ product, then direct attack by OH^- on the Cr(III) center of $({}^2T_1/{}^2E)-Cr(NN)_3^{3+}$ should yield the same seven-coordinate hydroxy-intermediate and final product. Therefore, by defining the quantum yield for photoaquation in terms of the rate constants and efficiencies of processes which deactivate $({}^2T_1/{}^2E)Cr(NN)_3^{3+}$, the efficiency for ${}^4T_2 \rightsquigarrow ({}^2T_1/{}^2E)$ intersystem crossing should be obtained under specified conditions.

The overall quantum yield for photoaquation of $Cr(bpy)_3^{3+}$ is

$${}^{4+2}\phi_{rx} = \frac{{}^4\eta_{isc} \sum k_{rx}'}{\sum k_{obs}} \quad (3-180)$$

where $\sum k_{rx}'$ represents the sum of all the first-order (and pseudo-first-order) rate constants of processes leading to product formation, and $\sum k_{obs}$ is the observed rate constant for the decay of $({}^2T_1/{}^2E)$ under specific experimental conditions.

The values of ${}^{4+2}\phi_{rx}$ for $Cr(bpy)_3^{3+}$ ($1 \times 10^{-3} M$), obtained in argon-purged solutions at $50^\circ C$ for $1.0 \times 10^{-4} M \leq [OH^-] \leq 1.0 M$ ($\mu = 1.0$ with NaCl), are presented in Table 3-30. All ${}^{4+2}\phi_{rx}$ values have been

corrected for any thermal reaction, and are thus attributable to photochemical aquation alone. Under the experimental conditions used, $^{4+2}\phi_{rx}$ includes contributions from ground-state quenching. Therefore, values of 2k_o and $^2k_{gsq}$ (see equation 3-16) were obtained by measuring the observed lifetime of $(^2T_1/^2E)Cr(bpy)_3^{3+}$ as a function of substrate concentration at various $[OH^-]$ and under identical conditions used to determine $^{4+2}\phi_{rx}$. The values of 2k_o and $^2k_{gsq}$ are collected in Table 3-30. Employing these 2k_o and $^2k_{gsq}$ values, $^2k_{obs}$ may be calculated from equation (3-16); these are included in Table 3-30.

Assuming that $^4\eta_{isc} \approx 1$, values of $^2k_{rx}'$ may be calculated from equation (3-180) and the experimentally-determined values of $^{4+2}\phi_{rx}$ and $^2k_{obs}$; $^2k_{rx}'$ values are included in Table 3-31. If it is assumed that $^2k_{rx}'$ is defined by equation (3-181), where $^2k_{rx}^{H_2O}$ represents the

$$^2k_{rx}' = ^2k_{rx}^{H_2O} + ^2k_{rx}^{OH^-} [OH^-] \quad (3-181)$$

nucleophilic attack on $(^2T_1/^2E)Cr(bpy)_3^{3+}$ to form the seven-coordinate aquo-intermediate at $[OH^-] \leq 0.10 \text{ M}$. At $[OH^-] \geq 0.10 \text{ M}$, $^2k_{rx}'$ must reflect, at a minimum, $^2k_{rx}^{H_2O} + ^2k_{rx}^{OH^-} [OH^-]$. This assumes that $(^2T_1/^2E)-Cr(bpy)_3^{3+}$ reacts with H_2O to form $Cr(bpy)_3(H_2O)^{3+}$ and directly with OH^- to form $Cr(bpy)_3(OH)^{2+}$. The value of $^2k_{rx}^{OH^-}$ can be obtained from the slope of a plot (shown in Figure 3-38) of 2k_o vs $[OH^-]$, where $[OH^-]$ ranges from 0.10 - 1.0 M; $^2k_{rx}^{OH^-} = 4.5 \times 10^3 \text{ M}^{-1} \text{ sec}^{-1}$. The contribution from $(^2T_1/^2E)Cr(bpy)_3^{3+} \rightarrow Cr(bpy)_3(OH)^{2+}$ is then $^2k_{rx}^{OH^-} [OH^-]$, the values of which are tabulated in Table 3-31. Values of $^2k_{rx}^{H_2O}$ can then be calculated from equation (3-182).

TABLE 3-30 : Rate Constants for the Intrinsic Decay, Ground-state quenching and Observed

Decay of $(^2T_1/{}^2E)Cr(bpy)_3^{3+}$ at 5°C as a Function of $[OH^-]$.

$[OH^-]$ (M)	$4 \rightarrow 2 \phi_{rx}$	${}^2k_o \times 10^{-3}$ (sec $^{-1}$)	${}^2k_{gsq} \times 10^{-6}$ (M $^{-1}$ sec $^{-1}$)	${}^2k_{obs} \times 10^{-4} a$ (sec $^{-1}$)
1.0×10^{-4}	--	6.1	1.0	0.71
1.0×10^{-3}	0.079	5.9	2.8	0.87
1.0×10^{-2}	0.078	6.2	3.2	0.95
0.10	0.096	6.2	3.8	1.0
0.30	0.122	7.45	3.4	1.1
0.50	0.251	8.1	4.4	1.25
0.70	0.410	9.9	5.0	1.49
1.00	0.661	10.2	6.4	1.66

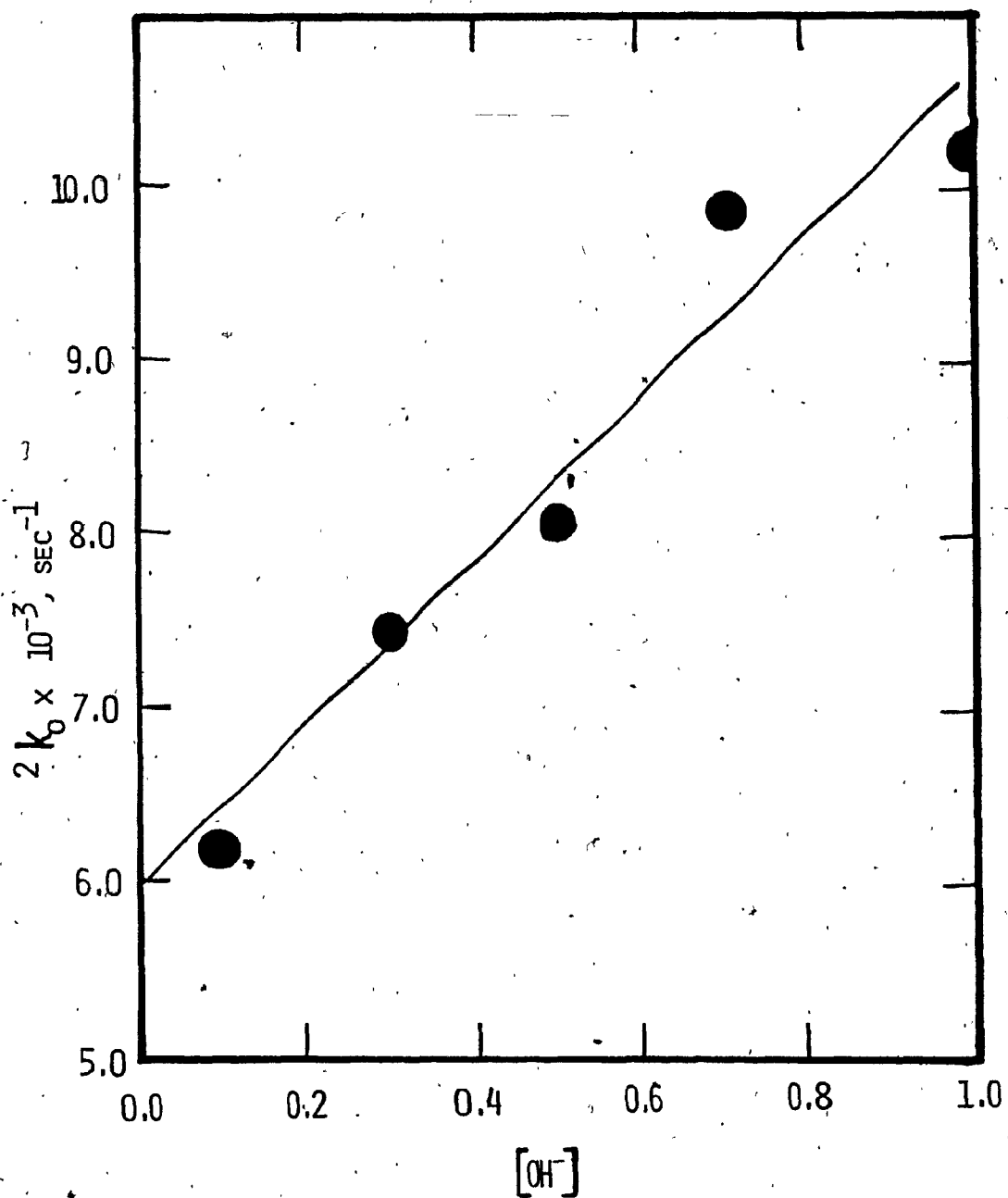
a Calculated from ${}^2k_{obs} = {}^2k_o + {}^2k_{gsq} [Cr(bpy)_3^{3+}]$, using $[Cr(bpy)_3^{3+}] = 1.0 \times 10^{-3}$ M.

TABLE 3-31: Values of $2k_{rx}^{OH^-}$, $2k_{rx}^{H_2O}$ for Cr(bpy)₃³⁺ at 5°C.

[OH ⁻] (M)	$2k_{rx}^{OH^-} \times 10^{-3}$ ^a (sec ⁻¹)	$2k_{rx}^{H_2O}$ [OH ⁻] $\times 10^{-3}$ ^b (sec ⁻¹)	$2k_{rx}^{H_2O}$ ^c (sec ⁻¹)
1.0×10^{-4}			
1.0×10^{-3}	0.687	0	6.87×10^2
1.0×10^{-2}	0.741	0	7.41×10^2
0.10	0.960	0.466	4.94×10^2
0.30	1.34	1.40	0
0.50	3.14	2.33	8.08×10^2
0.70	6.11	3.26	2.85×10^3
1.00	10.97	4.66	6.31×10^3

^a Calculated from equation (3-180). ^b Calculated using the slope of the plot in Figure 3-38 and the [OH⁻] values. ^c Calculated from equation (3-182).

FIGURE 3-38 : Plot of $2k_0$ vs $[\text{OH}^-]$ in the Range 0.10 - 1.00 M OH^- for $\text{Cr}(\text{bpy})_3^{3+}$ at 5°C .



$${}^2k_{rx}^{H_2O} = {}^2k_{rx}' - {}^2k_{rx}^{OH^-} [OH^-] \quad (3-182)$$

From Table 3-31, ${}^2k_{rx}^{H_2O}$ appears to decrease for $10^{-4} \text{ M} \leq [OH^-] \leq 0.3 \text{ M}$, and increase for $0.30 \text{ M} \leq [OH^-] \leq 1.0 \text{ M}$. The decrease in ${}^2k_{rx}^{H_2O}$ may be rationalized in terms of the Cr(III) center being preferentially solvated by OH^- as compared to H_2O ; as $0.30 \text{ M } OH^-$ is approached, there will be very few H_2O molecules around the Cr(III) core.

It seems unlikely that ${}^2k_{rx}^{H_2O}$ will actually increase for $[OH^-] > 0.30 \text{ M}$. If ${}^2k_{rx}^{OH^-} [OH^-]$ represents direct attack of OH^- on the (${}^2T_1/{}^2E$) species, then there must be some additional source of product. One might consider ground-state quenching as this product source; then ion-pairing between $Cr(bpy)_3^{3+}$ and Cl^- occurs as well as that between $Cr(bpy)_3^{3+}$ and OH^- . As $[OH^-]$ increases, ion-pair formation between $Cr(bpy)_3^{3+}$ and OH^- will predominate such that at $[OH^-] = 1.0 \text{ M}$ (where Cl^- is absent), only these ion-paired species will be present. Therefore, at $[OH^-] > 0.30 \text{ M}$,

$${}^2k_{gsq}' [Cr^{3+}] = {}^2k_{rx}' - {}^2k_{rx}^{OH^-} [OH^-] \quad (3-183)$$

where ${}^2k_{gsq}' [Cr^{3+}]$ is that part of the total ground-state quenching process that leads to product formation. It is known that Cl^- -mediated ground-state quenching does not yield product at low $[OH^-]$. Values of ${}^2k_{gsq}' [Cr^{3+}]$ are collected in Table 3-32 using values of ${}^2k_{rx}'$ and ${}^2k_{rx}^{OH^-} [OH^-]$ from Table 3-31, and $[Cr^{3+}] = 1.0 \times 10^{-3} \text{ M}$. Subsequently, the fraction F_{gsq} of ground-state quenching that is effective in yielding product can be calculated (see Table 3-32). Note that at $[OH^-] = 1.0 \text{ M}$,

TABLE 3-32 : Calculated values of $^2k_{\text{gsq}}$, F_{gsq} , F_{OH}^{-2} and $^2k_{\text{nr}}$ for Cr(bpy) $_3^{3+}$ at 5°C.

[OH ⁻] (M)	$^2k_{\text{gsq}}$, Cr $^{3+}$ a (sec ⁻¹)	F_{gsq} b	F_{OH}^{-2} c	$^2k_{\text{nr}} \times 10^{-3}$ c (sec ⁻¹)
1.0×10^{-4}				
1.0×10^{-3}	0	0	0	5.21
1.0×10^{-2}	0	0	0	5.56
0.10	0	0	0.01	5.24
0.30	0	0	0.09	6.20
0.50	8.08×10^2	0.184	0.25	5.77
0.70	2.85×10^3	-0.569	0.49	6.64
1.00	6.31×10^3	0.986	1.00	5.54
				ave (5.7 ± 0.5)

a $^2k_{\text{gsq}}[\text{Cr}^{3+}] = ^2k_{\text{rx}} - ^2k_{\text{rx}}[\text{OH}^-]$; b $F_{\text{gsq}} = ^2k_{\text{gsq}}$, where $^2k_{\text{gsq}}$ was obtained from Table 3-30 and $[\text{Cr}^{3+}] = 1.0 \times 10^{-3}$ M. c $^2k_{\text{nr}}$ was calculated from $^2k_{\text{nr}} = ^2k_{\text{obs}} - ^2k_{\text{rx}}[\text{OH}^-] - ^2k_{\text{gsq}}[\text{Cr}^{3+}] - ^2k_{\text{rx}}$.

$F_{\text{gsq}} \sim 0.99$, virtually all ground-state quenching leads to product formation. A comparison of the fraction of ground-state quenching with the fraction of OH^- present in solution can be made by plotting F_{gsq} vs $[\text{OH}^-]$ and $[\text{OH}^-]$ vs $[\text{OH}^-]$, as in Figure 3-39; the fraction F_{gsq} does not follow the fraction OH^- present. At low $[\text{OH}^-]$, there does not appear to be any ground-state quenching that gives product; however, at 1 M $[\text{OH}^-]$, all ground-state quenching leads to product formation.

If one assumes that both OH^- and Cl^- will ion-pair with 1×10^{-3} M $(^4\text{A}_2)\text{Cr}(\text{bpy})_3^{3+}$ and $(^2\text{T}_1/^2\text{E})\text{Cr}(\text{bpy})_3^{3+}$ to approximately the same extent, then all $(^4\text{A}_2)$ and $(^2\text{T}_1/^2\text{E})$ species will be ion-paired. Furthermore, the fraction of these molecules which are ion-paired by OH^- probably approximates the fraction of OH^- ion present in solution. If it is assumed that F_{OH^-} is the fraction of $\text{Cr}(\text{bpy})_3^{3+}$ molecules ion-paired with OH^- and equal to $[\text{OH}^-]$, then $F_{\text{OH}^-} = 1$ at 1.0 M $[\text{OH}^-]$ and $F_{\text{OH}^-} = 0$ at $[\text{OH}^-] \leq 0.1$ M. If effective ground-state quenching giving product formation necessitates an $\text{OH}^- - \text{OH}^-$ interaction of $(^4\text{A}_2)\text{Cr}(\text{bpy})_3^{3+}$ and $(^2\text{T}_1/^2\text{E})\text{Cr}(\text{bpy})_3^{3+}$, then a fraction F_{gsq} of the ground-state quenching that is effective in yielding products must equal $F_{\text{OH}^-}^2$ since the probability that $\text{OH}^- - \text{OH}^-$ ion-pairing will occur is related to $[\text{OH}^- \text{ ion-pair}]^2$. Plots of F_{gsq} vs $[\text{OH}^-]$ and $F_{\text{OH}^-}^2$ (see Figure 3-40) show reasonable agreement; the trend of $F_{\text{OH}^-}^2$ follows that of F_{gsq} .

Inasmuch as $^2k_{\text{obs}} = ^2k_{\text{rx}}^{\text{OH}^-} [\text{OH}^-] + ^2k_{\text{gsq}} [\text{Cr}^{3+}] + ^2k_{\text{rx}}^{\text{H}_2\text{O}} + ^2k_{\text{nr}}$, one can calculate all the rate constants on the basis of the above assumptions; values of $^2k_{\text{nr}}$ are presented in Table 3-32. It would seem that deviations in $^2k_{\text{nr}}$ are negligible, $^2k_{\text{nr}}(\text{ave}) = (5.7 \pm 0.5) \times 10^3 \text{ sec}^{-1}$. $^2k_{\text{nr}}$ is not expected to change very much in the medium used in these experiments.

FIGURE 3-39 : Plots of F_{gsq} vs $[\text{OH}^-]$, (\blacktriangle), and $[\text{OH}^-]$ vs $[\text{OH}^-]$, (\blacksquare), in the Range 0.10 - 1.00 M OH^- for $\text{Cr}(\text{bpy})_3^{3+}$ at 5°C .

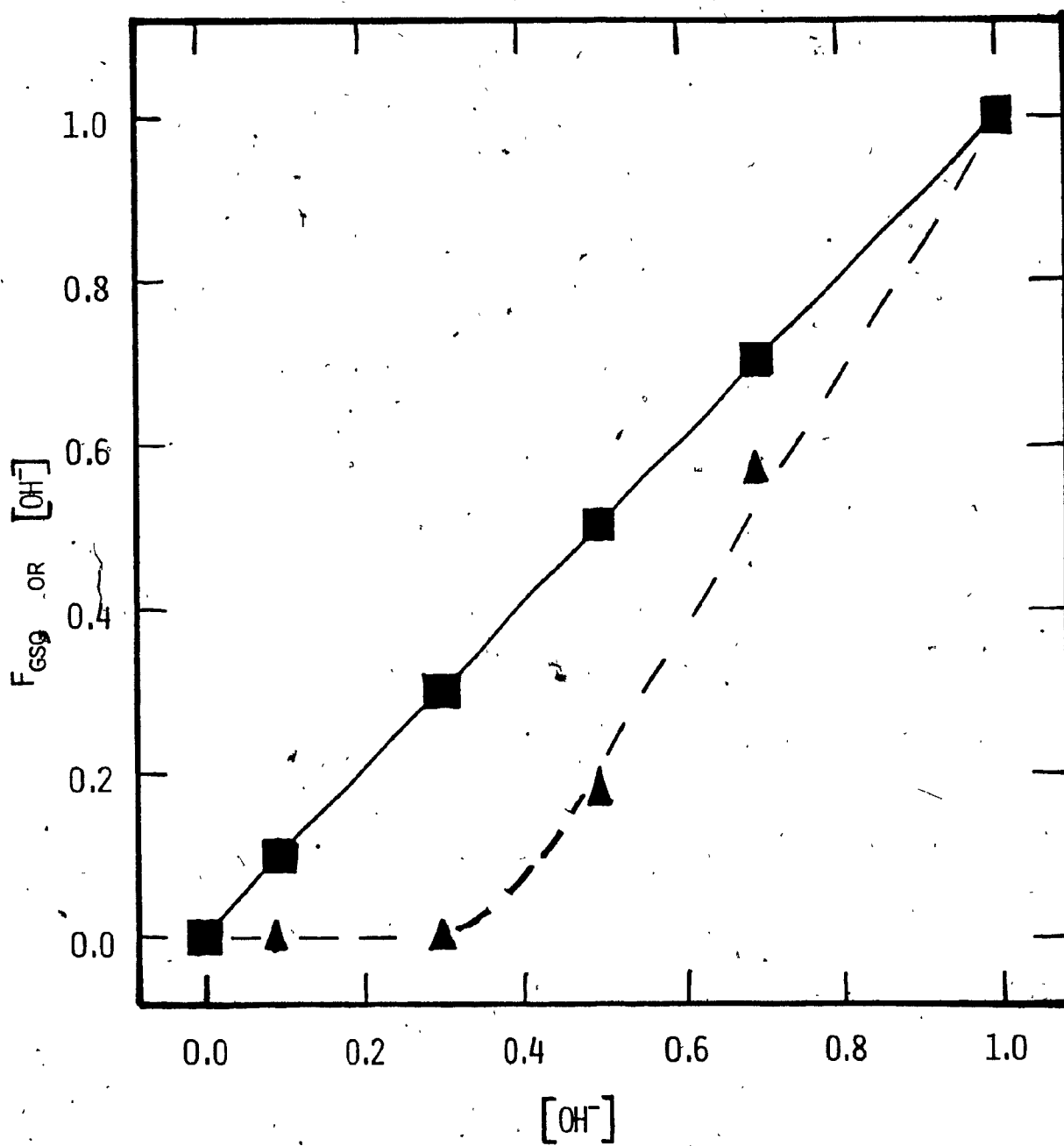
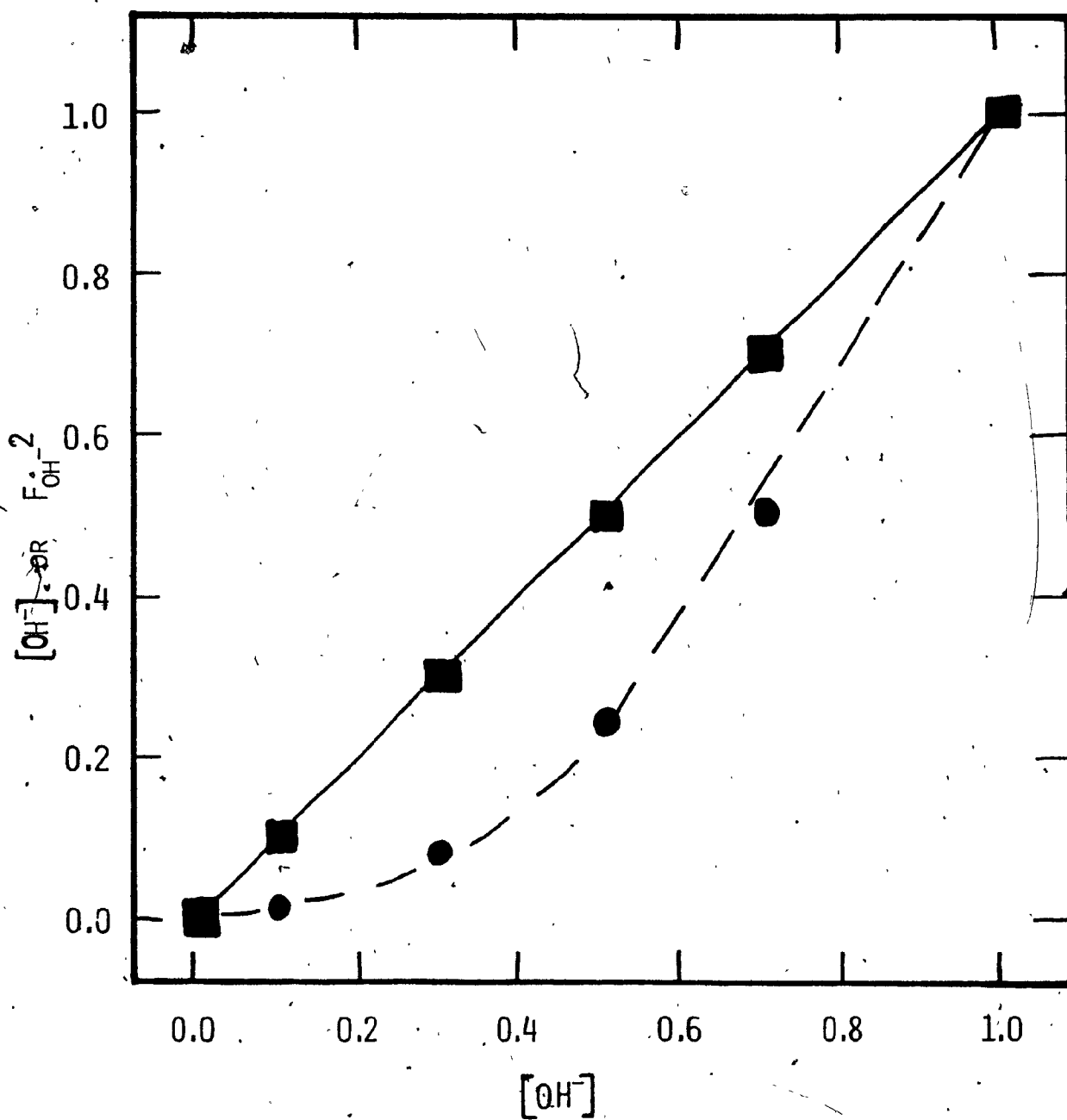


FIGURE 3-40 : Plots of $[\text{OH}^-]$ vs $[\text{OH}^-]$, (\blacksquare), and $F_{\text{OH}^-}^{-2}$ vs $[\text{OH}^-]$, (\bullet), for $\text{Cr}(\text{bpy})_3^{3+}$ at 5°C in the Range $0.10 - 1.00 \text{ M OH}^-$.



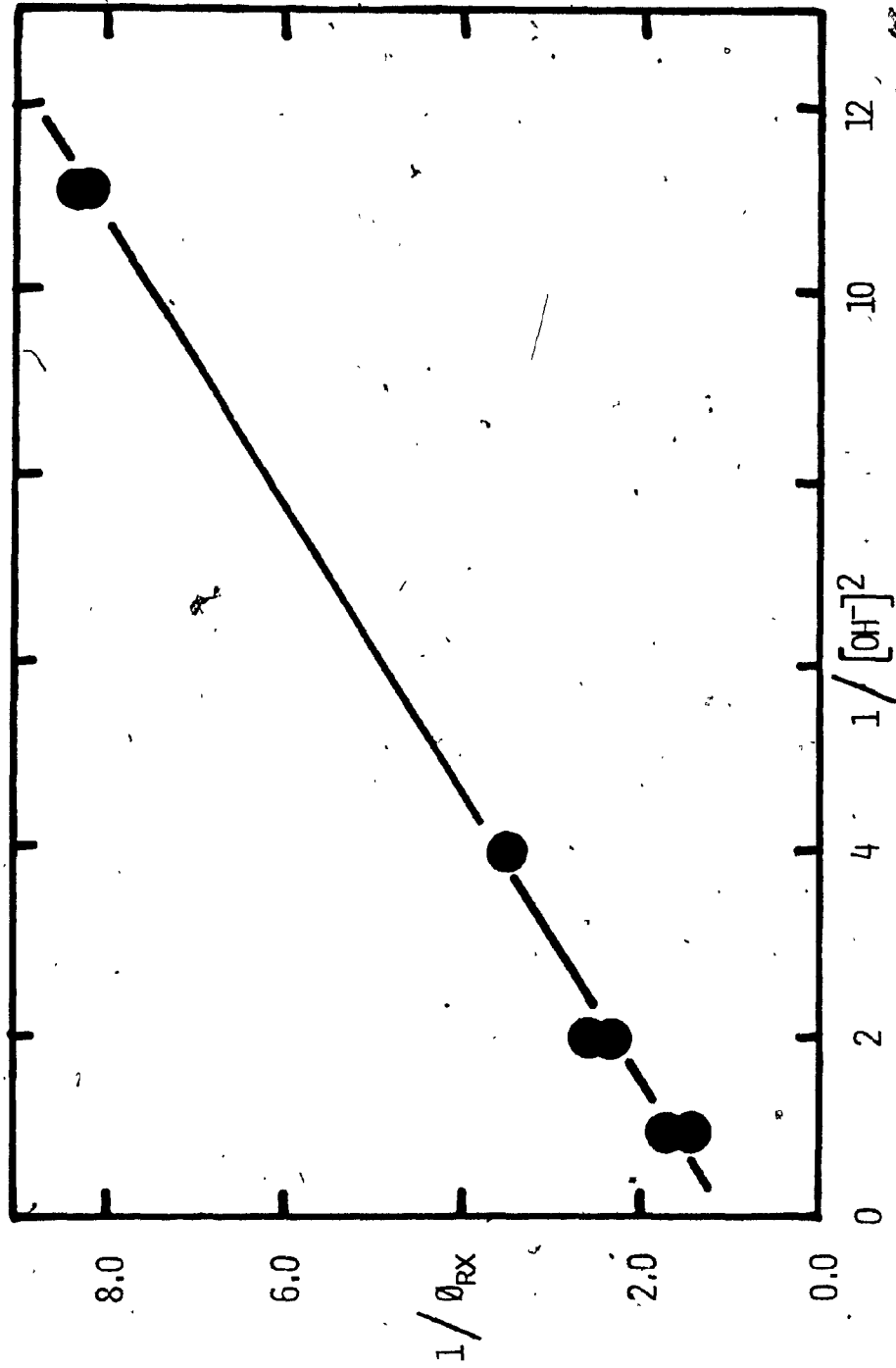
Returning to the dependence of ${}^{4+2}\phi_{RX}$ on $[OH^-]$, ${}^{4+2}\phi_{RX}$ is defined

$${}^{4+2}\phi_{RX} = \frac{{}^2k_{RX}^{H_2O} + {}^2k_{RX}^{OH^-} [OH^-] + {}^2k_{gsq} [Cr^{3+}] F_{OH^-}^{-2}}{{}^2k_{obs}} \quad (3-184)$$

When $F_{OH^-}^{-2} \leq 0.1$, the ground-state quenching term in equation (3-184) is not significant and ${}^{4+2}\phi_{RX}$ is some function of $[OH^-]$. When $F_{OH^-}^{-2} > 0.1$, the ground-state quenching term becomes important, and the relationship between ${}^{4+2}\phi_{RX}$ and $[OH^-]$ becomes quadratic in the limit of $[OH^-] = 1.0$.

A plot of $1/{}^{4+2}\phi_{RX}$ vs $1/[OH^-]^2$ is illustrated in Figure 3-41 for $0.3 \text{ M} \leq [OH^-] \leq 1.0 \text{ M}$. The plot is linear, and must have a slope = 1 since it was assumed in the previous analyses that ${}^4\eta_{isc} = 1$. The slope of the plot = 1.09. This plot suggests, though does not prove, the value of ${}^4\eta_{isc} \approx 1$ from the experimental results obtained. However, ${}^4\eta_{isc}$ is probably very close to 1. The data do indicate that direct attack by OH^- on $({}^2T_1/{}^2E)Cr(bpy)_3^{3+}$ yields a seven-coordinate intermediate which subsequently gives rise to quantitative formation of products. Furthermore, the data show that ground-state quenching is the predominant source of product formation at high OH^- concentrations.

FIGURE 3-41 : Plot of $1/4+2\phi_{IX}$ vs $1/[\text{OH}^-]^2$ in the Range 0.30 -
1.00 M OH^- for $\text{Cr}(\text{bpy})_3^{3+}$ at 5°C .



3.11. WAVELENGTH DEPENDENCE OF $^{4+2} \phi_{rx}$, $^4 \phi_{rx}$ AND I' FOR $Cr(bpy)_3^{3+}$.

The photoaquation reaction of $Cr(bpy)_3^{3+}$ in basic aqueous media to yield $Cr(bpy)_2(OH)_2^+$ is one of the few Cr(III) complexes for which direct reaction from ($^2T_1/{}^2E$) is postulated for the quenchable component of the reaction. Furthermore, the unquenchable component of the reaction is believed to originate from quartet excited states, and the intersystem crossing ($^4T_2 \rightsquigarrow ^2T_1/{}^2E$) yield of ca. unity for excitation at 313 nm. In light of these observations and postulations, and the recent report by Langford and Sasseville¹²⁴ which hints at a wavelength-dependent quantum yield for reaction and phosphorescence yields of $Cr(bpy)_3^{3+}$, we have undertaken a detailed investigation of this system in an effort to elucidate the roles of the 4T_2 and 2E excited states. Wavelength dependencies for reaction and phosphorescence yields of Cr(III) complexes have been cited for $Cr(en)_3^{3+}$,³⁶ $Cr(NH_3)_6^{3+}$,¹²⁵ trans- $Cr(en)_2(NCS)(F)^+$,¹²⁶ and trans- $Cr(en)_2(NCS)_2^+$.¹²⁰

The wavelength dependence of the total photoaquation quantum yield (ϕ_{rx}^{tot}), the unquenchable photoaquation quantum yield ($^4 \phi_{rx}$), and the phosphorescence intensity (I') of $Cr(bpy)_3^{3+}$ have been studied in air-equilibrated aqueous solution (pH 9.6, $\mu = 1.0 \text{ M NaCl}$) at 22°C. $^4 \phi_{rx}$ was measured in the presence of $0.15 \text{ M } I^-$, such that more than 99.9% of the reaction from the ($^2T_1/{}^2E$) manifold was quenched. The data for ϕ_{rx}^{tot} , $^4 \phi_{rx}$ and I' are tabulated in Table 3-33, and Figures 3-42 and 3-43 reveal the wavelength dependence of these data. One notes the sharp decrease in both ϕ_{rx}^{tot} and $^4 \phi_{rx}$ in the excitation wavelength region 470 - 510 nm; also, the ($^2T_1/{}^2E$) phosphorescence intensity I' varies in a similar manner under identical experimental conditions, as revealed in Figure 3-43.

The phosphorescence intensity I' is directly proportional to the

FIGURE 3-42 : Plots of $^4\phi_{rx}$ and I' vs Excitation Wavelength for $Cr(bpy)_3^{3+}$ at pH 9.6 and 22°C in Air-equilibrated Solutions.

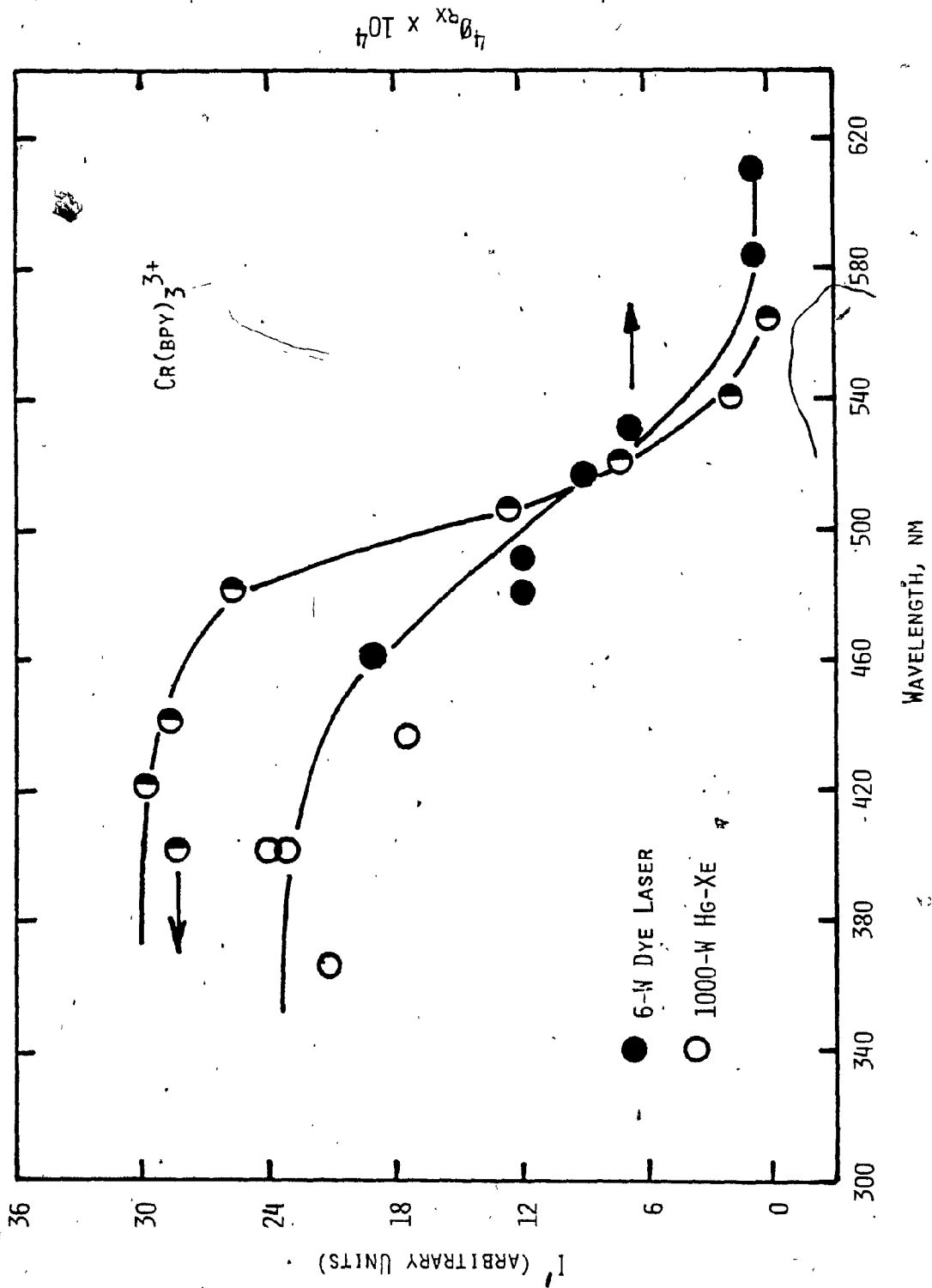


FIGURE 3-43 : Plot of ϕ_{rx}^{tot} vs Excitation Wavelength for $\text{Cr}(\text{bpy})_3^{3+}$
at pH 9.6 and 22°C in Air-equilibrated Solutions.

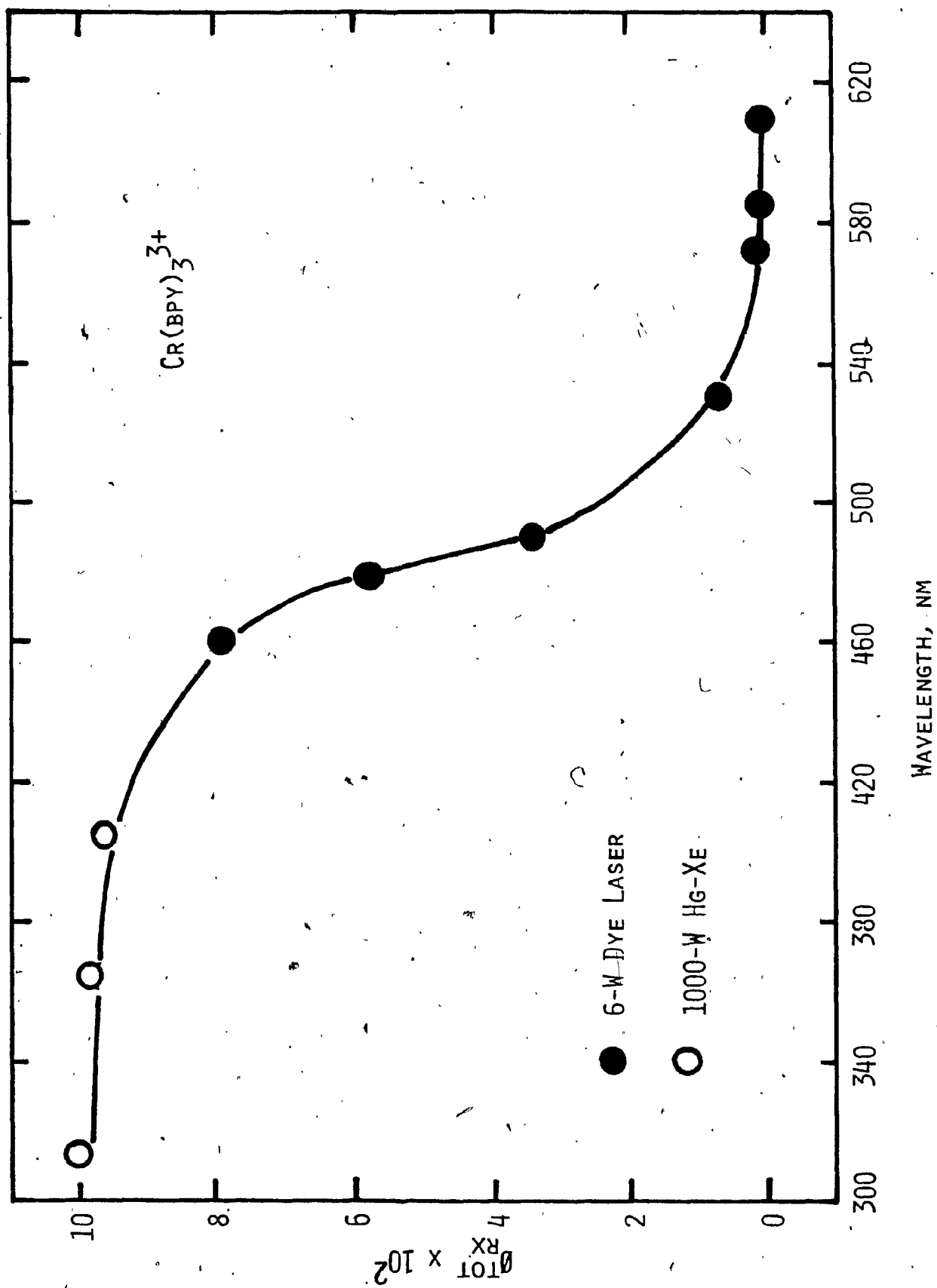


TABLE 3-33 : Photoaquation Quantum Yields in the Absence and Presence of Iodide Ion and Phosphorescence Intensities of $\text{Cr}(\text{bpy})_3^{3+}$ as a Function of Excitation Wavelength in Air-equilibrated Solutions at pH ~ 9.5 and 22°C .

λ , nm	${}^{4+2}\phi_{\text{rx}}^{\text{a}}$	${}^4\phi_{\text{rx}}^{\text{b}}$	I^{c}
313	0.10	--	--
365	0.094	0.0021	--
400	--	0.0023	28.4
420	--	--	29.6
440	--	--	28.7
458	0.079	0.0019	--
460	--	--	34.8
477	0.058 ^a	0.0012	--
480	--	--	25.7
488	0.034	0.0012	--
505	--	--	13.0
514	--	0.0009	--
520	--	--	7.3 ₆
529	0.007	0.0007	--
540	--	--	2.1 ₄
565	--	--	0.3
573	0.0006	--	--
584	0.0003	0.0001	--
611	0.0003	0.0001	--

^a Estimated error 15-20%. ^b Estimated error 15-20%.

^c Estimated error 10%.

phosphorescence yield from (${}^2T_1/{}^2E$), so that as I' decreases there is a concomitant decrease in the phosphorescence yield, ${}^2\phi_{\text{rad}}$. The data obtained have been normalized to reveal the coincidence of the wavelength dependence, and are depicted in Figure 3-44. A comparison of the absorption spectrum of $\text{Cr}(\text{bpy})_3^{3+}$ with the variation in $\phi_{\text{rx}}^{\text{tot}}$, ${}^4\phi_{\text{rx}}$ and I' (Figure 3-44) reveals the experimentally-measured reaction and phosphorescence yields begin to decrease in the low-energy tail of the first quartet-quartet absorption band. Previous observations of this nature have been attributed to the wavelength dependence of the (${}^4T_2 \rightsquigarrow {}^2E$) intersystem crossing efficiency, ${}^4\eta_{\text{isc}}$, such that at lower levels of vibrational excitation, the 4T_2 state is unable to efficiently come into resonance with vibronic components of the 2E manifold.³⁴

An energy-level diagram is illustrated in Figure 3-45 which depicts energy level against distortion; this can be used to rationalize the wavelength dependence of the $\text{Cr}(\text{bpy})_3^{3+}$ system. Absorption of light yields a Franck-Condon excited state, ${}^4\text{FC}$; the molecule is in a vibronic state corresponding to a vibrationally-excited level of a particular electronic state. In solution, the excess vibrational energy is rapidly dissipated to the surroundings via collision with solvent molecules, leading to vibrational relaxation, ${}^4k_{\text{ic}}$. At normal temperatures, vibrational relaxation occurs in about $10^{11} - 10^{13} \text{ sec}^{-1}$, depending on the amount of excess energy that must be dissipated. The thermally-equilibrated (or "thexi") state, ${}^4T_2^0$, is lower in energy and distorted inasmuch as the bond length and bond angle change relative to the 4A_2 ground-state geometry. During the equilibration process, prompt intersystem crossing, ${}^4k_{\text{pisc}}$, to the (${}^2T_1/{}^2E$) manifold may occur; alternatively, quartet-doublet intersystem crossing may proceed from ${}^4T_2^0$ to (${}^2T_1/{}^2E$), ${}^4k_{\text{isc}}$. (${}^2T_1/{}^2E$) may undergo back-

FIGURE 3-44 : Normalized Plots of $^4\phi_{rx}$, ϕ_{rx}^{tot} and $^2\phi_p^{rel}$ vs. Excitation Wavelength for $Cr(bpy)_3^{3+}$ at pH 9.6 and 22°C in Air-equilibrated Solutions.

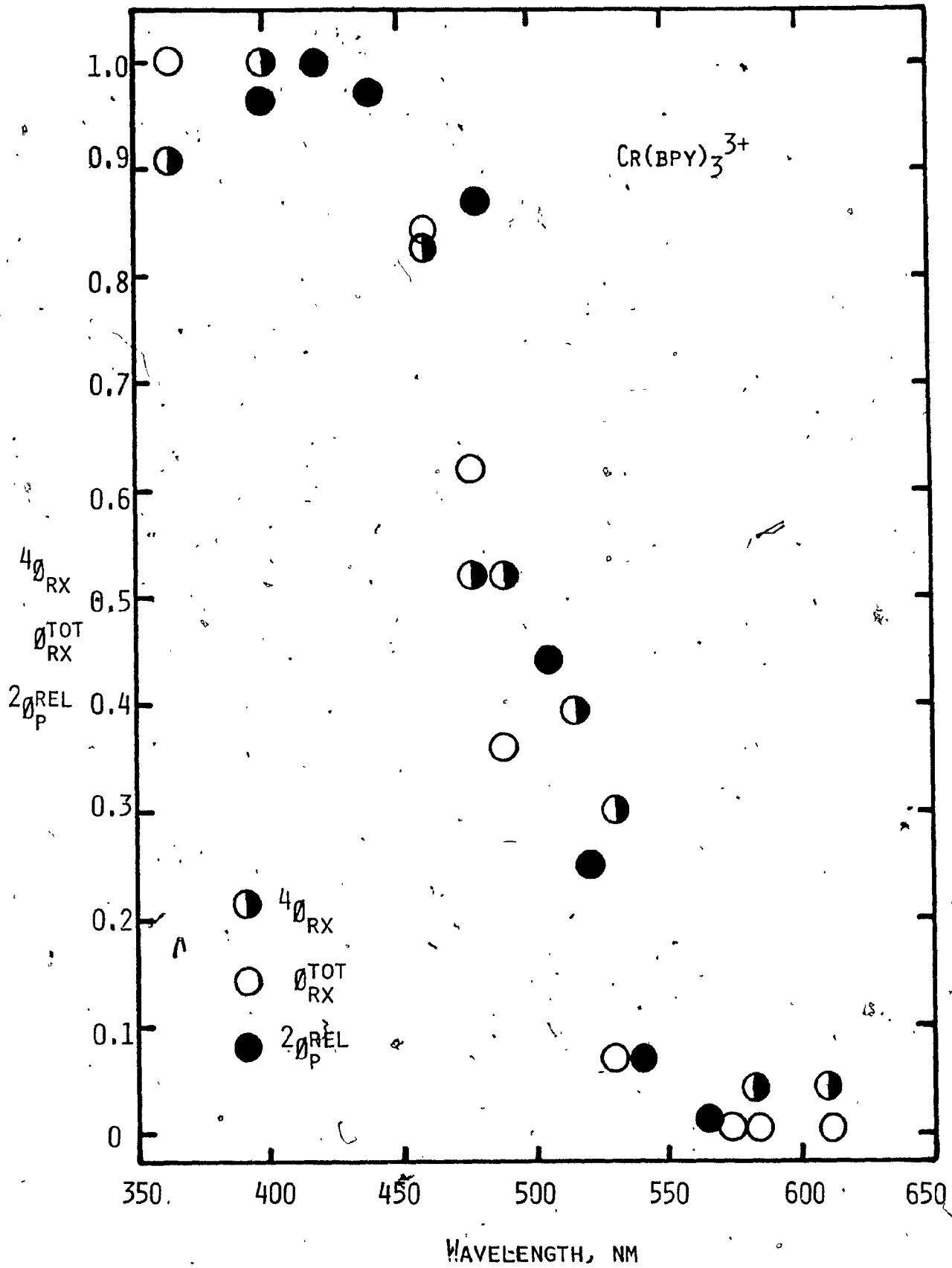
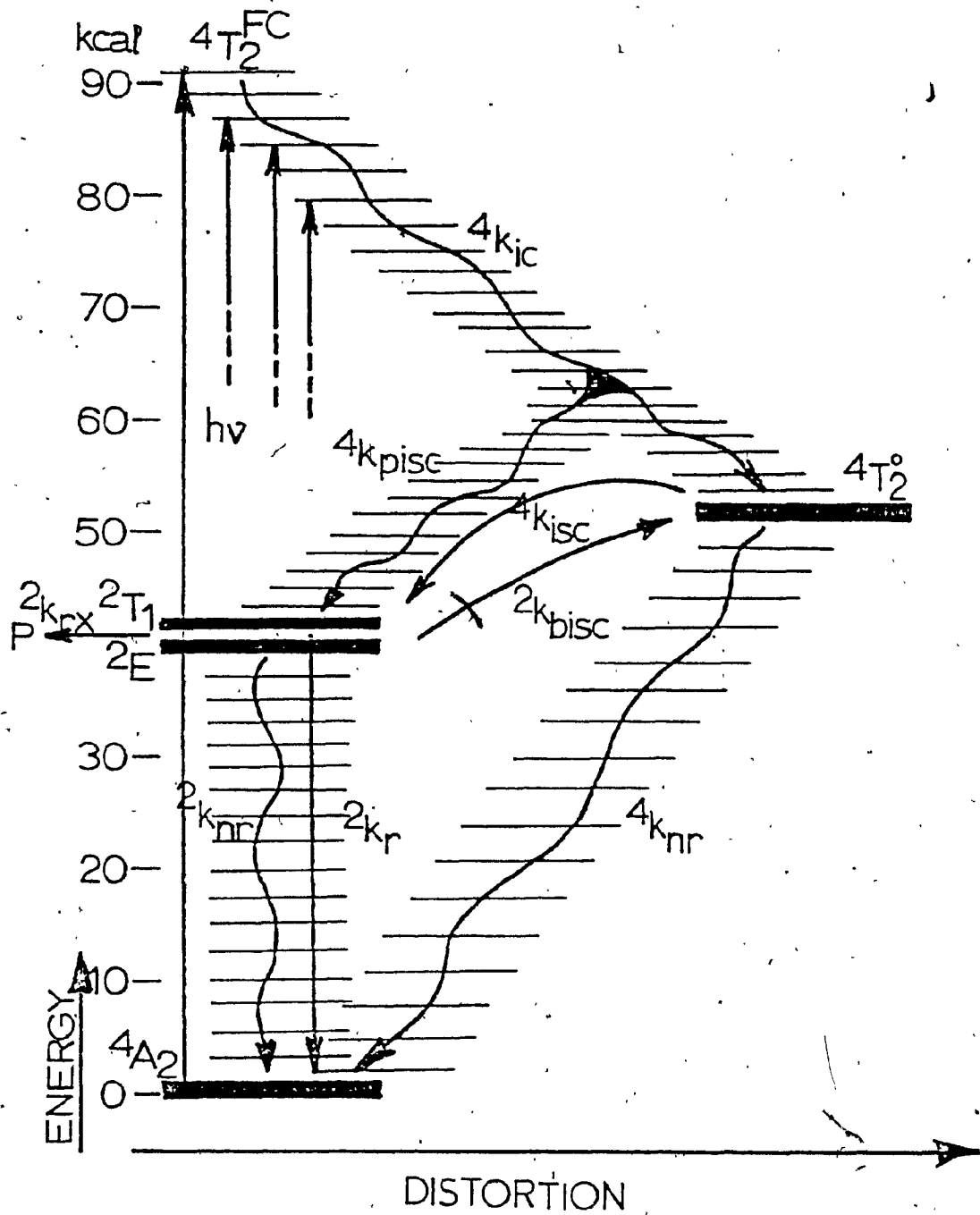


FIGURE 3-45 : Simplified Energy-level Diagram for the Wavelength
Dependence of the Photoaquation of $\text{Cr}(\text{bpy})_3^{3+}$ at
pH 9.6 and 22°C in Air-equilibrated Solutions.



intersystem crossing, $^2k_{\text{bisc}}$, to $^4T_2^0$; chemical reaction is then expected from $^4T_2^0$. If there is no back-intersystem crossing, then chemical reaction occurs from $(^2T_1/{}^2E)$.

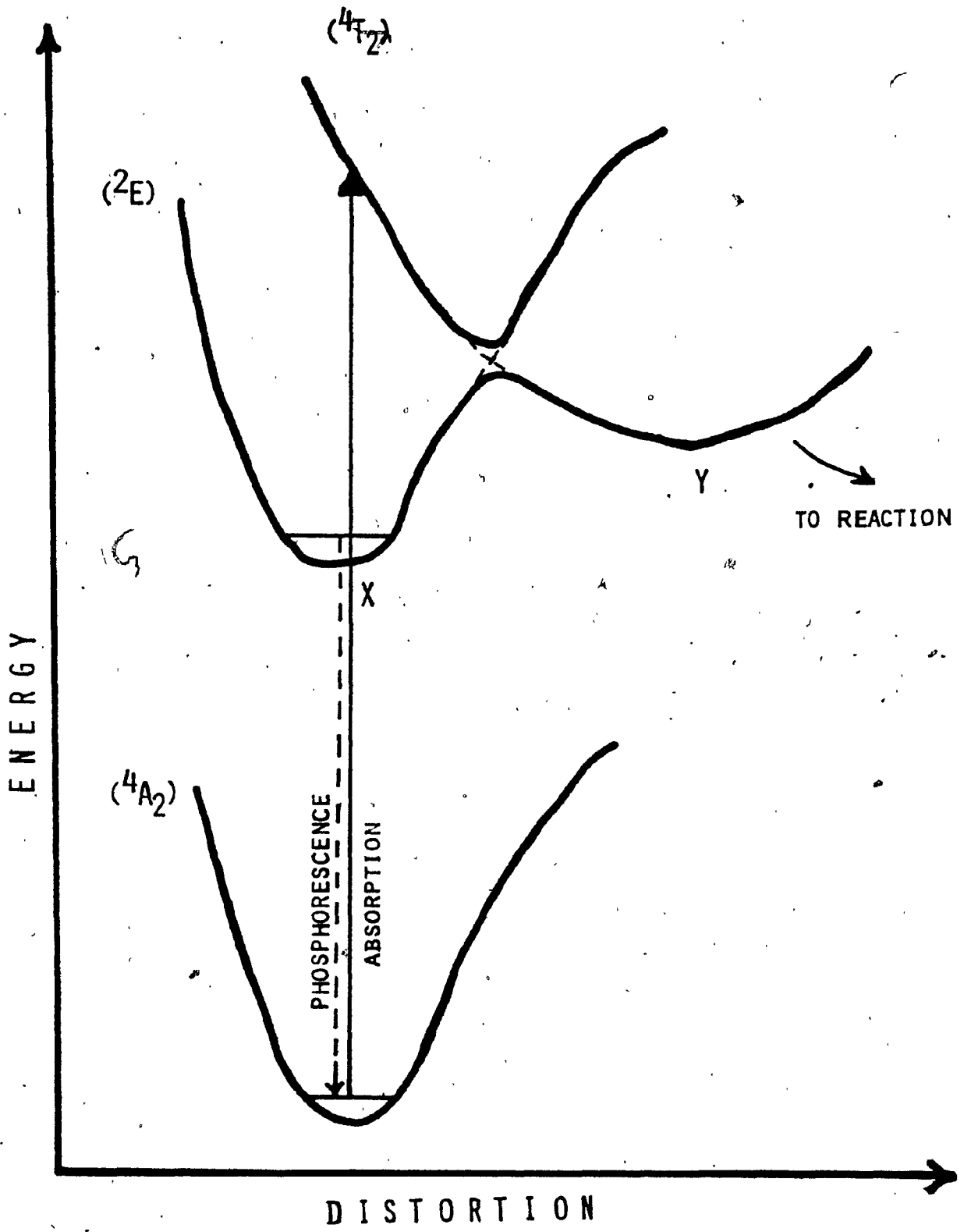
Depending on the amount of excess vibrational energy available, $^4k_{\text{ic}}$ will vary; the greater the available energy, the faster the relaxation process will be. As the amount of energy becomes less, $^4k_{\text{ic}}$ may decrease sufficiently, such that other processes (e.g., prompt intersystem crossing or prompt reaction from the quartet) may compete with the relaxation process. Thus, as the excitation energy decreases (excitation wavelength increases), these other processes may become competitive with $^4k_{\text{ic}}$. It has been proposed¹²⁷ that the reactive excited states are those which are thermally-equilibrated; that is, the $^4T_2^0$ and the 2E states.

For the $\text{Cr}(\text{bpy})_3^{3+}$ system, the spectroscopic energies of the 4T_2 , 4T_1 and $(^2T_1/{}^2E)$ electronic states are known; however, the energy of the $^4T_2^0$ state remains unknown. Further, the quartet excited states are expected to be severely distorted relative to the 4A_2 ground state inasmuch as the electron configurations are $t_{2g}^2 e_g^1$ and t_{2g}^3 , respectively. The $(^2T_1/{}^2E)$ states are not expected to be distorted since they belong to the t_{2g}^3 configuration, and there is no Stokes shift observed between the ${}^4A_2 \longleftrightarrow (^2T_1/{}^2E)$ absorption and emission maxima. This distortion is revealed in Figure 3-45. Keeping previous mechanistic evaluations in mind, it is quite apparent that there is no simple, straight-forward explanation for the observed wavelength dependence; the behavior cannot be attributed solely to prompt 4T_2 reaction, to ${}^4T_2^0$ reaction subsequent to back-intersystem crossing from 2E , nor to direct reaction from ${}^4T_2^0$.

Some analogies between the results obtained herein for $\text{Cr}(\text{bpy})_3^{3+}$ and those for trans- $\text{Cr}(\text{en})_2(\text{NCS})^+$ can be drawn. Sandrini and coworkers¹²⁰

have shown that for $\text{Cr(en)}_2(\text{NCS})_2^+$ the quantum yield for NCS^- release, ϕ_{NCS^-} , and the quantum yield for proton uptake, ϕ_{H^+} , remain constant for excitation in the wavelength range 365 - 560 nm; however, the relative phosphorescence quantum yield, $\phi_{\text{p}}^{\text{rel}}$, remains constant in the 330 - 450 nm region and then decreases somewhat in the low-energy side of the lowest quartet-quartet absorption band ($\lambda_{\text{max}} = 487 \text{ nm}$). Similar phosphorescence quantum yield behavior has been observed for Cr(en)_3^{3+} and $\text{Cr}(\text{NH}_3)_6^{3+}$.^{36,125} Furthermore, there exists an unquenchable component of each photoreaction for $\text{Cr(en)}_2(\text{NCS})_2^+$ which necessarily must originate via direct reaction from $^4\text{T}_2$. The quenchable reaction component of the photoreaction has two possible fates: i) direct reaction from ^2E , or ii) delayed reaction from $^4\text{T}_2$ after passing through the ^2E manifold. Whereas the ratio for the two photoreactions, $\phi_{\text{NCS}^-} / \phi_{\text{H}^+}$, is the same for both the quenchable and unquenchable reaction components, it was suggested¹²⁰ that both the quenchable and unquenchable reactions originate from the $^4\text{T}_2$ state, via prompt and delayed reactions, respectively. Thus, back-intersystem crossing ($^2\text{E} \rightsquigarrow ^4\text{T}_2$) must be an important decay process of the ^2E state of this complex ion. We have previously noted that the back-intersystem crossing process, $^2k_{\text{bisc}}$, is thought to be unimportant for $\text{Cr}(\text{bpy})_3^{3+}$. The results obtained for the $\text{Cr(en)}_2(\text{NCS})_2^+$ system were interpreted¹²⁰ on the basis of interaction between the $^4\text{T}_2$ and ^2E states, both states having a common component when complete (spin + orbital) wave functions are considered. This leads to an "avoided crossing" situation, in which two energy minima exist. Figure 3-46 illustrates this situation for which X and Y denote the two minima. At excitation energies greater than the "mixing region" (e.g., to point P in Figure 3-46), the excited-state molecule can relax to either the X or Y minimum; whereas, for

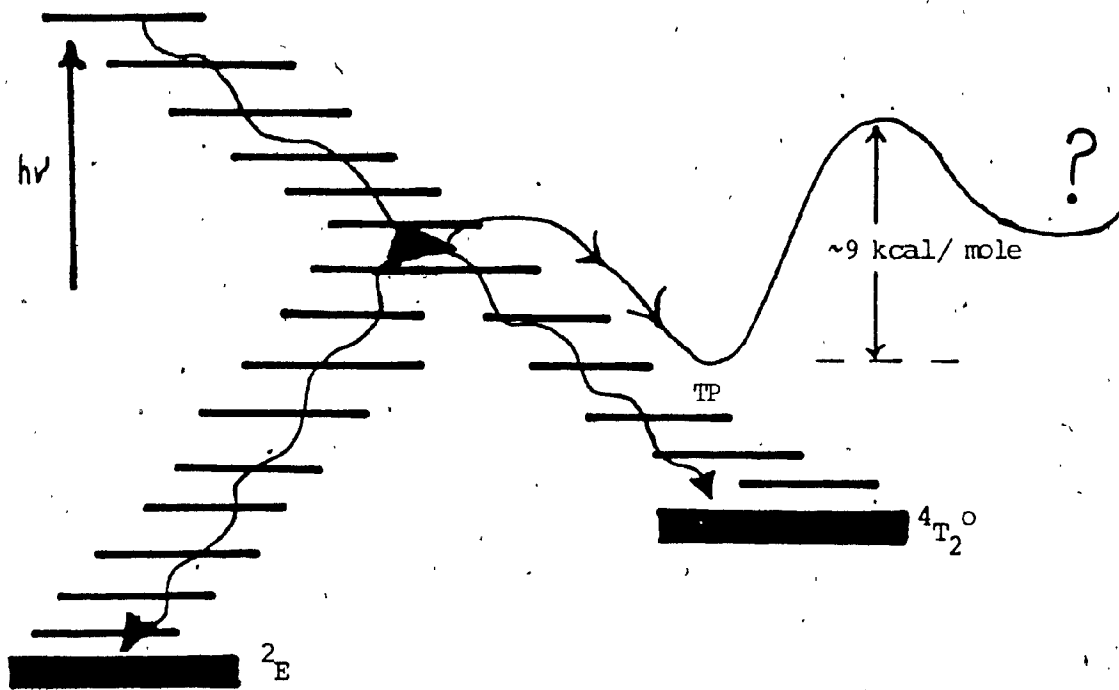
FIGURE 3-46 : Schematic Representation of the Quartet-doublet Excited-state Mixing in trans-Cr(en)₂(NCS)₂⁺; from Figure 5 in Reference 120.



excitation into vibrational levels corresponding to energies lower than the "mixing region", excited-state molecules would preferentially relax into the Y minimum. In such a case, the phosphorescence yield, ϕ_p^{rel} , would necessarily be expected to be less than in the case for relaxation to minimum X. The Y-X energy barrier is expected to be low inasmuch as intersystem crossing is an adiabatic process.¹²⁰ The result of such an interpretation is the possibility of reaction from the Y minimum, as well as reaction from X, such that any molecules reaching Y directly from excitation to P can undergo a prompt reaction. Those molecules reaching X upon excitation to P can either deactivate through phosphorescence or back-intersystem cross to Y and then react. Whether the ligand substitution reactions occur directly from Y or from another intermediate (Z) was not discernable;¹²⁰ but a concerted associative mechanism was thought most probable.

A reaction scheme can be suggested at this point which represents the results observed for the wavelength dependence exhibited by $\text{Cr}(\text{bpy})_3^{3+}$ and takes into consideration the energy level diagram of Figure 3-45 and Sandrini's interpretation of the results obtained for $\text{Cr}(\text{en})_2(\text{NCS})_2^+$. This is presented in Scheme 3-7. The wavelength dependence observed for the photoaquation of both the quenchable and unquenchable reaction components reveals that, in fact, the thermally-equilibrated quartet excited state, ${}^4T_2^0$, is not involved in the prompt photoaquation reaction inasmuch as both $\phi_{\text{RX}}^{\text{tot}}$ and ${}^4\phi_{\text{RX}}$ begin to decrease at ca. 470 nm; an unquenchable reaction quantum yield (${}^4\phi_{\text{RX}} \approx 7 \times 10^{-4}$) is measurable up to ca. 530 nm. Therefore, it would seem that excited-state quartet reaction must originate from some other vibrational level of the quartet manifold, designated as Δ in Scheme 3-7. Whereas the luminescence intensity shows

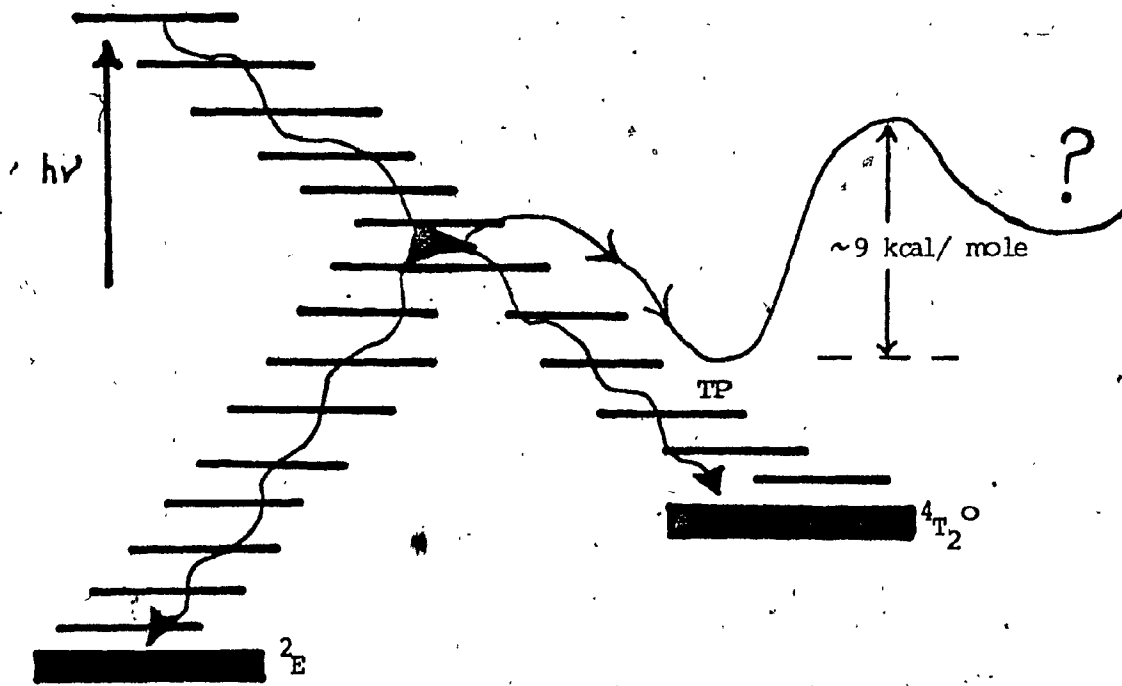
Scheme 3-7



excitation into vibrational levels corresponding to energies lower than the "mixing region", excited-state molecules would preferentially relax into the Y minimum. In such a case, the phosphorescence yield, ϕ_p^{rel} , would necessarily be expected to be less than in the case for relaxation to minimum X. The Y-X energy barrier is expected to be low inasmuch as intersystem crossing is an adiabatic process.¹²⁰ The result of such an interpretation is the possibility of reaction from the Y minimum, as well as reaction from X, such that any molecules reaching Y directly from excitation to P can undergo a prompt reaction. Those molecules reaching X upon excitation to P can either deactivate through phosphorescence or back-intersystem cross to Y and then react. Whether the ligand substitution reactions occur directly from Y or from another intermediate (Z) was not discernable;¹²⁰ but a concerted associative mechanism was thought most probable.

A reaction scheme can be suggested at this point which represents the results observed for the wavelength dependence exhibited by $\text{Cr}(\text{bpy})_3^{3+}$ and takes into consideration the energy level diagram of Figure 3-45 and Sandrini's interpretation of the results obtained for $\text{Cr}(\text{en})_2(\text{NCS})_2^+$. This is presented in Scheme 3-7. The wavelength dependence observed for the photoaquation of both the quenchable and unquenchable reaction components reveals that, in fact, the thermally-equilibrated quartet excited state, $^4T_2^0$, is not involved in the prompt photoaquation reaction inasmuch as both ϕ_{rx}^{tot} and $^4\phi_{rx}$ begin to decrease at ca. 470 nm; an unquenchable reaction quantum yield ($^4\phi_{rx} \approx 7 \times 10^{-4}$) is measurable up to ca. 530 nm. Therefore, it would seem that excited-state quartet reaction must originate from some higher vibrational level of the quartet manifold, designated as \blacktriangle in Scheme 3-7. Whereas the luminescence intensity shows

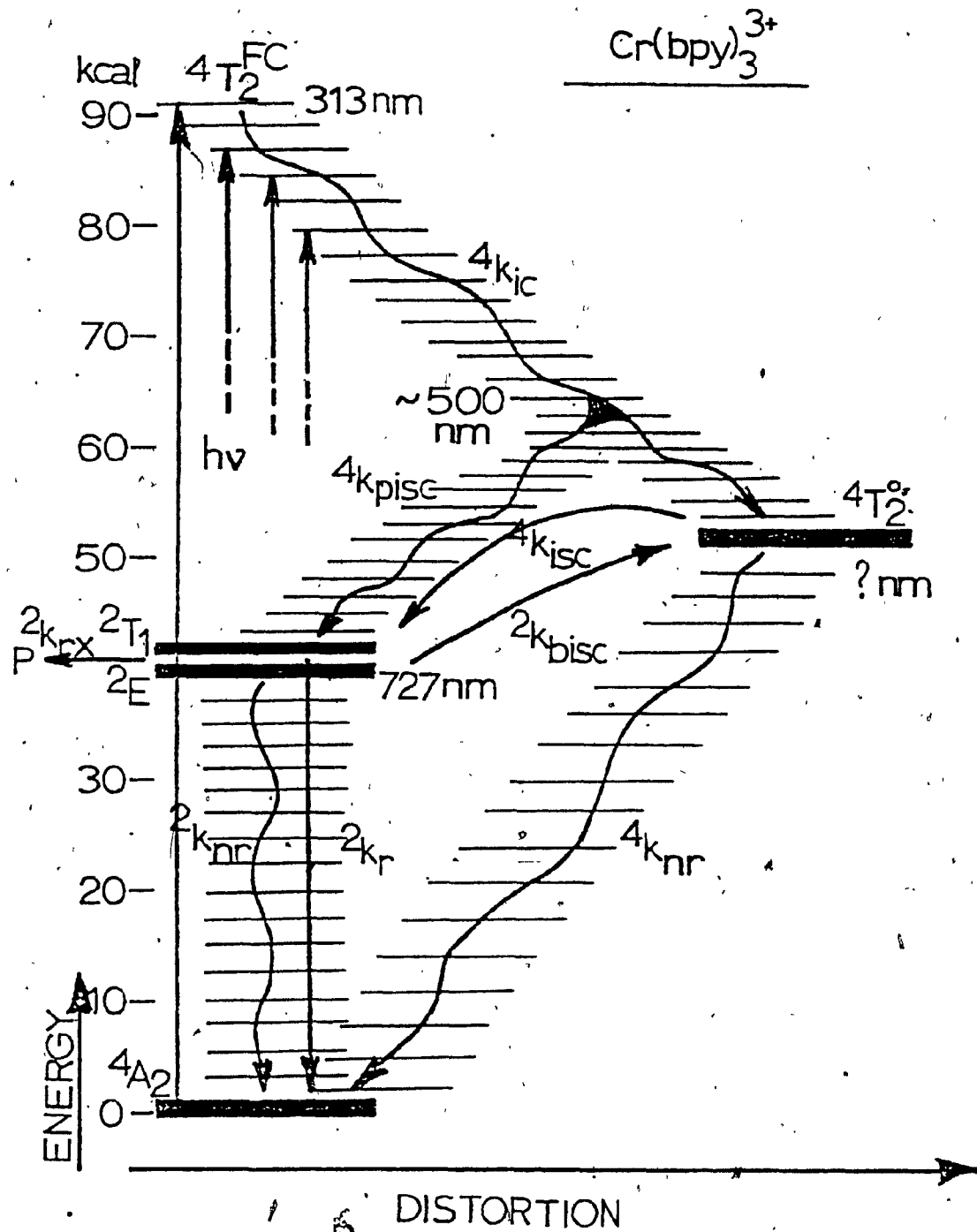
Scheme 3-7



a similar wavelength dependence in the 470-510 nm region, the (${}^2T_1/{}^2E$) doublet manifold population must also begin to decrease at this point. In consequence, there would appear to be two processes, chemical reaction and intersystem crossing, which compete with vibrational relaxation from the initially-populated Franck-Condon state. The nature of the (?) species in Scheme 3-7 is tenuous at this point, since one cannot delineate whether it is a ground-state chemical species or an excited-state species.

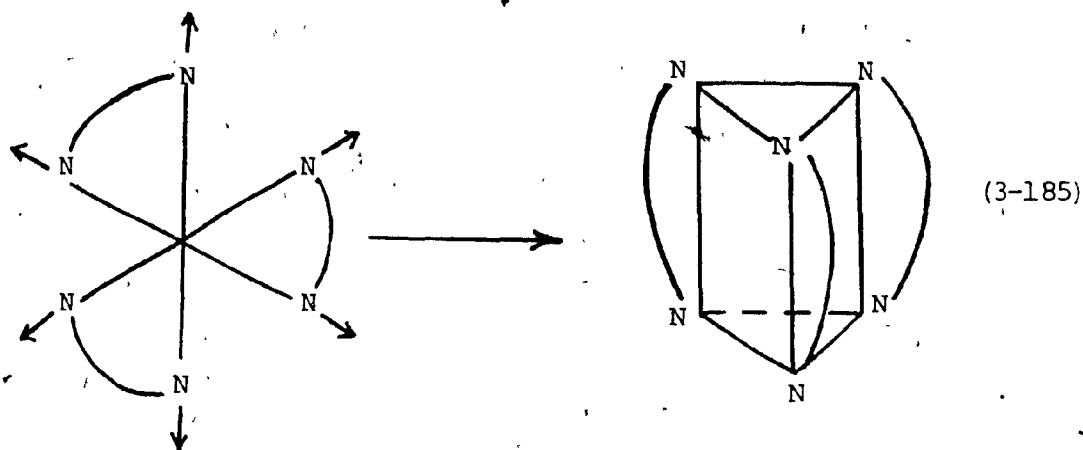
It is possible, however, to construct a potential energy surface diagram for the $\text{Cr}(\text{bpy})_3^{3+}$ (Figure 3-47) somewhat analogous to that for $\text{Cr}(\text{en})_2(\text{NCS})_2^+$ in order to postulate a plausible photoreactivity model. Excitation energies above 460 (i.e., $\lambda > 460$ nm) initially yield a Franck-Condon quartet state, 4FC , which rapidly deactivates via vibrational relaxation. Excited-state molecules so produced can relax into either the X or Y minimum (see Figure 3-46), for which relaxation into X gives rise to the observed photoaquation from the (${}^2T_1/{}^2E$) manifold, ${}^2k_{rx}$, and to phosphorescence, ${}^2k_{rad}$. Those excited-state molecules relaxing into Y can undergo prompt reaction from Y, ${}^4k_{rx}$, deactivate non-radiatively, ${}^4k_{nr}$, and/or intersystem cross to the (${}^2T_1/{}^2E$) manifold, ${}^4k_{pisc}$. Intersystem crossing is expected to be rapid inasmuch as it must compete with vibrational relaxation, which is expected to be very fast ($\sim 10^{-12}$ sec). Excitation into the "mixing region", where some quartet-doublet interaction is assumed, occurs in the 470 - 510 nm region where ϕ_{rx}^{tot} , ${}^4\phi_{rx}$ and I^1 all exhibit a sharp decrease. Excited-state molecules thus produced can relax into the X and the Y minima as well. However, the decrease in the phosphorescence quantum yield indicates that the Y minimum is preferentially occupied. Since there is measurable photoreaction to ca. 530 nm, it is likely that the majority of excited-state molecules also relax to the Y

FIGURE 3-47 : Energy-level Diagram Depicting Wavelength Dependence
of ϕ_{rx}^{tot} , $^4\phi_{rx}$ and I' for $Cr(bpy)_3^{3+}$ in Air-Equilibrated
Solutions at pH 9.6 and 22°C.

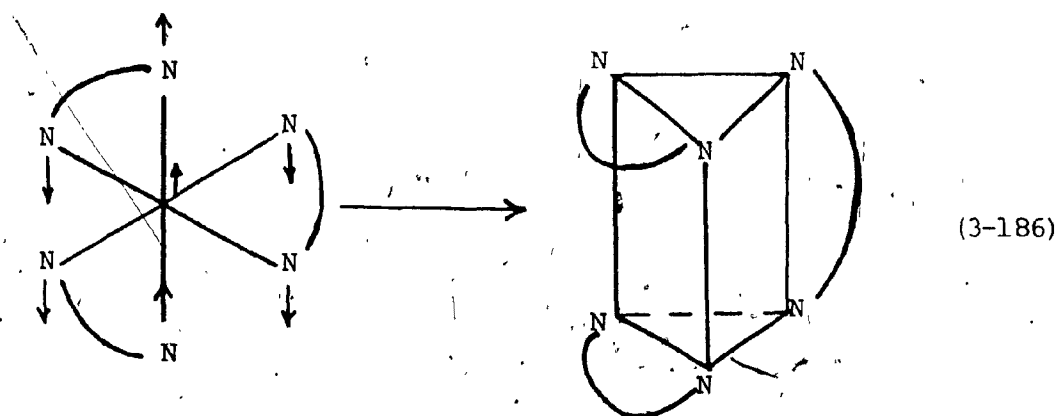


minimum.

Additionally, one can speculate on the nature of the species in the Y minimum generated from the relaxation down the vibrational manifold which accompanies ligand-field transitions in octahedral d^3 complexes. Two vibrational modes accompany the ${}^4A_2 \rightarrow {}^4T_2$ transition, namely the symmetrical breathing mode a_{1g} and the buckle mode t_{1u} , as shown by Hollebhone's tensorial model.¹²³ The symmetrical breathing mode essentially causes an octahedron to undergo a 60° rotation of one of its trigonal faces to yield a trigonal prismatic (TP) geometry.

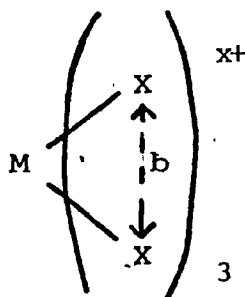


Excitation into the 4T_2 manifold is also accompanied by the buckle mode, which may be strong enough to expose the metal center on one of the faces of the octahedron. The exposed face could certainly facilitate nucleophilic attack by H_2O , and thereby lower the energy required to form the



seven-coordinate aquo-intermediate. From these considerations, a trigonal prismatic geometry (TP) could be associated with the Z species in Sandrini's¹²⁰ work (see Figure 3-46), and the activation energy (ca. 9 kcal/mole) associated with the ${}^4\phi_{rx}$ reaction can be attributed to the energy required for the formation of the seven-coordinate intermediate from the trigonal prismatic species. Figure 3-47 can then be modified to illustrate the wavelength dependence for ϕ_{rx}^{tot} , ${}^4\phi_{rx}$ and I' for the $Cr(bpy)_3^{3+}$ system including the aforementioned considerations; this is depicted in Figure 3-48.

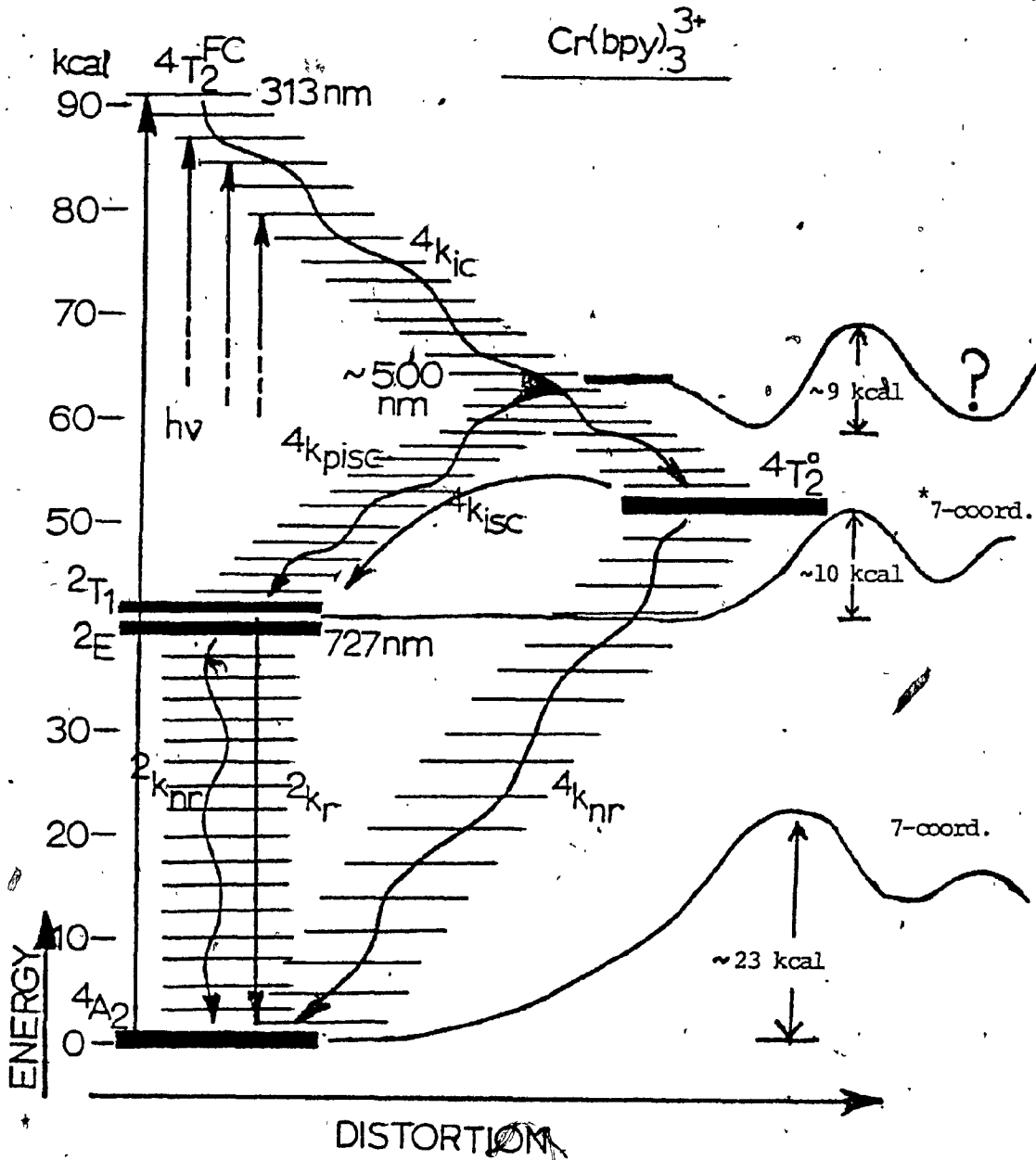
Support for a trigonal prismatic (TP) geometry⁵ for the Z species may be obtained from X-ray crystal structure data for various tris-chelate complexes, $M(\text{bidentate})_3^{x+}$, which have approximate D_3 symmetry and geometries ranging from nearly octahedral (O_h) to trigonal prismatic (TP). From such data, the "bite" b of the chelate ligand may be determined,



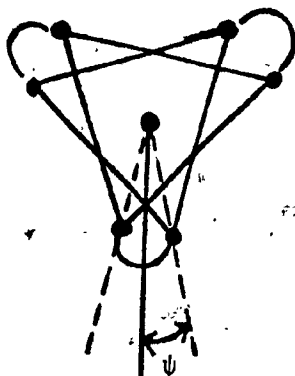
(3-187)

and can be used to give an indication of the coordination geometry. In general, as the "bite" of the ligand is progressively decreased, a continuous change from regular O_h to TP geometry is expected.¹²⁸ In addition to the "bite" of the ligand, the pitch angle, ψ , (angle of twist between the upper and lower triangular faces of an octahedron) is indicative of the coordination geometry; $\psi = 30^\circ$ for O_h geometry and $\psi = 0^\circ$

FIGURE 3-48 : Energy-level Diagram Depicting Wavelength Dependence
and Reaction Pathways from the Various Ground- and
Excited-state Manifolds of $\text{Cr}(\text{bpy})_3^{3+}$.



for TP geometry.



(3-188)

Normalization of the "bite" b (by assuming a metal-donor atom distance of unity) for several $M(\text{bidentate})_3^{x+}$ species of $\sim D_3$ symmetry reveals such trends in "bite" and pitch angle. Some data is collected in Table 3-34 part A for various N- and S-donor atom tris-chelates; the data reveal that as the "bite" b is decreased, TP geometry becomes more favorable. Other trends, as well, are observed: i) O_h geometry is favored by addition of electrons to the complex, ii) the "bite angle" X-M-X increases as the M-X distance decreases, and iii) the "bite angle" is independent of electron configuration, although the M-X distance increases with the addition of electrons in the t_{2g} subshell.

A comparison of the data in part A of Table 3-34 with that in part B for the polypyridyl complex ions would seem to suggest that it would not be difficult for the polypyridyl complexes to distort to a TP geometry. Furthermore, excitation of the $\text{Cr}(\text{bpy})_3^{3+}$ complex is accompanied by an increase in the M-N distance, which necessarily decreases the N-M-N angle; this would cause a decrease in the "bite" of the bipyridyl ligand, and thereby favor a TP geometry.

TABLE 3-34 : Known Values of the "bite" b and the Pitch Angle, ψ , for Some Tris(bidentate)-Transition Metal Complexes.

Complex ^a	X-X bite, b , (Å)	Pitch angle, ^c (°)	Reference
Mn(acac) ₃	1.5	33.8	<u>d</u>
Cr(acac) ₃	1.43	30.8	<u>d</u>
Co(en) ₃ ³⁺	1.39	28.5	<u>e</u>
Cr(en) ₃ ³⁺	1.31	25.2	<u>f</u>
Cu(en) ₃ ⁺	1.30	24.5	<u>g</u>
Co(S ₂ COEt ₂) ₃	1.23	21.8	<u>h</u>
Fe(S ₂ COEt ₂) ₃	1.22	20.5	<u>i</u>
Cr(MBz) ₃	1.21	---	<u>j</u>
Fe(Et ₂ (dtc)) ₃	1.20	0	<u>k</u>
Ru(Et ₂ (dtc)) ₃	1.19	0	<u>k</u>

TABLE 3-34, cont'd.

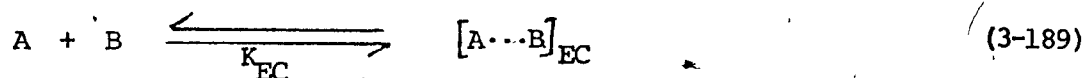
PART B-

Complex ^c	X-X bite, b, ^b (Å)	Reference
Fe(phen) ₃ ²⁺	1.32	<u>m</u>
Ru(bpy) ₃ ²⁺	1.27	<u>n</u>
Cu(phen) ₃ ²⁺	1.24	<u>o</u>

^a (acac) = acetylacetonato; (en) = ethylenediamine; (MBz) = 4-morpholine carbodithioato; (Et₂dtc) = N,N-diethyldithiocarbamate. ^b X = donor atom, b has been normalized. ^c see (3-188). ^d B. Morosin, J.R. Brathovde, Acta Cryst., 17, 705 (1964). ^e K. Nakatsu, Bull. Chem. Soc. Japan, 35, 832 (1962). ^f K.N. Raymond, P.W.R. Corfield, Inorg. Chem., 7, 1362 (1968). ^g D.L. Cullen and E.C.L. Lingafetter, Inorg. Chem., 9, 1858 (1970). ^h S. Merlino, Acta Cryst., Sect. B, 24, 1441 (1968). ⁱ B.F. Hoskins, B.P. Kelly, J. Chem. Soc., Chem. Comm., 45, (1970). ^j R.J. Butcher and E. Sinn, J. Am. Chem. Soc., 98, 2440 (1976). ^k L.H. Pignolet, Inorg. Chem., 13, 2051 (1974). ^m A. Zalkin, D.H. Templeton and T. Ueki, Inorg. Chem., 12, 1641 (1973). ⁿ D.P. Rillema, D.S. Jones, J. Chem. Soc., Dalton Trans., 1237, (1973).

3.12. EXCITED-STATE BEHAVIOR OF $\text{Cr}(\text{bpy})_3^{3+}$ IN $\text{CH}_3\text{CN}/\text{H}_2\text{O}$ MIXTURES.

The first step in a bimolecular reaction is the diffusion of two reactants A and B to form an encounter complex (EC),



the nature and fate of which are governed by the solvent cage. The kinetic behavior is described by the following rate expression

$$\text{Rate} = k_{\text{obs}}[\text{A}] = \frac{k_1 K_{\text{EC}} [\text{B}]}{1 + K_{\text{EC}} [\text{B}]} [\text{A}] \quad (3-191)$$

When $[\text{B}] \gg [\text{A}]$, as is the case in solvolysis reactions, the value of $K_{\text{EC}}[\text{B}] > 1$, and the rate = $k_1[\text{A}]$; this is so because encounter complex formation is unavoidable. Thus, solvolysis reactions are always first-order in $[\text{A}]$.

From a coordination chemist's point of view, the encounter complex in solvolysis reactions can be seen as the solvation of reactant A. The solvation shell of A is composed of a primary coordination sphere and a secondary coordination sphere. The former comprises the nearest neighbors of the central atom in A, and is highly ordered as a result of solute and solvent influences. The secondary coordination sphere is composed of encounter partners, and of encounter partners and bulk solvent in dilute solution.

In thermal solvolysis reactions the nucleophilic character of the solvent tends to lower the barrier to substitution via bond-formation stabilization of the transition state. In photo-solvolysis reactions, on the other hand, the nucleophile may interact with an excited-state solute species possessing energy greater than the barrier to thermal substitution. As a result, the nucleophile (solvent in solvolysis) in the photo-reaction can take part in the selection of excited-state deactivation pathways rather than in lowering the substitution barrier.

In solvolytic reactions where the nucleophile (reactant B) is a solvent mixture, the question arises as to which nucleophilic component preferentially solvates reactant A. Hersey¹²⁹ has employed ¹H-NMR solvent relaxation methods to investigate the exchange of proton nuclei between a paramagnetic chromium(III) environment (primary coordination sphere) and the diamagnetic bulk solvent environment (secondary coordination sphere); specifically, the preferential solvation of $\text{Cr}(\text{bpy})_3^{3+}$ in $\text{CH}_3\text{CN}/\text{H}_2\text{O}$ mixtures. It must be recognized that there is rapid exchange of solvent molecules between the primary and secondary coordination spheres on the NMR time scale.

One parameter that can be extracted from the NMR studies is η/η_0 . As applied to the $\text{Cr}(\text{bpy})_3^{3+}$ ion in $\text{CH}_3\text{CN}/\text{H}_2\text{O}$ mixtures, η/η_0 describes the number of water molecules in encounter with $\text{Cr}(\text{bpy})_3^{3+}$ in the mixed solvent system (η) as compared to the number of water molecules in encounter with $\text{Cr}(\text{bpy})_3^{3+}$ in pure water (η_0); thus, η/η_0 compares the probability of encounter between H_2O and $\text{Cr}(\text{bpy})_3^{3+}$ in a mixed solvent system to the encounter probability when all of the primary coordination sphere sites are occupied by water (equal to unity).

If the composition of the primary coordination sphere is the same as

that for the secondary coordination sphere, then a plot of η/η_0 vs mole fraction CH_3CN ($\chi_{\text{CH}_3\text{CN}}$) would be linear with a slope of +1 for the methyl protons of CH_3CN ; a similar plot would be linear with slope of -1 for the protons of water.^{130,131} This situation is revealed in Figure 3-49 by the dashed lines, and corresponds to no preferential solvation of $\text{Cr}(\text{bpy})_3^{3+}$ by either CH_3CN or H_2O . Thus, where no preferential solvation by either solvent component occurs, η/η_0 is equal to the mole fraction of solvent component. If, however, $\text{Cr}(\text{bpy})_3^{3+}$ is preferentially solvated by CH_3CN , then the plot of η/η_0 vs $\chi_{\text{CH}_3\text{CN}}$ should reveal data points for the CH_3CN protons above the line of slope +1; and the data for the H_2O protons would appear below the line of slope -1,^{130,131} as illustrated by the solid lines in Figure 3-49. Figure 3-50 depicts Hersey's¹²⁹ results for the $\text{Cr}(\text{bpy})_3^{3+}$ - $\text{CH}_3\text{CN}/\text{H}_2\text{O}$ system, for which the η/η_0 values for the CH_3CN protons increase gradually as $\chi_{\text{CH}_3\text{CN}}$ increases, while η/η_0 for the H_2O protons exhibits a much sharper initial decrease as $\chi_{\text{CH}_3\text{CN}}$ increases. Furthermore, the results show conclusively that CH_3CN occupies the primary coordination sphere sites preferentially over H_2O . For example, at $\chi_{\text{CH}_3\text{CN}} = 0.5$, η/η_0 for the methyl protons of CH_3CN fall on a curve which is positive with respect to the situation of no preferential solvation, and η/η_0 for the H_2O protons fall on a curve below the no preferential solvation situation. However, one notes that the η/η_0 vs $\chi_{\text{CH}_3\text{CN}}$ plots for $\text{Cr}(\text{bpy})_3^{3+}$ (Figure 3-50) do not exhibit ideal preferential solvation behavior, when compared to the solid lines in Figure 3-49. As Hersey¹²⁹ has pointed out, the non-complimentary behavior of η/η_0 vs $\chi_{\text{CH}_3\text{CN}}$ may be due to a dependency of T_2 , the observed average relaxation time, on the primary coordination sphere composition as a result of some interaction between the aromatic bipyridine ligands

FIGURE 3-49 : η/η_0 vs $\chi_{\text{CH}_3\text{CN}}$ for a Complex Undergoing Preferential Solvation; dashed lines represent the case of no preferential solvation. From reference 129.

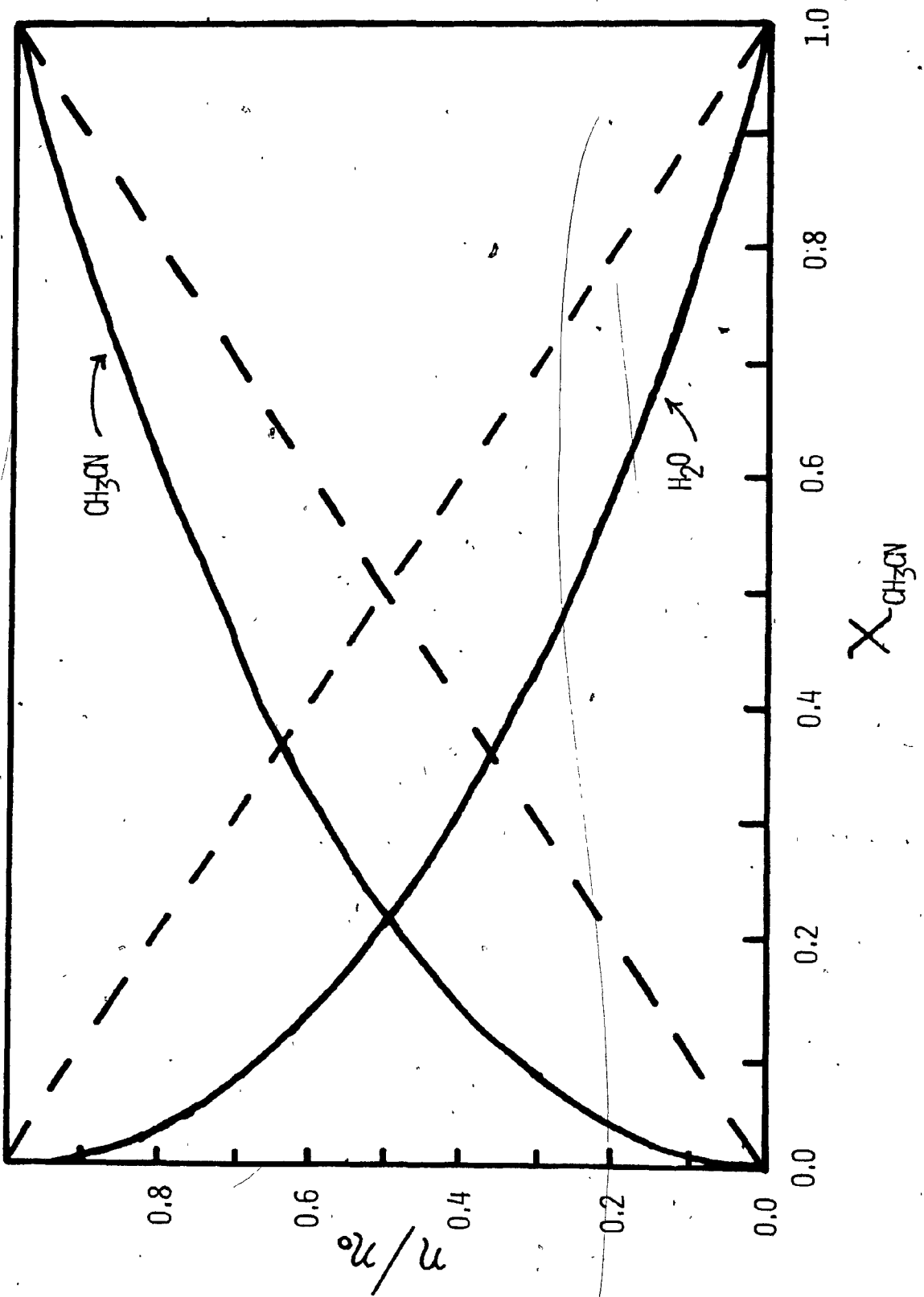
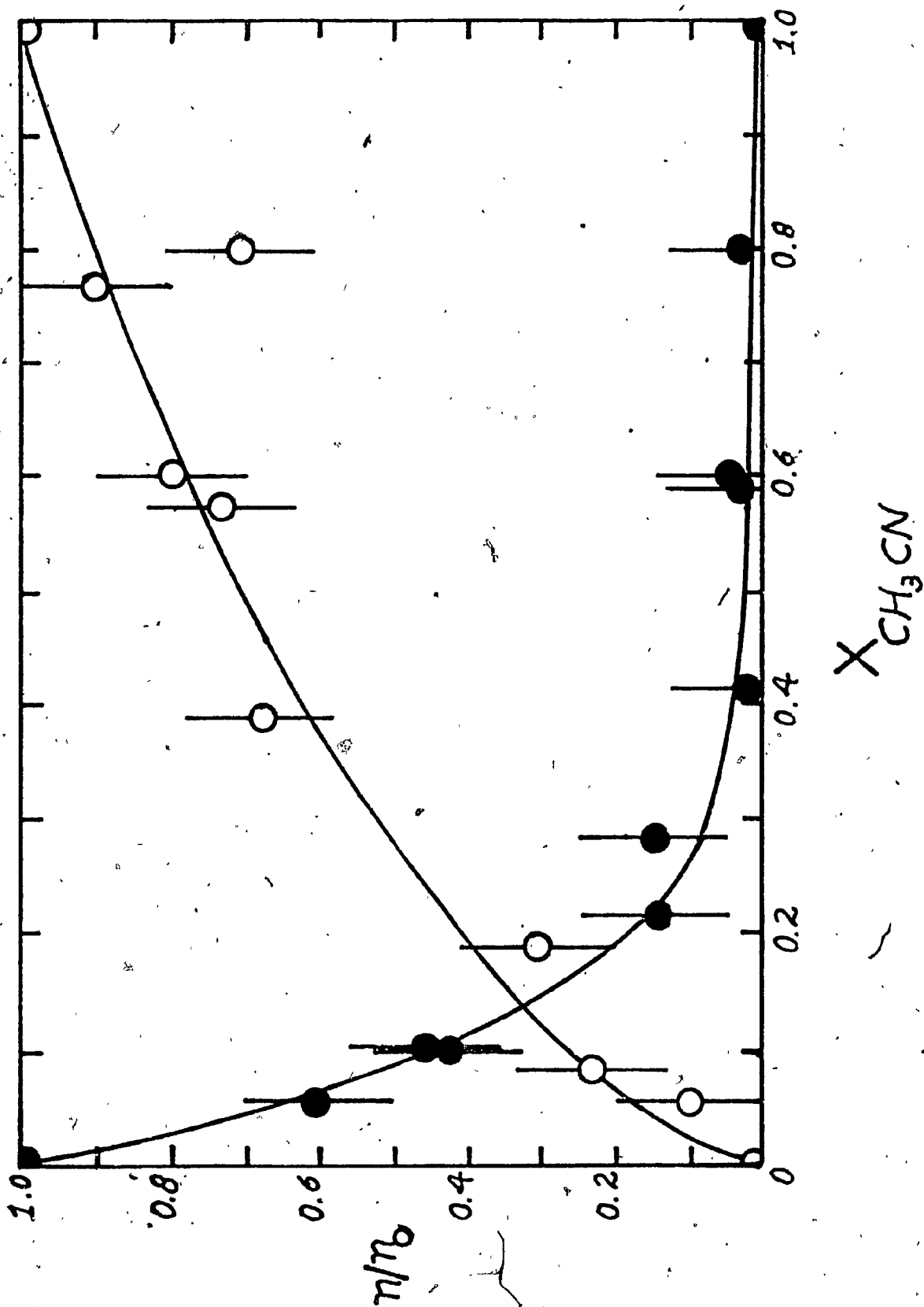


FIGURE 3-50 : Preferential Solvation Data for $\text{Cr}(\text{bpy})_3^{3+}$ at 25°C
Plotted as η / η_0 vs Mole Fraction of CH_3CN for $\text{CH}_3\text{CN}/$
 H_2O Mixtures. Solid circles show value of η / η_0
derived from NMR linewidths of H_2O protons; open circles
refer to data derived from the NMR linewidths of the
methyl protons of CH_3CN ; from reference 129.



and CH_3CN . In addition, the "interligand pockets" present in $\text{Cr}(\text{bpy})_3^{3+}$ can accommodate water molecules, and thus the system would require that these molecules be displaced prior to CH_3CN solvation of the paramagnetic center. This, then, may account for the sharp decrease in η/η_0 with increasing $\chi_{\text{CH}_3\text{CN}}$ (Figure 3-50).

Recently, several groups^{49,51,122,132-134} have reported on the sensitivity of Cr(III) photoprocesses towards changes in medium. A basic question in the understanding of such effects is to distinguish effects which are static from those which are dynamic in nature. An aid to this distinction would include information on solvent molecule distribution about the Cr(III) complex. As an extension to the ground-state preferential solvation of $\text{Cr}(\text{bpy})_3^{3+}$ by CH_3CN reported by Hersey,¹²⁹ the effects of solvent composition on the photosolvolytic of $\text{Cr}(\text{bpy})_3^{3+}$ was investigated in $\text{CH}_3\text{CN}/\text{H}_2\text{O}$ mixtures. Specifically, the quantum yield for photo-reaction, and the phosphorescence intensity and lifetime of $\text{Cr}(\text{bpy})_3^{3+}$ were studied as a function of $\text{CH}_3\text{CN}/\text{H}_2\text{O}$ solvent composition in air-equilibrated solutions at 22°C.

Figure 3-51 depicts the variation in the observed lifetime of $(^2\text{T}_1/^2\text{E})\text{Cr}(\text{bpy})_3^{3+}$ for various $\chi_{\text{CH}_3\text{CN}}$ in air-equilibrated and argon-purged solutions; the lifetime varies with solvent composition, though not exponentially. These results contrast those reported by Henry and Hoffman⁴⁹ wherein the decay rate of the transient absorption of $(^2\text{T}_1/^2\text{E})\text{Cr}(\text{bpy})_3^{3+}$ remained constant (at $1.6 \times 10^4 \text{ sec}^{-1}$ within experimental error) for $0 \leq \chi_{\text{CH}_3\text{CN}} \leq 1$. Henry⁵⁰ attributed this behavior to the inability of solvent polarity to sufficiently perturb the system so as to alter the rate of non-radiative decay, $^2k_{\text{nr}}$. Similar results were obtained⁴⁹ for $0 \leq \chi_{\text{DMF}} \leq 0.1$ in $\text{DMF}/\text{H}_2\text{O}$ media, though more recently Porter and Van

Houten^{51,122} observed an exponential decrease in ${}^2\phi_{\text{obs}}$ with increasing X_{DMF} in the range $0 \leq X_{\text{DMF}} \leq 0.1$. The latter observations suggest that quenching of the (${}^2T_1/{}^2E$) species by DMF involves an increase in ${}^2k_{\text{nr}}$ while ${}^2k_{\text{rad}}$ remains constant. Moreover, the relative phosphorescence lifetimes parallel those of the relative intensities of (${}^2T_1/{}^2E$)Cr(bpy)₃³⁺ in CH₃CN/H₂O mixtures, as shown in Figure 3-52. The (${}^2T_1/{}^2E$) phosphorescence intensity I is given by equation (3-192). For comparative purposes,

$$I = {}^2\phi_{\text{rad}} = {}^2k_{\text{rad}} {}^4\eta_{\text{isc}} {}^2\tau \quad (3-192)$$

equation (3-192) may be rewritten as (3-193), where the superscripts H and S denote H₂O and solvent mixture (CH₃CN/H₂O), respectively.

$$\frac{I^S}{I^H} = \frac{{}^2\phi_{\text{rad}}^S}{{}^2\phi_{\text{rad}}^H} = \frac{{}^2k_{\text{rad}}^S}{{}^2k_{\text{rad}}^H} \frac{{}^4\eta_{\text{isc}}^S}{{}^4\eta_{\text{isc}}^H} \frac{{}^2\tau^S}{{}^2\tau^H} \quad (3-193)$$

Inasmuch as ${}^2k_{\text{rad}}$ is proportional to the refractive index of the solvent, it is expected that ${}^2k_{\text{rad}}^S$ and ${}^2k_{\text{rad}}^H$ would differ; but the refractive indices of H₂O (1.333)³ and CH₃CN (1.342)³ are very similar, and thus it is assumed that ${}^2k_{\text{rad}}^S$ and ${}^2k_{\text{rad}}^H$ are also similar (${}^2k_{\text{rad}}^S \approx {}^2k_{\text{rad}}^H$). The value of ${}^4\eta_{\text{isc}}^H$ is known to be ≈ 1 from previous work (see Section 3.10.); thus,

$$\frac{I^S}{I^H} = \frac{{}^4\eta_{\text{isc}}^S}{{}^4\eta_{\text{isc}}^H} \frac{{}^2\tau^S}{{}^2\tau^H} \quad (3-194)$$

Figure 3-52 and the data in Table 3-35 show that (I^S / I^H) and $({}^2\tau^S / {}^2\tau^H)$

FIGURE 3-51 : Dependence of Emission Lifetime of $(^2T_1/{}^2E)Cr(bpy)_3^{3+}$ Species on Solvent Composition Expressed as Mole Fraction CH_3CN . Closed circles denote data obtained in air-equilibrated solutions; open circles refer to data for argon-purged solutions.

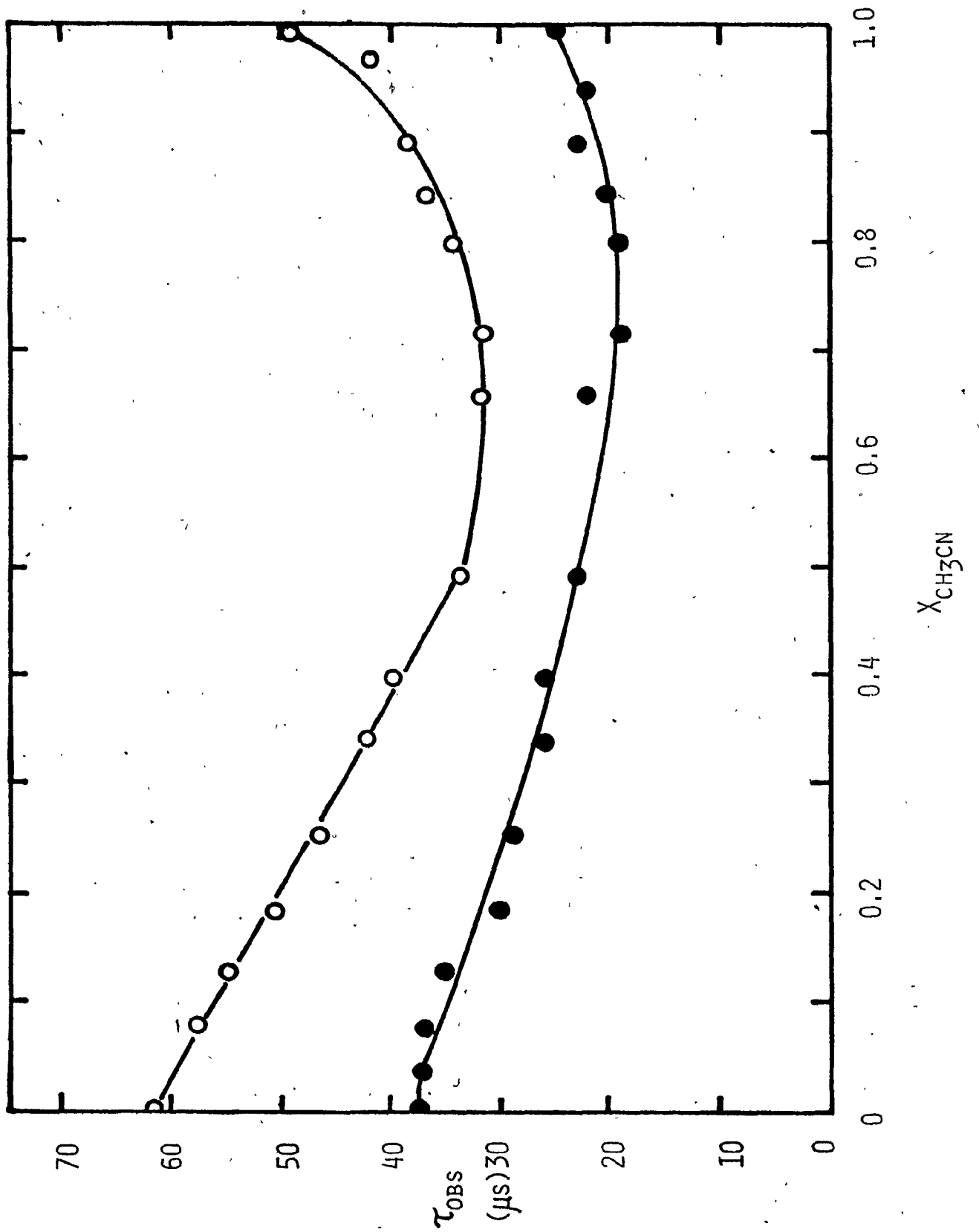


FIGURE 3-52 : Effect of Added CH_3CN on the Luminescence Intensity and Emission Lifetime of $(^2T_1/{}^2E)\text{Cr}(\text{bpy})_3^{3+}$ Species Expressed as a Function of Mole Fraction of CH_3CN .
Temperature, 22°C ; air-equilibrated solutions;
 $[\text{Cr}(\text{bpy})_3^{3+}] = 1.5 \times 10^{-4} \text{ M}$.

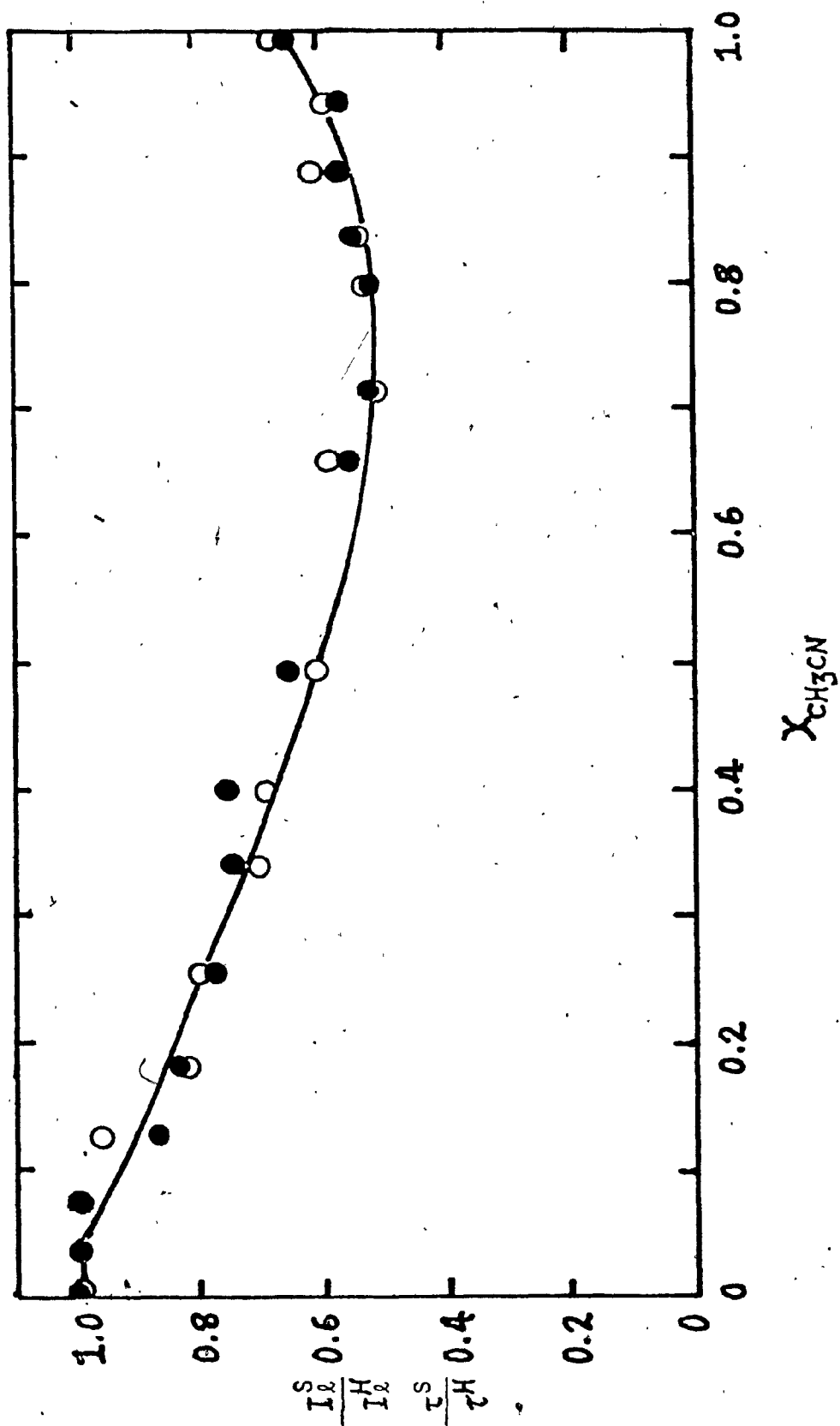


TABLE 3-35 : Relative Values of $(\eta/\eta_0)_{\text{CH}_3\text{CN}}$, Phosphorescence Intensities I, and Lifetimes for $\text{Cr}(\text{bpy})_3^{3+}$ at 22°C as a Function of CH_3CN Composition.

$x_{\text{CH}_3\text{CN}}$	$(\eta/\eta_0)_{\text{CH}_3\text{CN}}$	(I^S / I^H)	(τ^S / τ^H)
1.000	1.00	0.650	0.678
0.9439	0.97	0.565	0.589
0.8918	0.95	0.575	0.614
0.8432	0.93	0.550	0.543
0.7978	0.90	0.519	0.524
0.7158	0.85	0.525	0.514
0.6591	0.82	0.560	0.594
0.4942	0.76	0.654	0.608
0.3999	0.70	0.750	0.689
0.3399	0.62	0.738	0.697
0.2556	0.56	0.771	0.789
0.1862	0.48	0.828	0.816
0.1283	0.40	0.869	0.957
0.0790	0.23	1.009	0.995
0.0367	0.13	0.988	0.997
0.000	0.00	1.000	1.000

have the same value for the same solvent composition; this observation indicates that ${}^4\eta_{isc}^S$ also equals ~ 1 in neat CH_3CN as well as in $\text{CH}_3\text{CN}/\text{H}_2\text{O}$ mixtures. In consequence, the variations in $({}^2\tau^S / {}^2\tau^H)$ and (I^S / I^H) must arise from an increase in ${}^2k_{nr}$, the rate constant for non-radiative decay of $({}^2T_1/{}^2E)\text{Cr}(\text{bpy})_3^{3+}$. This is most likely the case for $0 \leq X_{\text{CH}_3\text{CN}} \leq 0.7$; however, in the range $0.7 \leq X_{\text{CH}_3\text{CN}} \leq 1$, there is a large increase in ${}^2\tau^S$ in argon-purged solutions for which a slower rate of chemical quenching of $({}^2T_1/{}^2E)$ by H_2O is indicated. Thus, at $X_{\text{CH}_3\text{CN}} > 0.7$, quenching of $({}^2T_1/{}^2E)$ by CH_3CN probably occurs at diffusional rates. The similar values of (I^S/I^H) and $({}^2\tau^S / {}^2\tau^H)$ lend additional credence to the value of ${}^4\eta_{isc}^S \approx 1$. This is consistent with Porter's results^{51, 122} which showed a diminution in relative lifetimes and phosphorescence yield in DMF/ H_2O media. The results obtained could not be attributed to "variations in the population of the 2E state arising from either changes in the decay of the 4T_2 precursor state nor to changes in the efficiency of intersystem crossing to the 2E state".

The variation in phosphorescence intensities and lifetimes in the region where $0.80 \leq X_{\text{CH}_3\text{CN}} \leq 1.00$ are revealed in Figure 3-53; conventional Stern-Volmer kinetics for quenching of $({}^2T_1/{}^2E)$ by H_2O are observed, as defined by equation (3-195). The plot of ${}^2\tau_0 / {}^2\tau$ vs $[\text{H}_2\text{O}]$ of

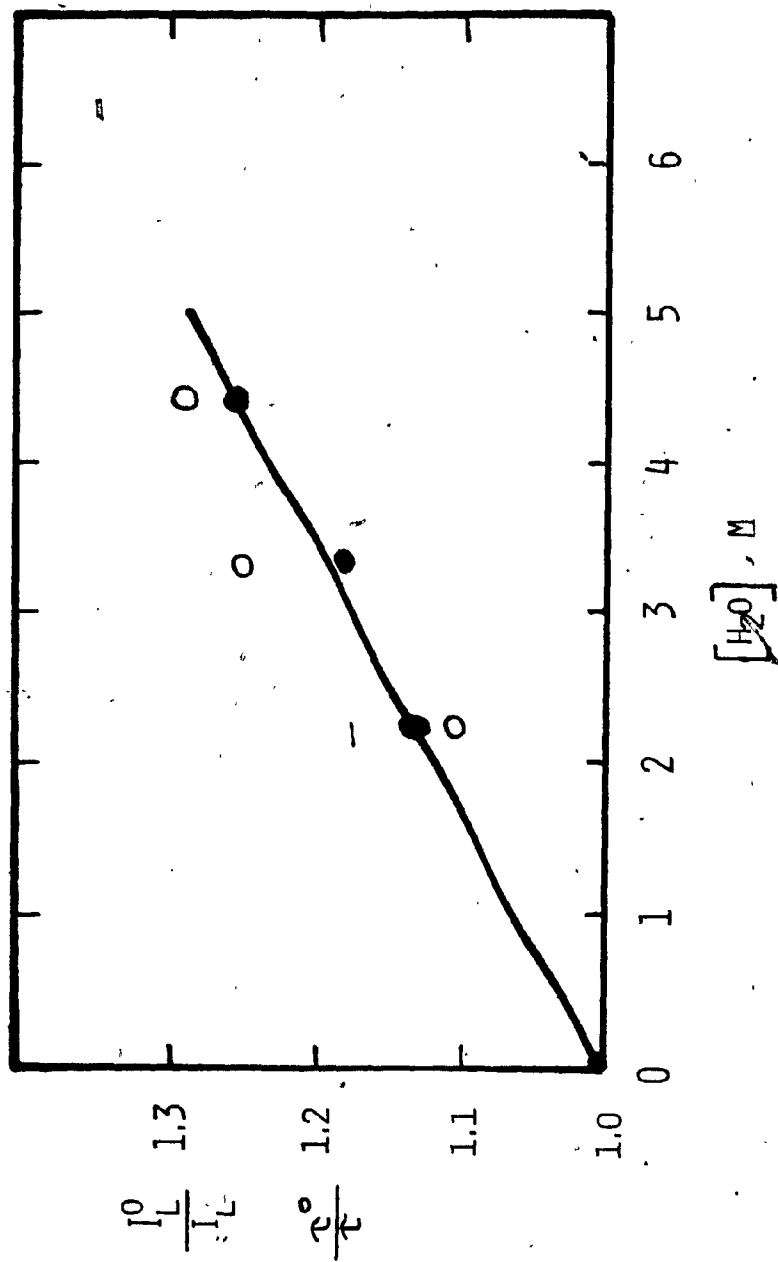
$$\frac{{}^2\tau_0}{{}^2\tau} = 1 + K_{sv} [\text{H}_2\text{O}] = 1 + {}^2k_q {}^2\tau_0 [\text{H}_2\text{O}] \quad (3-195)$$

Figure 3-53 yields a quenching rate constant ${}^2k_q(\text{H}_2\text{O}) = 2.67 \times 10^3 \text{ M}^{-1} \text{ sec}^{-1}$, in satisfactory agreement with a value of ${}^2k_q(\text{H}_2\text{O}) = 2.97 \times 10^3 \text{ M}^{-1} \text{ sec}^{-1}$ from the plot of I_0/I vs $[\text{H}_2\text{O}]$ in Figure 3-53.

FIGURE 3-53 : Stern-Volmer Plot for the Water Quenching of the Phosphorescence Intensity and Emission Lifetimes of $\text{Cr}(\text{bpy})_3^{3+}$ in $\text{CH}_3\text{CN}/\text{H}_2\text{O}$ Mixtures (0.80 - 1.00 mole fraction CH_3CN). Solid circles denote intensity data; open circles denote lifetime data.

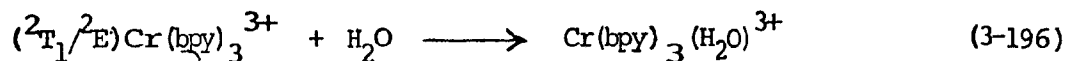
Temperature, 22°C ; argon-purged solutions;

$$[\text{Cr}(\text{bpy})_3^{3+}] = 1.5 \times 10^{-4} \text{ M.}$$



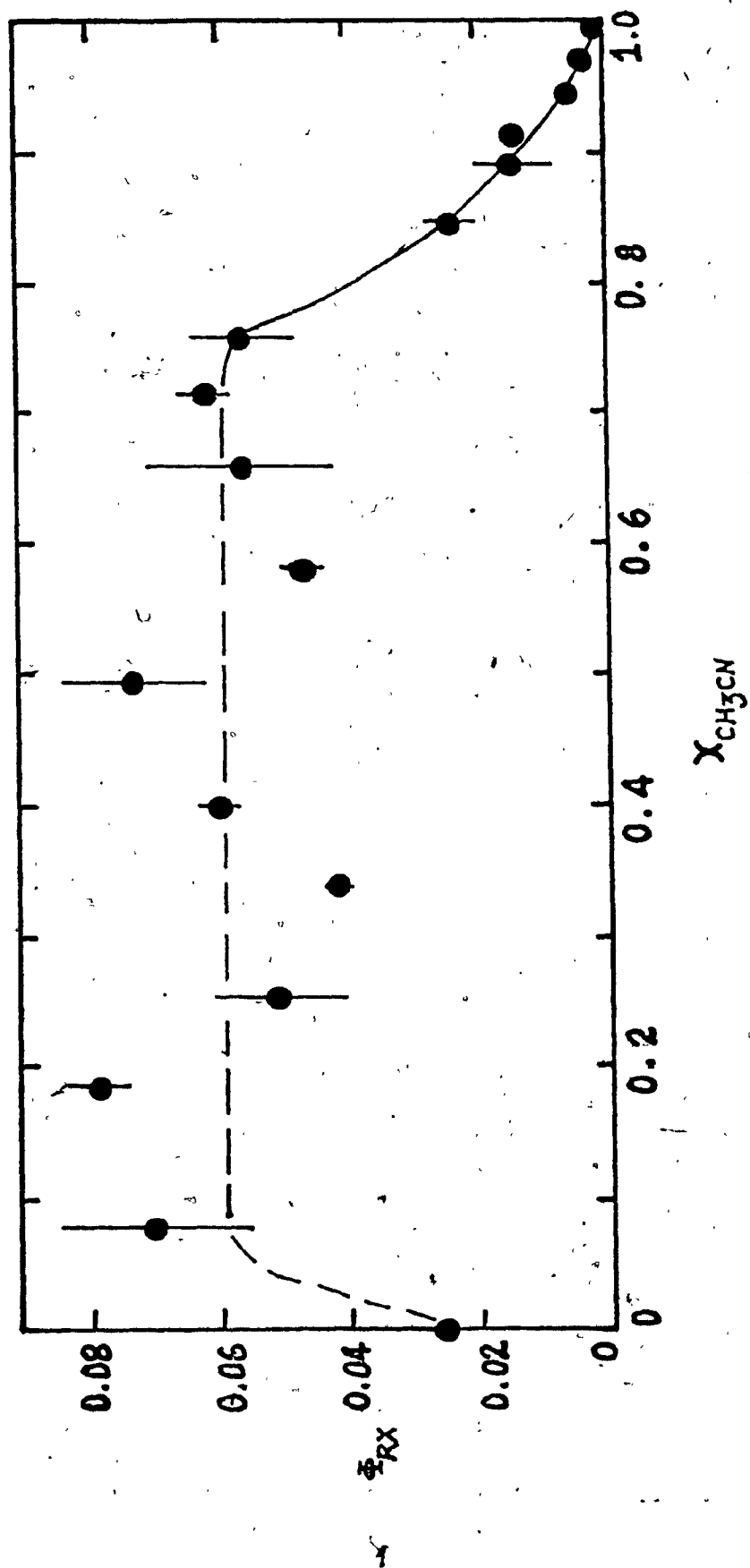
In addition to phosphorescence intensity and lifetime measurements in $\text{CH}_3\text{CN}/\text{H}_2\text{O}$ mixtures, the quantum yield of photosolvolysis (ϕ_{rx}) of $\text{Cr}(\text{bpy})_3^{3+}$ in air-equilibrated $\text{CH}_3\text{CN}/\text{H}_2\text{O}$ mixtures at 22°C has been determined; the results are depicted in Figure 3-54. It is apparent that ϕ_{rx} exhibits three distinct regimes: (a) ϕ_{rx} initially increases as $x_{\text{CH}_3\text{CN}}$ varies from 0.00 to 0.08; (b) ϕ_{rx} remains essentially constant (0.062 \pm 0.011) from 0.08 to 0.75 mole fraction CH_3CN ; (c) in the region where $0.75 \leq x_{\text{CH}_3\text{CN}} \leq 1.00$, ϕ_{rx} shows a sharp decrease with increasing $x_{\text{CH}_3\text{CN}}$ such that at $x_{\text{CH}_3\text{CN}} = 1.00$, $\phi_{\text{rx}} < 1 \times 10^{-4}$. In region (a), preferential solvation results indicate that the available solvation sites are becoming occupied by H_2O molecules rather than CH_3CN molecules. In region (c), ϕ_{rx} increases with increasing $[\text{H}_2\text{O}]$ and reaches a limiting value (at $x_{\text{CH}_3\text{CN}} \sim 0.75$, $x_{\text{H}_2\text{O}} \sim 0.25$) before a situation occurs in which H_2O is a significant component in the primary coordination sphere of the $\text{Cr}(\text{bpy})_3^{3+}$ ion.

The results seem to indicate that it is not necessary to invoke a solvolysis mechanism different from that outlined in reactions (3-86) to (3-100) for $\text{Cr}(\text{bpy})_3^{3+}$ in aqueous alkaline solution. Assuming this, the rate of formation of the seven-coordinate intermediate (reaction 3-196)



should be proportional to the probability of encounter between $(^2T_1/{}^2E)\text{Cr}(\text{bpy})_3^{3+}$ and H_2O ; as such, a linear relationship between the rate of formation of $\text{Cr}(\text{bpy})_3(\text{H}_2\text{O})^{3+}$ and η/η_0 would be expected. However, these rate data are not available, though plots of ϕ_{rx} vs η/η_0 and vs $x_{\text{CH}_3\text{CN}}$ are virtually the same. From the available results, it is

FIGURE 3-54 : Dependence of the Photosolvolysis Quantum Yield on the Solvent Composition for $\text{Cr}(\text{bpy})_3^{3+}$ in $\text{CH}_3\text{CN}/\text{H}_2\text{O}$ Mixtures. Temperature, 22°C ; air-equilibrated solutions; $[\text{Cr}(\text{bpy})_3^{3+}] = (1-2) \times 10^{-4} \text{ M}$.



concluded that reaction (3-196) represents an equilibrium situation which lies to the left in region (a) where $\chi_{\text{H}_2\text{O}}$ is small, and becomes saturated in region (c) wherein subsequent removal of H_2O molecules (increasing $\chi_{\text{CH}_3\text{CN}}$) has no effect on the equilibrium.

Employing the ground-state preferential solvation, emission lifetime and intensity data for $\text{Cr}(\text{bpy})_3^{3+}$ in $\text{CH}_3\text{CN}/\text{H}_2\text{O}$, a comparison with analogous data for the trans- $\text{Cr}(\text{NH}_3)_2(\text{NCS})_4^-$ (R^-) complex ion allows for some interesting distinctions to be made. The preferential solvation profile for trans- $\text{Cr}(\text{NH}_3)_2(\text{NCS})_4^-$ in $\text{CH}_3\text{CN}/\text{H}_2\text{O}$ mixtures is presented in Figure 3-55; a comparison with the analogous profile for $\text{Cr}(\text{bpy})_3^{3+}$ (Figure 3-54) indicates that both complexes are preferentially solvated by CH_3CN in their ground states. Furthermore, the point at which the composition of the solvation shell contains equimolar amounts of CH_3CN and H_2O (the equisolvation point) occurs at $\chi_{\text{CH}_3\text{CN}} \approx 0.10$ for both trans- $\text{Cr}(\text{NH}_3)_2(\text{NCS})_4^-$ and $\text{Cr}(\text{bpy})_3^{3+}$. However, the similarities between R^- and $\text{Cr}(\text{bpy})_3^{3+}$ for the data obtained do not go beyond this point. The doublet-state lifetime of R^- in air-equilibrated neat H_2O at 23°C is ca. 6 nsec (extrapolated from low-temperature data) and increases to 106 nsec in air-equilibrated CH_3CN at 23°C ; ¹³² whereas, the doublet-state lifetime of $\text{Cr}(\text{bpy})_3^{3+}$ in air-equilibrated neat H_2O at 22°C is 42 μsec and decreases to ca. 19 μsec in air-equilibrated neat CH_3CN at 22°C (determined in this work). The consequence is that the doublet-state $\text{Cr}(\text{bpy})_3^{3+}$ species is capable of undergoing a great many more successive encounters with solvent molecules than are possible for the doublet-state R^- species. Analogous data to those in Figure 3-54 for $\text{Cr}(\text{bpy})_3^{3+}$ are presented in Figure 3-56 for the phosphorescence lifetime quenching of R^- in $\text{CH}_3\text{CN}/\text{H}_2\text{O}$ mixtures. The results for R^- show that τ_0 / τ varies linearly with $\eta / \eta_0(\text{H}_2\text{O})$, though

FIGURE 3-55 : Preferential Solvation Data of $\text{trans-Cr}(\text{NH}_3)_2(\text{NCS})_4^-$ at 25°C . Circles denote data from the NMR linewidths of CH_3CN protons; squares show values derived from the NMR linewidths of H_2O protons; reproduced from reference 135.

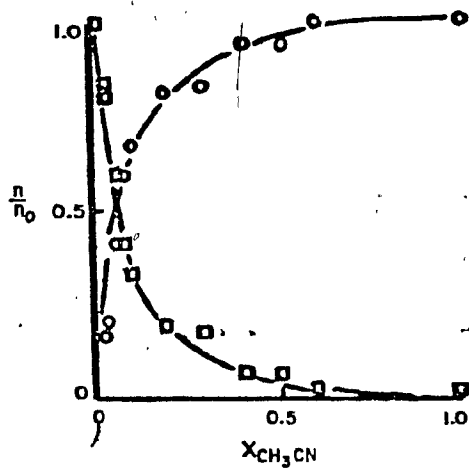
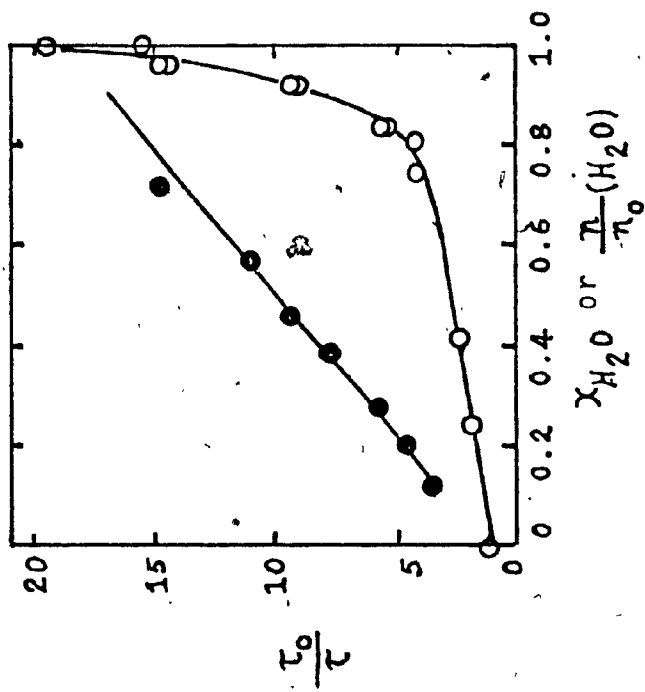
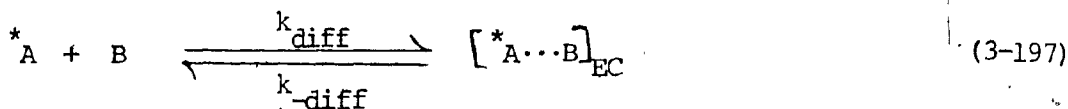


FIGURE 3-56 : Effect of Water on the Emission Lifetimes of trans-
 $\text{Cr}(\text{NH}_3)_2(\text{NCS})_4^-$ in $\text{CH}_3\text{CN}/\text{H}_2\text{O}$ Mixtures. Open circles
denote τ_0/τ vs. Mole Fraction of Water; solid circles
denote τ_0/τ against η/η_0 of water; reproduced (in
part) from reference 132.



the dependence of τ_0/τ on the number of moles of water in the solvation shell in the mixed solvent system, $\chi_{\text{H}_2\text{O}}$, is not a simple one.

It would appear at this point that the behavioral differences between excited-state trans-Cr(NH₃)₂(NCS)₄⁻ and Cr(bpy)₃³⁺ in CH₃CN/H₂O mixtures can be attributed to static vs dynamic effects of the solvent system on the complex ion. Dynamic effects involve diffusional processes wherein the reactant A and solvent B form the encounter complex [^{*}A...B]_{EC} (equivalent to reaction 3-188 at diffusional rates). Therefore, reaction (3-188 becomes (3-197) for an excited-state species ^{*}A. On the other hand,



static effects are dependent on prior physical or chemical "association" between A and B. The following arguments favor static effects of solvent on trans-Cr(NH₃)₂(NCS)₄⁻ and dynamic effects on Cr(bpy)₃³⁺ to account for the photo-sensitivity of chromium(III) complexes to changes in medium composition. (1) The much shorter doublet-state lifetime of R⁻ limits the magnitude of the number of excited-state encounters with solvent molecules; whereas the much longer (²T₁/²E)Cr(bpy)₃³⁺ lifetime increases the probability of such encounters. As a result, ground-state encounter complex formation is favored for trans-Cr(NH₃)₂(NCS)₄⁻ and excited-state encounter complex formation is favored for Cr(bpy)₃³⁺. The increase in the emission lifetime of R⁻ in going from neat H₂O to neat CH₃CN solvent was attributed¹³² to enhanced vibrational communication between R⁻ and hydrogen-bonding solvent molecules. Hydrogen-bond acceptance is possible from the (NH₃) ligand, but not from the (bpy) ligand; hence, analogous behavior

from $\text{Cr}(\text{bpy})_3^{3+}$ is not expected on the basis of hydrogen-bonding ability of the solvent to the complex ion. In terms of observed doublet-state lifetimes, the R^- complex ion would be expected to favor a static process, while $\text{Cr}(\text{bpy})_3^{3+}$ would favor a dynamic process. (2) The linear relationship between τ_0/τ and $\eta/\eta_0(\text{H}_2\text{O})$ for R^- (Figure 3-57) is expected for a static process inasmuch as quenching by H_2O is proportional to the number of 1:1 encounters between R^- and H_2O , and the results in Figure 3-57 have been attributed¹³² to quenching of R^- by H_2O via chemical reaction (photosubstitution). Linearity in η/η_0 for ground-state solvolysis of $\text{Cr}(\text{NCS})_6^{3-}$ was attributed^{135,136} to a 1:1 reaction of the solvolytically-reactive solvent with the complex ion without significant involvement of other solvating molecules. For the $\text{Cr}(\text{bpy})_3^{3+}$ system, a dynamic quenching process is evidenced in the region $0.80 \leq \chi_{\text{CH}_3\text{CN}} \leq 1.0$ (Figure 3-53) where H_2O does not make an important contribution to the population of the ground-state equilibrium solvation shell, and thus does not contribute significantly to the initially-formed excited-state solvation shell. Further, the non-linear preferential solvation curve (Figure 3-50) clearly indicates that if any occupancy by H_2O does occur, it is non-linearly dependent on bulk solvent composition; however, in a dynamic process, the collisional probability will depend on the composition of bulk solvent as long as $\chi_{\text{H}_2\text{O}}$ remains small. In fact, a dynamic quenching process predicts conventional Stern-Volmer plots (equation 3-195, Figure 3-53) as well as parallelism between emission lifetime and intensity quenching measurements.⁶⁵ The similar values of $^2k_q(\text{H}_2\text{O})$ from the lifetime and intensity quenching measurements for $\text{Cr}(\text{bpy})_3^{3+}$ where $0 \leq \chi_{\text{H}_2\text{O}} \leq 0.20$ support a dynamic quenching process for this system.

The results obtained for the quantum yields of photosolvolysis of

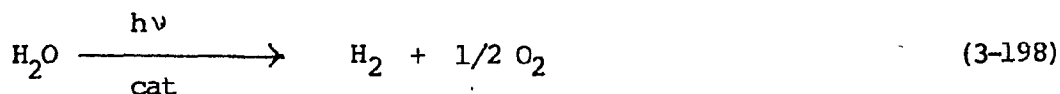
$\text{Cr}(\text{bpy})_3^{3+}$ (Figure 3-54) and R^- cannot be used to argue for or against static or dynamic processes, though a comparison of their photoreactivities in H_2O , CH_3CN and $\text{CH}_3\text{CN}/\text{H}_2\text{O}$ mixtures contributes to an understanding of the relative roles of the quartet and doublet excited states, as well as some of the photophysical properties.

Chen and Porter^{26,137} originally postulated that 50% of the photoaquation of R^- in methanol/water/ethylene glycol (2:1:1) at -65°C occurs directly from the quartet excited state, the remainder occurring from the quartet state subsequent to passing through and return from the unreactive doublet excited states. In room-temperature aqueous solution, $\phi_{\text{rx}} = 0.26$ in CH_3CN .¹³³ Adamson's¹³² investigation of the emission lifetimes and their apparent activation energies in various solvents and solvent mixtures led to the suggestion that the doublet-state lifetime is controlled by a single process - chemical reaction from the doublet state, $2k_{\text{rx}}$. Thus, it was proposed¹³² that the quenchable yield for photoaquation results from direct reaction from the doublet state. An investigation of the relative behavior of the photoaquation and phosphorescence quantum yields for R^- in the temperature range -195 to 25°C was interpreted²⁰ in terms of the presence of a non-radiative decay process which competes with radiative decay but leads to photoaquation; this conclusion suggested reaction from the quartet excited state. A detailed analysis by Shipley and Linck¹³⁸ of the various results support a mechanism for photoaquation in which the quenchable reaction component comes from the quartet excited state subsequent to back-intersystem crossing from the doublet state. As Kirk¹⁵ has recently pointed out, those studies which support direct doublet-state reaction for R^- remain inconclusive.

4.0. CONCLUSIONS.

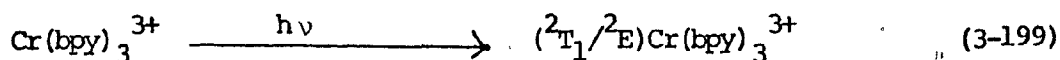
Over the last ten years, the photochemistry of transition metal polypyridyl complexes has been extensively investigated in view of the recognition that these complexes possess several favorable characteristics for incorporation into the development of solar energy conversion and storage schemes. Any endoergic photoreaction is capable of converting light energy into chemical energy. The product of such a reaction, if stable, may be considered a potential fuel to be stored, transported and converted to a material with concomitant evolution of energy.

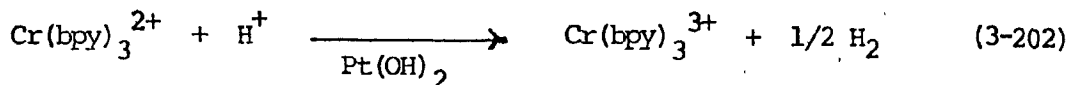
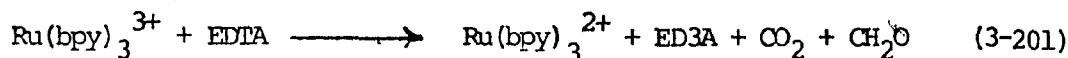
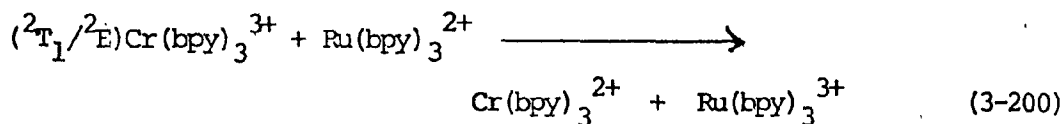
One of the more attractive ways to utilize solar energy is the photocatalysed splitting of water to yield dihydrogen and dioxygen:



Direct photolysis of H_2O with solar radiation is not feasible inasmuch as the absorption spectrum of H_2O does not overlap the solar emission spectrum; thus, the reaction must be sensitized by redox catalysts in some cyclic scheme.

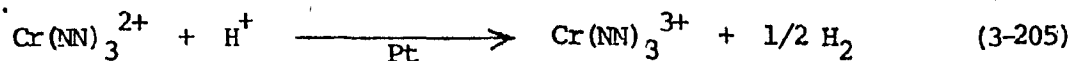
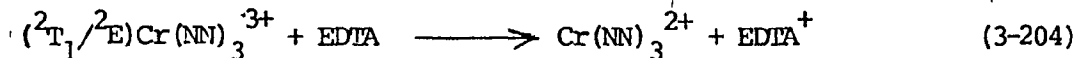
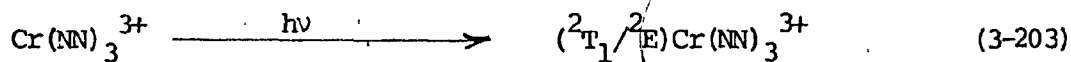
While the vast majority of the investigations on photosensitizer species have focussed on $\text{Ru}(\text{bpy})_3^{2+}$, polypyridyl complexes of $\text{Cr}(\text{III})$ have also been studied. Miller and McLendon¹³⁸ have observed hydrogen evolution from systems incorporating $\text{Cr}(\text{bpy})_3^{3+}$ or $\text{Cr}(4,4'\text{-Me}_2\text{bpy})_3^{3+}$. An aqueous solution (pH 4) containing $\text{Cr}(\text{bpy})_3^{3+}$, $\text{Ru}(\text{bpy})_3^{2+}$, EDTA and $\text{Pt}(\text{OH})_2$ was irradiated (410 - 500 nm) to produce hydrogen with a $\phi \sim 0.002$, based on $\text{Cr}(\text{bpy})_3^{3+}$.¹³⁸ The following reactions were proposed:





An analogous scheme for a system comprised of $Cr(4,4'-Me_2bpy)_3^{3+}$, $Ru(terpy)_2^{2+}$, EDTA and $Pt(OH)_2$ at pH 4.9 has been reported,¹³⁸ with $\phi \leq 0.003$. $Cr(NN)_3^{3+}$ serves as the light harvester because of its higher concentration (than Ru^{2+}) in the system, the Ru^{2+} complex serves as the reductive quencher of $({}^2T_1/{}^2E)Cr(NN)_3^{3+}$, while EDTA acts as the "sacrificial" species to reduce Ru^{3+} prior to back electron transfer between Ru^{3+} and Cr^{2+} . The advantages of $Cr(4,4'-Me_2bpy)_3^{3+}$ over $Cr(bpy)_3^{3+}$ include its longer (${}^2T_1/{}^2E$) lifetime, stronger reducing ability and decreased reactivity toward photosolvolysis.

More recently, Ballardini and coworkers¹³⁹ have reported H_2 evolution from aqueous solutions using $Cr(NN)_3^{3+}$ as the photosensitizer in systems composed of $Cr(NN)_3^{3+}$, EDTA and a platinum catalyst. The reactions are:



The investigation demonstrated that only those $\text{Cr}(\text{NN})_3^{3+}$ complex ions possessing sufficiently negative reduction potentials to reduce H^+ at pH 4.8 were capable of photosensitizing H_2 production. Thus, H_2 evolution was observed for $\text{NN} = \text{phen}$, 4,4'- Me_2bpy , and 4,7- Me_2phen ; yields were ≤ 0.001 , 0.025 and 0.035 ml H_2 /min irradiation, respectively.¹³⁹

Electricity generation is also a potential avenue of use for $\text{Cr}(\text{NN})_3^{3+}$ complexes. Langford and coworkers¹⁴⁰ have observed a cathodic photocurrent in a photoelectrochemical cell upon irradiation, (457 - 514 nm) of 10^{-2} M $\text{Cr}(\text{bpy})_3^{3+}$ in deaerated 0.1 M H_2SO_4 . Employing a transparent n-type SnO_2 semiconductor and a platinum counter electrode, the photocurrent observed results from the reduction of $(^2\text{T}_1/^2\text{E})\text{Cr}(\text{bpy})_3^{3+}$ at the electrode to yield $\text{Cr}(\text{bpy})_3^{2+}$. Addition of a reducing scavenger ($\text{Fe}^{\text{II}}\text{EDTA}$) to the solution caused the photocurrent to become anodic, due to oxidation of $\text{Cr}(\text{bpy})_3^{2+}$ at the platinum electrode.¹⁴⁰ Though the system was not optimized, utilization of complexes with longer lifetimes should increase the efficiency of such a photoelectrochemical cell.

Successful utilization and comprehension of the potential applicability of $\text{Cr}(\text{NN})_3^{3+}$ species as photosensitizers in solar energy conversion and storage schemes necessitates knowledge of the photochemical and photophysical properties of these complexes. As well, these properties are required to elucidate the role(s) of the various excited states in these complex ions. Furthermore, with this knowledge, it is possible to compare the photoreactivity models of $\text{Cr}(\text{NN})_3^{3+}$ with those of other $\text{Cr}(\text{III})$ complexes, as well as other transition metal polypyridyl complexes.

The investigations of the ground-state,¹ and photophysical and photochemical behavior of $\text{Cr}(\text{NN})_3^{3+}$ has allowed for intensive characterization of the lowest excited doublet manifold, including its lifetime, the factors

affecting its lifetime and chemical reactivity, and its chemical reactivity in aqueous and mixed solvent systems. More specifically, the lowest excited state of $\text{Cr}(\text{NN})_3^{3+}$ has been identified as the thermally-equilibrated (${}^2\text{T}_1/{}^2\text{E}$). The observed lifetimes of (${}^2\text{T}_1/{}^2\text{E}$) $\text{Cr}(\text{NN})_3^{3+}$ are relatively long when compared to other Cr(III) complexes and $\text{M}(\text{NN})_3^{n+}$, and vary with the nature of the substituent on the bpy or phen framework. This variation has been attributed to the capability of the ligand to act as both an oscillating perturbation dipole and as an energy acceptor.

The lifetime of (${}^2\text{T}_1/{}^2\text{E}$) $\text{Cr}(\text{NN})_3^{3+}$ is affected by the presence of large concentrations of anions such as $\text{X}^- = \text{ClO}_4^-$, NO_3^- , Cl^- and HSO_4^- . The observed increase in the observed lifetime is attributed to a decrease in both ${}^2k_{\text{rx}}$ and ${}^2k_{\text{nr}}$, with the greater effect on ${}^2k_{\text{rx}}$. The decrease in ${}^2k_{\text{nr}}$ arises from extensive ion-pairing between (${}^2\text{T}_1/{}^2\text{E}$) $\text{Cr}(\text{NN})_3^{3+}$ and X^- which places the anion in the interligand pockets, with the consequence that the vibrational freedom of the ligand and the efficiency of electronic-to-vibrational energy transfer processes are decreased. The decrease in ${}^2k_{\text{rx}}$ results from the occupation of the interligand pockets by the anions as well as in the solvation sphere, which results in decreased access to the Cr(III) core by the water molecule. Ground-state quenching of (${}^2\text{T}_1/{}^2\text{E}$) $\text{Cr}(\text{NN})_3^{3+}$ has also been observed in the presence of added anions. Quenching constants have been evaluated for several $\text{Cr}(\text{NN})_3^{3+}$ species in Cl^- media, as well as for $\text{Cr}(\text{bpy})_3^{3+}$ and $\text{Cr}(\text{phen})_3^{3+}$ in the presence of various anions. The ground-state quenching phenomenon is seen as arising from collision-induced encounter of ground-state ion-paired species with excited-state ion-paired species to form an "ion-bridged excimer".

The long-lived (${}^2\text{T}_1/{}^2\text{E}$) $\text{Cr}(\text{NN})_3^{3+}$ species are capable of engaging in

a wide variety of excited-state bimolecular reactions. Quenching studies have shown that $(^2T_1/{}^2E)Cr(NN)_3^{3+}$ is a strong oxidizing agent. The excited-state redox potentials have been calculated for $(^2T_1/{}^2E)Cr(NN)_3^{3+}$ from the corresponding ground-state potentials and spectroscopic energies. $Cr(NN)_3^{2+}$, the electron transfer product of reductive quenching of $(^2T_1/{}^2E)Cr(NN)_3^{3+}$, have been identified and characterized by their absorption spectra. Several bimolecular electron-transfer quenching reactions have been investigated, along with the energy transfer process which occurs between $(^2T_1/{}^2E)Cr(NN)_3^{3+}$ and molecular oxygen.

Investigations of the photochemical reactivity of $Cr(NN)_3^{3+}$ in aqueous alkaline solution reveal that $(^2T_1/{}^2E)Cr(NN)_3^{3+}$ is produced with near-unitary efficiency from the initially-populated Franck-Condon quartet excited states for irradiation at $\lambda < 450$ nm. $(^2T_1/{}^2E)Cr(NN)_3^{3+}$ undergoes photoaquation via nucleophilic attack by H_2O at the Cr(III) center to yield a seven-coordinate intermediate, $Cr(NN)_3(H_2O)^{3+}$. Deprotonation of $Cr(NN)_3(H_2O)^{3+}$, followed by ring-opening, leads irreversibly and quantitatively to the observed products, $Cr(NN)_2(OH)_2^+$ and (NN) . The pH and temperature profiles of ϕ_{rx} for the $(^2T_1/{}^2E)Cr(NN)_3^{3+}$ (NN = bpy and phen) photoaquation reaction at pH 9 - 10.5 implicate a reaction mechanism similar to the thermal aquation of these complexes.¹

On quenching > 99.9% of the $(^2T_1/{}^2E)Cr(bpy)_3^{3+}$ photoaquation reaction with iodide ion, there remains an unquenchable reaction component which presumably originates from the short-lived quartet excited state. This unquenchable component has been observed for NN = bpy and phen. Studies of the pH and temperature profiles of the unquenchable reaction component of $Cr(bpy)_3^{3+}$ indicate that reaction mechanism is indistinguishable from that proposed for the $(^2T_1/{}^2E)$ and 4A_2 aquation reactions. Temperature

dependence studies of the unquenchable reaction component for $\text{Cr}(\text{phen})_3^{3+}$ were not easy to rationalize inasmuch as Arrhenius-type plots were non-linear.

The wavelength dependence of the quenchable and unquenchable reaction components, as well as the phosphorescence intensity, of $\text{Cr}(\text{bpy})_3^{3+}$ was investigated in the 313 - 611 nm region in order to determine if a chemical reaction and/or a prompt intersystem crossing process was capable of competing with vibrational relaxation down the quartet excited state manifold. A coincidental sharp decrease in ${}^4\text{T}_2$ ϕ_{rx} , ${}^4\text{T}_1$ ϕ_{rx} and I' at 470 - 510 nm was observed. The results have been interpreted in terms of the presence of prompt intersystem crossing to (${}^2\text{T}_1/{}^2\text{E}$) in the 500-nm region, along with prompt chemical reaction from some higher quartet vibrational level than ${}^4\text{T}_2^0$. The reactive pathway presumably leads to some species having trigonal prismatic geometry.

Examination of the photosolvolytic of $\text{Cr}(\text{bpy})_3^{3+}$ in $\text{CH}_3\text{CN}/\text{H}_2\text{O}$ mixtures reveals the preferential solvation of $\text{Cr}(\text{bpy})_3^{3+}$ by CH_3CN , although no simple model can account for its reactivity. However, a detailed comparison of the $\text{Cr}(\text{bpy})_3^{3+}$ system with that of $\text{Cr}(\text{NH}_3)_2(\text{NCS})_4^-$ in the same solvent system suggests that dynamic effects predominate in the $\text{Cr}(\text{bpy})_3^{3+}$ system whereas static effects are responsible for the behavior of $\text{Cr}(\text{NH}_3)_2(\text{NCS})_4^-$. Additionally, it is not necessary to invoke a photosubstitution mechanism different from that in aqueous media for the mixed solvent system.

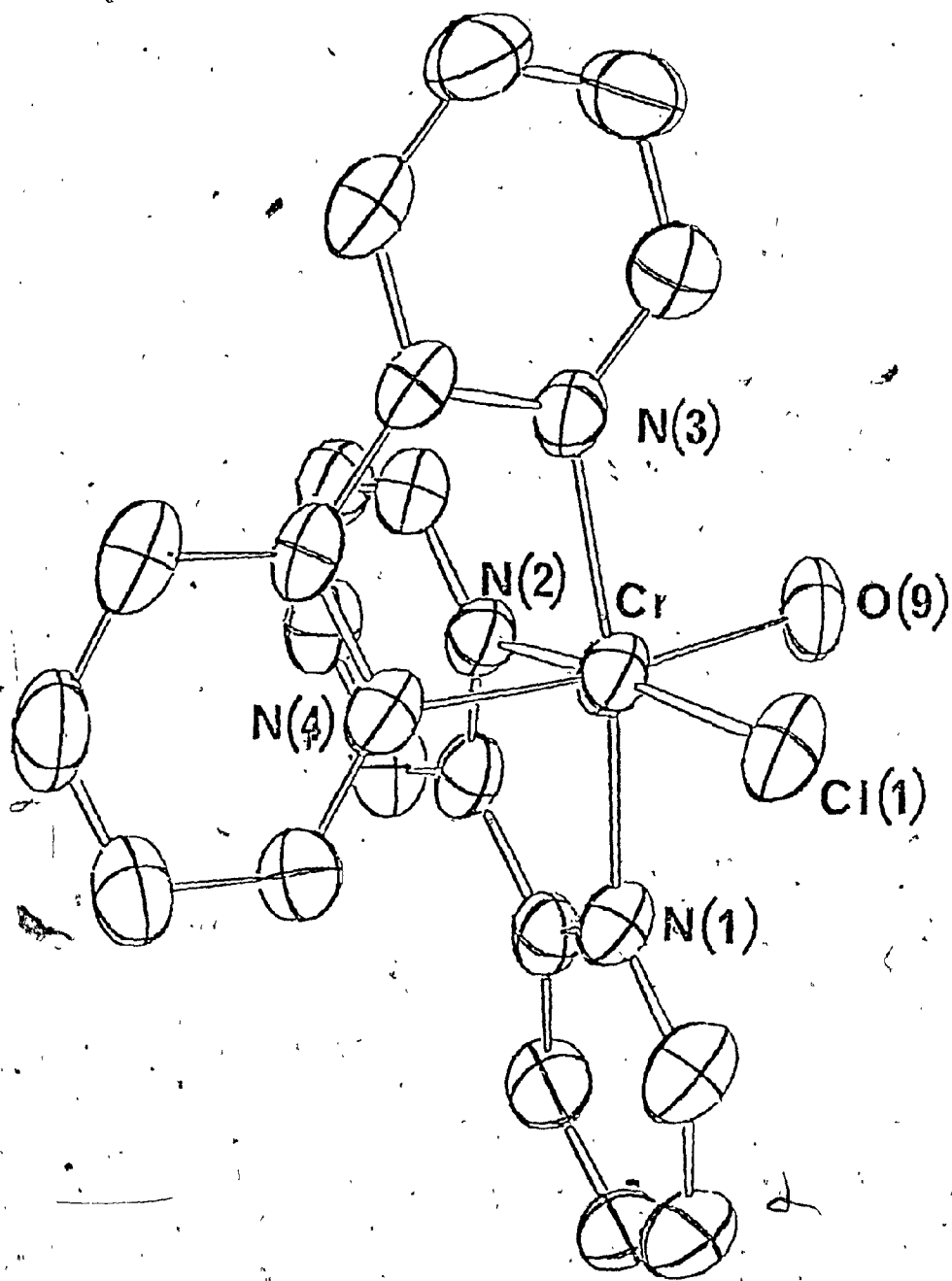
ADDENDA

Characterization of the Chromium(III) Product from the Reaction
Between CrCl_2 and 2,2'-bipyridine Under Slow Oxidation.

The bright yellow $[\text{Cr}(\text{bpy})_3](\text{ClO}_4)_3 \cdot 1/2 \text{H}_2\text{O}$ compound is usually prepared by a modified procedure of Baker and Mehta,⁸⁹ in which an oxygen-free, acidic CrCl_2 solution is added to an oxygen-free aqueous suspension of 2,2'-bipyridine. The resulting dark suspension, $\text{Cr}(\text{bpy})_3(\text{ClO}_4)_2$, is subsequently oxidized with chlorine gas to yield the bright yellow crude product. However, in the synthesis of this compound, a pink product was often obtained. It was of interest to examine the nature of this product, which presumably arises from the slow oxidation of $\text{Cr}(\text{bpy})_3^{2+}$.

The X-ray crystal structure of this pink product (Figure 3-57) was kindly determined by W.A. Wickramasinghe and P.H. Bird. Their results show that this product is $[\text{Cr}(\text{bpy})_2(\text{H}_2\text{O})\text{Cl}](\text{ClO}_4)_3 \cdot 2\text{H}_2\text{O}$. The molecular geometry about the central chromium atom consists of two bidentate bipyridyl ligands, and a chloro group and a H_2O molecule in a cis position. The Cr-N [N(1), N(3), N(4)] distances are $2.037 \pm 0.005 \text{ \AA}$, except for the Cr-N(2) bond distance which is $2.059(5) \text{ \AA}$. The longer Cr-N(2) bond distance probably is due to a small trans influence by the chloro-group. The Cr-Cl and Cr-O(9) (water) bond distances are $2.259(2)$ and $1.975(4) \text{ \AA}$, respectively; C-N distances are $1.34 \pm 0.01 \text{ \AA}$. Intra-ligand N-Cr-N bond angles are $79.0(2)^\circ$ and $79.6(2)^\circ$, which are comparable to the corresponding angles found for $\text{Cu}(\text{bpy})_3^{2+}$.¹⁴² The two water molecules are hydrogen-bonded¹⁴³ to the coordinated water; O(9)-O(water) distances are 2.67 and 2.64 \AA . There are six ClO_4^- units about the $\text{Cr}(\text{bpy})_2(\text{H}_2\text{O})\text{Cl}^{2+}$ cation within 3.3 \AA of a non-hydrogen atom. One of these ClO_4^- species has oxygen atoms wedged in the pocket defined by the two bipyridyl ligands, reminiscent of ion-pairing in the solid state.¹⁴⁴

FIGURE 3-57 : Geometry of the cis-Cr(bpy)₂(H₂O)Cl²⁺ Cation; made available by N. Serpone.



Further (spectrophotometric) characterization was afforded by recording the visible absorption spectrum of the pink product in acidic and basic media. In 0.01 M OH^- solution, the spectrum reveals a broad band at 550 nm ($\epsilon = 65$) which sharpens and blue shifts to 520 nm ($\epsilon = 56$) in 0.01 M HCl. By comparison, the $\text{Cr}(\text{bpy})_2(\text{OH})_2^+$ complex cation has the corresponding band at 518 nm ($\epsilon = 49$) and $\text{Cr}(\text{bpy})_2(\text{H}_2\text{O})_2^{3+}$ at 492 nm ($\epsilon = 48$).¹⁰ Furthermore, the visible absorption spectrum of $\text{Cr}(\text{bpy})_2(\text{H}_2\text{O})_2^{3+}$ exhibits bands at ~ 490 nm ($\epsilon = 40$) which red-shifts to ~ 520 nm ($\epsilon = 40$) upon addition of base.¹⁴⁵ Thus, in acidic media, the pink product species exists as $\text{Cr}(\text{bpy})_2(\text{H}_2\text{O})\text{Cl}^{2+}$, and in basic media as $\text{Cr}(\text{bpy})_2(\text{OH})\text{Cl}^+$. The spectral observations for the $\text{Cr}(\text{bpy})_2(\text{H}_2\text{O})\text{Cl}^{2+}$ complex ion are consistent with expectations since Cl affords a weaker ligand field than either OH^- or H_2O , and thus d-d transitions occur at longer wavelengths (i.e., lower energies). Interestingly, Tucker and co-workers¹⁴⁶ reported the same compound $[\text{Cr}(\text{bpy})_2(\text{H}_2\text{O})\text{Cl}](\text{ClO}_4)_2 \cdot 2\text{H}_2\text{O}$ prepared from a complicated electrolytic reduction procedure. Elemental analyses for C, H, N, Cr and total Cl were in good agreement with calculated values; a test for free Cl^- was positive only after heating the salt, but no spectral data were reported. Ng and Garner¹⁴⁷ have synthesized cis- $\text{Cr}(\text{bpy})_2(\text{H}_2\text{O})\text{Cl}^{2+}$ by aquation of the cis-dichloro complex and isolated it in aqueous solution by cation exchange chromatography. Visible absorption spectra for the $\text{Cr}(\text{bpy})_2(\text{H}_2\text{O})\text{Cl}^{2+}$ and $\text{Cr}(\text{bpy})_2(\text{H}_2\text{O})_2^{3+}$ species in 4 F HCl reveal d-d bands at 517 nm ($\epsilon = 43.5$) and 492 nm ($\epsilon = 44.5$), respectively.

As a further examination of the nature of the pink product, the pK_a values of $\text{Cr}(\text{bpy})_2(\text{H}_2\text{O})\text{Cl}^{2+}$ and $\text{Cr}(\text{phen})_2(\text{H}_2\text{O})_2^{3+}$ were determined under identical conditions; it was assumed that the pK_a values of $\text{Cr}(\text{bpy})_2(\text{H}_2\text{O})_2^{3+}$

and the analogous phen complex would be very nearly the same. Thus, in 1.0 M NaNO_3 solution, the potentiometric titration of $\text{Cr}(\text{bpy})_2(\text{H}_2\text{O})\text{Cl}^{2+}$ gave a curve typical of a monobasic acid, with $\text{pK}_a = 4.6$ (error ≈ 0.2). Under identical conditions, the potentiometric titration of $\text{Cr}(\text{phen})_2(\text{H}_2\text{O})_2^{3+}$ yielded a curve reminiscent of a dibasic acid with $\text{pK}_1 = 3.0$ and $\text{pK}_2 = 6.0$ (error ≈ 0.2). These latter results are in good agreement with those reported by Inskip and Bjerrum¹⁴⁵ for which $\text{pK}_1 = 3.5$ and $\text{pK}_2 = 6.1$ in 0.1 M NaNO_3 for the $\text{Cr}(\text{phen})_2(\text{H}_2\text{O})_2^{3+}$ cation.

5.0. REFERENCES.

1. M.A. Jamieson, "A Kinetic Investigation of the Hydrolysis of Tris-(1,10-phenanthroline)chromium(III) and Tris(2,2'-bipyridyl)chromium(III) and the Preparation of Some New Chromium(III) polypyridyl Complexes", M.Sc. Thesis, Concordia Univ., Montreal, April, 1978.
2. C. Mongay and V. Cerda, *Ann. Chim. (Paris)*, 64, 409 (1974).
3. R.C. Weast, Ed., "CRC Handbook of Chemistry and Physics", 51st Edition, 1970-1971, The Chemical Rubber Company, Cleveland, Ohio. The densities of CH_3CN and H_2O were taken as 0.78 g/ml at 20°C and 0.99707 g/ml at 25°C , respectively.
4. J. Demas and C.M. Flynn, Jr., *Anal. Chem.*, 48, 353 (1976).
5. E.E. Wegner and A.W. Adamson, *J. Am. Chem. Soc.*, 88, 394 (1966).
6. C.A. Parker, "Photochemistry of Solutions", Elsevier Co., New York, N.Y., 1968.
7. J.G. Calvert and J.N. Pitts, Jr., "Photochemistry", J. Wiley and Sons, New York, N.Y., 1966.
8. E. Konig and S. Herzog, *J. Inorg. Nucl. Chem.*, 32, 585 (1970).
9. J. Josephsen and C.E. Schaffer, *Acta Chem. Scand.*, Ser. A, A31, 813 (1977).
10. M. Maestri, F. Bolletta, N. Serpone, L. Moggi and V. Balzani, *Inorg. Chem.*, 15, 2048 (1976).
11. R.D. Gillard, *Coord. Chem. Rev.*, 16, 67 (1975).
12. R.J. Watts, J.S. Harrington and J. Van Houten, *J. Am. Chem. Soc.*, 99, 2179 (1977).
13. G.W. Bushnell, K.R. Dixon and M.A. Khan, *Can. J. Chem.*, 52, 1367 (1974).
14. P.D. Fleischauer, A.W. Adamson and G. Sartori, *Progr. Inorg. Chem.*, 17, 1 (1972).
15. A.D. Kirk, *Coord. Chem. Rev.*, 39, 225 (1981).
16. V. Balzani and V. Carassiti, "Photochemistry of Coordination Compounds", Academic Press, New York, (1970).
17. G.B. Porter and H.L. Schlafer, *Z. Phys. Chem. (Frankfurt)*, 37, 104 (1963).
18. G.B. Porter, S.N. Chen, H.L. Schlafer and H. Gausmann, *Theor. Chim. Acta*, 20, 81 (1971).

19. A.D. Kirk and G.B. Porter, *J. Phys. Chem.*, 84, 887 (1980).
20. A.W. Adamson, *J. Phys. Chem.*, 71, 798 (1967).
21. A.W. Adamson, *Pure & Appl. Chem.*, 51, 313 (1979).
22. H.L. Schlafer, *J. Phys. Chem.*, 69, 2201 (1965).
23. R.A. Plane and J.P. Hunt, *J. Am. Chem. Soc.*, 79, 3343 (1957).
24. R.A. Plane and M.R. Edelson, *J. Phys. Chem.*, 63, 327 (1959).
25. R.A. Plane and MR. Edelson, *Inorg. Chem.*, 3, 231 (1964).
26. S. Chen and G.B. Porter, *Chem. Phys. Lett.*, 6, 41 (1971).
27. C.H. Langford and L. Tipping, *Can. J. Chem.*, 50, 887 (1972).
28. R. Ballardini, G. Varani, F. Wasgestian, L. Moggi and V. Balzani, *J. Phys. Chem.*, 77, 2947 (1973).
29. M.C. Cimolino and R.G. Linck, *Inorg. Chem.*, 20, 3499 (1981).
30. R. Fukuda, R.T. Walters, H. Macke and A.W. Adamson, *J. Phys. Chem.*, 83, 2097 (1979).
31. X. Yang, C.A. Sutton and C. Kotal, *Inorg. Chem.*, 21, 2893 (1982).
32. F. Wasgestian, *Ber. Bunsenges. Phys. Chem.*, 75, 1143 (1971).
33. N.A.P. Kane-Maguire and C.H. Langford, *J. Am. Chem. Soc.*, 94, 2125 (1972).
34. R. Sasseville and C.H. Langford, *J. Am. Chem. Soc.*, 101, 5834 (1979).
35. A.D. Kirk, P.E. Hoggard, G.B. Porter, M.G. Rockley and M.W. Windsor, *Chem. Phys. Lett.*, 37, 199 (1976).
36. N.A.P. Kane-Maguire, J.P. Phifer and G.C. Toney, *Inorg. Chem.*, 15, 593 (1976).
37. H.L. Schlafer, *Z. Phys. Chem. (Frankfurt)*, 11, 65 (1957).
38. M. Maestri, F. Bolletta, L. Moggi, V. Balzani, M.S. Henry and M.Z. Hoffman, *J. Am. Chem. Soc.*, 100, 2694 (1978).
39. M.S. Henry and M.Z. Hoffman, personal communication.
40. A.D. Liehr, *J. Phys. Chem.*, 67, 1314 (1963).
41. J.R. Perumareddi, *Coord. Chem. Rev.*, 4, 73 (1969).
42. T. Ohno and S. Kato, *Bull. Chem. Soc. Japan*, 43, 8 (1970); *ibid.*, 46, 1602 (1973).

43. N.A.P. Kane-Maguire, J. Conway and C.H. Langford, *J. Chem. Soc., Chem. Commun.*, 801 (1974).
44. C.T. Lin, W. Bottcher, M. Chou, C. Creutz and N. Sutin, *J. Am. Chem. Soc.*, 99, 6536 (1976).
45. D. Nicollin, P. Bertels and J.A. Koningstein, *Can. J. Chem.*, 58, 1334 (1980).
46. M. Asano and J.A. Koningstein, *J. Chem. Phys.*, 73, 688 (1980).
47. R. Sriram, M.Z. Hoffman and N. Serpone, *J. Am. Chem. Soc.*, 103, 997 (1981).
48. A.D. Kirk and G.B. Porter, *J. Phys. Chem.*, 84, 887 (1980).
49. M.S. Henry and M.Z. Hoffman, *Adv. Chem. Ser.*, 168, 91 (1978).
50. M.S. Henry, *J. Am. Chem. Soc.*, 99, 6138 (1977).
51. J. Van Houten and G.B. Porter, *Inorg. Chem.*, 18, 2053 (1978).
52. F. Bolletta, M. Maestri and V. Balzani, *J. Phys. Chem.*, 80, 2499 (1976).
53. L. Johansson, *Chem. Scr.*, 9, 30 (1976); *ibid.*, 10, 72 (1976).
54. J.B. Birks, "Photophysics of Aromatic Molecules", Wiley-Interscience, New York, 1970.
55. N.A.P. Kane-Maguire and C.H. Langford, *Inorg. Chem.*, 15, 464 (1976).
56. V. Balzani, F. Bolletta, M.T. Gandolfi and M. Maestri, *Topics in Curr. Chem.*, 75, 1 (1978).
57. J.F. Endicott, in "Concepts in Inorganic Photochemistry", A.W. Adamson and P.D. Fleischauer, Eds., John Wiley, New York, 1975.
58. R. Memming, *J. Electrochem. Soc.*, 116, 785 (1969).
59. H. Shizuka and H. Ouchi, *J. Phys. Chem.*, 86, 1297 (1982).
60. C.K. Jorgensen, "Absorption Spectra and Chemical Bonding in Complexes", Pergamon Press, Oxford, 1962.
61. M.J. Blandamer and M.F. Fox, *Chem. Rev.*, 70, 59 (1970).
62. A.D. Kirk and G.B. Porter, *J. Phys. Chem.*, 84, 2998 (1980).
63. D.R. Stranks, *Pure & Appl. Chem.*, 38, 303 (1974).

64. F.B. Ueno, Y. Sasaki, T. Ito and K. Saito, *J. Chem. Soc., Chem. Commun.*, 328 (1982).
65. V. Balzani, L. Moggi, M.F. Manfrin, F. Bolletta and G.S. Lurance, *Coord. Chem. Rev.*, 15, 321 (1975).
66. A.A. Lamola, in "Energy Transfer and Organic Photochemistry", A.A. Lamola and N.J. Turro, Eds., Interscience, New York, 1969.
67. N.J. Turro, J.C. Dalton and D.S. Weiss, in "Organic Photochemistry", Vol. 2, O.L. Chapman, Ed., Marcel Dekker, New York, 1969.
68. A. Yekta and N.J. Turro, *Chem. Phys. Lett.*, 17, 31 (1972).
69. A. Pfeil, *J. Am. Chem. Soc.*, 93, 5395 (1971).
70. H. Linschitz and L. Pekkarinen, *J. Am. Chem. Soc.*, 82, 2411 (1960).
71. C. Steel and H. Linschitz, *J. Phys. Chem.*, 66, 2577 (1962).
72. T.L. Banfield and D. Hussain, *Trans. Faraday Soc.*, 63, 1985 (1969).
73. T. Ohno and S. Kato, *Bull. Chem. Soc. Japan*, 42, 3385 (1969).
74. H.F. Wastegian and G.S. Hammond, *Theor. Chim. Acta*, 20, 186 (1971).
75. A. Adamczyk and F. Wilkinson, *J. Chem. Soc., Faraday Trans. 2*, 68, 2031 (1972).
76. F. Bolletta, M. Maestri, L. Moggi and V. Balzani, *J. Am. Chem. Soc.*, 95, 7864 (1973).
77. J.N. Demas and A.W. Adamson, *J. Am. Chem. Soc.*, 93, 1800 (1971).
78. I. Fujita and H. Kobayashi, *Ber. Bunsenges. Phys. Chem.*, 76, 115 (1972).
79. R.A. Marcus, *J. Chem. Phys.*, 24, 966 (1956).
80. R.A. Marcus, *Ann. Rev. Phys. Chem.*, 15, 155 (1964).
81. D. Rehm and A. Weller, *Ber. Bunsenges. Phys. Chem.*, 73, 834 (1969).
82. D. Rehm and A. Weller, *Isr. J. Chem.*, 8, 259 (1970).
83. C. Creutz and N. Sutin, *J. Am. Chem. Soc.*, 99, 241 (1977).
84. R.A. Marcus, *J. Phys. Chem.*, 43, 2654 (1965).
85. R.A. Marcus, *J. Phys. Chem.*, 43, 679 (1965).
86. B. Brunshwig and N. Sutin, *J. Am. Chem. Soc.*, 100, 7568 (1978).

87. N. Sutin, in "Tunneling in Biological Systems", B. Chance, Ed., Academic Press, New York (1979).
88. T. Sagi and S. Aoyagui, *Electroanal. Chem. Interfac. Electrochem.*, 60, 1 (1975).
89. B.R. Baker and B.D. Mehta, *Inorg. Chem.*, 4, 848 (1965).
90. M.C. Hughes and D.J. Macero, *Inorg. Chem.*, 13, 2739 (1974).
91. C.T. Lin and N. Sutin, *J. Phys. Chem.*, 80, 97 (1976).
92. C.R. Bock, T.J. Meyer and D.G. Whitten, *J. Am. Chem. Soc.*, 97, 2909 (1975).
93. R. Ballardini, G. Varani, M.T. Indelli, F. Scandola and V. Balzani, *J. Am. Chem. Soc.*, 100, 7219 (1978).
94. P. Delaive, J.T. Lee, H. Abruna, H.W. Sprintschnik, T.J. Meyer, and D.G. Whitten, *Adv. Chem. Ser.*, 168, 28 (1978).
95. R. Ballardini, G. Varani, F. Scandola and V. Balzani, *J. Am. Chem. Soc.*, 98, 7432 (1976).
96. F. Bolletta, M. Maestri, L. Moggi and V. Balzani, *J. Chem. Soc., Chem. Commun.*, 901 (1975).
97. A. Juris, M.F. Manfrin, M. Maestri and N. Serpone, *Inorg. Chem.*, 17, 2258 (1978).
98. C. Creutz, *Inorg. Chem.*, 17, 1046 (1978).
99. G.J. Ferraudi and J.F. Endicott, *Inorg. Chim. Acta*, 37, 219 (1979).
100. J.F. Endicott and G.J. Ferraudi, *J. Am. Chem. Soc.*, 99, 5812 (1977).
101. J. Silverman and R.W. Dodson, *J. Phys. Chem.*, 56, 846 (1952).
102. R.A. Marcus and N. Sutin, *Inorg. Chem.*, 14, 213 (1975).
103. Y. Saito, J. Takemoto, B. Hutchinson and K. Nakamoto, *Inorg. Chem.*, 11, 2003 (1972).
104. I. Fujita, T. Yazaki, Y. Torii and H. Kobayashi, *Bull. Chem. Soc. Japan*, 45, 2156 (1972).
105. Y. Narisawa, M. Kimura and K. Nakano, *Bull. Chem. Soc. Japan*, 47, 2017 (1974).
106. P.M. Lutz, G.J. Long and W.A. Baker, Jr., *Inorg. Chem.*, 8, 2529 (1969).
107. C.K. Jorgensen, "Oxidation Numbers and Oxidation States", Springer, New York, 1969.

108. "Sadtler Index of UV Spectra", Sadtler Research Laboratories, Inc., 1967.
109. V. Balzani and F. Bolletta, *J. Am. Chem. Soc.*, 100, 7404 (1978).
110. F. Wilkinson and A. Farnilo, *J. Chem. Soc., Faraday Trans. 2*, 72, 604 (1976).
111. D.O.L. Gijzeman, F. Kaufman and G. Porter, *J. Chem. Soc., Faraday Trans. 2*, 69, 708 (1973), and references therein.
112. D.R. Kearns, *Chem. Rev.*, 71, 395 (1971).
113. C.S. Foote, *Accts. Chem. Res.*, 1, 104 (1968).
114. K. Gollnick, *Adv. Photochem.*, 6, 1 (1968).
115. J.N. Demas, E.W. Harris, C.M. Flynn and D. Diemente, *J. Am. Chem. Soc.*, 97, 3838 (1975).
116. J.N. Demas, E.W. Harris and R.P. McBride, *J. Am. Chem. Soc.*, 99, 3547 (1977).
117. J.S. Winterle, D.S. Kliger and G.S. Hammond, *J. Am. Chem. Soc.*, 98, 3719 (1976).
118. C. Herzberg, "Spectra of Diatomic Molecules", Van Nostrand, Princeton, New Jersey, 1950.
119. W. Siebrand, *J. Chem. Phys.*, 44, 4055 (1966); *ibid.*, 46, 440 (1967); *ibid.*, 47, 2411 (1967).
120. D. Sandrini, M.T. Gandolfi, L. Moggi and V. Balzani, *J. Am. Chem. Soc.*, 100, 1463 (1978).
121. S. Glasstone, K.J. Laidler and H. Eyring, "The Theory of Rate Processes", McGraw-Hill, New York, New York, 1941.
122. G.B. Porter and J. Van Houten, *Inorg. Chem.*, 19, 2903 (1980).
123. B.R. Hollebone, C.H. Langford and N. Serpone, *Coord. Chem. Rev.*, 39, 181 (1981).
124. C.H. Langford and R.L.P. Sasseville, *Inorg. Chem.*, 19, 2850 (1980).
125. N.A.P. Kane-Maguire, D.E. Richardson and C.J. Toney, *J. Am. Chem. Soc.*, 98, 3996 (1976).
126. A.D. Kirk, L.A. Frederick and S.G. Glover, *J. Am. Chem. Soc.*, 102, 7120 (1980).
127. R.T. Walters and A.W. Adamson, *Acta Chem. Scand., Ser. A*, A33, 53 (1979).

128. D.L. Kepert, *Inorg. Chem.*, 11, 1561 (1972).
129. M.W. Hersey, "Preferential Solvation and the Photochemical Behavior of the Tris(2,2'-bipyridine)Chromium(III) Ion in Mixed Solvents", Undergraduate Thesis, Carleton Univ., Ottawa, 1979.
130. L.S. Frankel, C.H. Langford and T.R. Stengle, *J. Phys. Chem.*, 74, 1376 (1970).
131. C.H. Langford and T.R. Stengle, "NMR of Paramagnetic Molecules", G.N. LaMar, W. Harrocks and R.H. Holm, Eds., Academic Press, New York, 1973, Chapter 9.
132. A.R. Gutierrez and A.W. Adamson, *J. Phys. Chem.*, 82, 902 (1978).
133. M. Cusumano and C.H. Langford, *Inorg. Chem.*, 17, 2222 (1978).
134. C.F.C. Wong and A.D. Kirk, *Can. J. Chem.*, 54, 3794 (1976).
135. V.S. Sastri, R.W. Herwood, S. Behrendt and C.H. Langford, *J. Am. Chem. Soc.*, 94, 753 (1972).
136. C.H. Langford and J.P.K. Tong, *Accts. Chem. Res.*, 10, 258 (1977).
137. S.N. Chen and G.B. Porter, *J. Am. Chem. Soc.*, 92, 3196 (1970).
138. N.J. Shipley and R.G. Linck, *J. Phys. Chem.*, 84, 2490 (1980).
139. D.S. Miller and G. McLendon, 178th Am. Chem. Soc. National Meeting, Washington D.C., September, 1979, INOR-119.
140. R. Ballardini, A. Juris, G. Varani and V. Balzani, *Nouv. J. Chim.*, 4, 563 (1980).
141. M.W. Hersey, T.J. Vandermoot, and C.H. Langford, *Inorg. Chim. Acta*, 29, 1233 (1978).
142. O.P. Anderson, *J. Chem. Soc., Dalton Trans.*, 2579 (1979); *ibid*, 1237 (1973).
143. S.N. Vinogradov and R.H. Linnell, "Hydrogen Bonding", Van Nostrand Reinhold Co., New York, 1971, pp. 177.
144. W. Wickramasinghe, P.H. Bird, M.A. Jamieson and N. Serpone, *J. Chem. Soc., Chem. Commun.*, 798 (1979).
145. R.G. Inskoop and J. Bjerrum, *Acta Chem. Scand.*, 15, 62 (1961).
146. B.V. Tucker, I.M. Fitzgerald, L.G. Hargis, L.B. Rogers, *J. Electroanal. Chem.*, 13, 400 (1967).
147. S.Y.J. Ng and C.S. Garner, *Inorg. Chim. Acta*, 5, 365 (1971).

CONCORDIA UNIVERSITY

CURRICULUM VITAE

1. Name: Mary Alain JAMIESON

2. Address: 5526 Ashdale Avenue, apt. no. 114,
Cote St. Luc, Quebec, Canada H4W 2B7

Date of Birth: May 2, 1951

Place of Birth: Oslo, Norway First Language: English

3. Thesis Title : THE PHOTOCHEMICAL AND PHOTOPHYSICAL CHARACTERIZATION
OF CHROMIUM(III) POLYPYRIDYL COMPLEXES IN FLUID
MEDIA.

Department: Chemistry Thesis Supervisor: Dr. Nick Serpone

Major Area of Study: Inorganic Photochemistry and Photophysics.

4. University Education:

<u>Degree</u>	<u>Major Subject</u>	<u>University (year)</u>
Bachelor of Science	Chemistry	Concordia (1975)
Master of Science	Chemistry	Concordia (1978)

5. Experience:

<u>Dates</u>	<u>Institution</u>	<u>Responsibility</u>
1975 - 1980 (academic terms)	Concordia	Teaching Assistant
1973 (summer)	Hoffman LaRoche	Summer Research Assistant
1974 (summer)	General Foods	Summer Technician
1982 (Jan.-May)	Dawson College	Lecturer, Chemistry 111

6. Publications:

"Hydroxide Ion assisted Aquation of Tris-(2,2'-bipyridine)chromium-
(III) Ion", Mary A. Jamieson, N. Serpone, and M. Maestri, Inorg.
Chem., 17, 2432 (1978).

"Oxygen Quenching of Metal-centered Excited States of Polypyridyl
Complexes of Chromium(III)", N. Serpone and M.A. Jamieson, and
M.Z. Hoffman, Inorg. Chim. Acta, 31, 1447 (1978).

"Temperature-dependence of the Photoaquation of Tris-(2,2'-bipyridine) chromium(III) Ion in Alkaline Solution", M.A. Jamieson, N. Serpone, M.S. Henry and M.Z. Hoffman, *Inorg. Chem.*, 18, 214 (1978).

"Excited State Behavior of Polypyridyl Complexes of Chromium(III)", N. Serpone; M.A. Jamieson, M.S. Henry, M.Z. Hoffman, F. Bolletta and M. Maestri, *J. Am. Chem. Soc.*, 101, 2907 (1979).

"Interligand Pockets in Polypyridyl Complexes. The Crystal and Molecular Structure of the $\text{Cr}(2,2',2''\text{-terpyridine})_2^{3+}$ Ion", W. Wickramasinghe, P.H. Bird, M.A. Jamieson and N. Serpone, *J. Chem. Soc., Chem. Commun.*, 798 (1979).

"Ground-State Quenching of the 2E Excited State of $\text{Cr}(\text{bpy})_3^{3+}$ and $\text{Cr}(\text{phen})_3^{3+}$ ", R. Sriram, M.Z. Hoffman, M.A. Jamieson, N. Serpone, *J. Am. Chem. Soc.*, 102, 1754 (1980).

"Chromium(II)-Polypyridyl Complexes: Formation, Spectra, and Electron Transfer Kinetics", N. Serpone, M.A. Jamieson, S.S. Emmi, P.G. Fucchi, Q.G. Mulazzani and M.Z. Hoffman, *J. Am. Chem. Soc.*, 103, 1091 (1981).

"Oxidative Substitution Reaction of the Osmochrome $\text{Os}(\text{OEP})[(\text{OMe})_3]_2$ in Chlorinated Solvents", N. Serpone, M.A. Jamieson and T. Netzel, *J. Photochemistry*, 15, 295 (1981).

"Photophysics and Photochemistry of Polypyridyl Complexes of Chromium(III)", N. Serpone, M.A. Jamieson, R. Sriram and M.Z. Hoffman, *Inorg. Chem.*, 20, 3983 (1981).

" $^4T_2 \rightarrow ^2E$ Intersystem Crossing Efficiency in the $\text{Cr}(\text{bpy})_3^{3+}$ and $\text{Cr}(\text{phen})_3^{3+}$ Ions in Aqueous Media", N. Serpone, M.A. Jamieson and M.Z. Hoffman, *J. Chem. Soc., Chem. Commun.*, 1006 (1980)

"Advances in the Photochemistry and Photophysics of Chromium(III) Polypyridyl Complexes in Fluid Media", M.A. Jamieson, and N. Serpone, and M.Z. Hoffman, *Coord. Chem. Rev.*, 39, 121 (1981).

"Characterization of the Chromium(III) Product from the Reaction Between CrCl_2 and 2,2'-bipyridine Under Slow Oxidation", W.A. Wickramasinghe, P.H. Bird, M.A. Jamieson, N. Serpone and M. Maestri, *Inorg. Chim. Acta*, 64, L85 (1982).

"Medium Effects in Cr(III) Photochemistry: Dynamic vs Static Processes in tris-(bipyridine) Chromium(III) and trans-diammine tetrathiocyanato Chromium(III) Ions in $\text{CH}_3\text{CN}/\text{H}_2\text{O}$ Mixtures", M.A. Jamieson, C.H. Langford, N. Serpone, and M.W. Hersey, accepted for publication.

"Covalent Hydration and Pseudo-base Formation in Transition Metal Polypyridyl Complexes. Reality or Myth?", N. Serpone, G. Ponterini, M.A. Jamieson, F. Bolletta and M. Maestri, *Coord. Chem. Rev.*, accepted for publication.

"Photochemical, Photophysical, and Thermal Behavior of Tris-(1,10-phenanthroline) Chromium(III) Ion in Aqueous Solution", F. Bolletta, M. Maestri, L. Moggi, M.A. Jamieson, N. Serpone, M.S. Henry and M.Z. Hoffman, submitted for publication.

Communications Presented at Conferences:

"Lifetimes and photoaquation quantum yields of polypyridyl Cr(III) Complexes", N. Serpone, M.A. Jamieson, M.Z. Hoffman and R. Sriram, CIC Conference, Ottawa, Ontario, June, 1980, Abstract IN-6.

"Photophysics and photochemistry of Cr(III) polypyridyl complexes", R. Sriram, M.Z. Hoffman, M.A. Jamieson and N. Serpone, 4th Microsymposium on the Photochemistry and Photophysics of Coordination Compounds, Mont Gabriel, Quebec, July 30 - August 1, 1980, Abstract No. 7.

"The nature of intermediates in the excited state redox reactions: Cr(II), Rh(II) and Rh(I) polypyridyl complexes", M.Z. Hoffman, N. Serpone, M.A. Jamieson, Q.G. Mulazzani, S. Emmi, P.G. Fucchi, and M. Venturi, 3rd International Conference on the Photochemical Conversion and Storage of Solar Energy, SERI, Boulder, Colorado, August 3 - 10, 1980, Abstract IV-3.

"Probing of the picosecond-lived 4T_2 excited state of $Cr(bpy)_3^{3+}$ ", M.A. Jamieson, N. Serpone and M.Z. Hoffman, Conference on Inorganic Reaction Mechanisms, Wayne State University, Detroit, Michigan, June 10 - 12, 1981.

"Photoreactivity from a short-lived excited state", M.A. Jamieson, N. Serpone and M.Z. Hoffman, NERM-11 ACS Meeting, Rochester, N.Y., October, 1981, Abstract 250.

"Anion effects on the phosphorescence lifetimes of Cr(III) polypyridyl complexes in fluid media", M.A. Jamieson, N. Serpone, M.Z. Hoffman and R. Sriram, NERM-12 ACS Meeting, June 27 - 30, 1982, Burlington, Vermont, Abstract 217.

Date : October, 1982

Signature :

Mary A. Jamieson

